Physiological and cellular effects of TENin1, a novel small molecule inhibitor of endomembrane protein trafficking

Rupesh Paudyal

Submitted in accordance with the requirements of the degree of Doctor of Philosophy

University of Leeds

School of Biology, Faculty of Biological Sciences

September 2013

Supervisors: Professor Alison Baker and Dr Stuart L. Warriner

I confirm that the work submitted is my own and that appropriate credit has been given where reference has been made to the work of others.

This copy has been supplied on the understanding that it is copyright material and that no quotation from the thesis may be published without proper acknowledgement.

Acknowledgements

This thesis is dedicated to my grandparents

Mr Umakanta Paudyal and Mrs Min Kumari Paudyal

Abstract

Gravitropic response is required for proper orientation of plant growth and development. One of the factors that influence gravitropism in plants is the polar distribution of the plant hormone auxin, which is maintained by auxin transporters at the plasma membrane (PM). These endomembrane proteins are transported to the PM via the secretory pathway and undergo constitutive endocytic recycling from the PM. This thesis characterises an inhibitor of endomembrane protein trafficking, Trafficking & ENdocytosis inhibitor 1 TENin1 (TE1), that reduces gravitropic response in *Arabidopsis thaliana* seedlings. Short term TE1 treatment causes intracellular accumulation of membrane proteins including brassinosteroid receptor BRI1, aquaporin PIP2a, and auxin transporters PIN2 and PIN7. All the accumulated experimental evidence gained throughout the duration of this project also suggest that TE1 interferes with the endomembrane recycling to the TGN both from the pre-vacuolar compartment (PVC) and the PM therefore causing accumulation of PIN2-GFP at the PVC, which is eventually re-directed to the vacuole. The long term effects of TE1 were also characterised and revealed dose-dependent growth inhibition of whole plants and reduction in organelle dynamics. In a separate study in the laboratory two *Arabidopsis thaliana* accessions that displayed resistance to the effects of TE1 were identified. A library of *Arabidopsis thaliana* recombinant inbred lines (RILs) generated by crossing a TE1 resistant accession with the sensitive Columbia accession was commercially available. Therefore, 174 and 117 RILs were screened for different traits to identify a region of the genome responsible for the resistance to the effects of TE1. The data generated from the RIL screens revealed a major resistant locus lies within 9 to 16 Mb in the chromosome 5. A further study is now required to map the target gene(s) responsible for the resistance to TE1.

Contents

5　Chapter Five – Identification of *Arabidopsis thaliana* natural accessions that display resistance to TENin1 and genetic mapping of the resistant loci　128

List of Figures

List of Tables

List of abbreviations

2,4-D	2,4-dichlorophenoxyacetic acid
A23	Tyrphostin A23
ABC	ATP binding cassette
ABCB	ABC transporter subfamily B
ABD2	Actin binding domain 2
ABP1	Auxin binding protein 1
ADP	Adenosine 5' diphosphate
AFB	Auxin binding F-box protein
AP	Adapter protein
ARA7	Rab 5 small GTPase (RabF2b)
ARF	ADP-ribosylation factor
ARL	Average root length
ASK1	Supressor of kinetochore protein 1 (SKP1)
ATP	Adenosine-5'-triphosphate
AUX1	Auxin resistant 1
BFA	Brefeldin A
BR	Brassinosteroid
BRI1	Brassinosteroid insensitive 1
BSA	Bovine serum albumin
CAPS	Cleaved amplified polymorphic sequences
CCV	Clathrin coated vesicle
CDF	Cumulative distribution frequency
CFP	Cyan fluorescent protein

CHX	Cycloheximide
CIM	Composite interval mapping
CLASP	Cytoplasmic linker associated protein
CME	Clathrin mediated endocytosis
Col-0	*Arabidopsis thaliana* Columbia accession
COP	Coatomer protein complex
CUL1	Cullin 1
DIC	Differential interference contrast
DMSO	Dimethyl sufoxide
DNA	Deoxyribonucleic acid
EMS	Ethyl methanesulfonate
ER	Endoplasmic reticulum
ERAD	ER associated protein degradation
ERES	Endoplasmic reticulum exit site
ES1	Endosidin 1
ESCRT	Endosomal sorting complex required for transport
FLS	Flagellin sensitive
GAP	GTPase activating factor
GDP	Guanosine diphosphate
GE	Gel electrophoresis
GEF	Guanine nucleotide exchange factor
GFP	Green fluorescent protein
GNL	GNOM-like
GTP	Guanosine-5'-triphosphate

H$_2$O	Water
HKT2-4	*Arabidopsis thaliana* Heiligkreuztal-2 accession
IAA	Indole-3-acetic acid
KS	Kolmogorov-Smirnov
LatB	Latrunculin B
LAX	Like AUX1
Ler	*Arabidopsis thaliana* Landsberg erecta accession
LOD	Logarithm of the odds
LPVC	Late prevacuolar compartment
MS	Murashige and Skoog
mRNA	messenger RNA
MTR	Multiple trait
MVB	Multi vesicular bodies
NAA	Naphthaleneacetic acid
NAG	N-acetylglucosaminyl transferase
NASC	Nottingham Arabidopsis Stock Centre
NSF	N-ethylmaleimide sensitive fusion protein
PAT	Polar auxin transport
PBS	Phosphate buffered saline
PCR	Polymerase chain reaction
PFA	Paraformaldehyde
PGP	P-glycoprotein
PI3K	Phosphoinositide-3-kinase
PID	Pinoid

PILS	PIN LIKES
PIN	PIN-FORMED
PIP2a	Plasma membrane intrinsic protein 2a
PP2A	Protein phosphatase 2A
PSR	Percentage survival rate
PTS	Peroxisome targeting signal
PVC	Pre-vacuolar compartment
QTL	Quantitative trait locus
RBX	Ring box
RE	Restriction endonuclease
RFLP	Restriction fragment length polymorphism
RFP	Red fluorescent protein
RIL	Recombinant inbred line
RNA	Ribonucleic acid
ROP	Rho of plants
RUB	Ubiquitin related protein
SAR	Structure activity relationship
SCF	ASK1-CUL1-F-box protein
secGFP	Secreted green fluorescent protein
Sha	*Arabidopsis thaliana* Shahdara accession
SGR	Shoot gravitropism
SKS	SKU SIMILAR
SKU	SKEWED
SNARE	Soluble NSF attachment protein receptor

SNP	Single nucleotide polymorphism
SNX	Sorting nexin
SPK1	SPIKE1
SSLP	Single sequence length polymorphism
ST	Sialyl transferase
SYP	Syntaxin of plants
T-DNA	Transferred DNA
TE1	TENin1; Trafficking and endocytosis inhibitor 1
TIR1	Transport inhibitor response 1
TGN	Trans-Golgi network
TPL	Topless
VAM	Vacuolar morphology
VAN	Vascular network defective
VHAa1	Vacuolar proton-ATPase a1
VPS	Vacuollar protein sorting
VSR	Vacuolar sorting receptor
VTI	Vesicle transport v-SNARE family protein
Ws2	*Arabidopsis thaliana* Wassilewskija accession
YFP	Yellow fluorescent protein

List of symbols and units

½	Half
°C	Degrees Celsius
μl	Microlitre
μM	Micromolar
μm	Micrometer
A	Adenine
bp	Base pairs
cM	Centimorgan
C	Cytosine
D	Displacement rate
G	Guanine
g	Relative centrifugal force
h	Hour
kb	Kilobase
kDa	KiloDalton
l	Litre
M	Molar
Mbp	Mega base pairs
mg	Milligram
MI	Meandering index
min	Minute
ml	Millilitre
mM	Millimolar
mm	Millimeter
n	Number
nM	Nanomolar

p	Probability value
s	Second
SE	Standard error
T	Thymine
V	Velocity
v/v	Volume/volume
w/v	Weight/volume

1   Chapter One – Introduction

1.1   Plant endomembrane trafficking

Endomembrane dependent protein trafficking is essential for the survival of eukaryotic organisms. The plant endomembrane is a complex system in which proteins undergo trafficking through several distinct membrane-bound compartments to reach their designated destination (Figure 1.1 and Figure 1.2). The endomembrane system consists of different membrane-bound organelles such as the endoplasmic reticulum (ER), Golgi apparatus and Golgi derived vesicles trans-Golgi network (TGN). Other organelles that are also part of the endomembrane system include multi-vesicular bodies or pre-vacuolar compartments (PVCs), endosomes, the vacuole, the cell plate (CP) and the plasma membrane (PM).

1.1.1   ER–Golgi interface

After the transcription in the nucleus the mature messenger ribonucleic acid (mRNA) is transported to the cytosol through the nuclear pores. In the cytosol, translation of mRNA into polypeptides occurs on free ribosomes. Endomembrane proteins are synthesised on the ribosomes that are bound to the ER. From this point onwards, proteins destined for the secretory pathway need to be transported (translocated) into the ER from the cytosol. Protein translocation through the translocation channel into the ER lumen can take place as the protein is being synthesised (co-translationally) or after protein synthesis (post-translationally). Both of these mechanisms require the following processes, (1) the identification of protein to be targeted into the ER by the signal (recognition) peptide, (2) protein association to the ER translocation machinery and protein import, and (3) protein folding and maturation in the ER (Rapoport, 2007).

From the ER, trafficking of the newly synthesised and correctly folded proteins to their designated destination starts with transport to the Golgi apparatus (Figure 1.1). The ER is typically organised in a polygonal network, connected by three way junctions, that consists of tubules, cisternae and the nuclear envelope (Sparkes et al., 2009c). The function of the ER ranges from biosynthesis of phospholipids, glycosylation and controlling cellular calcium homeostasis to folding and quality control of secretory proteins (Vitale et al., 1993). Only the proteins that are correctly

folded leave the ER to be taken further to their destination(s). The proteins that are not folded properly are retained in the ER lumen until they can be refolded properly. However, if this process is still unsuccessful then incorrectly folded proteins undergo ER-associated protein degradation (ERAD), where they are retro-translocated from the ER lumen to the cytosol (Stolz and Wolf, 2010). These misfolded proteins are then ubiquitinated in the cytosol, by ubiquitin proteasome system, that marks these proteins to be degraded by the proteasomes. The anterograde transport of secretory proteins from the ER to Golgi takes place at the ER exit sites (ERES) in vesicles covered with coatomer protein complex II (COPII) (Marti et al., 2010).

Vesicles are small compartments that travel from one organelle to another allowing inter-compartmental transport to take place. Most vesicles that are involved in the secretory transport of protein or lipid are usually covered in coat proteins such as clathrin, COPI or COPII. The type of vesicle coat helps determine the sorting of the vesicle and its constituents to the designated destination within the cell. The COPII mediated transport from the ER to Golgi apparatus is initiated when a small GTP binding protein, secretion associated Ras related protein 1 (Sar1), exchanges GTP for GDP with the help of Sec12, a guanine nucleotide exchange factor (GEF) that is bound to the ER membrane (d'Enfert et al., 1991; Barlowe et al., 1994). This allows recruitment of COPII from the cytosol to the Sec23/24 core and that recruits and Sec13/31 complex to form a heterotetrametic subcomplex (Marti et al., 2010). COPII is also required for membrane curvature that will form the COPII vesicles and when membrane deformation is complete Sar1-GTP is hydrolysed to Sar1-GDP, with the action of ARF-GTPase activating proteins (GAPs), that causes dissociation and uncoating of the vesicle (Marti et al., 2010).

There is also evidence that suggests there might be a physical connection between the ERES and the cis-Golgi as Golgi is visualised to localise adjacent to the ERES for brief periods. The ER-Golgi connection was displayed by manipulating Golgi movement using laser traps and allowing the cortical ER tubule to follow the path of Golgi movement (Sparkes et al., 2009b). The Golgi apparatus typically consists of many stacks of membrane bound cisternae designated cis to medial to trans face moving away from the ER (Richter et al., 2009). The function of Golgi bodies in the plant cell includes the synthesis of the cell wall polysaccharides, protein

glycosylation and protein sorting to the PM or to the vacuole. Trafficking to the PM is also dependent on organelles that are derived from the Golgi.

Retrograde transport from Golgi to the ER and trafficking between the Golgi cisternae faces might be carried out by COPI coated vesicles (Figure 1.1). It has been recently reported that the staple proteins in the cisternal stack in the central region of Golgi cisternae are static and the rims of cisternae containing soluble aggregates are mobilised in a process termed as rim progression (Lavieu et al., 2013). COPI is a protein complex composed of 7 subunits. The assembly of COPI at the membrane is mediated by a small GTP binding protein, adenosine diphosphate (ADP)-ribosylation factor 1 (ARF1). ARF1 is GDP bound in its inactive state but GEFs defined by a central Sec7 domain show an ability to change GDP to GTP. This then allows ARF to bind in to the membrane and COPI multimers, which allows the formation and the budding of a new vesicle (Bethune et al., 2006).

The retrograde transport is equally as important as the anterograde transport to maintain the protein equilibrium that maintains organelle integrity. If the rate of anterograde-retrograde trafficking is favoured towards the anterograde trafficking then an imbalanced situation may arise where Golgi size and population would increase in the expense of the ER. Vice versa in tobacco cells, treatment with fungal toxin brefeldin A (BFA) causes re-localisation of Golgi proteins to the ER, an effect that can be recovered upon BFA washout (Matsuoka et al., 1995; Boevink et al., 1999). BFA inhibits the action of GNOM protein that acts as an ARF-GEF (Steinmann et al., 1999), that is required for COPI mediated retrograde trafficking from the Golgi to the ER. Inhibition of this step by BFA is also seen due to the loss of ERES integrity (Ritzenthaler et al., 2002; daSilva et al., 2004; Stefano et al., 2006), which suggests that there is a counter effect in trafficking to the Golgi which results in re-localisation of the Golgi proteins into the ER by fusing the ER and Golgi membranes (Nebenfuhr et al., 2002). Similarly in *Arabidopsis thaliana* protoplasts, a dominant negative mutant of ARF1 proteins caused re-distribution of proteins to the ER indicating that ARF1 is required for the ER to Golgi export (Lee et al., 2002). Remarkably, BFA does not affect the identity of Golgi in *Arabidopsis thaliana* cells indicating that in *Arabidopsis thaliana* GNOM is not the GEF for ARF1 that is required for trafficking from the ER to Golgi. Instead, GNOM homolog GNOM-like 1 (GNL1) is required for the ER to Golgi transport. A point mutation in GNOM at amino

acid position 696 from methionine to leucine in the sec7 domain, required for ARF interaction, caused BFA resistance making it similar to GNL1 (Geldner et al., 2003).
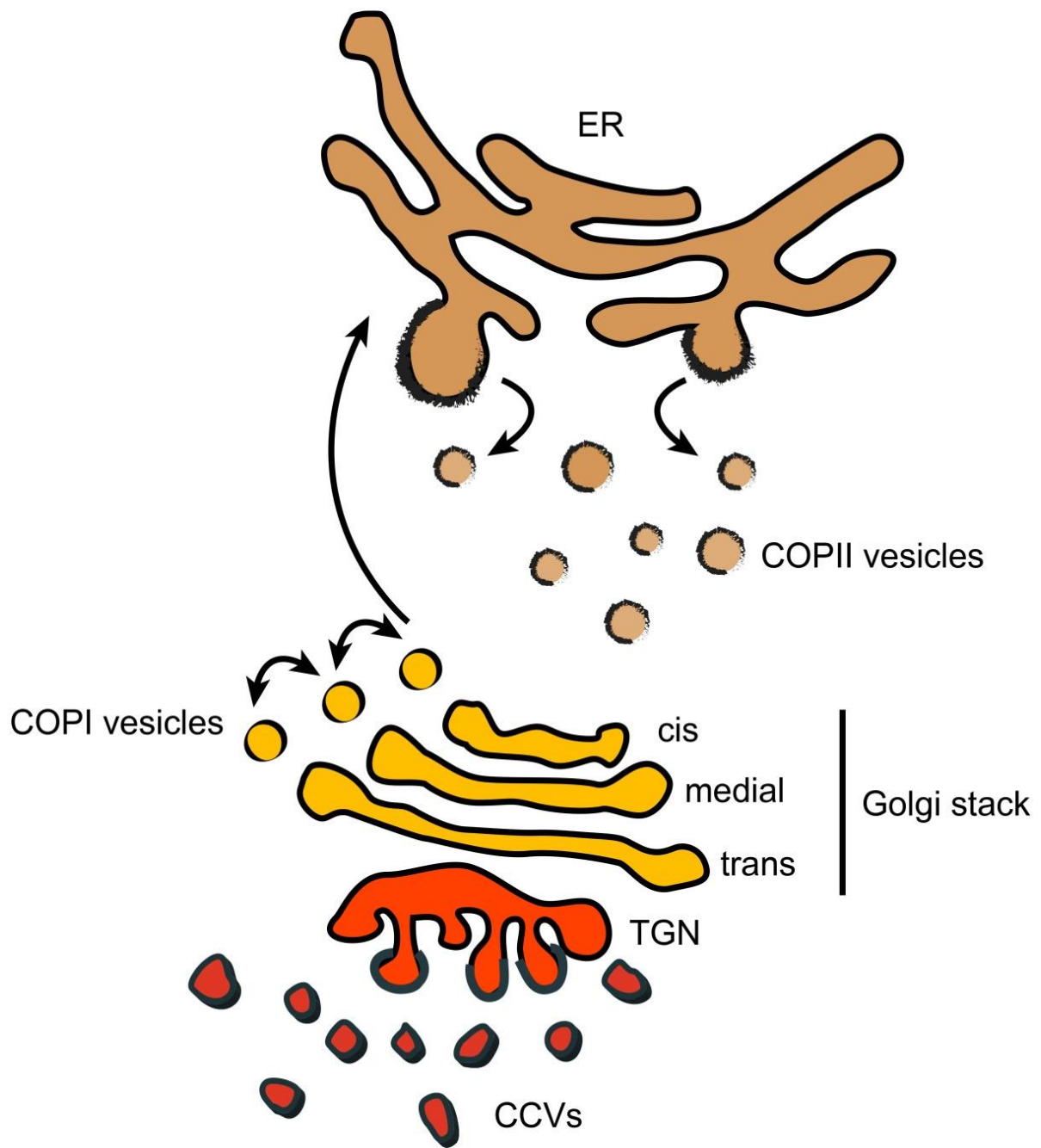
Figure 1.1. The ER-to-Golgi interface.

Anterograde and retrograde trafficking between the ER and Golgi stacks. ER; endoplasmic reticulum, COP; coat protein complex, TGN; trans-Golgi network, CCVs; clathrin coated vesicles.

1.1.2 TGN and beyond

It is thought that the TGN serves as a central junction in the secretory and the endocytic trafficking. Trafficking of the newly synthesised proteins towards the PM or towards the vacuole and the proteins recycling from the PM, both those designated to be recycled back to the PM and those destined for the vacuole for degradation are thought to pass through the TGN. However, there might be a direct route from the Golgi to the PM. Direct evidence of protein trafficking to the PM from the TGN is still missing but ECHIDNA protein localised to the TGN was shown to be required for secretory trafficking but not endocytosis (Gendre et al., 2011). Even though the TGN is occasionally found adjacent to the trans face of the Golgi cisternae, it is an independent organelle. The TGN is often confused with the trans-Golgi cisternae that are part of the Golgi apparatus. Sialyl transferase (ST) fusions that localise to the trans-Golgi cisternae are frequently used as Golgi markers and they do not co-localise with TGN marker soluble N-ethylmaleimide-sensitive factor attachment protein receptor (SNARE), SYP61 (Foresti and Denecke, 2008).

1.1.2.1 Protein trafficking to- and from- the plasma membrane

Biosynthetic trafficking to the TGN is poorly characterised. One possibility is the trafficking to the TGN from the Golgi takes place through the clathrin coated vesicles (CCVs), which fuse to the TGN. Trafficking of the secreted green fluorescent protein (secGFP), that is transported from the ER to the apoplast (extracellular space), passes through the Golgi apparatus and displays weak accumulation of signal in the apoplast (Batoko et al., 2000; Zheng et al., 2004). This is consistent with the finding that secretory trafficking to the PM is a default pathway for protein cargoes (Denecke et al., 1990). In dividing cells, proteins that are typically routed towards the PM/apoplast are localised to the cell plate (CP) and its surroundings (Yokoyama and Nishitani, 2001). However, only a low level of co-localisation of the cytokinesis syntaxin KNOLLE with ARA7, a Rab5 GTPase that is targeted to the PVC was observed (Reichardt et al., 2007). During cytokinesis, KNOLLE is generally localised to the phragmoplast and it is involved in vesicle fusion required for CP formation (Lauber et al., 1997). Expression of KNOLLE in non-dividing cells caused targeting of the protein to the PM (Volker et al., 2001). This suggests that the default protein targeted to the PM is redirected towards the CP during cytokinesis but trafficking towards the PVC remains unchanged.
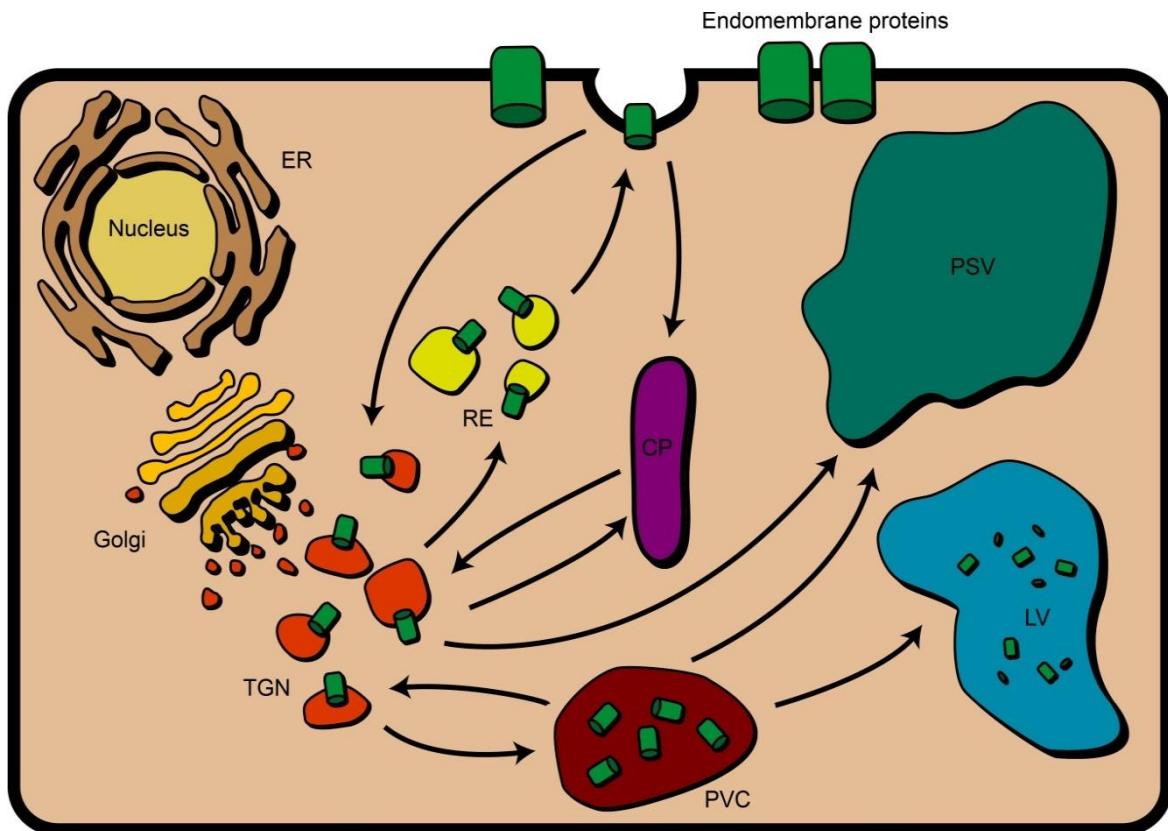
Figure 1.2. Simplified model of the plant endomembrane based trafficking in plants.

Proteins synthesised in the endoplasmic reticulum (ER) are taken to the Golgi apparatus followed by trafficking to the trans-Golgi network (TGN) mediated by vesicles fusing away from Golgi. From the TGN proteins may be taken to the plasma membrane. In dividing cells, proteins are also targeted to the cell plate (CP). Proteins are also recycled from the PM through the TGN pathway back to the PM via recycling endosomes (RE). Alternatively, proteins from the TGN may also be taken to the lytic vacuole (LV) for protein degradation via the pre-vacuolar compartment (PVC) or to the protein storage vacuole (PSV).

There is some evidence for the existence of a distinct compartment often referred as recycling endosome (RE) that may act as an intermediate in the trafficking from TGN to the PM and perhaps is only involved in endocytic trafficking (only in recycling of the proteins from the PM and not in the secretory protein trafficking of the newly synthesised proteins). It is however not backed up with concrete evidence. Existence of a recycling endosomal compartment was concluded based on the failure to co-localise GNOM-GFP, that is thought be involved specifically in endocytic recycling to the PM, with other markers of secretory system and partial co-localisation of endocytic tracer dye FM4-64 (Geldner et al., 2003). FM4-64 is a fluorescent styryl dye, widely used to trace endocytic trafficking, that has a lipophilic tail therefore binds to the PM and is internalised to the endosomal compartments by endocytosis eventually reaching the vacuole membrane (Figure 1.3). Divergence of secretory and endocytic recycling therefore is thought to exist but experimental evidence backing these hypotheses is still weak. However, the TGN in plants has been shown to act as a crossroads in trafficking as the newly synthesised proteins pass through TGN to the PM or the vacuole. Proteins recycling from the PM also pass through the TGN, either to be recycled back to the PM or to be degraded at the vacuole (Dettmer et al., 2006).

Trafficking to the PM requires fusion of the vesicle carrying the cargo, which may include peripheral/integral membrane proteins or enzymes and other molecules at the apoplast required for the cell wall synthesis. Either way, PM trafficking requires vesicle formation for cargo uptake from the donor membrane and fusion at the target membrane to release the cargo. Typically, clathrin mediated vesicle formation, whether for the trafficking to the PM or endocytosis from the PM requires a combination of several proteins. Clathrin heavy chain (CHCs) and clathrin light chains (CLCs) are required to form each leg of the clathrin triskelion that is recruited to the donor membrane (Chen et al., 2011). ARF catalyses the synthesis of phosphatidylinositol 4,5-bisphosphate at the PM and the synthesis of phosphatidylinositol 4-phosphate at the trans-Golgi cisternae as a mark for the recruitment site for vesicle generation. In the post-Golgi trafficking, the activated ARF GTPase generally helps in the recruitment of the adaptor protein (AP) complexes at the donor membrane. In mammalian cells ARF6 has been reported to play a part in

clathrin recruitment to the PM (Ge et al., 2001; Aikawa and Martin, 2005) however, this process is not well defined in plants.

Clathrin does not directly interact with the membrane or its cargo therefore this interaction is mediated by the AP complex that is also recruited to the membrane for the CCV formation (Barth and Holstein, 2004; Happel et al., 2004). AP complexes in eukaryotes exist as heterotetrameric protein and the subunits are often referred as adaptins. AP complexes are composed of two large adaptins (α/γ/δ/ε and β), one medium (μ) and a small adaptin (σ) (McMahon and Boucrot, 2011). Accumulation of polymerising clathrin triskelia and AP complexes at the donor membrane site (i.e. at the PM or the TGNs) causes membrane invagination therefore loading the cargoes into the forming vesicle and finally the bud undergoes scission mediated by GTPases, dynamin or dynamin-related proteins (DRPs) (Chen et al., 2011). Once the CCV is released, the clathrin coat is quickly dismantled. Different AP complexes appear to have distinct role in vesicle formation, AP-2 is required for clathrin mediated endocytosis (CME) from the PM (Ortiz-Zapater et al., 2006; Dhonukshe et al., 2007; Bar et al., 2009). Recently, a μ-adaptin of AP-1 complex was shown to be localised at the TGN, and AP-1 was implicated in protein trafficking/recycling to the PM, the vacuole and the cell plate but it is not required for endocytosis from the PM (Park et al., 2013; Teh et al., 2013; Wang et al., 2013). AP-3 β subunit was shown to be predominantly localised to the cytosol and was shown to be required for biogenesis of the lytic vacuole but not the embryonic storage vacuole (Feraru et al., 2010). Another component of the AP-3, the δ subunit, was also identified and implicated in the vacuolar biogenesis and function (Zwiewka et al., 2011).

ARF-GEF GNOM and ARF-GAP VASCULAR NETWORK DEFECTIVE (VAN) 3 were both reported to be required for endocytosis from the PM (Naramoto et al., 2010). However, this does not fit in with the observations that show accumulation of proteins in the BFA compartment, originating from the PM (Geldner et al., 2001; Geldner et al., 2003; Paciorek et al., 2005). Since, this was suggested by studies in genetic knockout mutants, there remains a possibility that when GNOM, required for trafficking to the PM, is knocked out then a pleiotropic effect is observed where endocytosis is also inhibited as a consequence of inhibition of exocytosis. Therefore, modulation of these pathways using small molecule inhibitors, which can be transiently used to determine the primary function of a protein, can be advantageous.

Clathrin independent endocytosis also exists in plants. Some examples include the internalisation of leucine-rich repeat receptor kinases brassinosteroid (BR) receptor, brassinosterioid insensitive 1 (BRI1) and flagellin receptor, flagellin sensitive 2 (FLS2). BRI1 is normally inactive due to the binding of BRI1 kinase inhibitor 1 which is phosphorylated upon BR binding. This liberates BRI1 to form a heterodimer with BRI1-associated kinase 1, which is ready to be internalised from the PM (Vert, 2008). FLS2 has also been shown to form a complex with BAK1 minutes after ligand binding (Chinchilla et al., 2007) followed by internalisation of the receptor complex. Recently, uptake of glucose and internalisation of fluorescent protein-flotillin1, that localises to the PM, were shown to be take place via clathrin independent endocytic process (Bandmann and Homann, 2012; Li et al., 2012).
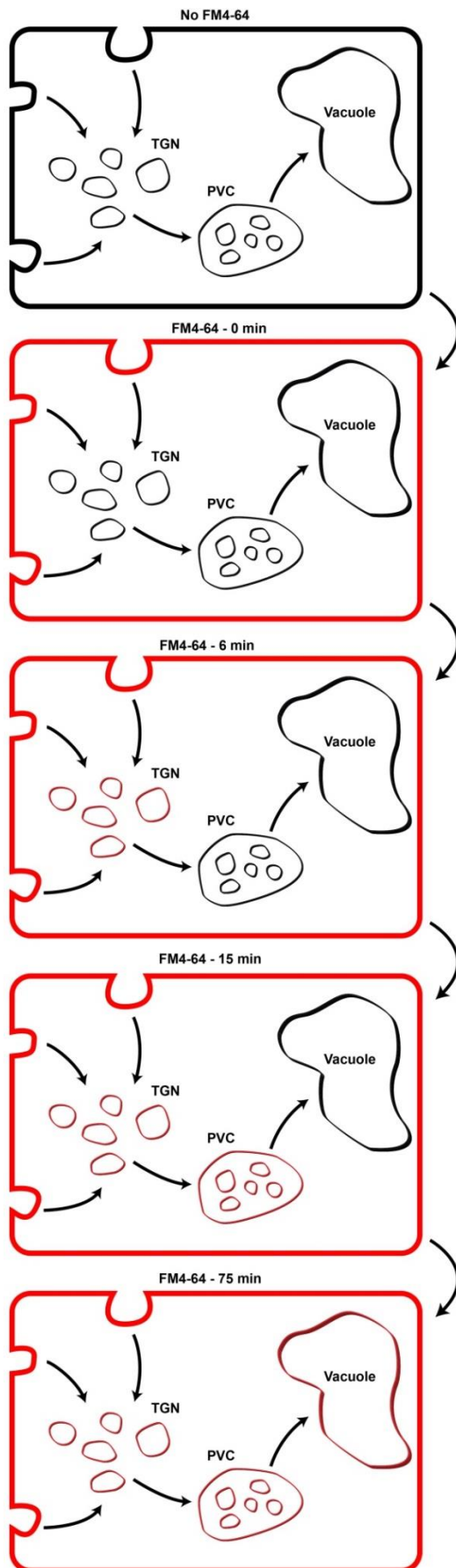
Figure 1.3. FM4-64 uptake in *Arabidopsis thaliana* root cells.

Upon Incubation, *Arabidopsis thaliana* root in FM4-64 dye immediately binds the lipids in the plasma membrane. Internalisation of membrane into endosomal compartments can be traced with FM4-64, and FM4-64 co-localises with the TGN marker VHAa1-GFP 6 min after FM4-64 incubation and eventually partial co-localisation with the PVC marker ARA7 is observed after 15 min (Dettmer et al., 2006). Eventually FM4-64 reaches the vacuole membrane after 75 min incubation (Bassil et al., 2011). Red outline of the endomembrane organelles represents FM4-64 labelling. However, this does not exclude the possibility of FM4-64 passing through another intermediate compartment before reaching the TGN.

1.1.2.2 Vacuolar trafficking and recycling from the prevacuolar compartment

Secretory trafficking to the vacuole requires a vacuolar sorting signal that is detected by the family of vacuolar sorting receptors (VSRs), which consists of seven members in the model plant *Arabidopsis thaliana* (De Marcos Lousa et al., 2012). The fusion of TGN derived vesicles to the PVC helps release the VSRs therefore they are possibly recycled back to the TGN of Golgi for another round of trafficking. The PVC then fuses with the vacuole to releasing the cargo proteins into the vacuole. Recently, a late prevacuolar compartment (LPVC) has been proposed to mediate trafficking between the PVC and the vacuole in tobacco (Foresti et al., 2010). PVCs are multi-vesicular bodies that form by the internalisation of endosomal vesicles into the PVC structure therefore producing an internal compartment within the PVC termed as intraluminal vesicles (ILVs). This type of formation of the PVC is thought to be mediated by clathrin although concrete evidence is still missing. During the fusion of PVCs to the vacuole, the ILVs are exposed to the vacuolar lumen for degradation of proteins and lipids and the remainder of proteins/lipids outside the ILVs but within the PVC are probably used for vacuole membrane (Babst, 2011). Therefore, the proteins that are designated to be degraded in the lytic vacuole need to be compacted into these ILVs. The proteins that are targeted to the ILVs are marked by ubiquitination of a lysine residue. Ubiquitin tags are then recognised by the endosomal sorting complex required for transport (ESCRT) that helps target proteins into the ILVs. An alternative process of the PVC formation is also proposed that suggests PVCs mature from the TGN (Scheuring et al., 2011). This report also showed that vacuolar trafficking can still take place in the absence of functional clathrin mediated trafficking, although trafficking to the vacuole required the action of the ESCRT components. Therefore, multiple mechanisms for the PVC formation may exist in plants.

FM4-64 in *Arabidopsis thaliana* localises at the PVC after 30 min incubation, as shown by FM4-64 co-localisation with a known PVC marker BP80, a VSR protein 80 kDa (Tse et al., 2004). Another report showed FM4-64 co-localisation with ARA7, another PVC marker, 15 min after incubation (Dettmer et al., 2006). Either way, this indicated that the PVC also acts in the endocytic pathway and indicates the position of the PVC to be after TGN in the endocytic trafficking as TGNs were labelled just after 5 min FM4-64 incubation (Dettmer et al., 2006). It is known that the VSRs do

not localise to the PM but they are predominantly identified at the PVC indicating that biosynthetic trafficking towards the vacuole also takes place through the PVC. Therefore like the TGN compartments, PVCs also overlap between the biosynthetic trafficking and endocytic trafficking.

Protein recycling from the PVC to the TGN or Golgi is mediated by the retromer complex. This recycling process is inhibited by the action of drug wortmannin (daSilva et al., 2005), which interferes with the action of the enzyme phosphatidylinositol 3-kinase, that is responsible for the production of lipid phosphatidylinositol 3-phosphate (PI3P). The subunits of the retromer complex interact with PI3P to mediate the retrograde trafficking to recycle the VSRs therefore the action of wortmannin also inhibits trafficking to the vacuole. This effect redirects the vacuolar cargoes towards the PM and which is then secreted (daSilva et al., 2005). The endomembrane based trafficking pathways discussed before are shown in the Figure 1.2.

1.2 Effects of endomembrane trafficking on auxin signalling

Along with the components required for the formation of the cell wall, the plasma membrane and the vacuole, plant endomembrane based trafficking and recycling is pivotal for cellular response to the external stimuli, plant development and tropic responses. One special feature of the endomembrane trafficking is its ability to generate cellular polarity by focusing the protein trafficking to one end of the cell. This is particularly important in generating asymmetric distribution of the plant hormone auxin that is important for many aspects of plant development including cell division, cell elongation, plant organogenesis and maintaining shoot and root tropic responses.

1.2.1 Auxin signalling

Auxin signalling activates or represses the expression of several classes of genes that in turn regulate the developmental aspects controlled by auxin (Finet and Jaillais, 2012). The auxin signalling cascade is a complex process and is generally controlled by two gene families, the Aux/IAAs and the auxin response factors that encode transcriptional activators or repressors. In *Arabidopsis thaliana*, the Aux/IAA gene family has 29 members and the auxin response factor family has 23 gene members. An important breakthrough in this signalling was the identification of the

family of F-box proteins TIR1 (transport inhibitor response 1) that acts as an auxin receptor (Dharmasiri et al., 2005; Kepinski and Leyser, 2005a). Several other F-box proteins AFBs (auxin signalling F-box proteins) were also later on shown to bind to natural auxin indole-3-acetic acid (IAA) (Parry et al., 2009; Calderon Villalobos et al., 2012). TIR1/AFBs together with suppressor of kinetochore protein 1 (SKP1 or ASK1 in plants), cullin 1 (CUL1) and ring box (RBX) form an E3 ubiquitin ligase complex commonly known as SKP1-CUL1-F-box protein (SCF)$^{TIR1/AFB}$ complex (Chapman and Estelle, 2009). Under low level of auxin IAA, Aux/IAA repressors and topless (TPL) co-repressors bind to the auxin response factors that control auxin responsive gene expression (Figure 1.4). However higher level of intracellular auxin IAA leads to the binding of IAA to TIR1/AFBs. This also recruits Aux/IAAs with IAA acting as molecular glue between these two proteins. Therefore, auxin promotes the poly-ubiquitination of the Aux/IAA repressors, by the action of the SCF$^{TIR1/AFB}$ E3 ubiquitin ligase that acts as a mark for protein degradation by the 26S proteasome. TIR1/AFBs proteins are components of ubiquitin-protease system. Degradation of repressor Aux/IAAs liberates the activating auxin response factor to initiate the transcription of auxin responsive genes by binding to the auxin responsive element region, with a consensus sequence (TGTCTC), at the promoter of auxin responsive genes (Chapman and Estelle, 2009). Auxin mediated induction of gene expression is summarised in Figure 1.4. The auxin induced genes include the Aux/IAA family therefore they can repress the free auxin response factors to prevent excessive gene expression.
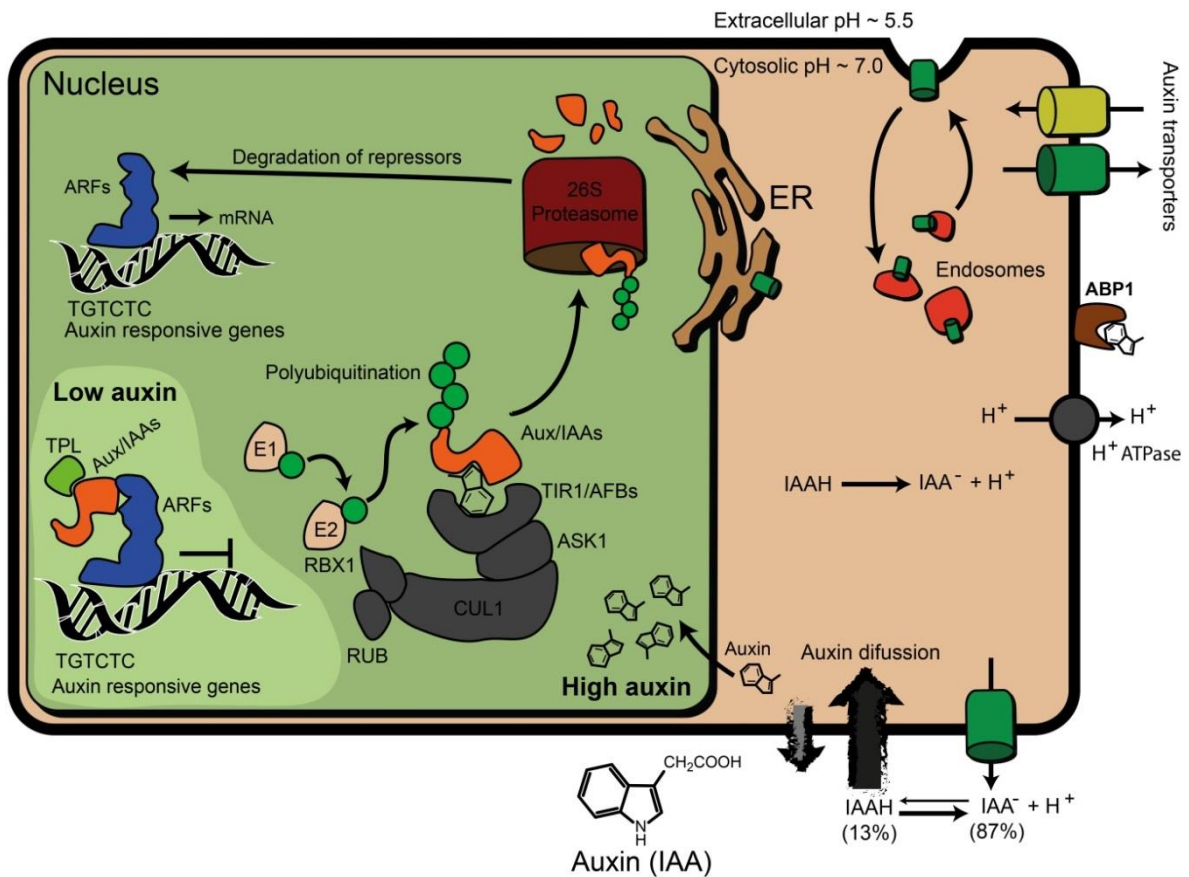
Figure 1.4. Auxin signalling and auxin transport pathway.

Auxin, indole-3-acetic acid (IAA), may be imported into the cell by diffusion (rough arrow) or by auxin influx carriers AUX/LAX that localise to the plasma membrane (PM). Auxin binding protein (ABP1) is also present on the PM. IAA requires efflux carriers, PINs or ABCBs, at the PM to be exported from the cell. The auxin carriers are undergoing constant endocytic recycling at the PM. Some PINs are also found in the ER membrane. Under low auxin level in the nucleus, auxin responsive gene expression is prohibited due to repression of transcription factors, auxin response factors (ARFs), by the binding of repressor proteins Aux/IAAs. However, in high auxin concentration auxin acts as a molecular glue to bind TIR1/AFB proteins with Aux/IAAs and ASK1-CUL1-F-box protein (SCF)$^{TIR1/AFB}$ protein complex helps the polyubiquitination of the Aux/IAAs by E3 ubiquitin ligase enzyme that marks for Aux/IAAs to be degraded by 26S proteasome. This liberates the auxin response factors that can bind to the consensus sequence (TGTCTC) in auxin response genes to start transcription.

1.2.2 Auxin transport

The plant hormone auxin, in its most abundant natural form, mainly exists as a weak organic acid that is composed of an indole ring with a carboxylic acid side group (indole-3-acetic acid; IAA, Figure 1.4). As the Cholodny-Went theory proposes, the differential distribution of auxin creates a gradient therefore this allows a wide range of developmental processes to be mediated by one small molecule. This gradient of auxin distribution is mediated by the active cell-to-cell transport of auxin molecules, a process termed as polar auxin transport (PAT), that is predominantly mediated by the auxin influx and the efflux carriers that are typically localised at the PM (Grunewald and Friml, 2010).

The hydrophobic lipid composition at the PM does not allow passive transport of polarised molecules or proteins however non-polar substances may pass through with relative ease (Figure 1.4). The driving force behind the PAT lies within the pH difference seen across the PM generated by the PM localised H^+ ATPases. The pH of the apoplast is relatively acidic (pH ~5.5) and the pH across the membrane in the cytosol is relatively neutral (pH ~7.0). The pKa constant of IAA is 4.75. Therefore, at the acidic apoplastic pH, some of the carboxyl group in the IAA is protonated (IAA-H $\leftrightarrow$ IAA$^-$ + H$^+$) into its neutral form. However at the neutral cytosolic pH IAA-H is deprotonated (IAA-H $\rightarrow$ IAA$^-$ + H$^+$) shifting the equilibrium towards the polar IAA$^-$ (Peer et al., 2011). Therefore this chemical feature of auxin makes efflux from the cell the rate limiting factor in the PAT (Petrasek et al., 2006). The role of the auxin efflux carriers therefore defines the auxin distribution in plants.

1.2.2.1 Auxin transport carriers

Alongside import of non-polar IAA by passive transport across the membrane, auxin import into the cell is also carried out by the family of plasma membrane auxin permeases, AUX/Like AUX (LAX). *Arabidopsis thaliana* genome contains four genes in this family AUX1 and LAX1-3. It is predicted that the import of IAAs through the AUX/LAX transporters occurs as H$^+$ symport (Sabater and Rubery, 1987). However the nature of auxin, as described below, also makes a huge difference to uptake by the AUX/LAX importers. The synthetic auxin 2,4-dichlorophenoxyacetic acid (2,4-D) requires auxin influx carriers to be imported into the cell however, another synthetic auxin 1-naphthalene acetic acid (NAA) does not require auxin influx carriers and is

able to diffuse freely through the PM due to its lipophilic properties (Delbarre et al., 1996).

There are at least two families of proteins that display auxin efflux activity at the PM. These are PIN-FORMED (PIN) and type B transporters of the ATP-binding cassette (ABC) protein transporters superfamily (ABCB/P-glycoprotein; PGP/multidrug resistance) (Bandyopadhyay et al., 2007). In *Arabidopsis thaliana* the PIN protein family has eight members (PIN1-8) that are divided into two subclasses as determined by the length of the cytosolic hydrophilic loop in the middle of the protein chain that separates hydrophobic trans-membrane regions either side of the cytosolic loop (Krecek et al., 2009). PIN1-4 and PIN7 are localised at the PM and are often referred as canonical or 'long' PINs. PIN6 also belongs to the long PIN subgroup due to its sequence similarity at the trans-membrane (TM) domains and only a slight reduction to the hydrophilic cytosolic loop. The predicted TM topology of PM localised PIN2 protein (Ganguly et al., 2010), that represents TM topology of long PINs, is displayed in Figure 1.5. In contrast to the PM localised long PINs, short PINs, PIN5 and PIN8, have been shown to be localised at the ER membrane in *Arabidopsis thaliana* (Mravec et al., 2009; Dal Bosco et al., 2012; Ding et al., 2012). Subcellular localisation of PIN6 is still not well characterised but it was recently reported to be localised to the ER (Bender et al., 2013).

The second auxin efflux proteins belong to the ABCB superfamily which is conserved amongst bacteria and eukaryotes. Two subgroups of the ABCB families, ABCB1, ABCB4 and ABCB19, have been predicted to display auxin transport in plants (Bandyopadhyay et al., 2007). They have been shown to be localised at the PM in a non-polarised manner and use ATP to move their substrate across the membrane. Recently, a new family of proteins PIN-LIKES (PILS) have been shown to be localised to the ER and contributes to maintain the intracellular auxin homeostasis (Barbez et al., 2012).
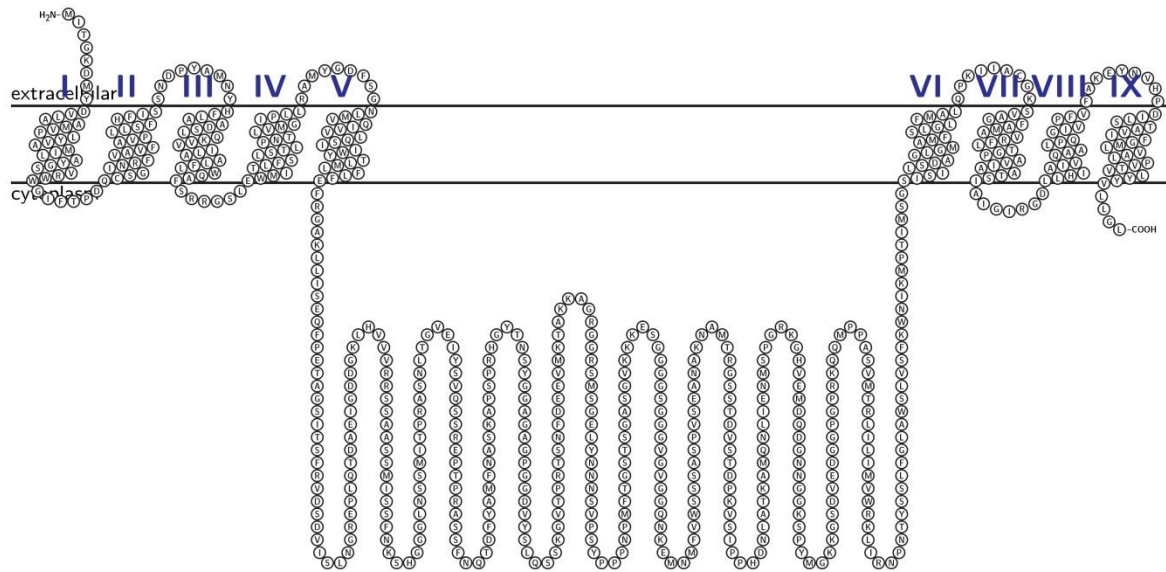
Figure 1.5. Trans-membrane topology of long PINs.

The coding DNA sequence of *AtPIN2* was translated to amino acids that revealed 647 aa sequence. This was entered in TMHMM Server v. 2.0 software (http://www.cbs.dtu.dk/services/TMHMM-2.0/) that predicts topology of trans-membrane (TM) proteins. The predicted TM topology was then inputted into LaTeX software (with help from Dr. Vincent Postis, University of Leeds) to generate the PIN2 TM topology model.

1.2.3 Subcellular positioning of auxin transporters

All the auxin transporters AUX/LAX, PINs and ABCBs display tissue-specific expression patterns that may overlap in some cases. As it is known that the rate limiting factor in auxin transport is auxin efflux, the subcellular localisation of PIN proteins seems to have an extra impact in the development and external responses, such as the plants response to gravity perception termed as gravitropism, a process that is mediated by the formation of transient auxin gradient (Band et al., 2012).

Different members from the family of PIN proteins operate in different cell types, and show distinct polarisation in the membrane according to the cell type and expression level (Krecek et al., 2009). A list of subcellular localisation of PINs and AUX1 in different cellular layers of *Arabidopsis thaliana* root is listed in Table 1-1. In *Arabidopsis thaliana* root, PIN1 and PIN2 are polarised basally ('rootwards') in the stele and young cortex, respectively, AUX1 and PIN2 are polarised apically ('shootwards') in the epidermis and PIN3 and PIN7 are non-polar in the columella (Table 1-1). In simple terms, auxin transport in *Arabidopsis thaliana* roots is controlled predominantly by PIN1, PIN2 and PIN3 (Figure 1.6C) (Feraru and Friml, 2008). As auxin is mainly synthesised in the young shoot tissues (Ljung et al., 2001), it is transported basally towards the root tip via PIN1 proteins that are typically basally polarised in the stele layer (Figure 1.6B and C). When auxin reaches the root meristem, it is then transported laterally towards the root cap and the epidermis layer by PIN3 protein that is localised in a non-polar manner at the root columella region (Figure 1.6B and C) (Feraru and Friml, 2008). The auxin level is higher at the root meristem region, partly due to the synthesis of auxin at the root meristem (Ljung et al., 2005) and perhaps the rate of auxin transport by PIN1 from the stele is higher than PIN3 dependent auxin efflux from the columella. Auxin is then transported up the root by the action of PIN2 proteins that display apical polarisation in the root epidermis cells (Figure 1.6B and C).

Table 1-1. Tissue specific subcellular polarisation of plasma membrane localised AUX1 and PIN proteins in *Arabidopsis thaliana* root

Tissue	Protein	Localisation
Mature root	PIN1	Stele, polar basal
Elongation and transition zone	AUX1	Epidermis, polar apical
	PIN1	Stele, polar basal
	PIN2	Epidermis, polar apical/lateral
	PIN3	Pericycle, polar lateral
	PIN7	Stele, polar basal/lateral
Root tip	AUX1	Columella and lateral root cap, non-polar
	PIN1	Pro-vasculature, polar basal
	PIN2	Epidermis, polar apical/lateral; cortex, polar basal
	PIN3	Columella, non-polar
	PIN4	Pro-vasculature, polar basal; QC, non-polar
	PIN7	Columella, non-polar

AUX1/long PINs and their polarisation status in different tissue and cell layer of *Arabidopsis thaliana* root are specified. QC, quiescent centre.
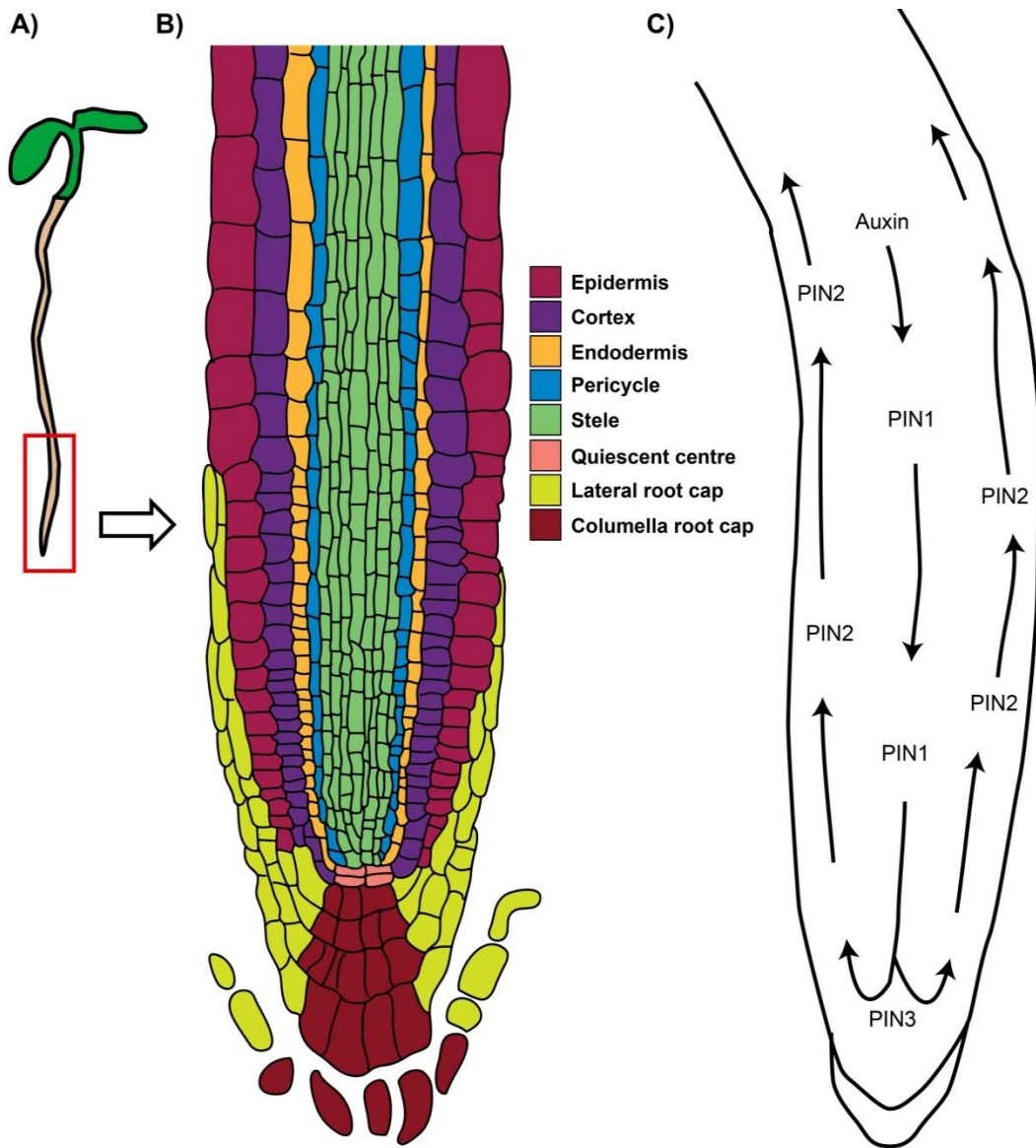
Figure 1.6. Auxin transport in *Arabidopsis thaliana* root.

Cartoon of an *Arabidopsis thaliana* seedling is shown (A), and magnified diagram of the root tip is also displayed (B) that allows visualisation of different cell layers. Auxin transport model and the directional auxin efflux of PIN1, PIN2 and PIN3 is also shown (C).

1.2.4 Maintaining polarity of PINs

As discussed above, plants need auxin gradients that are required for proper growth and orientation, maintained by polarised PIN proteins at the PM. The polarised distribution of PIN proteins arises by continuous endocytic recycling between the PM and the endomembrane derived vesicles often referred as endosomes (Geldner et al., 2001). The polarity of the PM proteins may be switched if required in response to external cues and according to the developmental stage of plants growth. As discussed above, the polarity of PIN localisation drives auxin transport and disruption to the PIN polarisation disrupts auxin gradients and which in turn causes a range of auxin defective/insensitive like phenotypes in plants (Krecek et al., 2009).

Impairment in clathrin function and inhibitor studies have been used to show that PINs undergo clathrin mediated endocytosis (CME) from the PM (Dhonukshe et al., 2007). Moreover, the ARF-GEF GNOM was shown to be required for PIN1 recycling back to the PM and other ARF-GEFs have been predicted to be required for trafficking and recycling of other PINs to the PM (Steinmann et al., 1999; Geldner et al., 2001). Therefore, constitutive endocytic recycling of PIN proteins is mediated by clathrin-mediated endocytosis from the PM and an ARF-GEF dependent recycling back to the PM (Geldner et al., 2001; Dhonukshe et al., 2007).

After synthesis, PIN proteins are initially taken to the PM in a non-polarised manner. It is from the PM they are internalised into endosomes and they are then targeted to the designated side of the membrane to create polarity (Figure 1.7). This was shown by the use of real time live cell imaging after photo bleaching the existing PIN markers (Dhonukshe et al., 2008a). Therefore, a two-step model of PIN polarity establishment was proposed based on this finding that implies an essential role played by clathrin mediated endocytosis and ARF-GEF dependent recycling to establish PIN polarity in the membrane.

Recent advances in PIN polarity have led to the identification of protein kinase AGC-3 family members, PINOID (PID), WAG1 and WAG2 which display the ability to phosphorylate auxin transporters which causes PINs to be localised to the apical side of the PM (Kleine-Vehn et al., 2009; Dhonukshe et al., 2010). PID, WAG1 and WAG2 were specifically observed to be expressed in the root epidermis and lateral root caps, where PIN2 is polarised apically (Dhonukshe et al., 2010).

Overexpression of PID causes basal to apical switch of PIN proteins including PIN1, which in turn results in loss of the auxin gradient at the primary root meristem, and other auxin defective phenotypes such as defective embryo formation are also observed (Friml et al., 2004). Similarly, loss of function of protein phosphatase 2A (PP2A), that acts antagonistically to PID and de-phosphorylates PINs, causes PINs to be polarised apically in the PM (Michniewicz et al., 2007). One of the side effects of the loss of PIN polarisation due to change in the PIN phosphorylation state is the loss of gravitropic response in plants (Michniewicz et al., 2007; Dhonukshe et al., 2010).
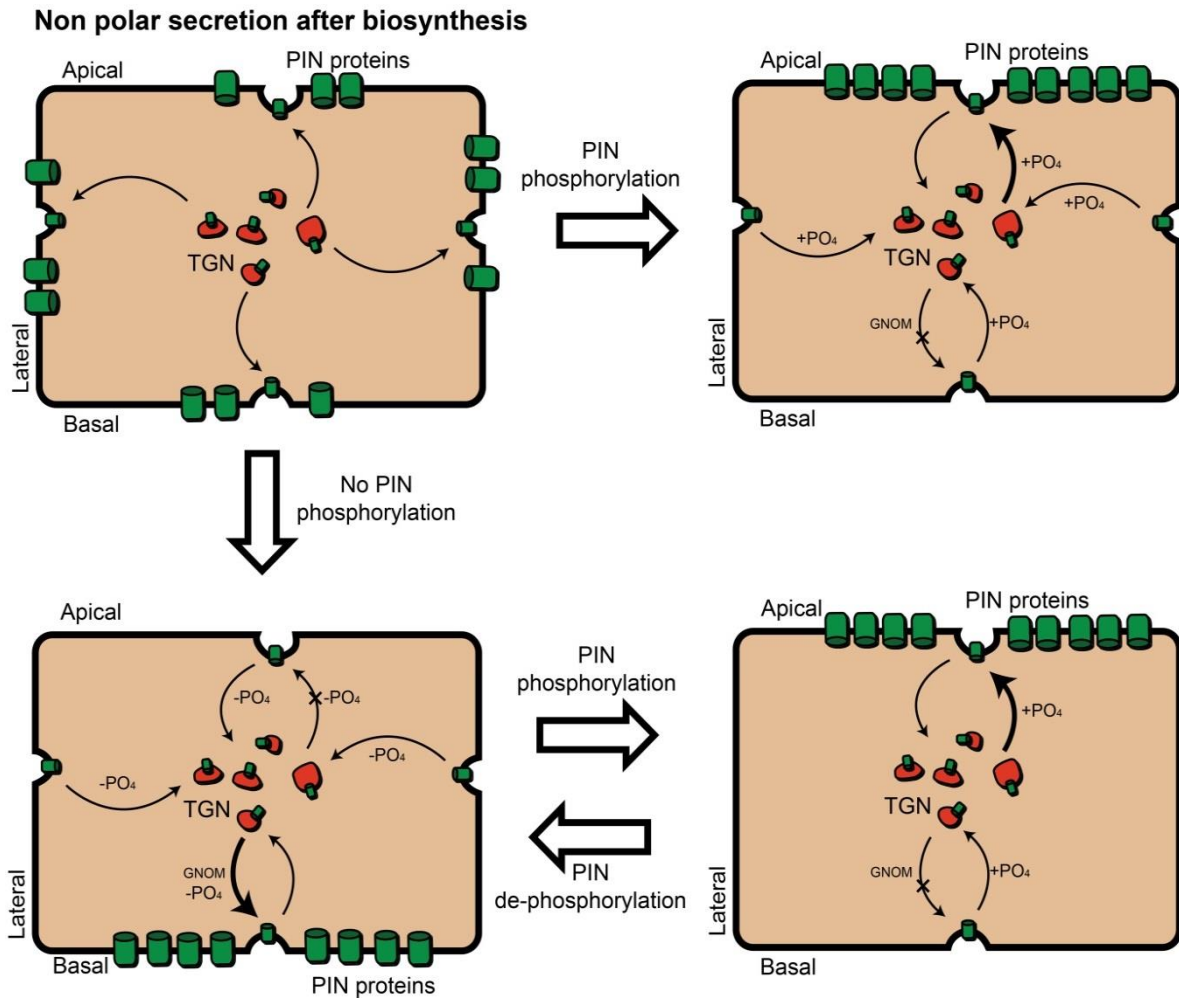
Figure 1.7. Determination of PIN polarity.

PIN proteins are initially trafficked to the membrane in a non-polar manner, where they are phosphorylated by the family of AGC-3 kinases, if a PIN protein is phosphorylated then it competes with GNOM dependent basal targeting therefore PIN proteins are recycled to apical plasma membrane. If phosphorylation activity is low, then PINs undergo GNOM mediated recycling to the basal membrane. Basally polarised PINs may be phosphorylated which would cause apical transcytosis. Alternatively, phosphorylated PINs may be de-phosphorylated by the action of protein phosphatases which antagonises the action of AGC-3 kinases to cause transcytosis of PINs to basal localisation.

1.2.5 Gravitropism

Gravity induced reorientation of plant growth (gravitropism) is important to maintain plant posture and access to nutrients. In *Arabidopsis thaliana*; roots, hypocotyls and inflorescence stems exhibit a gravitropic response. Genetic studies have been used to show that there are genes with overlapping function in control of gravitropism in these organs but there are also genes that function specifically in gravitropic response of a particular organ (Tasaka et al., 1999). For example, shoot gravitropism (*SGR*) genes were identified by characterising mutants that displayed abnormal shoot gravitropism in *Arabidopsis thaliana* (Fukaki et al., 1996; Yamauchi et al., 1997). Further investigation into the *SGR* identified them as elements required for endomembrane protein trafficking (Kato et al., 2002; Yano et al., 2003). For example, *Arabidopsis thaliana SGR3* was shown to encode syntaxin vacuolar morphology 3 (VAM3), which localises to the PVC. The same paper also showed interaction of VAM3 with VTI11, and implicated SNARE complex containing VAM3 and VTI11 is required for vacuolar trafficking and shoot gravitropic response (Yano et al., 2003). Indeed, *VTI11* was shown to be encoded by *SGR4*, required for vacuolar trafficking (Kato et al., 2002).

Gravity sensing in shoot and root takes place in the endodermis and root columella cells, respectively. Even though the gravity sensing cell types are different for root and shoot, they share a common mechanism to sense gravity. These cells are often referred as statocytes because they contain sedimentable amyloplasts, statoliths, capable of gravity recognition. In *Arabidopsis thaliana*, the amyloplasts in the statocytes contain high quantities of starch and sedimentation of starch grains in response to gravity has been noted (Morita, 2010). However, shoot and root of *Arabidopsis thaliana* starch deficient mutant were still able to exhibit gravitropic response albeit the effect was reduced (Kiss et al., 1989; Kiss et al., 1997). Therefore, although starch granules contribute to the initial gravity perception they are not essential for the gravitropic response.

Vertically orientated *Arabidopsis thaliana* roots show polarised auxin distribution that is mainly maintained by PIN1, PIN2 and PIN3 proteins. PIN3 proteins, distributed in a non-polar manner in the gravity sensing columella cells, are especially important in re-distribution of auxin laterally from the root tip towards epidermis to be taken up the

root (Figure 1.8A). As shown in Figure 1.8A PIN3, like other PIN proteins, is undergoing constitutive endocytic recycling through to the TGN back to the PM. When a seedling encounters a gravity stimulation, i.e. horizontally orientated seedling, the statoliths in the statocytes detect gravity and sediment to the new bottom of the gravity vector. Therefore, non-polar PIN3 proteins in the root columella region start targeting to the new base and are polarised basally (Friml et al., 2002). This shifts the auxin gradient to the basal side of the root (Figure 1.8B) which inhibits cell elongation at the bottom side of the root causing root bending towards the vertical gravity vector (Figure 1.8C). Although the underlying mechanisms have been described, details of how the gravity sensing and signalling process that dictate conditional polar endocytic recycling of PIN3 are still unresolved.
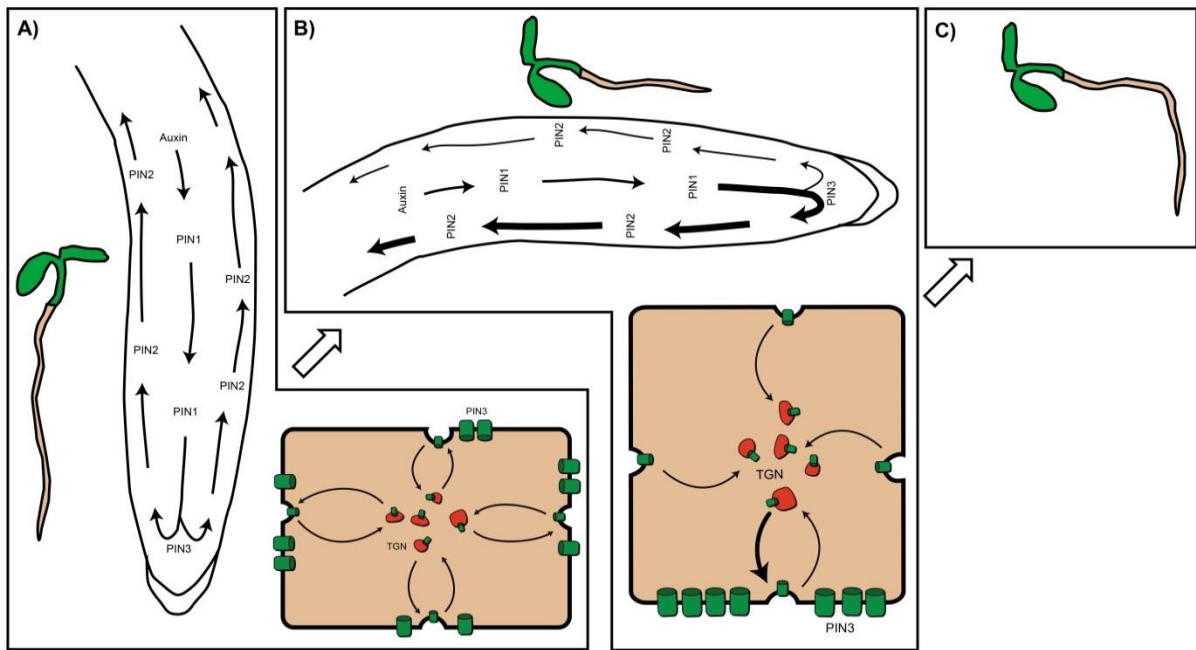
Figure 1.8. Root gravitropic response and auxin gradient manipulation by endocytic recycling.

Arabidopsis thaliana seedling in vertical orientation (A) displays uniform auxin distribution predominantly manipulated by PIN1, PIN2 and PIN3 proteins that undergo constitutive endocytic recycling. When the seedling encounters a gravity stimulation and is lying in horizontal orientation (B) the endosomes containing PIN3 at the root columella recycle to the new gravity base and are polarised basally, which shifts auxin concentration towards the bottom of the root. This in turn inhibits cell elongation at the bottom side therefore causing root bending towards the gravity vector (C).

1.2.6 Actin cytoskeleton

Dynamics of plant organelles is dependent on the integrity of actin filaments. Depolymerisation of the actin cytoskeleton inhibits the movement of all organelles including Golgi, the ER, peroxisomes, and mitochondria (Shimmen and Yokota, 2004). However, there seems to be a little effect on organelle dynamics if microtubules are depolymerised. The actin cytoskeleton has also been reported to be required for trafficking of secretory and endocytic vesicles (Ovecka et al., 2005). Various studies have used the actin depolymerising compound latrunculin B (LatB) to show it causes internalisation of PIN proteins (Geldner et al., 2001; Kleine-Vehn et al., 2009). However, depolymerising the microtubules did not affect the localisation or the internalisation of PIN proteins suggesting that PIN trafficking is dependent on actin rather than microtubules (Geldner et al., 2001).

Auxin transport and actin dynamics share a close relationship. In fact the chemicals that were initially identified as inhibitors of auxin transport such as 2,3,5-triiodobenzoic acid and 2-(1-pyrenoyl) benzoic acid were shown to inhibit vesicle trafficking by stabilising actin filaments (Dhonukshe et al., 2008b). Therefore, actin stabilisation leads to inhibition of PIN dynamics at the plasma membrane, even though PIN localisation is unaffected, which has an inhibitory effect in auxin efflux activity. The actin cytoskeleton is not only required for early endocytic events, it is also thought to be involved in PIN trafficking to the vacuole (Kleine-Vehn et al., 2008). This also correlates well with the gravitropic response, as stabilising the actin filaments decreased root gravitropism (Mancuso et al., 2006) and enhanced gravitropic response is observed in roots treated with LatB (Hou et al., 2003; Hou et al., 2004). A small molecule that displayed selective inhibitory activity on PIN2, AUX1, BRI1 and AUX1 and caused protein accumulation at the TGN (Robert et al., 2008) was also later on shown to stabilise and then consequently reduce depolymerisation of the actin filaments (Toth et al., 2012).

Recently, genetic studies have been used to establish a link between the actin cytoskeleton and auxin signalling. Auxin-binding protein 1 (ABP1), contributes to the recruitment of clathrin to the PM for endocytosis. Addition of exogenous auxin has been proposed to bind to ABP1 and interfere with this function (Robert et al., 2010). This is initiated shortly after auxin binds to the ABP1 at the apoplast. ABP1 is thought to be anchored to the membrane by SKEWED5 (SKU5) or SKU5 SIMILAR6

(SKS6) (Shimomura, 2006). This then allows IAA to move into the PM and signal is relayed on to Rho of plants (ROP)-GEF SPIKE1 (SPK1), to activate GTP-ROP (Murphy and Peer, 2012). The role of ROP GTPases in downstream signalling of ABP1 binding of auxin was recently demonstrated (Chen et al., 2012; Lin et al., 2012; Nagawa et al., 2012). Loss of function of SPK1 increased internalisation of PIN2, which could not be inhibited by addition of auxin (Lin et al., 2012). Similarly, ROP6 and its downstream effector RIC1 has also been reported to be play a part in clathrin association in the PM for endocytosis (Chen et al., 2012). This is consistent with the findings that show GTPases and their effectors inhibit PIN endocytosis by stabilising the actin cytoskeleton, an effect that could be overturned by depolymerisation of the actin filaments (Lin et al., 2012).

In summary, a polarised auxin gradient is required to maintain proper orientation of plant growth and perception to gravity. This is predominantly maintained by polarised auxin efflux carriers that mainly function at the PM. These auxin transporters are taken to the PM through endomembrane trafficking. They are undergoing constitutive recycling at the PM by endocytic uptake into endomembrane compartments, which could also be destined to be degraded in the vacuole. The trafficking of the endomembrane compartments is dependent on the actin filaments and the cytoskeleton network.

1.3 Chemical genetics

As discussed above, there are many unanswered question in plant protein trafficking pathways and further research needs to be performed to achieve a better understanding of these processes. However, using genetically encoded fusion proteins, i.e. green fluorescent protein (GFP) and its spectral variants, allows the visualisation of cells, cellular compartments and its elements. This technology has proven to be an invaluable tool and revolutionised the field by enabling visualisation of real-time intracellular dynamics, and dissection the cellular processes (Tsien, 1998). There are large number of T-DNA insertion mutants or ethyl methane sulphonate induced point mutation stocks that are readily available from the Arabidopsis stock centre (http://Arabidopsis.info/) that can facilitate the genetic studies of many cellular and developmental processes including endomembrane trafficking. Studies of gravitropism and links to protein trafficking in combination with the genetic and biochemical approaches can be complemented by the use of small

molecule inhibitors that target specific pathways of endomembrane trafficking (Hicks and Raikhel, 2010).

Chemical genetics is a term used to define the study of endogenous effects displayed by a small molecule. One common way of identification of small molecule modulators of endogenous processes is by a large scale screen using extensive libraries of compounds looking for particular phenotype or binding to a desired protein that is known to cause the phenotype. Subsequently, identification of protein/gene function is enabled by the identification of the chemical modulator of the protein/gene. Such process is an extension of chemical genetics and maybe termed as chemical genomics. Like genetic studies, chemical genetics also usually involves a forward or reverse approach. Forward chemical genetics usually starts by screening library of small molecules to identify a desired phenotype and then subsequent identification of the target causing the phenotype. In contrast reverse chemical genetics starts with a target and searches for small molecules that bind and modulate function. Some advantages of using chemical genetics includes the possibility of direct manipulation of (families of) proteins in a controlled fashion with desired dose and treatment time, rather than indirect manipulation of proteins by gene mutation that is often irreversible. This type of study can also be used to bypass genetic redundancy and lethality that may be seen in genetic mutants (Hicks and Raikhel, 2009, 2012).

Use of small molecule modulators of endomembrane trafficking have aided our understanding of this system vastly. In particular, the fungal toxin, brefeldin A (BFA) have been used to dissect various pathways in endomembrane trafficking. As mentioned above, in *Arabidopsis thaliana*, BFA inhibits the action of GNOM ARF-GEF required for endocytic recycling back to the PM (Geldner et al., 2003). In tobacco, BFA also causes the fusion of the ER and Golgi apparatus (Jiang and Rogers, 1998). However, this effect is not observed in *Arabidopsis thaliana* as GNOM-like 1 (GNL1) is required for Golgi to ER COPI mediated retrograde trafficking (Richter et al., 2007). As BFA has been reported only to interfere with endocytic recycling and not the secretion of newly synthesised proteins (Teh and Moore, 2007), it may also be used to dissect the difference between these processes. High concentrations of BFA has also been reported to affect vacuolar

trafficking revealing the requirement of a partially BFA sensitive ARF-GEF to mediate this process (Tse et al., 2006; Kleine-Vehn et al., 2008).

In addition, another fungal metabolite wortmannin is also widely used to dissect components of vacuolar trafficking pathway. Wortmannin inhibits PI3K activity (Jung et al., 2002) which is required for VSR recycling from the PVC (daSilva et al., 2005). This causes a backlog of VSRs in the PVC therefore proteins cannot be taken forward towards the vacuole. Tyrphostin A23 (A23), a structural analogue of tyrosine (Tyr, Y), is also widely used in dissect endocytic processes. A cytosolic motif in trans-membrane proteins containing crucial Tyr residue, with sequence YXXΦ (where Φ is a bulky hydrophobic residue) is capable of interacting with the AP-2 complex and acts as internalisation motif. A23 can compete with Tyr due to its structural similarity for AP-2 binding therefore inhibiting clathrin mediated endocytosis (Banbury et al., 2003). Therefore, A23 can be used to dissect clathrin mediated and clathrin independent endocytic events. Concanamycin A inhibits vacuolar H$^+$-ATPase activity (Huss et al., 2002) and eventually alters Golgi and TGN morphology therefore interferes with the trafficking to the vacuole (Dettmer et al., 2006). Endosidin1 causes intracellular accumulation of apically polarised proteins such as PIN2 and AUX1, and non-polarised brassinosteroid receptor BRI1, however it did not affect the localisation of PIN1, PIN7 or PIP2a (Robert et al., 2008). This also helped establish the possibility of multiple endocytic recycling pathways taken by membrane proteins. Other small molecules that have also been used to dissect the endomembrane trafficking pathway in plants are listed in Table 1-2.
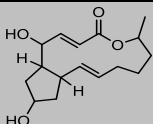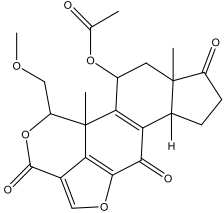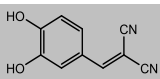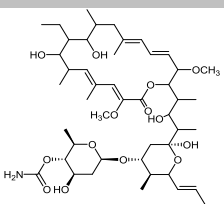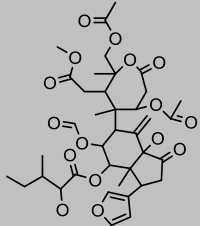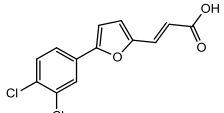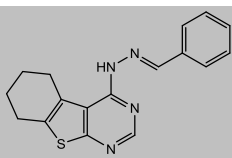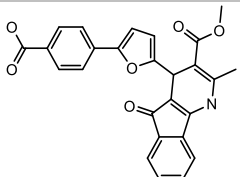
Compound	Structure	Effect; Target	Reference
Brefeldin A		Blocks exocytosis; inhibits the action of ARF-GEF GNOM	(Steinmann et al., 1999; Geldner et al., 2001)
Wortmannin		Blocks vacuolar trafficking by obstructing VSR recycling; inhibits PI3K	(daSilva et al., 2005)
Tyrphostin A23		Blocks CME; inhibits cargo recognition of AP2 complex	(Banbury et al., 2003)
Concanamycin A		Blocks vacuolar trafficking at the TGN; inhibits vacuolar H$^+$-ATPases	(Huss et al., 2002)
Endosidin1		Selective inhibition of endosomal recycling at the TGN	(Robert et al., 2008)
Gravacin		Blocks auxin transport and vacuolar trafficking by inhibiting ABCB19	(Surpin et al., 2005; Rojas-Pierce et al., 2007)
LG8		Changes morphology of the ER and Golgi	(Sorieul et al., 2011)
Sortin1		Changes vacuolar morphology and biogenesis	(Zouhar et al., 2004)

Table 1-2. Brief list of inhibitors of plant endomembrane trafficking.

1.4 Project aims

The aim of this project was to characterise and identify the subcellular pathway affected by a small molecule inhibitor of plant gravitropic response. This chemical was initially identified in a chemical genomics screen using library of 10,000 small molecules to identify compounds that alter hypocotyl gravitropism (Surpin et al., 2005). This same paper also reported that chemical, 6067962 (ChemBridge ID), renamed TENin1 (TE1) in this thesis, is an inhibitor of hypocotyl gravitropism in *Arabidopsis thaliana* seedlings. Therefore the aims of this thesis were:

➢ Characterisation of the long term chronic effects of TE1 at cellular and whole plant level.

➢ Characterisation of the short term effects of TE1 on endomembrane trafficking and auxin gradient to establish how it effects gravitropic response.

➢ Attempt to identify the molecular target of TE1 by using various genetic and biochemical strategies.

2 Chapter Two – Materials and Methods

2.1 Materials

2.1.1 Reagents

Analar grade reagents used for experiments were obtained from Sigma-Aldrich, Duchefa Biochemie B.V. and Fisher scientific unless otherwise specified.

2.1.1.1 Water

Water was purified to purity over 1MΩ.cm by Purite Purewater 300 that uses reverse osmosis and ion-exchange deionisation technology. Water was sterilised by autoclaving at 121°C, 15 p.s.i. for 20 min.

2.1.2 Buffers and solutions

2.1.2.1 ½ MS medium

Murashige and Skoog (MS) (Duchefa Biochemie B.V.) mineral salts (2.36 g/l) in water, pH adjusted to 5.7 with 500 mM KOH. For growth in 24-well microplates, 0.3% (w/v), or for vertical plant growth on petri dishes or 6-well plates, 0.8% (w/v) Phyto agar (Duchefa Biochemie B.V.) was added.

2.1.2.2 10X PBS (Phosphate buffered saline)

NaCl (80 g/l), KCl (2 g/l), Na_2HPO_4 (11.5 g/l), KH_2PO_4 (2 g/l); pH to 7.4 with KOH and used at a final concentration of 1×.

2.1.3 Chemicals

For all the chemicals stocks were made using DMSO as described below and 12 µl working stocks were aliquoted in sterile eppendorf tubes and stored at -20°C. The working stocks were not re-used once thawed unless specified otherwise.

2.1.3.1 TE1, HLL6 and JW analogues of TE1

25 mM stock of compound TE1, JW analogues (synthesised by James Warren, M. Chem student, University of Leeds) and HLL6 (synthesised by Helen Lightfoot, M. Chem student, University of Leeds), were made using 100% DMSO. For experimentation, working stocks were further diluted 1:25 to make 1 mM working stock with sterile H_2O and used at 25 µM unless specified otherwise.

2.1.3.2 BFA

50 mM stock of brefeldin A was made using 100% DMSO. For experimentation, working stocks were diluted to 50 µM BFA in ½ MS medium.

2.1.3.3 CHX

25 mM stock of cycloheximide was made using 100% DMSO. For experimentation, working stocks were diluted to 50 µM CHX in ½ MS medium.

2.1.3.4 FM4-64

5 mM stock of FM4-64 was made using 100% DMSO. For experimentation, working stocks were diluted to 5 µM FM4-64 liquid ½ MS medium. Working stocks were re-used again.

2.1.3.5 LatB

1 mM stock of latrunculin B was made using 100% DMSO. For experimentation, working stocks were diluted to the 1000× required working concentration using H_2O and used at 1:1000 in ½ MS.

2.1.3.6 Auxin

For auxin treatment, 1 mg/ml 1-Naphthaleneacetic acid (NAA; Sigma Aldrich) stock, stored at 4°C, was diluted to 5 µM in ½ MS for experimentation.

2.1.4 Plants

2.1.4.1 Marker lines

List of *Arabidopsis thaliana* marker lines and references are listed below in Table 2-1. I thank Prof Natasha Raikhel and Dr. Glenn Hicks (University of California, Riverside, USA) for kind donation of the endomembrane marker lines, AUX1-YGP, BRI1-GFP, PIN7-GFP and PIP2a-GFP, Dr. Stephanie Robert (SLU, Umea, Sweden) for GFP-ARA7, SYP61-CFP, NAG-GFP and VHAa1-GFP, Dr. Lorenzo Frigerio (University of Warwick, UK) for donation of secGFP and Dr. Stefan Kepinski (University of Leeds, UK) for PIN2-GFP.

Table 2-1. List of markers lines

Marker	Localisation/representation	Reference
GFP-PTS1	Peroxisomes	(Cutler et al., 2000)
RFP-PTS1	Peroxisomes	(Pracharoenwattana et al., 2005)
PTS2-GFP	Peroxisomes	(Pracharoenwattana et al., 2005)
ST-GFP	Golgi, trans cisternae	(Saint-Jore et al., 2002)
GFP-HDEL	Endoplasmic reticulum	(Batoko et al., 2000)
DR5-GFP	Auxin responsive expression	(Friml et al., 2003)
PIN2-GFP	PM, PIN2 proteins	(Abas et al., 2006)
AUX1-GFP	PM, AUX1 proteins	(Swarup et al., 2004)
BRI1-GFP	PM/endosomes, brassinosteroid receptor	(Geldner et al., 2007)
PIN7-GFP	PM, PIN7 proteins	(Blakeslee et al., 2007)
PIP2a-GFP	PM, PIP2a proteins	(Cutler et al., 2000)
secGFP	Apoplast, secreted GFP	(Zheng et al., 2004)
NAG-GFP	Golgi, cis cisternae	(Grebe et al., 2003)
SYP61-CFP	TGN	(Robert et al., 2008)
VHAa1-GFP	TGN	(Dettmer et al., 2006)
GFP-ARA7	PVC	(Jaillais et al., 2006)
GFP-ABD2	Actin	(Sheahan et al., 2004)

2.1.4.2 Generated double marker lines

Double marker lines were generated by crossing RFP-PTS1 × PTS2-GFP, RFP-PTS1 × GFP-HDEL, RFP-PTS1 × GFP-ABD2, RFP-PTS1 × ST-GFP and RFP-PTS1 × PIN2-GFP. RFP-PTS1 was used as both male and female parent.

2.1.4.3 Natural accessions

For the natural accession screen, 80 *Arabidopsis thaliana* accessions from the 1001 genomes project (N76427), whose genome sequence is available, were purchased from Nottingham Arabidopsis Stock Centre (NASC). Three more accessions Columbia (Col-0), Landsberg erecta (Ler) and Wassilewskija (Ws2) were also screened. The list of *Arabidopsis thaliana* accessions screened against TE1 with the individual NASC code is listed below in Table 2-2. The screen was performed by Adam Jamaluddin MSc student and the results for Sha and HKT2-4 independently confirmed by me.

Table 2-2. List of *Arabidopsis thaliana* ecotypes screened against TE1

NASC Code	Accession name	NASC Code	Accession name
N1092	Col-0	N76368	Apost-1
N1642	Ler	N76369	Dobra-1
N1601	Ws2	N76370	Petro-1
N76347	Aitba-2	N76371	Lecho-1
N76348	Toufl-1	N76372	Jablo-1
N76349	Vezzano-2	N76373	Bolin-1
N76350	Vezzano-2	N76374	Shigu-2
N76351	Rovero-1	N76375	Shigu-1
N76352	Voeran-1	N76376	Kidr-1
N76353	Altenb-2	N76377	Stepn-2
N76354	Mitterberg-1	N76378	Stepn-1
N76355	Castelfed-4	N76379	Sij1
N76356	Castelfed-4	N76380	Sij2
N76357	Bozen-1	N76381	Sij4
N76358	Bozen-1	N76382	Sha
N76359	Ciste-1	N76383	Koz2
N76360	Ciste-2	N76384	Kly4
N76361	Monte-1	N76385	Kly1
N76362	Angel-1	N76386	Dog-4
N76363	Moran-1	N76387	Xan-1
N76364	Mammo-2	N76388	Lerik1-3
N76365	Mammo-1	N76389	Istisu-1
N76366	Angit-1	N76390	Lag2-2
N76367	Lago-1	N76391	Vash-1
N76392	Bak-2	N76417	Qui-0
N76393	Bak-7	N76418	Vie-0
N76394	Yeg-1	N76419	Slavi-1
N76395	Kastel-1	N76420	Copac-1
N76396	Koch-1	N76421	Borsk-2
N76397	Del-10	N76422	Krazo-2
N76398	Nemrut-1	N76423	Galdo-1
N76399	Ey1.5-2	N76424	Timpo-1
N76400	Star-8	N76425	Valsi-1
N76401	Tu-Scha-9	N76426	Leb-3
N76402	Nie1-2	N76409	Agu-1
N76403	Tu-SB30-3	N76410	Cdm-0
N76404	HKT2-4	N76411	Don-0
N76405	Tu-Wa1-2	N76412	Fei-0
N76406	Ru3.1-31	N76413	Leo-1
N76407	Tu-V-13	N76414	Mer-6
N76408	Wal-HasB-4	N76415	Ped-0
N76416	Pra-6		

2.1.4.4 Sha × Col-0 RILs

A total of 174 recombinant inbred lines (RILs) generated by Simon et al., (2008) were screened in a natural accession screen against TE1. RILs generated by Simon et al., (2008), crossed Sha as the female parent to Col-0 as the male parent to generate F_1 plants that were allowed to self to obtain F_7 seeds and RILs are F_8 seeds ordered from INRA, Versailles, France.   Recombinations were roughly mapped in F_7 plants (Simon et al., 2008). List of RILs screened against TE1 is listed below in Table 2-3.

Table 2-3. List of the RILs screened against TE1

INRA code for the Sha × Col-0 RILs; http://dbsgap.versailles.inra.fr/vnat					
13RV1	13RV66	13RV140	13RV213	13RV286	13RV381
13RV2	13RV71	13RV141	13RV220	13RV301	13RV387
13RV3	13RV72	13RV144	13RV222	13RV302	13RV388
13RV5	13RV78	13RV146	13RV223	13RV303	13RV392
13RV7	13RV79	13RV150	13RV226	13RV306	13RV395
13RV11	13RV80	13RV151	13RV227	13RV307	13RV402
13RV13	13RV81	13RV152	13RV229	13RV313	13RV403
13RV15	13RV85	13RV156	13RV232	13RV317	13RV404
13RV19	13RV89	13RV164	13RV234	13RV318	13RV405
13RV22	13RV90	13RV166	13RV235	13RV320	13RV409
13RV23	13RV95	13RV172	13RV237	13RV321	13RV410
13RV28	13RV97	13RV174	13RV247	13RV325	13RV411
13RV29	13RV98	13RV175	13RV248	13RV327	13RV412
13RV30	13RV100	13RV176	13RV252	13RV331	13RV416
13RV31	13RV107	13RV181	13RV254	13RV332	13RV418
13RV34	13RV108	13RV183	13RV255	13RV336	13RV420
13RV38	13RV114	13RV185	13RV256	13RV337	13RV421
13RV39	13RV116	13RV192	13RV257	13RV345	13RV425
13RV41	13RV121	13RV198	13RV260	13RV351	13RV428
13RV48	13RV124	13RV199	13RV266	13RV356	13RV431
13RV51	13RV126	13RV202	13RV272	13RV363	13RV432
13RV56	13RV132	13RV205	13RV273	13RV366	13RV434
13RV58	13RV136	13RV206	13RV275	13RV375	13RV435
13RV59	13RV137	13RV210	13RV283	13RV376	13RV439
13RV64	13RV139	13RV212	13RV284	13RV377	13RV440
13RV442	13RV450	13RV472	13RV482	13RV488	13RV501
13RV445	13RV451	13RV474	13RV484	13RV490	13RV505
13RV446	13RV460	13RV478	13RV485	13RV493	13RV509
13RV449	13RV471	13RV479	13RV487	13RV500	13RV512

2.1.4.5 Generated F_2 natural accession crosses

F_1 crosses were generated for Col-0 × Sha (both male and female), Col-0 × HKT2-4 (both male and female), and for Sha × HKT2-4 (both male and female). The F_1 seeds were allowed to self to generate the F_2 seeds.

2.1.5 Imaging

2.1.5.1 Confocal microscopy

Zeiss META 510 and 710 laser-scanning inverted microscopes with a ×63 and ×40 oil immersion objectives were used to generate confocal images. GFP was excited with a 488-nm argon laser and emission detected by 488/541 dichoroic mirror and 505- to 530-nm band pass filter. FM4-64 and anti-Rabbit-CY3 were excited using 543-nm laser and a 585- to 615-nm filter was used to detect emission. CFP was excited with a 405-nm laser and emission detected with a 470- to 500-nm filter. YFP was excited with a 514 laser and emission a 530- to 600-nm filter was used to detect emission.

For movement analysis, peroxisomes (GFP-PTS1) and Golgi (ST-GFP) were monitored by fast scanning, 7.5 fs^{-1} and 7.1 fs^{-1} respectively, at a selected region of interest. Peroxisomes and Golgi stacks were tracked for 200 frames- over 26.4 sec and 100 frames-per movie over 14 sec, respectively.

2.1.5.2 Confocal movies analysis

Volocity 3.0 (Improvision, Coventry, UK) was used to analyse the movies and quantitative data was generated for each organelle track identified. To determine statistical significance in track velocity (V), displacement rate (D) and meandering index (MI) for different organelles at various tissues, cumulative distribution frequency (CDF) plots were generated with reference to Sparkes et al., (Sparkes et al., 2008), courtesy of Dr. Imogen Sparkes (University of Exeter, UK). The Kolomogorov-Smirnov (KS) test was performed to determine whether differences observed in V, D or MI distributions were statistically significant for different conditions i.e. DMSO and TE1.

2.2 Methods

2.2.1 Plants

2.2.1.1 Plant growth and seed collection

Arabidopsis thaliana seeds, imbibed for 48 h at 4°C in the dark, were sown on to the compost mix (3: 1, soil: vermiculite for plants) in small pots. Plants were grown at 23°C in 16 h light per day. After 6 weeks plants start flowering and they were bagged when the siliques start shedding for seed collection. The seeds were left to dry in the bag for at least two weeks once the bag was removed from the plant.

2.2.1.2 Seed sterilisation

Arabidopsis thaliana seeds were incubated in seed sterilisation solution (25% Milton sterilising solution (v/v), 0.1% Tween-20 (v/v) in sterile water) with agitation for 20 min at the room temperature. This was followed by four washes with sterile water. They were then imbibed at 4°C in the dark for 48 h.

2.2.1.3 Seedling growth

Sterilised and imbibed seeds were transferred to ½ MS media containing 0.8% (w/v) plant agar for vertical growth on Petri dishes. Seedlings were grown in a constant temperature room maintained at 22°C. Seedlings were normally grown in the presence of light for 16 h per day. Alternatively for seedlings grown in the dark, petri dishes were wrapped in tin foil. The plates were left vertically upright to allow growth for 7 days, ready for experimentation unless specified.

2.2.1.4 Crosses

Several *Arabidopsis thaliana* plants were grown in small pots until they start flowering and crossed to generate double marker lines, or two ecotypes were crossed. All anthers were removed in a young flower on the female parent, without allowing pollen to shed into the pistil. An open flower was removed from a suitable male parent and transferred pollen from male flower to female pistil by gently brushing surface of male anthers to female stigma. The female flower was bagged once the siliques started forming after 72 h in successful crosses. Seeds were collected after 14 days and F_1 seeds were plated out and grown on soil. F_2 seeds were collected and subsequently plated again with respective selections, for generation of double marker lines, see Table 2-4 below. Finally, the homozygote

plates displaying resistant to selection were tested on confocal microscope and seeds were collected from the F_3 progeny.

Table 2-4. List of lines used to generate double markers and their selection

Lines	Selection	Reference
RFP-PTS1	Kanamycin	(Pracharoenwattana et al., 2005)
PTS2-GFP	Hygromycin	(Pracharoenwattana et al., 2005)
ST-GFP	Kanamycin	(Saint-Jore et al., 2002)
GFP-HDEL	Hygromycin	(Batoko et al., 2000)
GFP-ABD2	BASTA	(Sheahan et al., 2004)
PIN2-GFP	Hygromycin	(Abas et al., 2006)

2.2.2 Gravitropic response assays

2.2.2.1 Root gravitropic response assay

Arabidopsis thaliana seedlings were grown on ½ MS media containing 0.8% plant agar in light for 6 days and transplanted to fresh media containing respective concentration of TE1 or 0.1% DMSO as control. Transplanted 6 day old seedlings were gravistimulated by rotating the plate by 90° and left vertically to grow for 48 h. Root measurement was taken straight after the transplant and after 48 h growth to calculate average root growth during this period. The plates were scanned straight after the seedling transplantation and 48 h after transplantation. The root lengths were measured using ImageJ 1.46 software and difference in growth was calculated. Root bending was also measured using ImageJ 1.46 software.

2.2.2.2 Hypocotyl gravitropic response assay

Hypocotyl gravitropic response assays were carried out as described (Surpin et al., 2005). *Arabidopsis thaliana* seedlings were grown on ½ MS media containing 0.8% plant agar, containing 0.2% DMSO as control and respective concentrations of TE1, in the darkness for 4 days and the plates were gravistimulated at 90° after 4 days for 48 h.

2.2.2.3 DR5-GFP

7 day old seedlings were gravistimulated for 180 min at 90° in DMSO or TE1, before pre-treatment in the respective condition (DMSO or TE1) for 30 min at vertical axis relative to the gravity vector.

2.2.3 Short term treatments

2.2.3.1 Chemical treatments

Short term chemical treatment was performed in 6 well petri dishes. Indicated final concentration of chemical from the working stock was mixed with ½ MS media containing 0.8% plant agar and incubated at room temperature at vertical axis relative to the gravity vector, unless specified otherwise, for the time mentioned.

2.2.3.2 Short term recovery experiments

Seedlings treated in the media containing chemicals were transplanted to ½ MS media containing 0.1% DMSO and 0.8% plant agar and incubated at room

temperature standing upright at vertical axis relative to the gravity vector for indicated amount of time.

2.2.3.3 FM4-64

To trace endocytosis, seedlings treated in 0.1% DMSO or 25 µM TE1 for 120 min in ½ MS media containing 0.8% plant agar were transferred to 5 µM FM4-64 mixed in 1 ml ice cold liquid ½ MS medium containing either 0.1% DMSO or 25 µM TE1 in 24 well plates. Seedlings were incubated in FM4-64 for 5 min and then washed two times in ice cold ½ MS medium containing 0.1% DMSO or 25 µM TE1. Following the washes, seedlings were transferred to the microscope slides, at which point the timer was started to trace endocytosis min by min, and images were generated every min starting at 4 min.

2.2.3.4 Tracing vacuolar trafficking

PIN2-GFP trafficking to the vacuole was traced by incubating seedlings at room temperature in ½ MS media containing 0.8% plant agar with 0.1% DMSO or 25 µM TE1. Seedlings were incubated in the darkness for 6 h.

2.2.4 Immuno-localisation

Immuno-localisation of PIN2 using anti-PIN2 antibodies (kindly gifted by Professor Christian Luschnig, BOKU, Austria) was performed as described (Sauer et al., 2006). Seedlings incubated in TE1 or DMSO for 120 min were fixed in PFA (4% [w/v] paraformaldehyde in 1× PBS dissolved at 70 °C, and 0.1% [v/v] Triton X-100) for 60 min in vacuum followed by 3× washes each with triton-PBS (0.1% [v/v] Triton X-100 in 1× PBS solution) and triton-H_2O (0.1% [v/v] Triton X-100 in water) followed by 37°C in driselase (2% [w/v] driselase in PBS) for 30 min. The following process was performed with ProVSI Robot (Intavis). The samples then underwent series of washes; 3× in triton-PBS for 15 min each, 2× in igepal (300 µl Igepal to 1 ml 10% [v/v] DMSO in 8.7 ml PBS) for 30 min each, and 3× in triton-PBS 15 min each followed by incubation in blocking solution (3% BSA [w/v] in 1× PBS) for 60 min. Samples were then incubated in anti-PIN2 (1:1000) (Abas et al., 2006) raised in rabbit (gifted by Professor Christian Luschnig) at 37°C for 4 h and washed 5× in triton-PBS for 15 min each at room temperature. This followed 4 h incubation in secondary antibody (1:250), anti-Rabbit-CY3 raised in goat (Stratech), at 37°C, and 3× washes with triton-PBS 15 min each, and finally 3× washes with H_2O for 15 min

each. The samples were then mounted on to the microscope slides, ready to be visualised under confocal microscope.

2.2.5 QTL mapping

The markers and the genetic map are described (Simon et al., 2008) and the material is available for download (http://publiclines.versailles.inra.fr/page/13). QTL analysis was performed using Windows QTL Cartographer Version 2.5_009 (Silva Lda et al., 2012). The raw data generated, average root length and percentage survival for each RIL were formatted into WordPad to generate .txt file (a value in each line represented the trait value gained), and if the RIL was not screened then the trait value was replaced with a full stop. This raw data in .txt file was inputted into QTL cartographer for QTL analysis. Interval mapping was initially used to generate rough map of QTLs and composite interval mapping (CIM) was used afterwards using the same dataset to get more accurate prediction of putative QTLs. The parameters used were as suggested (El-Lithy et al., 2004; Loudet et al., 2005) were used for CIM. The number of cofactor was three and the window size was used at 3 cM. The walking speed chosen to analyse QTL was 0.5 cM. 1,000 permutations of the data generated by quantifying traits were analysed for each trait. The logarithm of odds (LOD) significance threshold was used at standard value of 2.5 LOD ensuing in overall confidence level of 95%. The multiple-trait mapping feature was used to map multiple QTLs followed by CIM selection, using same parameters as CIM analysis.

2.2.6 SNPs identification

The thirty nine natural accessions taken forward to the secondary screen to identify accessions that display resistance to the agravitropic growth caused by TE1 were used to identify SNPs. This was performed using POLYMORPH software (http://polymorph.weigelworld.org/cgi-bin/webapp.cgi), which is a tool available from the 1001 genomes project website (http://www.1001genomes.org/).

3 Chapter Three – Characterising long term effects of TENin1

3.1 Introduction

A chemical genomics screen, from the laboratory of Natasha Raikhel, using 10,000 different chemicals identified four small molecules that established a link between endomembrane trafficking and altered hypocotyl gravitropism in *Arabidopsis thaliana* seedlings (Surpin et al., 2005). The rest of the small molecules, 69 compounds that passed primary screen, for altered hypocotyl gravitropic response were not further characterised. Thus these small molecules, whose biological activity was already confirmed, were re-screened to identify compounds that altered peroxisome morphology (Brown et al., 2011). One of the identified compounds, TE1 (Figure 3.1), was initially identified as an inhibitor of hypocotyl gravitropism (Surpin et al., 2005) in seedlings grown in the darkness and also identified in another independent chemical genomic screen as an enhancer of hypocotyl elongation (Savaldi-Goldstein et al., 2008) in seedlings grown in the light. However, these studies did not further investigate this compound.

Previous observations in the laboratory showed that long term chronic exposure to TE1 altered peroxisome distribution in the epidermal layer of all tissue, including cotyledons, hypocotyls and primary roots, where peroxisomes were clustered in groups near the cell periphery. An example of peroxisome clustering observed in 6 day old root epidermis grown on 25 µM TE1 can be seen in Figure 3.2.

The aim of the experiments presented in this chapter was to characterise the effects of TE1 in 7 day old *Arabidopsis thaliana*, Col-0 accession seedlings. Effects of various concentrations of TE1 were monitored for alterations in primary root length, hypocotyl elongation, root hairs, gravitropic response, survival rates and germination. Long term effect of TE1 on different organelles, such as the ER, peroxisomes and Golgi, was also monitored by analysing their morphology and dynamics.
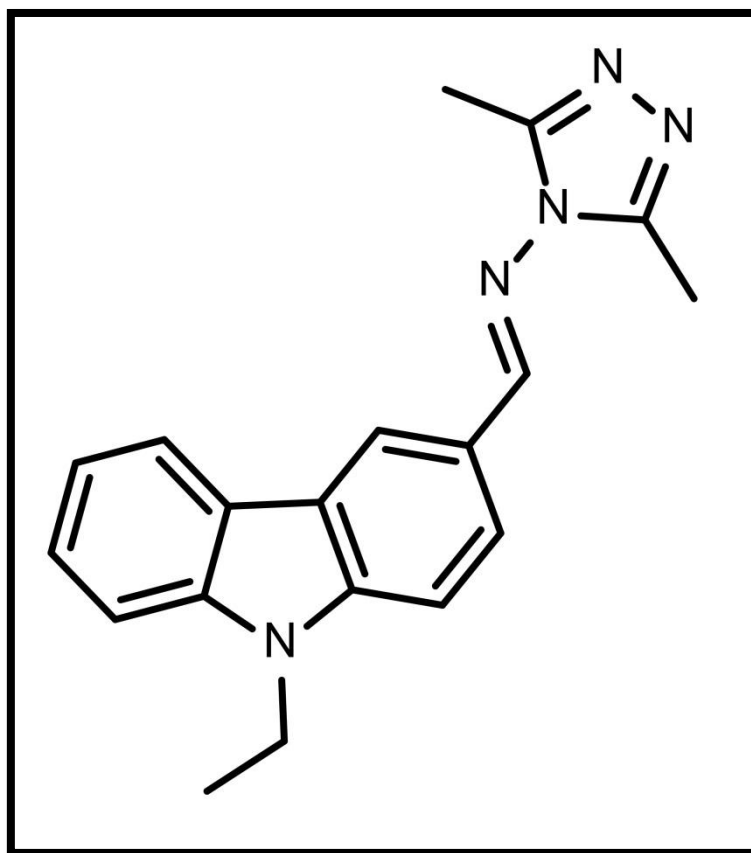
Figure 3.1. Chemical structure of TENin1 (TE1).

Full chemical name: N-[(9-ethyl-9H-carbazol-3-yl) methylene]-3,5-dimethyl-, [N(E)]-4H-1,2,4-Triazol-4-amine.
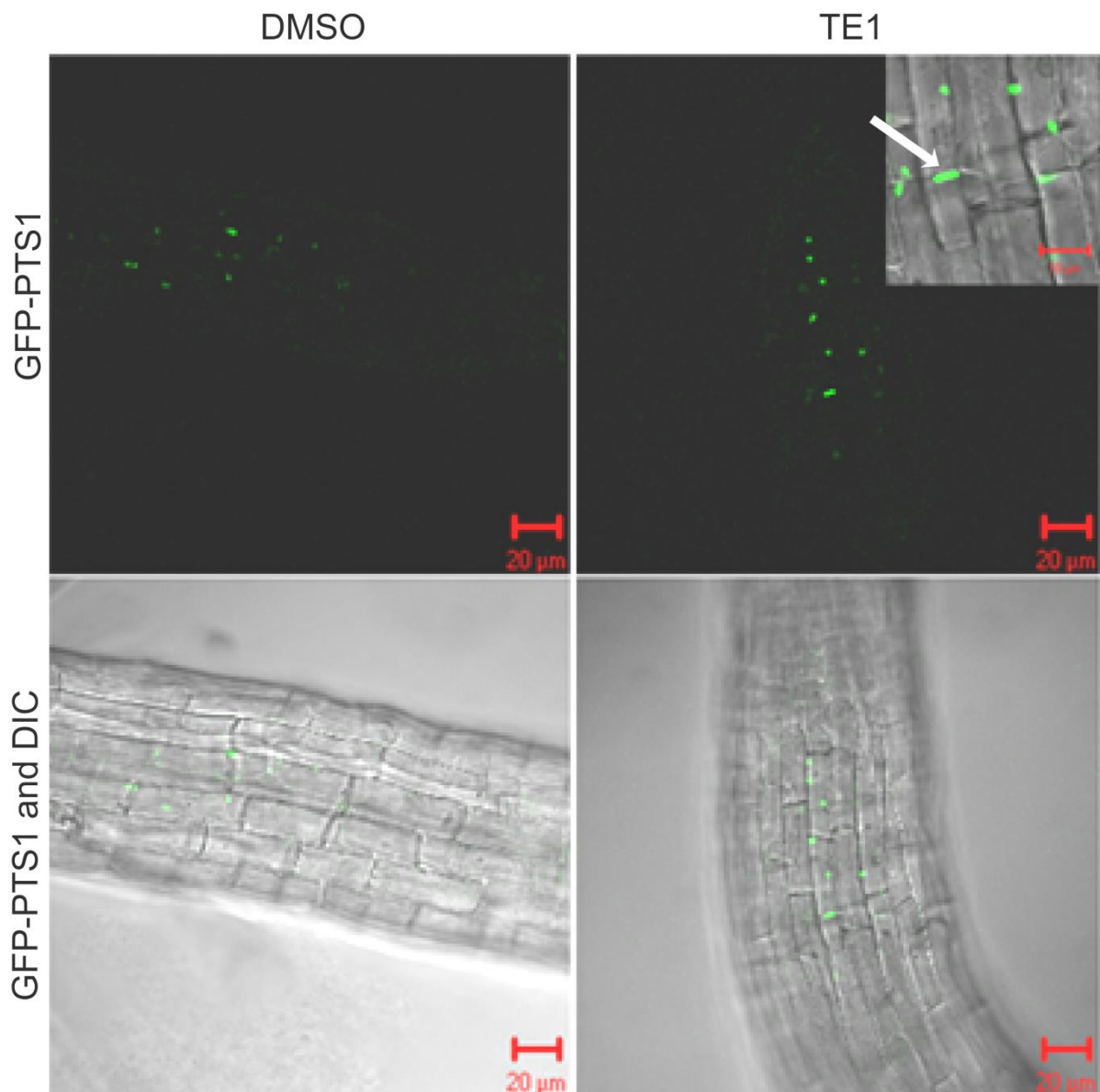
Figure 3.2. Groups of peroxisomes were observed in seedlings grown on TE1.

Peroxisomes (GFP-PTS1) in the root epidermis were visualised as bright green punctate structures, which were highly mobile in DMSO control. However, initial trial showed plants grown in the presence of 25 μM TE1 caused peroxisomes to cluster around cell periphery (see arrow). GFP-PTS1 and GFP-PTS1 with the digital interference contrast (DIC) is shown for both DMSO and 25 μM TE1. Scale bars, 20 μm and magnified scale bar, 5 μm. Image courtesy of Laura-Anne Brown and Alison Baker (University of Leeds, UK).

3.2 Characterisation of whole plant phenotype in seedlings grown on TE1

3.2.1 TE1 inhibits primary root growth

Treatment of plants with small molecule inhibitors of membrane trafficking such as BFA (Geldner et al., 2001) and wortmannin (Jaillais et al., 2006) are known to result in inhibition of root and hypocotyl elongation as well as disturbance of gravitropic responses. TE1 was also isolated as an inhibitor of gravitropic response in a chemical genomics screen (Surpin et al., 2005). To monitor the effect of TE1 on root development, primary root growth was monitored in 7 day old seedlings grown in 16 h light per day. Seedlings were grown on ½ MS media containing 0.2% DMSO (n=143), 1 µM TE1 (n=60), 5 µM TE1 (n=66), 10 µM TE1 (n=70), 15 µM TE1 (n=89), 20 µM TE1 (n=90), 25 µM TE1 (n=78), and 50 µM TE1 (n=80), respectively. Data collected from three comparable and independent repetitions, performed under strictly controlled conditions, were pooled together. Average length of the roots were measured after 7 days of growth in the specified concentration of TE1 and expressed as the percentage (%) average root length normalised against DMSO control (Figure 3.3).

As the concentration of TE1 increased, the average root length decreased. However, root growth appeared to be enhanced at 1 µM TE1, with average growth recorded at 111 ± 10% relative to DMSO control, however, the probability value (p) gained from statistical T-Test revealed this is not significant. Average root growth for 5 µM, 10 µM, 15 µM, 20 µM, 25 µM and 50 µM TE1, relative to DMSO control was recorded at 74 ± 9%, 45 ± 6%, 40 ± 5%, 36 ± 4%, 31 ± 3% and 26 ± 3%, respectively (Figure 3.3). T-test revealed p value ≤ 0.01, for all the concentrations from 5 µM to 50 µM TE1, suggesting the decrease in root length in presence of higher concentration of TE1 is statistically significant. Taken together data shows that TE1 inhibits the growth of primary root. Roots are sensitive to the effect of TE1 at 5 µM and higher.
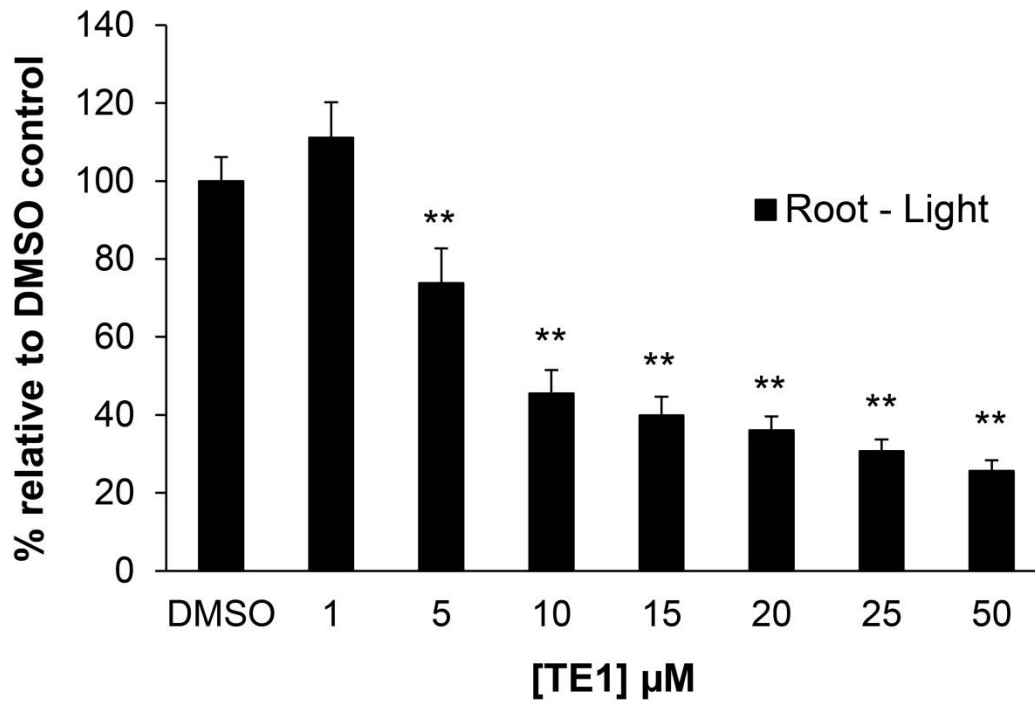
Figure 3.3. TE1 causes inhibition of primary root growth.

Root length of 7 day old seedlings grown in 16 h light in varying concentration of TE1 is shown. Root growth of plants grown on TE1 were standardised against DMSO control. Data merged from three repetitions, total 60-143 seedlings per condition were measured. Error bars represent SE, ** $p \leq 0.01$.

3.2.2 Effect of TE1 on whole plant

When grown on compound free media, 7 day old *Arabidopsis thaliana* seedlings displayed long primary roots, green cotyledons and the emergence of lateral roots was visible (Figure 3.4). At the same developmental stage, inhibition of primary root growth, decreased opening of cotyledons and impaired gravitropic growth was observed in seedlings grown on 10 µM TE1. Similarly, seedlings grown on 25 µM TE1 displayed shorter primary roots, decreased opening of cotyledons and grew at different angles relative to the gravity vector. No emerging lateral roots were observed in seedlings grown on 10 µM or 25 µM TE1 (Figure 3.4).
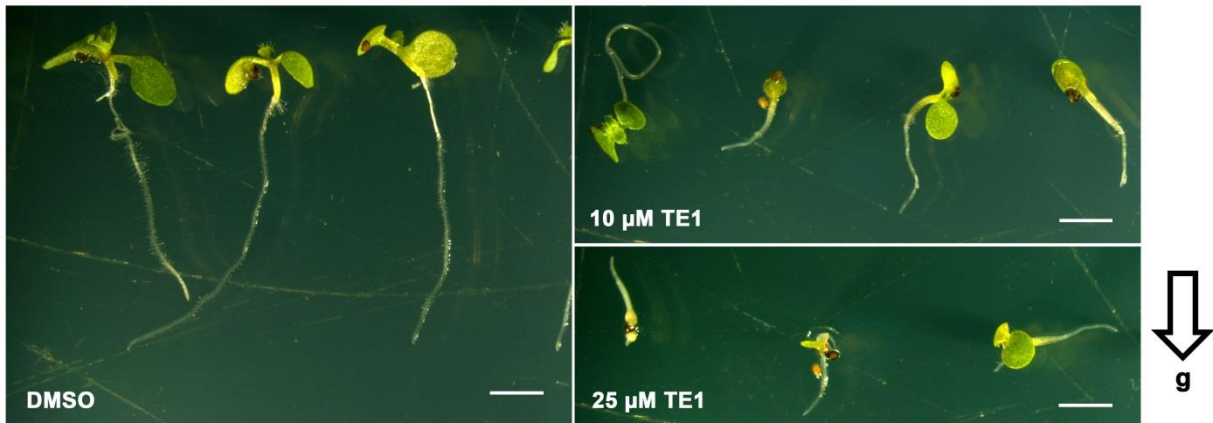
Figure 3.4. Effect of TE1 on whole plant.

7 day old seedlings grown on DMSO, 10 µM TE1 and 25 µM TE1 are shown. Arrow represents gravity (g) vector. Scale bars, 2 mm.

3.2.3 TE1 inhibits hypocotyl elongation of seedlings grown in the darkness

TE1 was isolated in another separate chemical genomics screen as an enhancer of hypocotyl elongation in seedlings grown in light (Savaldi-Goldstein et al., 2008). The effect of a range of TE1 concentrations on hypocotyl elongation was monitored in 7 day old seedlings grown in the darkness (Figure 3.5). Seedlings were grown on ½ MS media containing 0.02% DMSO (n=194), 1 µM TE1 (n=93), 5 µM TE1 (n=92), 10 µM TE1 (n=88), 15 µM TE1 (n= 112), 20 µM TE1 (n=105), 25 µM TE1 (n=85) and 50 µM TE1 (n=77). Data was merged from three independent experiments performed under strictly controlled conditions that produced comparable results. The average hypocotyl elongation of seedlings in the presence of TE1 was expressed as a percentage (%) average hypocotyl elongation standardised against the DMSO control.

Unlike primary root growth, hypocotyl elongation was inhibited at 1 µM TE1 displaying 69 ± 4% growth relative to the DMSO control. Average hypocotyl elongation for 5 µM, 10 µM, 15 µM, 20 µM, 25 µM and 50 µM TE1, relative to DMSO control was recorded at 52 ± 3%, 45 ± 3%, 42 ± 2%, 40 ± 2%, 41 ± 3% and 37 ± 4%, respectively (Figure 3.5). Inhibition of hypocotyl elongation caused by all TE1 concentrations was statistically significant, as p values were ≤ 0.01. This data shows that TE1 inhibits hypocotyl elongation in the dark at lower concentrations than required to affect the primary root growth.
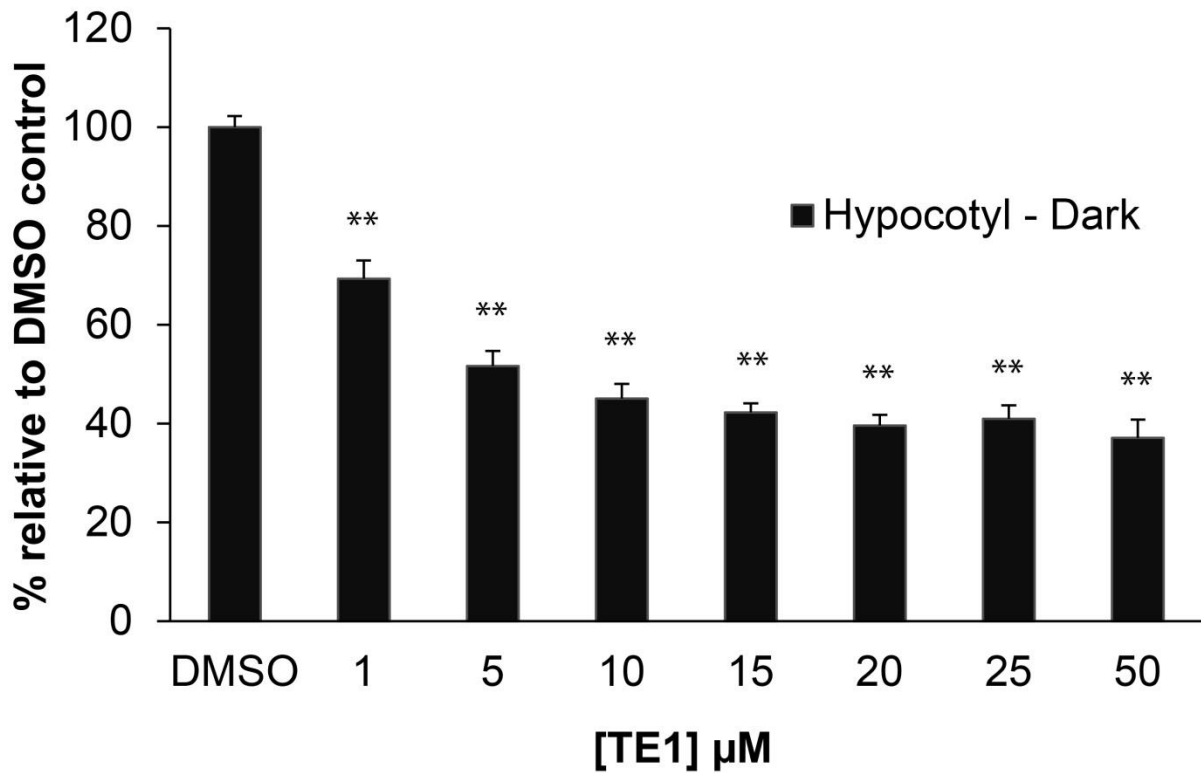
Figure 3.5. TE1 inhibits elongation of hypocotyl in the dark.

Effect of TE1 on hypocotyl lengths of 7 day old *Arabidopsis thaliana* seedlings grown in the darkness are shown. Plants grown on TE1 were standardised against DMSO control. Data merged from three repetitions and total 80-194 seedlings per condition were measured. Error bars represent SE, ** p ≤ 0.01.

3.2.4 Long term exposure to TE1 decreases survival of *Arabidopsis thaliana* seedlings

To determine if TE1 has toxic effects on plants, survival rates were monitored. 7 day old plants were grown on ½ MS media containing 0.02% DMSO (n=194), 1 µM TE1 (n=77), 5 µM TE1 (n=76), 10 µM TE1 (n=79), 15 µM TE1 (n=99), 20 µM TE1 (n=104), 25 µM TE1 (n=85) and 50 µM TE1 (n=92). Data was merged from three independent experiments performed under strictly controlled conditions that produced comparable results. Survival percentage was calculated by scoring the total number of seeds that germinated and taking the percentage of seeds that were still alive (Figure 3.6). This was determined by the amount of chlorophyll bleaching observed under a magnifying glass.

Seedlings grown on DMSO media showed 98 ± 0.2% survival. At 1 µM and 5 µM TE1 survival was recorded at 98 ± 0.3% and 95 ± 0.8%, respectively. T-Test revealed p values ≥ 0.25 for 1 µM and 5 µM TE1, suggesting that the decrease in survival percentage observed at 5 µM TE1 is not statistically significant. However percentage survival was recorded at 88 ± 0.6% for 10 µM TE1 with the p value of ≤ 0.05, revealing this slight decline in survival is statistically significant. Survival rates in the presence of 15 µM, 20 µM, 25 µM and 50 µM TE1 were recorded at 45 ± 0.6%, 21 ± 0.4%, 19 ± 1.1%, and 14 ± 0.4%, respectively. T-Test revealed the decline in survival rates at these concentrations is highly significant as revealed by p values ≤ 0.01 (Figure 3.6). These results demonstrate that *Arabidopsis thaliana* seedlings grown on media containing concentration higher than 10 µM TE1 are struggling for survival.
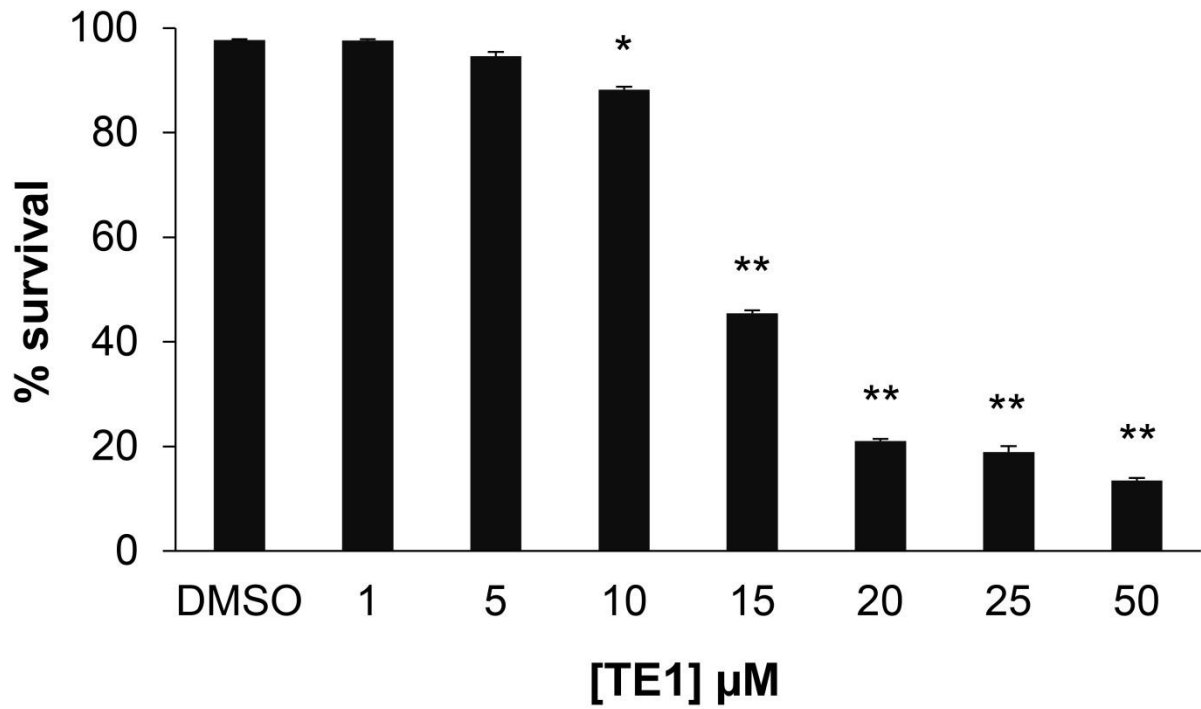
Figure 3.6. Long term exposure to TE1 decreases the survival of *Arabidopsis thaliana* seedlings.

Percentage survival of 7 day old seedlings grown in different concentration of TE1. Data merged from three repetitions, total of 76-194 seedlings were scored per condition. Error bars represent SE, * p ≤ 0.05, ** p ≤ 0.01.

3.2.5 TE1 does not affect germination

To determine whether TE1 affected germination, the percentage of seed germination was scored at different concentrations of TE1 (Figure 3.7). Sterilised seeds were imbibed for 48 h and plated on ½ MS media containing 0.02% DMSO (n=205), 1 µM TE1 (n=82), 5 µM TE1 (n=82), 10 µM TE1 (n=83), 15 µM TE1 (n=100), 20 µM TE1 (n=106), 25 µM TE1 (n=89), and 50 µM TE1 (n=97), respectively, and germination was monitored after 7 days. Data was merged from three independent replicates performed under strictly controlled conditions that produced similar results.

In the DMSO control, germination was scored at 94 ± 0.6%. Germinations rates for 1 µM, 5 µM, 10 µM, 15 µM, 20 µM, 25 µM and 50 µM TE1 were 94 ± 0.3%, 91 ± 1.5%, 95 ± 0.5%, 99 ± 0.2%, 98 ± 0.3%, 95 ± 0.3%, and 94 ± 0.5%, respectively. Changes observed in the germination percentage at different TE1 concentrations were not significant statically as the p values were ≥ 0.1 (Figure 3.7). These data show that germination is unaffected in the presence of TE1.
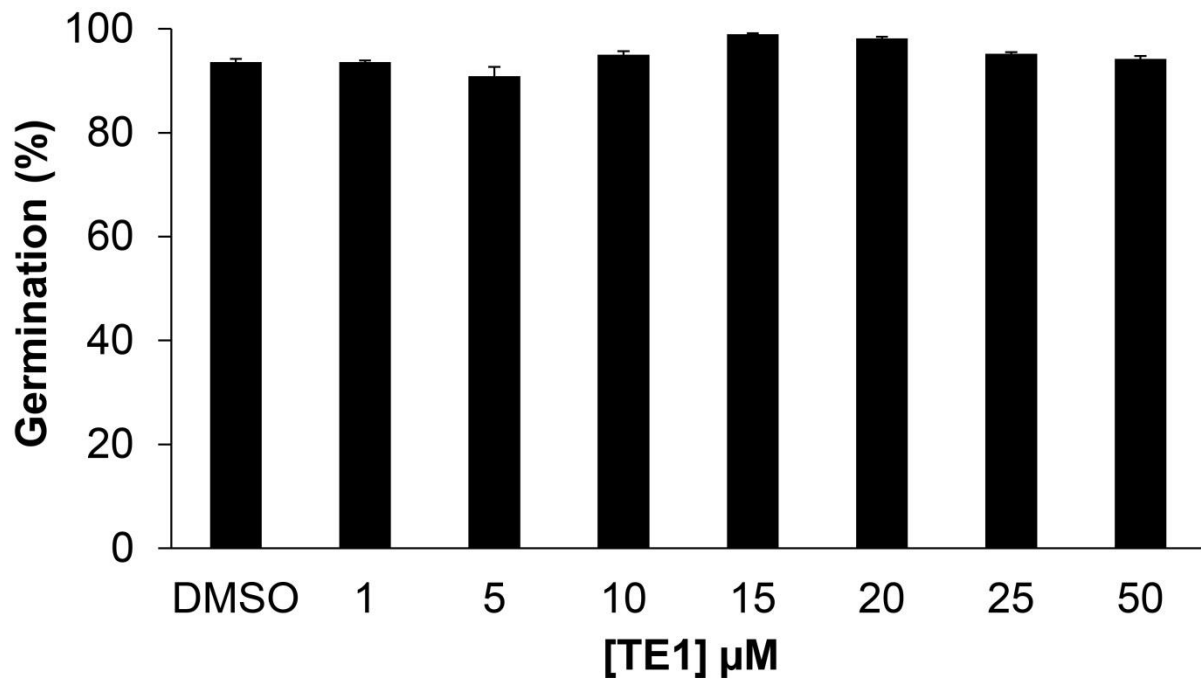
Figure 3.7. Percentage of germination of *Arabidopsis thaliana* is unaffected by TE1.

Germination percentage of wild type *Arabidopsis thaliana* in the presence of different concentration of TE1 is shown. Total of 82-205 seeds were counted to score germination per condition. Error bars represent SE.

3.2.6 TE1 inhibits root hair elongation

At 10 µM TE1 growth of primary root length was significantly reduced (Figure 3.3) but most plants were still alive at this concentration (Figure 3.6). Therefore, the effect of 10 µM TE1 was observed on root hair elongation. Root hair growth may be separated into four stages: selection of the trichoblast cell to form a root hair, swelling of cell causes bulge formation for root hair initiation, tip growth and maturation of the tip, reviewed in (Tominaga-Wada et al., 2011).

Long polarised root hairs were observed in the DMSO control but there were fewer root hairs observed in the presence of 10 µM TE1. Although some root hairs were observed in the presence of TE1, root hair elongation/maturation was inhibited (Figure 3.8). The data suggest that TE1 does not interfere with cell specification for root hair formation and initiation of root hairs, as bulge formation and root hair initiation was observed in the presence of TE1.

Figure 3.8. TE1 inhibits root hair elongation.

7 day old seedlings grown on DMSO (top row) and on 10 µM TE1 (bottom row) are shown.

3.2.7 Effects of TE1 on plant growth can be recovered

To determine whether the effects of TE1 on plant growth were permanent, transplant experiments were performed to see if growth inhibition phenotypes may be recovered. Seedlings were severely retarded in growth after 5 days on 25 µM TE1 (Figure 3.9B) compared to seedlings grown in medium containing 0.1% DMSO (Figure 3.9A). Five day old seedlings grown on ½ MS media containing 25 µM TE1 (Figure 3.9B) transplanted for further 5 days to TE1 free medium (Figure 3.9D) displayed recovery of growth. Cotyledons were green and expanded, primary leaves emerged, roots elongated and grew in accordance to gravity vector and root hairs developed. Seedlings grown on DMSO control transplanted to fresh media containing DMSO for further 5 days continued normal growth (Figure 3.9E), whereas almost all plants transplanted from TE1 to media containing TE1 for 5 more days did not display growth (Figure 3.9C). These results demonstrate that the effects of TE1 are reversible.

Figure 3.9. Growth inhibition caused by TE1 may be recovered.

5 day old seedlings grown on medium containing DMSO (A) and 25 µM TE1 (B). Plants transplanted from DMSO after 5 days to fresh DMSO medium for further 5 days (E), or from TE1 to TE1 for a further 5 days (C) or recovered from TE1 to DMSO (D). Scale bars, 2 mm.

3.3 Characterising the long term effect of TE1 on cellular organelles

3.3.1 TE1 does not interfere with peroxisome morphology and peroxisomal protein import

TE1 was initially identified to alter peroxisome positioning causing them to group in clusters in cell periphery (Figure 3.2). Therefore it was of interest to characterise the effects of TE1 on peroxisomes more thoroughly.

Peroxisome proteins imported into the peroxisomes contain one of two peroxisome targeting signal (PTS) peptides, PTS1 and PTS2, reviewed in (Hu et al., 2012). To test the effect of TE1 on peroxisome import machineries, homozygous *Arabidopsis thaliana* lines expressing PTS2-GFP and RFP-PTS1 were generated by crossing PTS2-GFP female parent with RFP-PTS1 male parent. Single marker lines were obtained from (Pracharoenwattana et al., 2005). Peroxisomes in the root epidermis of 7 day old seedlings grown on DMSO medium were bright and punctate. A high percentage of co-localisation between PTS2-GFP and RFP-PTS1 was observed, suggesting that the crosses generated were successful. In the presence of TE1, the appearance of both PTS1 and PTS2 targeted markers were comparable to the DMSO control, and no import defects into the peroxisomes were observed. A compound synthesised in the laboratory, HLL6, which inhibits the import of both PTS1 and PTS2 pathway (unpublished data) was used as a positive control. In presence of HLL6, inhibition of import of both PTS1 and PTS2 proteins is clearly visible as reported by dispersal of both GFP and RFP in the cytosol (Figure 3.10).
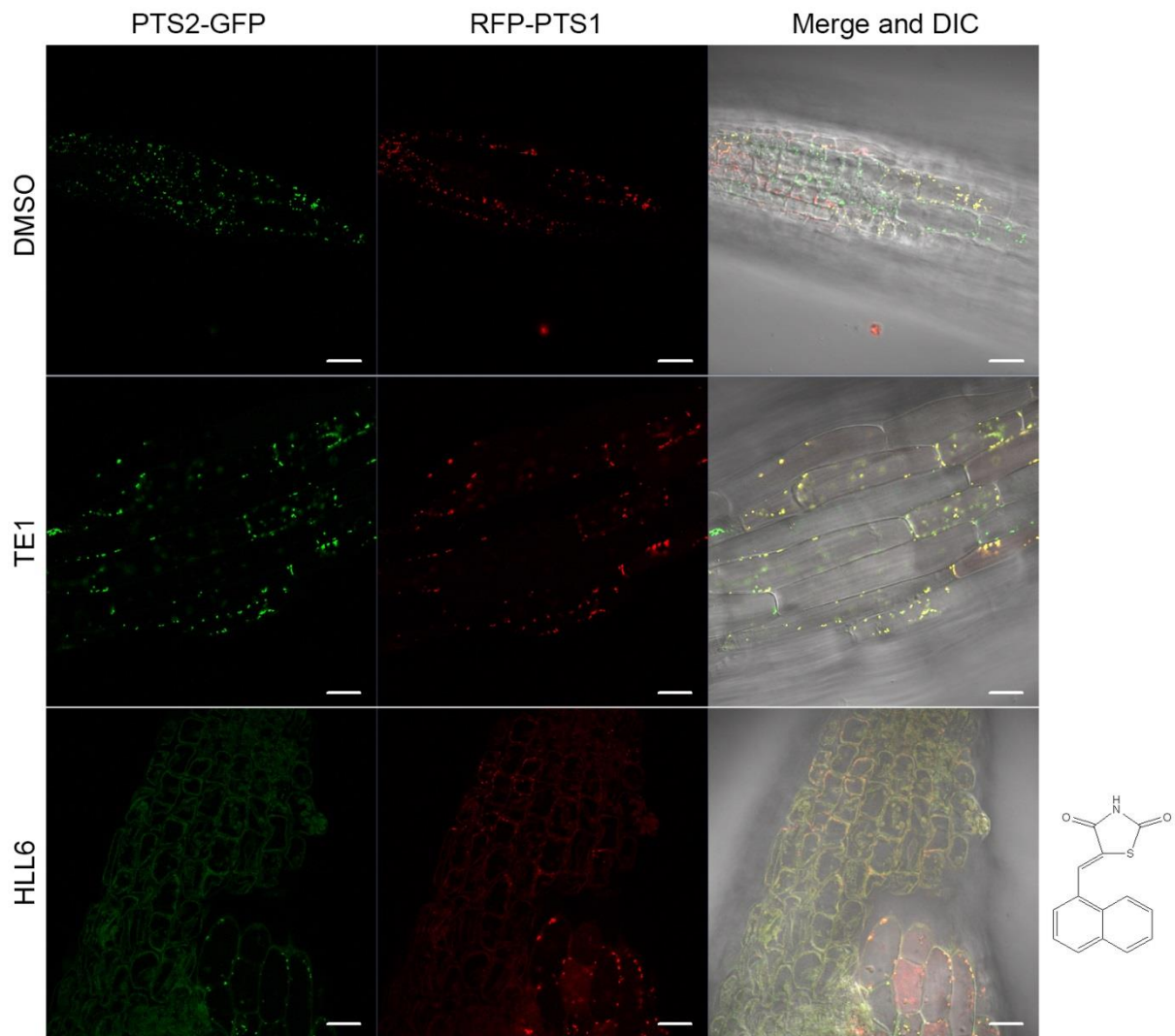
Figure 3.10. Peroxisome import pathways are functional in the presence of TE1.

7 day old *Arabidopsis thaliana* seedlings expressing PTS2-GFP (left column) and RFP-PTS1 (middle column), both labelling peroxisomes, co-localise together when merged together with DIC (right column). Seedlings were either grown of DMSO (top row), 25 µM TE1 (middle row) or 25 µM HLL6 (bottom row). Import defect can be seen in both PTS1 and PTS2 in the presence of HLL6. Scale bars, 20 µm.

The peroxisome clustering phenotype was also monitored in the epidermis cells of cotyledons, hypocotyls and roots in 7 day old seedlings grown on 25 µM TE1. However, no significant effect on peroxisome positioning was observed in the presence of TE1. Peroxisome morphology in hypocotyl epidermis is shown (Figure 3.11) as an example to demonstrate that peroxisome positioning in the presence of TE1 was comparable the DMSO control.
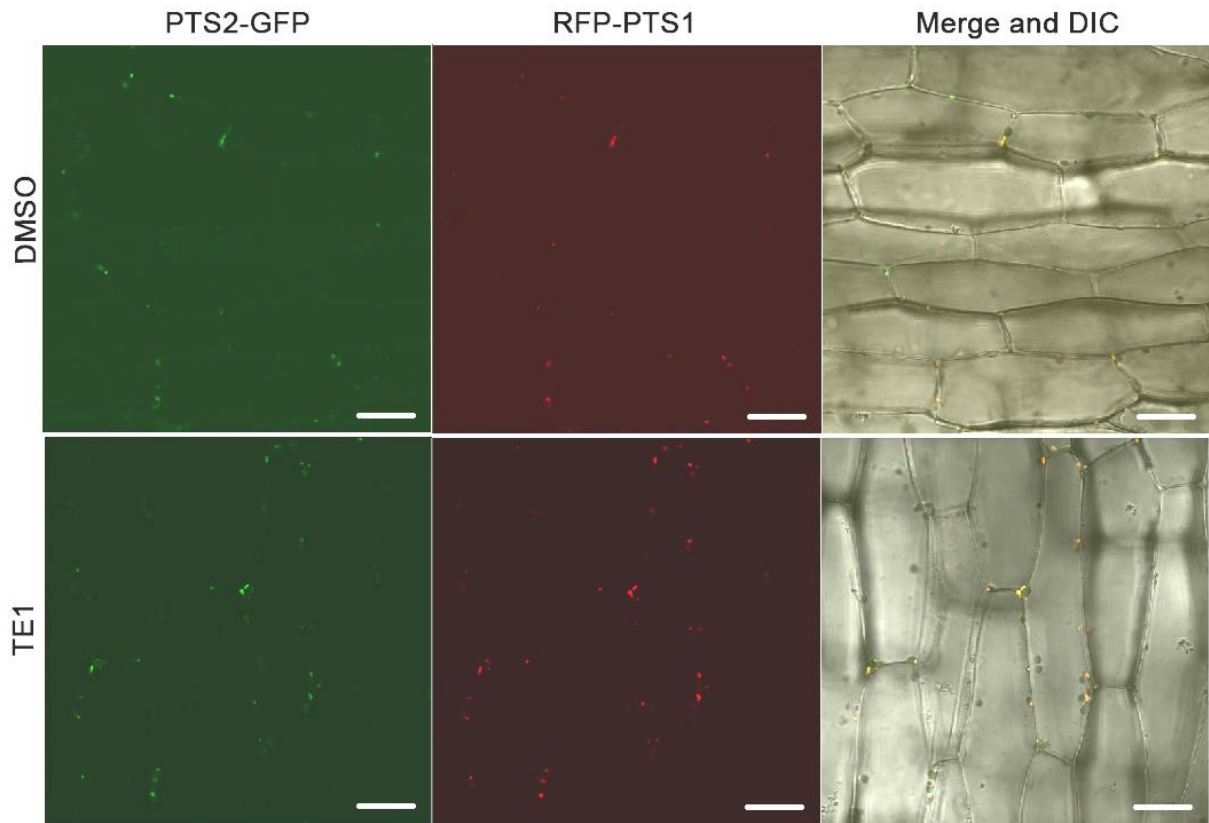
Figure 3.11. Peroxisomes in hypocotyl epidermis cells were visualised as normal in the presence of TE1.

7 day old *Arabidopsis thaliana* seedlings expressing PTS2-GFP (left column) and RFP-PTS1 (middle column), both labelling peroxisomes, co-localise together when merged together with DIC (right column). Seedlings were either grown on DMSO (top row) or in the presence of 25 µM TE1 (bottom row). Scale bars, 20 µm.

3.3.2 TE1 does not affect protein trafficking to the Golgi and positioning of Golgi stacks

The effect of TE1 on the positioning of Golgi and protein trafficking to the Golgi was also tested. Seven day old *Arabidopsis thaliana* seedlings expressing GFP fused with the N-terminal peptide from rat trans-Golgi enzyme sialyltransferase (ST; ST-GFP), which targeted to the trans-Golgi cisternae (Wee et al., 1998), were used to observe the effects of TE1 on Golgi in the epidermis cells of cotyledons, hypocotyl and primary root. Golgi stacks were visualised as bright and punctate structures in seedlings grown in the compound free media. In the presence of TE1, no visible change in Golgi positioning was observed as seen in the cotyledon (Figure 3.12). TE1 also did not seem to interfere with protein trafficking from the ER to Golgi, as no ER labelling was observed in the presence of the compound.
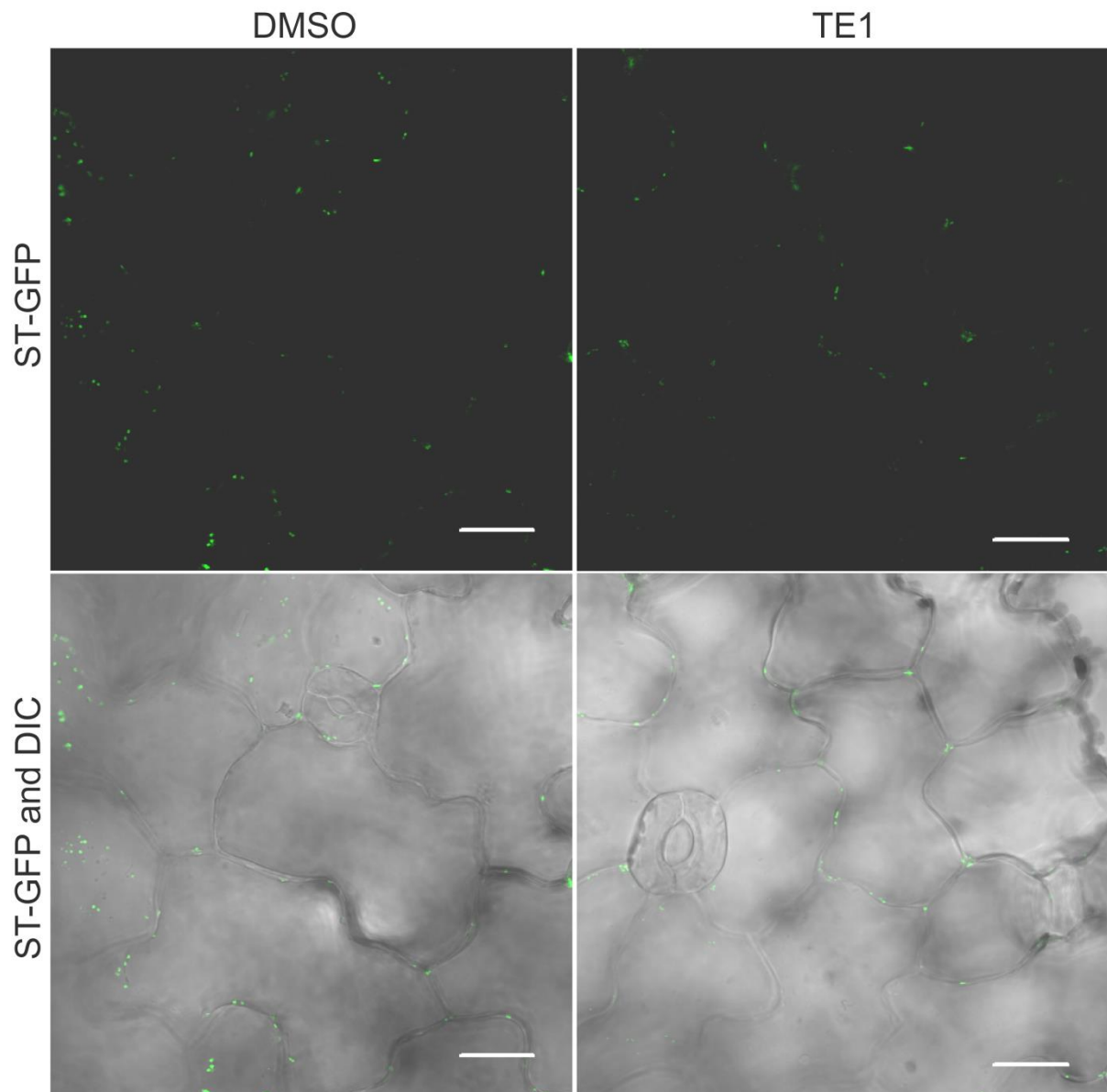
Figure 3.12. TE1 does not affect the morphology of Golgi stacks.

ST-GFP labelling Golgi stacks in the epidermis cells of 7 day old *Arabidopsis thaliana* seedlings grown on media containing DMSO (left column) and in the presence of 25 µM TE1 (right column) are shown. Bottom row shows ST-GFP merged with DIC. Scale bars, 20 µm.

3.3.3 TE1 causes change to the structure of the endoplasmic reticulum

The morphology of the endoplasmic reticulum (ER) in the presence of TE1 was tested using lines expressing GFP-HDEL for ER retention. Seedlings grown in the presence of 0.1% DMSO or 25 µM TE1 for 7 days were tested. ER networks in the cotyledon epidermal and hypocotyl epidermal cells were examined (Figure 3.13). In seedlings grown on DMSO, polygonal ER structures connected at anchor points were clearly visible in both cotyledon and hypocotyl epidermal cells (Figure 3.13A and Figure 3.13C). However, in the presence of TE1 a significant amount of damage to the ER network and ER clumping was observed in both hypocotyl and cotyledon epidermal cells (Figure 3.13B and Figure 3.13D). The 5 sided polygonal ER structures were mostly not visualised in the presence of TE1 and in some instances only the ER anchor points could be visualised in the cells. The result shows that TE1 causes changes to the ER network although trafficking to the Golgi seems to be functional as observed with functional trafficking of ST-GFP (Figure 3.12).
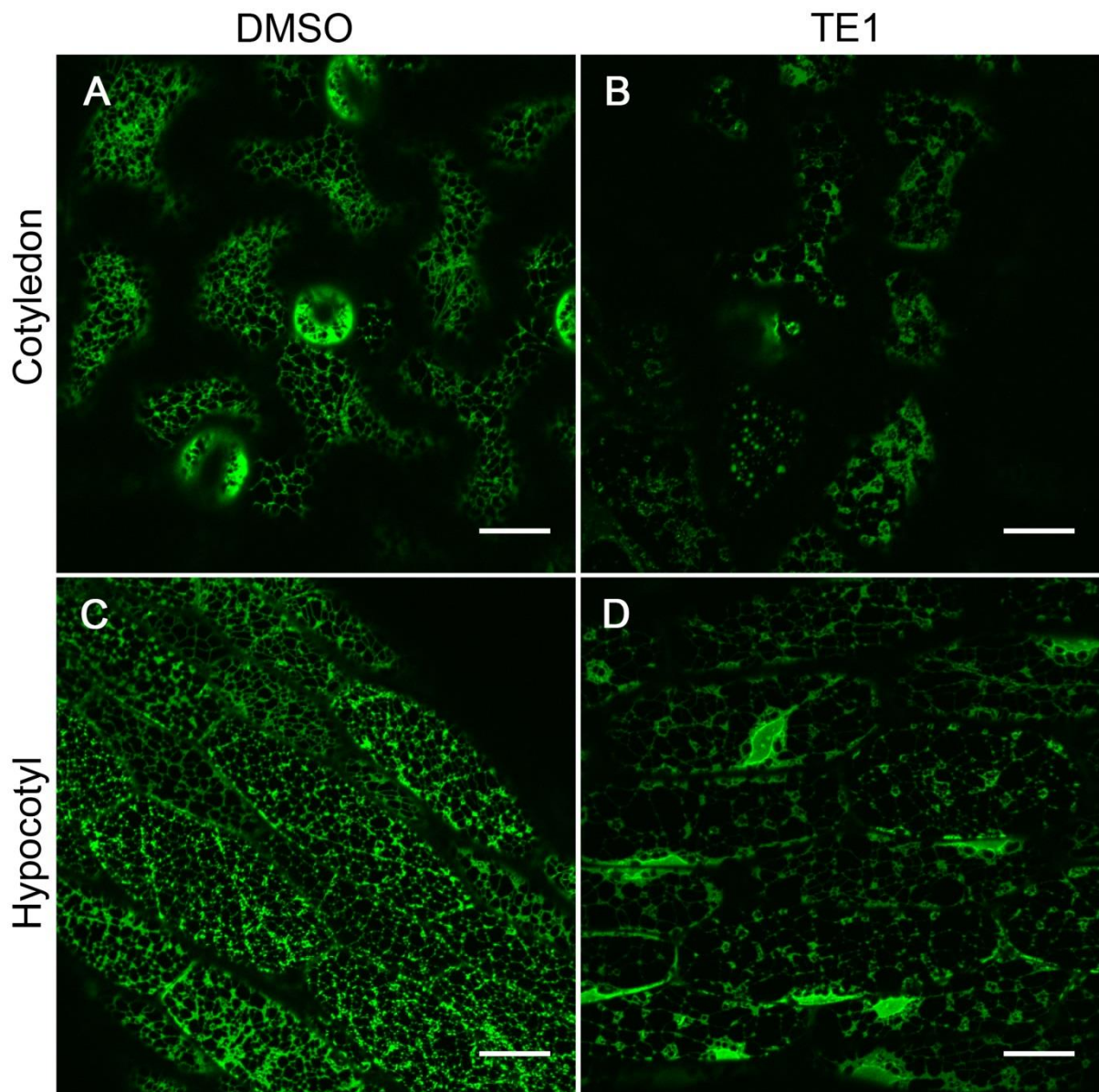
Figure 3.13. TE1 causes change to the ER structure.

7 day old *Arabidopsis thaliana* seedlings expressing GFP-HDEL targeted to the ER grown on DMSO (A and C) and on 25 μM TE1 (B and D). ER in the cotyledon (A and B) and hypocotyl (C and D) are shown. Scale bars, 20 μm.

3.3.4 Long term exposure to TE1 inhibits organelle movement

The effect of TE1 was tested on the movement of peroxisomes and Golgi in cotyledon, hypocotyl and root of 7 day old seedlings. Movies were generated for peroxisomes (GFP-PTS1) and Golgi (ST-GFP; cotyledons/ST-RFP; roots) using the confocal microscope, as described (Sparkes et al., 2008). These movies were used to generate data for track velocity, displacement rate and meandering index using *volocity 3* software. Track velocity (V; µm/s) represents the whole track length over a time frame. However, displacement rate (D; µm/s), does not cover the whole track length therefore it represents the shortest distance from the start to the end of a track over time. Finally, meandering index (MI; D/V), is a measure of organelle velocity with respect to movement directionality. The MI is calculated by dividing the V by D. Thus, organelles that demonstrate high saltatory movement may have a high V but it will have a low D, if it is compared to organelles that move away from the start point, even if the latter displays lower V than the former.

Cumulative distribution frequency (CDF) plots were generated, for peroxisome/Golgi movement analysis in roots and cotyledons, which describes the distribution of displacement rates within a given population of peroxisomes/Golgi in the presence or in the absence of chemical TE1. Data analysis using *volocity* was not performed for movies generated in hypocotyl because both peroxisomes and Golgi were not very mobile in hypocotyl epidermis. A minimum of eight movies were generated for each condition using 3-5 plants. The experiment was replicated twice and data showed similar results therefore it was pooled together. The CDF plots were made by Dr. Imogen Sparkes (University of Exeter), using the raw data I generated by analysing organelle movements in *volocity* software.

3.3.4.1 Quantification of peroxisome movement in cotyledons

For peroxisome movement in cotyledons, 7 day old seedlings were grown on media containing 0.1% DMSO or 10 µM TE1. Peroxisomes were tracked for DMSO n=734 and 10 µM TE1 n=564 (Figure 3.14). CDF plots indicate that TE1 has high impact on peroxisome velocity and displacement rate in cotyledon epidermis cells. CDFs show that in seedlings grown on DMSO, around 35% peroxisomes have velocity ≥ 2 µm/s and more than 65% peroxisomes display velocity ≥ 1 µm/s. In comparison for seedlings grown on 10 µM TE1, only 5% of the peroxisome population has velocity ≥ 2 µm/s and around 20% peroxisomes move faster than 1 µm/s (Figure 3.14A).

The CDF plot for displacement rate shows that in the presence of TE1 peroxisomes D in cotyledons is reduced. For DMSO, more than 20% peroxisomes displayed D ≥ 2 µm/s and 40% peroxisomes had D values ≥ 1 µm/s. Meanwhile, in the presence of 10 µM TE1, only 1% peroxisomes showed D ≥ 2 µm/s and 5% peroxisomes were observed to have D ≥ 1 µm/s (Figure 3.14B). Seedlings grown on DMSO control had around 75% peroxisomes that had MI ≥ 0.2, in comparison only 35% peroxisomes displayed MI ≥ 0.2 in the presence of TE1. Around 50% peroxisomes had MI ≥ 0.5 compared to only 15% that had MI ≥ 0.5 in seedlings grown on 10 µM TE1 (Figure 3.14C). The differences observed in peroxisome dynamics were statistically significant according to Kolmogorov-Smirnov (KS) statistical analysis that displayed $p \leq 0.01$. Tracks are shown for peroxisome movement over a typical movie time course in cotyledon epidermis of seedlings grown on DMSO and 10 µM TE1 (Figure 3.14D-E). These data show that movement of peroxisomes in the epidermis cells of cotyledons is reduced in the presence of TE1.
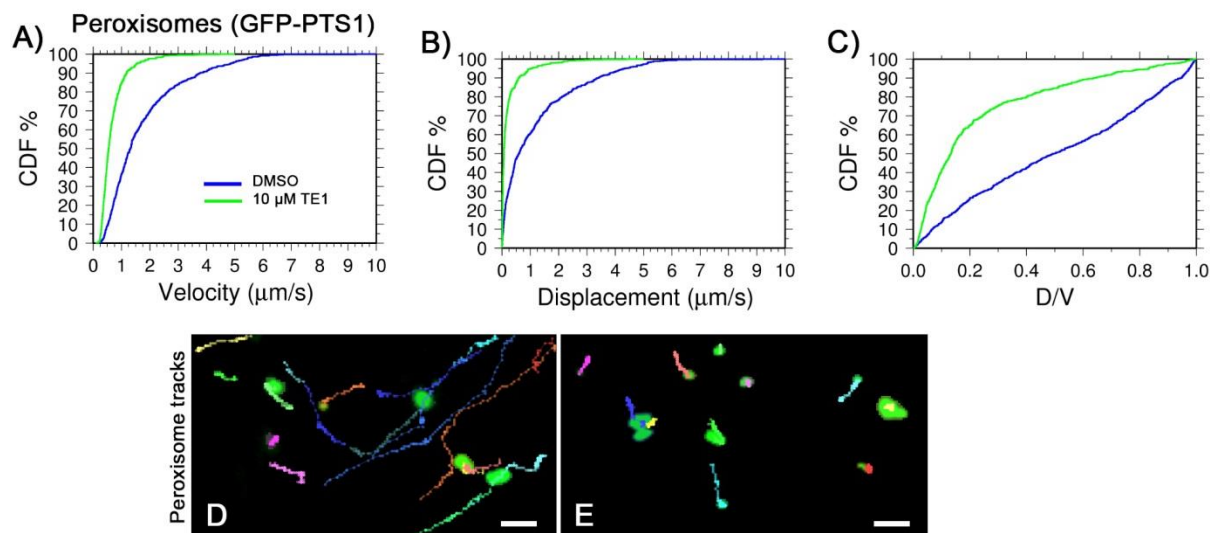
Figure 3.14. TE1 inhibits peroxisome movement in cotyledons.

(A-C) Statistical analysis of peroxisome movement in cotyledons of 7 day old *Arabidopsis thaliana* seedlings grown on medium containing DMSO (blue line) or 10 μM TE1 (green line). CDF graphs of track velocity (A), displacement rates (B) and meandering index (C) of tracked population of peroxisomes (GFP-PTS1) under specified conditions are displayed. Peroxisomes tracked, DMSO n=734 and 10 μM TE1 n=564. Tracks of peroxisomes movement over time course of a movie in cotyledons of plants grown on DMSO (D) and 10 μM TE1 (E) are also shown. Scale bars, 5 μm.

3.3.4.2 Quantification of Golgi movement in cotyledons

Golgi movement in cotyledons was quantified using 7 day old seedlings grown on media containing 0.1% DMSO or 10 µM TE1. Golgi stacks (ST-GFP) were tracked for DMSO n=826 and 10 µM TE1 n=995 (Figure 3.15). CDF graphs show that TE1 reduces Golgi velocity and displacement rate and MI in cotyledon epidermis cells. In the seedlings grown on DMSO, 45% of Golgi displayed V ≥ 1 µm/s and 15% of Golgi showed V ≥ 2 µm/s. This was significantly reduced in the presence of 10 µM TE1, where only 15% of Golgi had V ≥ 1 µm/s and 5% of Golgi showed ≥ 2 µm/s (Figure 3.15A).

The CDF for displacement rate shows that in the presence of TE1 Golgi D in cotyledons is reduced. In seedlings grown on DMSO, 25% of Golgi showed D ≥ 1 µm/s and 10% of Golgi were observed to have D ≥ 2 µm/s. However, in the presence of 10 µM TE1, 10% of Golgi had D ≥ 1 µm/s and just 2% of Golgi displayed D values ≥ 2 µm/s (Figure 3.15B). In the DMSO control, 65% of Golgi had a MI ≥ 0.2 and 40% of Golgi had a MI ≥ 0.5. In the presence of TE1 however, these values were significantly reduced, only 45% of Golgi stacks displayed a MI ≥ 0.2 and only 20% had a MI ≥ 0.5 (Figure 3.15C). The differences in dynamics of Golgi stacks as shown by the CDFs were statistically significant according to KS test that displayed p ≤ 0.01. Tracks are shown for Golgi movement over a typical movie time course in cotyledon epidermis of seedlings grown on DMSO and 10 µM TE1 (Figure 3.15D-E). These data show that movement of Golgi in the cotyledon epidermis cells is reduced in the presence of TE1.
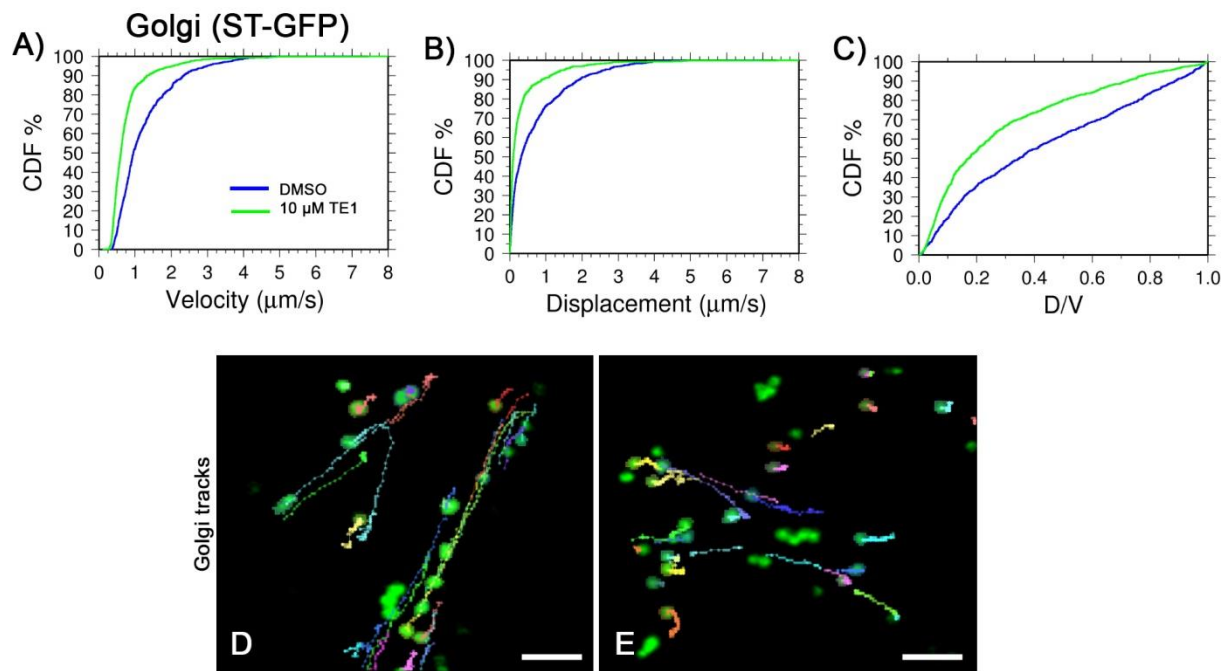
Figure 3.15. TE1 inhibits Golgi movement in cotyledons.

(A-C) Statistical analysis of Golgi movement in cotyledons of 7 day old *Arabidopsis thaliana* seedlings grown on medium containing DMSO (blue line) or 10 µM TE1 (green line). CDF graphs of track velocity (A), displacement rates (B) and meandering index (C) of tracked population of Golgi stacks (ST-GFP) under specified conditions are displayed. Golgi stacks tracked, DMSO n=826 and 10 µM TE1 n=995. Tracks of Golgi movement over time course of a movie in cotyledons of plants grown on DMSO (D) and 10 µM TE1 (E) are also shown. Scale bars, 5 µm.

3.3.4.3 Quantification of peroxisome movement in roots

For peroxisome movement in the primary roots, 7 day old seedlings were grown on media containing 0.1% DMSO or 25 µM TE1. Peroxisomes were tracked in the epidermis of the elongation zone for DMSO n=291 and 25 µM TE1 n=137 treated seedlings (Figure 3.16). CDF graphs show that TE1 has high impact on peroxisome V, D and MI in roots. In seedlings grown on DMSO, 65% of peroxisomes moved faster than 1 µm/s and 30% displayed V ≥ 2 µm/s. In the presence of TE1, only 15% of peroxisomes showed V ≥ 1 µm/s and only 5% of peroxisomes displayed V ≥ 2 µm/s (Figure 3.16A).

The CDF graph for displacement rate shows that in the presence of TE1, peroxisome D in the primary root is reduced. For DMSO, 40% of peroxisomes showed D ≥ 1 µm/s and 20% had D ≥ 2 µm/s. In the presence of TE1, only 5% of peroxisomes had D values ≥ 1 µm/s and 1% had D ≥ 2 µm/s (Figure 3.16B). In the roots of DMSO control seedlings 75% of peroxisomes had MI ≥ 0.2 and 50% had MI ≥ 0.5. In comparison, in the presence of TE1, 35% of peroxisomes had a MI ≥ 0.2, and 15% peroxisomes had a MI ≥ 0.5 (Figure 3.16C). The differences observed in peroxisome dynamics were statistically significant according to KS test that displayed p ≤ 0.01. Tracks are also shown for peroxisome movement over a typical movie time course in root epidermis of seedlings grown on DMSO and 25 µM TE1 (Figure 3.16D-E). This result demonstrates that TE1 inhibits the movement of peroxisomes in the epidermis cells of *Arabidopsis thaliana* roots.
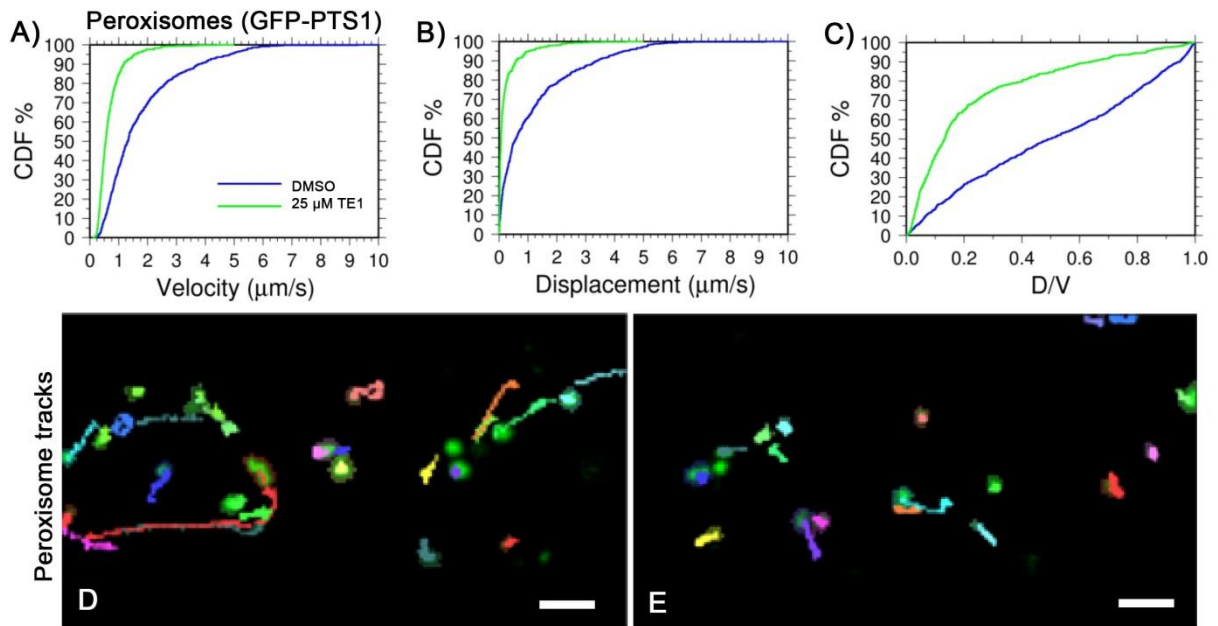
Figure 3.16. TE1 inhibits peroxisome movement in root.

(A-C) Statistical analysis of peroxisome movement in roots of 7 day old *Arabidopsis thaliana* seedlings grown on medium containing DMSO (blue line) or 25 µM TE1 (green line). CDF graphs of track velocity (A), displacement rates (B) and meandering index (C) of tracked population of peroxisomes (GFP-PTS1) under specified conditions are displayed. Peroxisomes tracked, DMSO n=291 and 25 µM TE1 n=137. Tracks of peroxisomes movement over time course of a movie in cotyledons of plants grown on DMSO (D) and 25 µM TE1 (E) are also shown. Scale bars, 5 µm.

3.3.4.4 Quantification of Golgi movement in roots

Dynamics of Golgi stacks in *Arabidopsis thaliana* roots were quantified using 7 day old seedlings grown on media containing 0.1% DMSO or 25 µM TE1. Golgi stacks were tracked in the epidermis of the elongation zone for DMSO n=397 and 25 µM TE1 n=235 grown seedlings (Figure 3.17). The CDF graphs show that TE1 inhibits Golgi movement including, V, D and MI in roots. In seedlings grown on DMSO, 50% of Golgi stacks displayed V ≥ 1 µm/s and 15% displayed V ≥ 2 µm/s. In the presence of TE1, 15% of the Golgi population displayed V ≥ 1 µm/s and only 5% of Golgi had V ≥ 2 µm/s (Figure 3.17A).

The CDF plot for displacement rate shows that in the presence of TE1 D for Golgi in roots is reduced. In seedlings grown on DMSO, 25% of the Golgi stacks displayed D ≥ 1 µm/s and 10% of Golgi displayed D ≥ 2 µm/s. In the presence of TE1 however, 10% of Golgi showed D ≥ 1 µm/s and just 2% of Golgi displayed D ≥ 2 µm/s (Figure 3.17B). In DMSO control, 65% of Golgi had a MI ≥ 0.2 and 40% of the Golgi population had a MI ≥ 0.5. However, in the presence of TE1, 45% of Golgi had a MI ≥ 0.2 and just 20% of Golgi had a MI ≥ 0.5 (Figure 3.17C). Inhibition of Golgi movement caused by TE1 as shown by the CDFs was statistically significant according to KS test that showed p ≤ 0.01. Tracks are shown for Golgi movement over a typical movie time course in the root epidermis of seedlings grown on DMSO and 25 µM TE1 (Figure 3.17D-E). This result shows that movement of Golgi in the root epidermis cells is reduced in the presence of TE1.
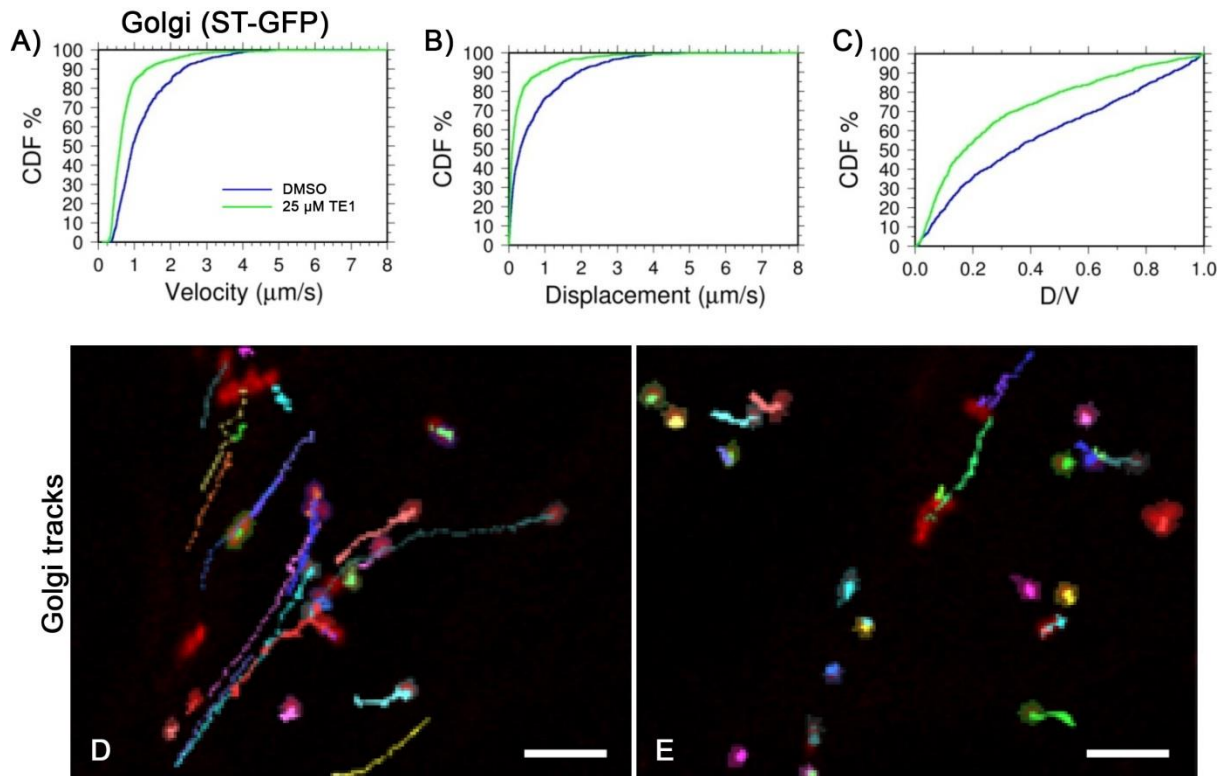
Figure 3.17. TE1 inhibits Golgi movement in roots.

(A-C) Statistical analysis of Golgi movement in roots of 7 day old *Arabidopsis thaliana* seedlings grown on medium containing DMSO (blue line) or 25 µM TE1 (green line). CDF graphs of track velocity (A), displacement rates (B) and meandering index (C) of tracked population of Golgi stacks (ST-RFP) under specified conditions are displayed. Golgi stacks tracked, DMSO n=397 and 25 µM TE1 n=235. Tracks of Golgi movement over time course of a movie in cotyledons of plants grown on DMSO (D) and 25 µM TE1 (E) are also shown. Scale bars, 5 µm.

3.3.5 Long term effect of TE1 on the actin cytoskeleton

Movement of the organelles in plants have been shown to be dependent on the myosin XI family of motor proteins, reviewed in (Morita et al., 2002). Myosin motors move on the actin filaments as demonstrated by the requirement of actin and not microtubule to mediate peroxisome movement in higher plants (Fukaki et al., 1998). Our previous observations showed that TE1 inhibits organelle movement in cotyledons and roots. Therefore, the effect of TE1 on the actin cytoskeleton was monitored in the cotyledons of 7 day old seedlings grown on DMSO and on 25 μM TE1. Actin filaments were visualised by GFP fused to actin binding domain (ABD) 2 of the *Arabidopsis thaliana* Fimbrin 1 protein. In plants grown on DMSO, actin filaments and bundles were clearly visualised and no indication of actin depolymerisation was observed. The actin cytoskeleton in the presence of TE1 was comparable to the DMSO control (Figure 3.18). The data shows that TE1 does not depolymerise or increase the bundling of actin filaments in the cotyledon epidermis.
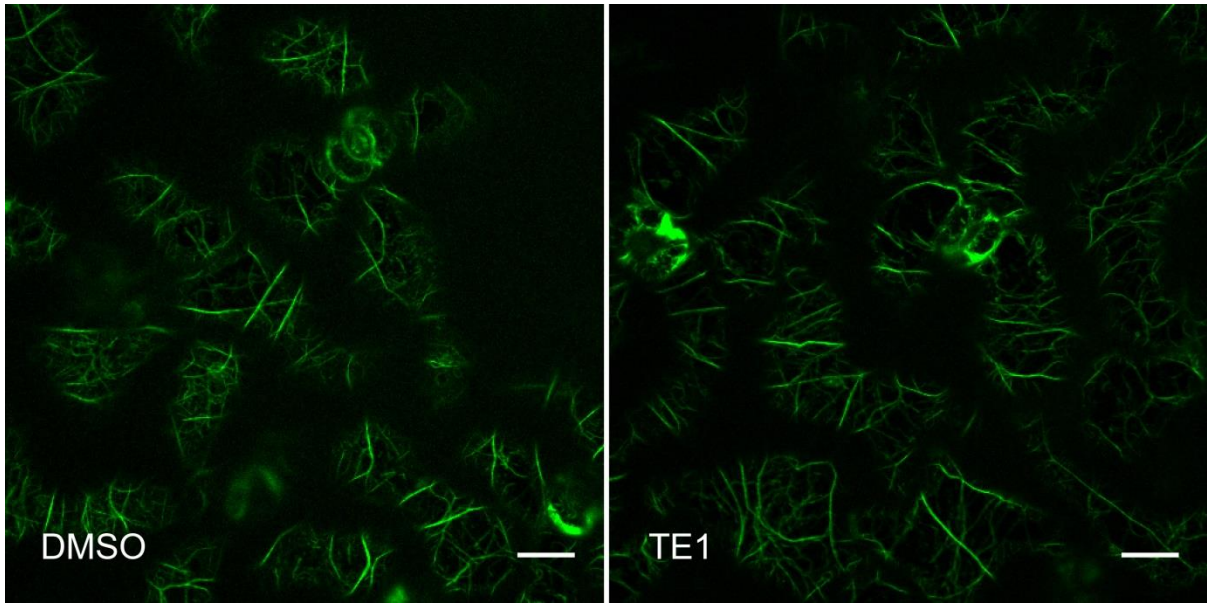
Figure 3.18. TE1 shows no obvious effect on the actin cytoskeleton.

7 day old *Arabidopsis thaliana* seedlings expressing GFP-ABD2 labelling actin filaments. Actin filaments from cotyledon epidermis cells can be seen from plants grown on DMSO and 25 μM TE1. Scale bars, 20 μm.

3.3.6 TE1 causes agravitropic growth of hypocotyl and roots

TE1 was isolated as an inhibitor of hypocotyl gravitropism in a large scale chemical genomics screen (Surpin et al., 2005). A range of concentrations 10-100 μM TE1 were used to identify the chemical as an inhibitor of hypocotyl gravitropism. This effect on hypocotyl gravitropism was replicated (Figure 3.19) under conditions described in (Surpin et al., 2005). The effect of TE1 was also checked on gravitropic response in roots (Figure 3.20).

3.3.6.1 Characterising the effect of TE1 on hypocotyl gravitropism

The effect of TE1 on hypocotyl gravitropism was investigated. In the darkness, *Arabidopsis thaliana* seedlings were grown upright for 4 days and gravistimulated at 90° for 48 h (Figure 3.19A). The hypocotyl of plants grown in the presence of DMSO mostly showed bending of hypocotyl in response to gravity stimulus, which indicates that they were responsive to gravity change (Figure 3.19B). However in the presence of 25 μM TE1 seedlings showed less directional change in response to gravistimulation (Figure 3.19C) and some seedlings are seen to be growing in a different orientation to the gravity vector. At 50 μM TE1, hypocotyl growth was observed in completely random orientations and no reorientation of hypocotyl was observed in response to gravistimulation (Figure 3.19D). As seen previously (Figure 3.5), hypocotyl growth is also observed to be inhibited in the presence of TE1. These results indicate that TE1 causes dysfunction of hypocotyl gravitropic response.
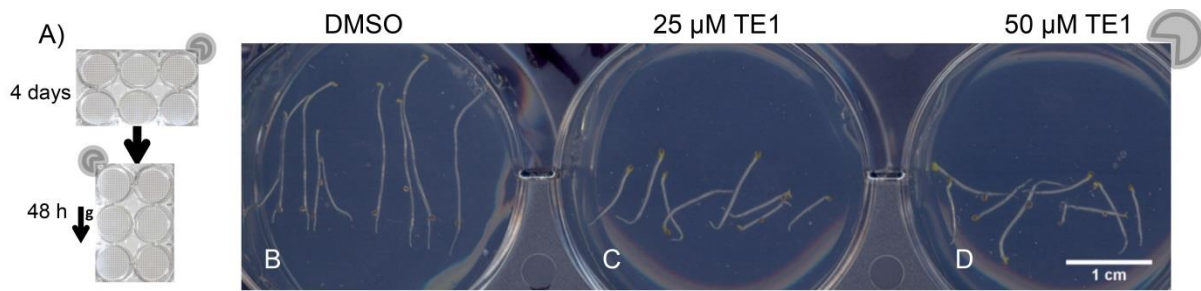
Figure 3.19. TE1 interferes with hypocotyl gravity perception.

Gravitropic response assay performed in *Arabidopsis thaliana* seedlings grown in the dark for 4 days and gravistimulated at 90° 48 h (A). Seedlings were grown in DMSO (B), 25 µM TE1 (C), and 50 µM TE1 (D). Scale bar, 10 mm.

3.3.6.2 Characterising the effect of TE1 on root gravitropism

The effect of the compound on root gravitropism was also investigated. Growth analysis of seedlings in the presence of TE1 displayed that TE1 inhibits the growth of both root (Figure 3.3) and hypocotyl (Figure 3.5). However, if hypocotyl bending away from the gravity vector after gravistimulation depends on the growth, then separating the effects is not possible. To eliminate this factor, a new gravitropic response assay was designed to quantify root gravitropism in the presence of TE1. *Arabidopsis thaliana* seedlings were grown in ½ MS media containing 0.1% DMSO for 6 days. This was followed by transplant to fresh media containing DMSO, 1 µM or 2 µM TE1 for 48 h, and change in gravity vector by 90° (Figure 3.20A). The length of roots was measured just after transplantation and after 48 h to ensure no difference in root growth was observed in the presence of TE1. Low concentrations of TE1 were chosen because concentrations ≥ 5 µM TE1 inhibit root growth, however, no root growth inhibition was observed at 1 µM TE1 (Figure 3.3).

In the presence of DMSO, average root bending in response to 90° gravistimulation was 81° (Figure 3.20B and Figure 3.20F). However in the presence of just 1 µM TE1, average root bending decreased by 26° in comparison to the DMSO control, to 55° Figure 3.20C and Figure 3.20G). Root bending was further reduced in the presence of 2 µM TE1 as only 48° angle change was observed in response to the 90° gravistimulation (Figure 3.20D and Figure 3.20H). In the presence of 1 µM and 2 µM TE1, the percentage of root growth after 48 h transplant/gravistimulation remained similar to the DMSO control (Figure 3.20E). These data show that TE1 inhibits gravity response of *Arabidopsis thaliana* root and this effect is not due to the inhibition of root growth.
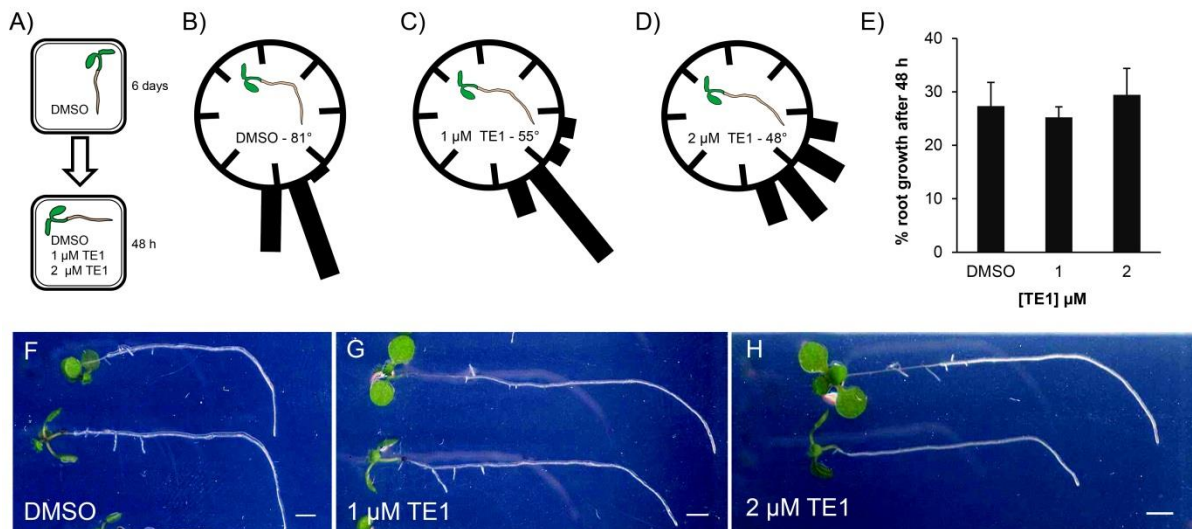
Figure 3.20. TE1 decreases root gravitropic response.

Arabidopsis thaliana seedlings grown in light for 6 days were gravistimulated for 48 h (A), in medium containing DMSO (B and F), 1 µM TE1 (C and G), and 2 µM TE1 (D and H). The average angle change of roots in response to gravistimulation after 48 h for DMSO was 81° (A), for 1 µM TE1 was 55° and for 2 µM TE1 was 48°. Root growth after transplantion onto DMSO, 1 µM and 2 µM TE1 for 48 h is also shown (E). Data represents a typical dataset from three repetitions, 15-24 seedlings per condition. Error bars represent SE. Scale bars, 5 mm.

3.4 Discussion

This chapter characterised the effects on whole plant phenotype and organelle morphology of long-term exposure to the small molecule TE1. The effects of TE1 on the appearance of peroxisomes, Golgi, the ER and actin filaments and the movement of peroxisomes and Golgi were tested using confocal laser scanning microscopy. The effect of the chemical was also tested at the whole plant level on relation to growth, survival, germination and gravitropism. The compound was initially isolated from a screen to identify altered hypocotyl gravitropic response (Surpin et al., 2005) and a subsequent screen in the laboratory classified it as altering peroxisome distribution within the cell (Figure 3.2). However, peroxisome clustering in the presence of TE1 could not be reliably reproduced (Figure 3.10 and Figure 3.11).

Characterisation of TE1 on the growth of 7 day old *Arabidopsis thaliana* seedlings revealed that TE1 inhibits primary root growth in light (Figure 3.3 and Figure 3.4), and hypocotyl elongation in the dark (Figure 3.5), in a dose dependent manner. Inhibition of hypocotyl elongation at 1 µM TE1 was observed whereas root length was unaffected at this concentration, which means that shoots are more sensitive to the effects of TE1 than roots. However, TE1 was also identified in a screen for compounds that increase hypocotyl length in the plants grown in light (Savaldi-Goldstein et al., 2008). This apparent contradiction can be explained by the finding that that auxin transport is required for hypocotyl growth in light grown seedlings but not in etiolated seedlings (Jensen et al., 1998).

Inhibition of plant growth by TE1 was only observed after a certain stage of development (Figure 3.4). The apical-basal axis in the embryo, with shoot meristem surrounded by embryonic leaves (cotyledons) in the apical side and root meristem at the basal side separated by embryonic stem (hypocotyl), forms a basic plant body shape during embryogenesis (Lau et al., 2012). Taken together these findings and the fact that germination was not affected by high concentrations up to 50 µM TE1 (Figure 3.7) suggest that the compound primarily affects post-germination processes. Alternatively, the compound may not penetrate through the seed coat to affect the early germination processes. Seedling survival percentage was decreased in the presence of high concentrations of TE1 after 7 days of growth. However, recovery of plant growth when transplanted to control conditions from TE1 (Figure

3.9) shows that no permanent damage was caused by the compound if the seedlings were transplanted after 5 days.

The effect of long-term TE1 treatment on organelle morphology was initially investigated. The data suggested that protein import into the peroxisomes and peroxisome positioning was unaffected in the presence of TE1 (Figure 3.10 and Figure 3.11). Long-term exposure to TE1 also had no effect on the trafficking to the Golgi or positioning of the Golgi stacks (Figure 3.12). This result suggests that transport of protein from the ER to Golgi is functional in the presence of TE1. However, significant change in the morphology of the ER is observed in the presence of TE1 (Figure 3.13).

Severe loss of the ER polygonal network and ER tubules were observed in seedlings grown on TE1 in the epidermis cells of both cotyledons and hypocotyls. The thick sheet-like structure of the ER visualised in the presence of TE1 may be due to the loss of ER tubules. ER membrane proteins, reticulons (RTNs), were shown to induce ER tubulation in artificial proteoliposomes in yeast (Hu et al., 2008). Similarly *Arabidopsis thaliana* reticulons, RTNLB1-4 and RTNLB13, localise to and constricts the ER tubular membranes (Tolley et al., 2008; Sparkes et al., 2010). RTNLB13 was also able to induce the ER membrane curvature and turn cisternal ER sheets into tubules in *pah1 pah2* double mutant (Tolley et al., 2010). *Arabidopsis thaliana* PAH1 and PAH2 phosphatidic acid phosphohydrolases were shown to redundantly inhibit phospholipid biosynthesis at the ER and double mutant *pah1 pah2* had higher level of phospholipids changing the ER into sheet structures (Eastmond et al., 2010). Although the structure of the ER is completely changed in the presence of TE1 (Figure 3.13), there is no evidence that suggest that the trafficking component from the ER is affected as protein was visible as normal in the Golgi stacks (Figure 3.12).

Similar to the findings shown here, abnormal arrangement of the ER network was also observed in multiple myosin XI mutants. 3KO *xik mya1 mya2 Arabidopsis thaliana* showed large ER aggregates around the cell periphery and unevenly distributed thick ER sheet-like structures. Unusually long ER bodies were also observed in the 3KO plants, this effect was much reduced in *mya1 mya2* 2KO plants, indicating that myosin XI-K is also important in preservation of the ER network and

shaping ER bodies although MYA1 and MYA2 are also involved in this process (Ueda et al., 2010).

In recent years, several studies on myosin XI have been carried out, showing it to be involved in remodelling and streaming of the ER network (Sparkes et al., 2009a; Ueda et al., 2010) and organelle mobility (Sparkes, 2010). TE1 inhibits the movement of peroxisomes and Golgi in both cotyledon and roots (Figure 3.14 to Figure 3.17). However, the extent of organelle movement inhibition in the presence of TE1 is not as severe as reported in multiple myosin XI KOs (Peremyslov et al., 2010) or total depolymerisation of actin filaments (Sparkes et al., 2008). This suggests that components required for organelle movement and interaction between actin filaments and myosins may be slightly affected by TE1. The network of actin filaments was seen to be intact in cotyledons (Figure 3.18), where organelle movement was inhibited in the presence of 10 µM TE1 (Figure 3.14 and Figure 3.15). Actin microfilaments and bundles were visible in the plants grown on TE1 therefore it is unlikely that organelle transport inhibition could be due to depolymerisation of the actin cytoskeleton.

Arabidopsis thaliana encodes eight actin (*ACT*) genes, *Arabidopsis thaliana act2* and *act8* mutants were shown to have defective root hair polarisation, whereas *act7* mutant did not affect root hair length but inhibited the length of primary root (Kandasamy et al., 2009). ACT7 is also required for auxin responsiveness for normal callus formation (Kandasamy et al., 2001) suggesting difficulties in cell differentiation and division without ACT7, which further supports the evidence for growth defects observed in *act7* mutants (Kandasamy et al., 2009). Seedlings grown on TE1 also caused defect in root hair elongation although root hair bulge formation was evident, tip growth was severely affected (Figure 3.8). Several factors have been reported to inhibit root hair cell elongation including, ACT2 and ACT8 (Kandasamy et al., 2009) and several class XI myosins (Ojangu et al., 2007; Peremyslov et al., 2008; Prokhnevsky et al., 2008).

The hypocotyl agravitropic response in the presence of TE1 as reported (Surpin et al., 2005) was also replicated (Figure 3.19). It was also demonstrated that the agravitropic growth caused by TE1 was not due to the inhibition of growth (Figure 3.20). It is well known that the gravitropic response in plants is dependent on the

distribution of auxin gradients and trafficking mechanisms. Functional characterisation of TE1 on trafficking components is investigated in detail in Chapter 4. Taken together the agravitropic phenotype and the sensitivity displayed by hypocotyl elongation in the presence of 1 µM TE1, at which concentration root growth was unaffected suggests that cell division is not significantly affected by TE1 as hypocotyl growth is not predominantly dependent on cell division (Gendreau et al., 1997). Therefore it can be hypothesised that the protein trafficking component required might be interfered by the function of TE1, which inhibits the hypocotyl elongation, but not root at low concentration of TE1.

Inhibition of gravitropic response and root hair elongation in the presence of TE1, both processes that are dependent of membrane trafficking, can also be used to back up the hypothesis that trafficking may be affected by TE1. It is generally accepted that polarised tip growth displayed by root hairs and pollen tubes is fundamentally controlled by localised protein trafficking towards the direction of growth within the cell. Secretory vesicles mainly carry components required for cell wall synthesis and addition of elongating plasma membrane (Carol and Dolan, 2002). Excess membrane proteins may be recovered by endocytosis to be ready for another round of trafficking. Trafficking of auxin carriers to the PM is essential to maintain auxin gradients which in turn control gravitropic response in plants. These data naturally leads towards the hypothesis that auxin gradient and membrane trafficking may be disrupted by the action of TE1. Therefore, Chapter 4 characterises the effects of TE1 on membrane trafficking, auxin distribution and auxin transporters.

4 Chapter Four – Short term cellular effects of TENin 1

4.1 Introduction

TE1 was initially isolated as an inhibitor of hypocotyl gravitropism (Surpin et al., 2005). As shown in Chapter 3, TE1 also inhibits root growth in the light and hypocotyl elongation in the dark. However, the agravitropic growth caused by TE1 was not due to the growth inhibition, Chapter 3 (Figure 3.20). Therefore, this chapter reports the effects of TE1 at cellular level. The complex endomembrane trafficking pathway was dissected using TE1 and other pharmacological tools to narrow down the pathway affected by TE1.

4.2 Results

4.2.1 Effect of TE1 on auxin responsiveness

TE1 was also identified as a stimulator of hypocotyl growth in the presence of light in a large scale chemical genomics screen. The same report also suggested the synthetic small molecules identified were potential pro-auxins (Savaldi-Goldstein et al., 2008). Effects of TE1 on auxin distribution were tested using the auxin responsive marker DR5-GFP. Recently, DR5 up-regulation in *Arabidopsis thaliana* root was shown to take place minutes after auxin treatment and this response peaked after 60 min (Brunoud et al., 2012). Rapid re-localisation of PIN3 proteins at the root columella upon gravistimulation (Friml et al., 2002) causes auxin translocation laterally that can be detected by DR5-GFP (Paciorek et al., 2005).

DR5-GFP seedlings incubated vertically in 0.1% DMSO or 25 µM TE1 for 210 min displayed a strong signal at the root columella (Figure 4.1A and B). Expression of DR5-GFP in the presence of TE1 was comparable to the DMSO control. Seedlings were also gravistimulated at 90° for 180 min in 0.1% DMSO or 25 µM TE1, following 30 min pre-incubation vertically in 0.1% DMSO or 25 µM TE1 (Figure 4.1C and D). Following gravistimulation, in the control seedlings, auxin redistribution was observed laterally towards the bottom of the root (Figure 4.1C). However, the redistribution of DR5-GFP signal to the bottom of root was not observed in seedlings gravistimulated in the presence of TE1 (Figure 4.1D). Overall, the data shows that TE1 does not cause up-regulation of DR5-GFP therefore it is not itself an auxin or metabolised into a compound with auxin-like activity inside *Arabidopsis thaliana* root. The symmetry of auxin distribution is also unaffected by TE1 in seedlings that do not experience a gravity stimulus. However, in seedlings that are gravistimulated the auxin re-localisation is inhibited by the presence of TE1 indicating that this compound may affect the trafficking of auxin transporters.
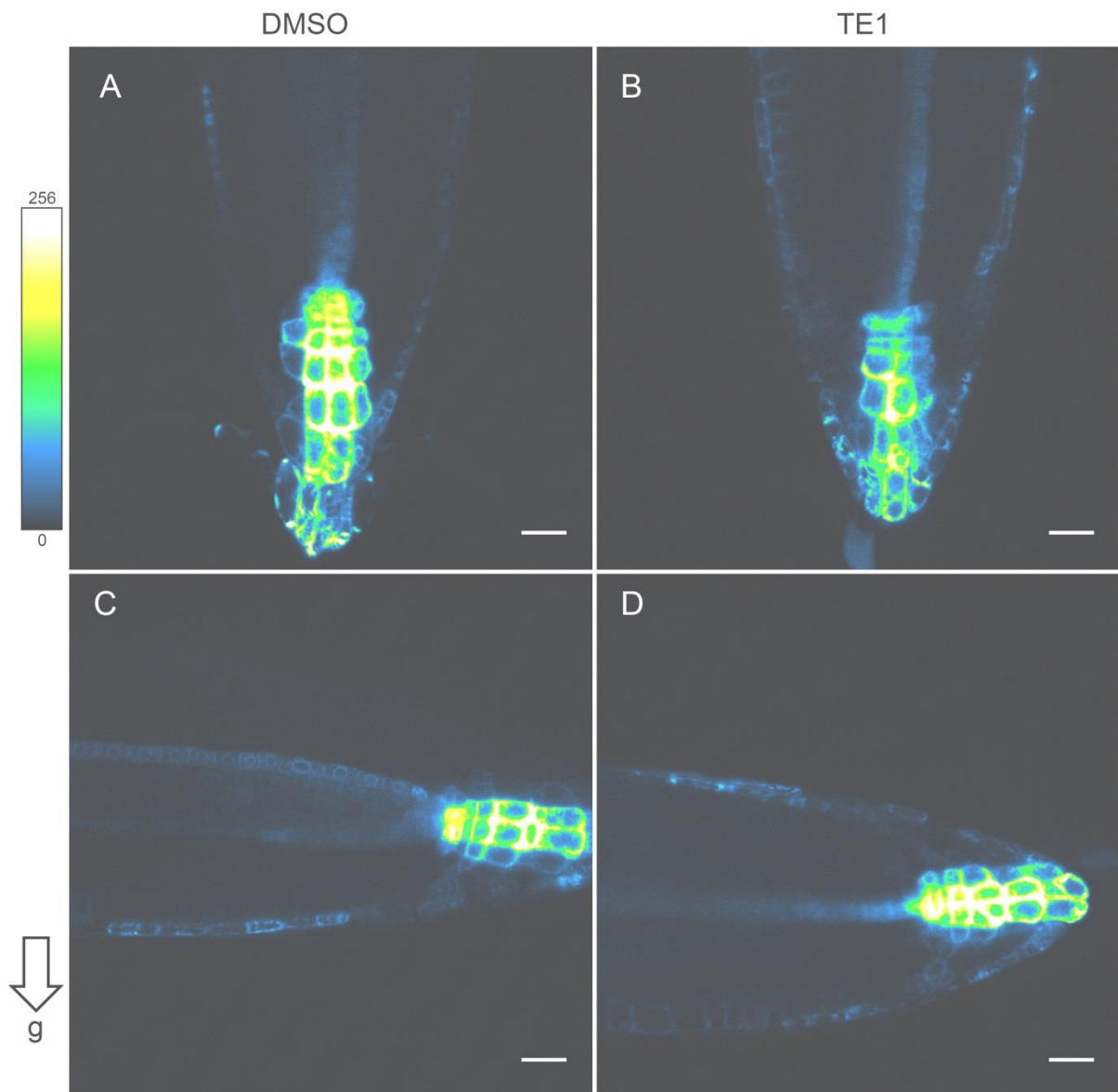
Figure 4.1. TE1 does not up-regulate DR5 expression but interferes with auxin re-localisation.

Heat map of fluorescence in 7 day old seedlings expressing DR5-GFP (A-D) incubated for 210 min in DMSO (A) and 25 µM TE1 (B) vertically aligned relative to the gravity vector (g). Seedlings were also gravistimulated perpendicularly relative to the gravity vector for 180 min in the presence of DMSO (C) or 25 µM TE1 (D). This was done following 30 min pre-incubation in DMSO (C) and 25 µM TE1 (D), where seedlings were aligned vertically relative to the g. Colour panel on the top left displays relative intensity of DR5-GFP from 0-256. Arrow represents g. Scale bars, 20 µm.

4.2.2 Characterising the effect of TE1 on endomembrane proteins

4.2.2.1 TE1 inhibits PIN2 trafficking in a reversible manner

As shown in Chapter 3, TE1 inhibits root gravitropism at concentrations as low as 1 µM (Figure 3.20). Plant gravitropism has been previously shown to be mediated by endomembrane trafficking, see (Dettmer and Friml, 2011). In particular, PIN2 proteins have been shown to play an important part in regulation of gravitropism in *Arabidopsis thaliana* (Chen et al., 1998; Luschnig et al., 1998; Muller et al., 1998; Utsuno et al., 1998). Therefore, the hypothesis that TE1 may affect the distribution of PIN2 was tested in *Arabidopsis thaliana* roots expressing PIN2-GFP.

7 day old seedlings grown on ½ MS media were transplanted to media containing 0.1% DMSO (Figure 4.2A) or 25 µM TE1 (Figure 4.2B) for 120 min. In untreated seedlings, PIN2-GFP shows a polarised distribution predominantly at the apical side of the membrane in the root epidermis cells (Figure 4.2A). Seedlings treated with 25 µM TE1 for 120 min caused accumulation of PIN2-GFP in intracellular bodies termed here as "TE1 bodies" (Figure 4.2B). This effect was recovered when seedlings treated in 25 µM TE1 for 120 min were transplanted to media containing 0.1% DMSO for 180 min (Figure 4.2C). Intracellular PIN2 agglomerations after short term treatment with TE1 suggest that it is a primary effect. Rapid inhibition of PIN2 trafficking may provide an explanation why TE1 causes growth inhibition and agravitropic response in the long term. These data show that TE1 interferes with trafficking of PIN2 proteins in a reversible manner.
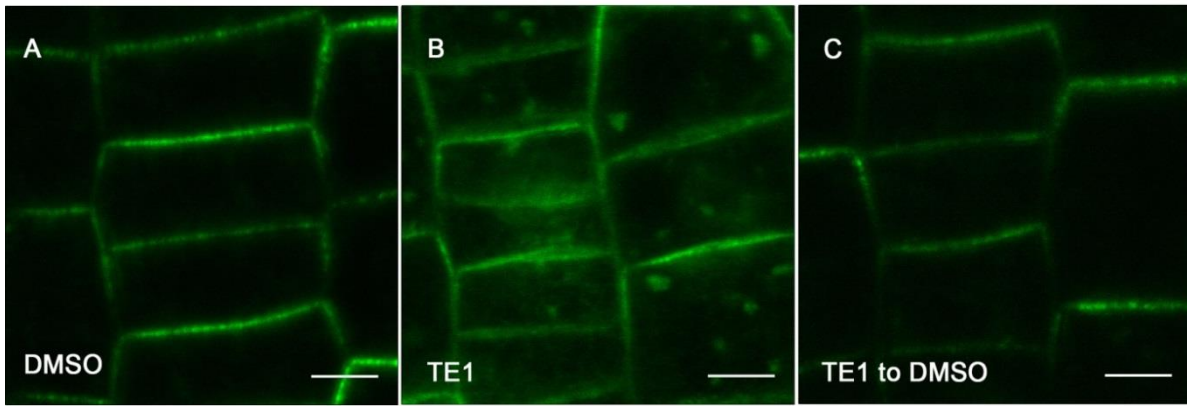
Figure 4.2. TE1 intereferes with PIN2 trafficking but the effects may be recovered.

Arabidopsis thaliana roots expressing PIN2-GFP were transplanted to medium containing DMSO (A) or 25 µM TE1 (B) for 120 min and effects on treated seedlings were recovered after a washout experiment was performed by transplanting seedlings from TE1 to compound free medium for 180 min (C). Scale bars, 5 µm.

4.2.2.2 Average intensity of PIN2-GFP is unchanged after short-term TE1 treatment

Inhibition of PIN2 trafficking in the presence of 25 µM TE1 after 120 min raised a question whether TE1 has an effect on the PIN2 expression or degradation. To monitor this, average fluorescent intensity was quantified in 20 different images generated using identical settings for DMSO or TE1 in 10 different seedlings expressing PIN2-GFP per condition. A typical example of a seedling incubated in 0.1% DMSO (Figure 4.3A) and 25 µM TE1 (Figure 4.3B) is shown. Quantification of average fluorescent intensity revealed that average fluorescent intensity for seedlings treated in DMSO was 423 ± 15 and for 25 µM TE1 average intensity was 412 ± 16 (Figure 4.3C). Statistical analysis revealed that there is no significant difference in average intensity in seedlings incubated in DMSO or 25 µM TE1 for 120 min. The result indicates that short term TE1 treatment does not change the average intensity of PIN2 in the cells.
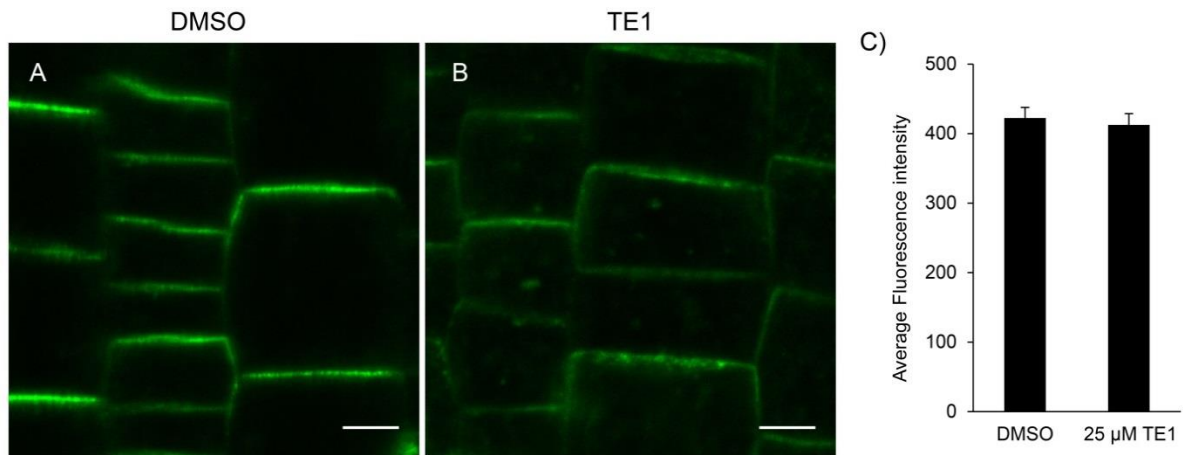
Figure 4.3. Average intensity of PIN2-GFP is unaffected in the presence of TE1.

Arabidopsis thaliana roots expressing PIN2-GFP were incubated in medium containing DMSO (A) and 25 µM TE1 (B) for 120 min. Average intensity of GFP fluorescence was measured in 20 images (≥ 180 cells) from 10 different seedlings treated with DMSO or 25 µM TE1 for 120 min (C). Scale bars, 5 µm. Error bars represent SE.

4.2.2.3 TE1 also inhibits trafficking of other membrane proteins

PIN2 proteins are synthesised in the ER and undergo trafficking through the endomembrane compartments (Grunewald and Friml, 2010). This process is common to other membrane proteins. Therefore to determine the specificity of TE1, its effect on other membrane proteins known to be recycled through endosomal compartments were examined. In the root epidermis cells, effects of TE1 were tested on auxin influx carrier AUX1 (Figure 4.4A and B), brassinosteroid receptor BRI1 (Figure 4.4C and D) and aquaporin PIP2a (Figure 4.4E and F). Effects of TE1 were also tested on auxin efflux carrier PIN7 (Figure 4.4G and H) in the root columella.

In the DMSO control, fluorescence is mostly visualised in the PM for all the membrane markers, AUX1-YFP, BRI1-GFP, PIN7-GFP and PIN2a-GFP (Figure 4.4A, C, E and G). Some intracellular bodies are also observed in DMSO control in AUX1-YFP and BRI1-GFP (Figure 4.4A and C) suggesting that at the steady state more of these proteins reside in the intracellular compartments compared to PIN2-GFP (Figure 4.2A), PIN7-GFP (Figure 4.4E) and PIP2a (Figure 4.4G). Unlike PIN2-GFP, 120 min incubation at 25 µM TE1 did not cause any visible effect on the localisation of AUX1-YFP or BRI1-GFP. However, increased intracellular accumulations were clearly seen when AUX1-YFP and BRI1-GFP seedlings were incubated for 180 min in medium containing 35 µM TE1 (Figure 4.4B and D). Similarly to PIN2-GFP, seedlings expressing PIN7-GFP and PIP2a-GFP incubated in 25 µM TE1 for 120 min also displayed intracellular accumulation in the TE1 bodies (Figure 4.4F and H). These results show that TE1 interferes with trafficking of all these plasma membrane proteins regardless of whether they localise apically like PIN2 in epidermis, basally like PIN2 in cortex or if they are non-polarised like PIP2a and PIN7 in columella in the PM. TE1 sensitivity displayed by PIN7-GFP at the root columella and other membrane proteins at the root epidermis also shows that the immediate effect of TE1 is not only limited to one cell type.
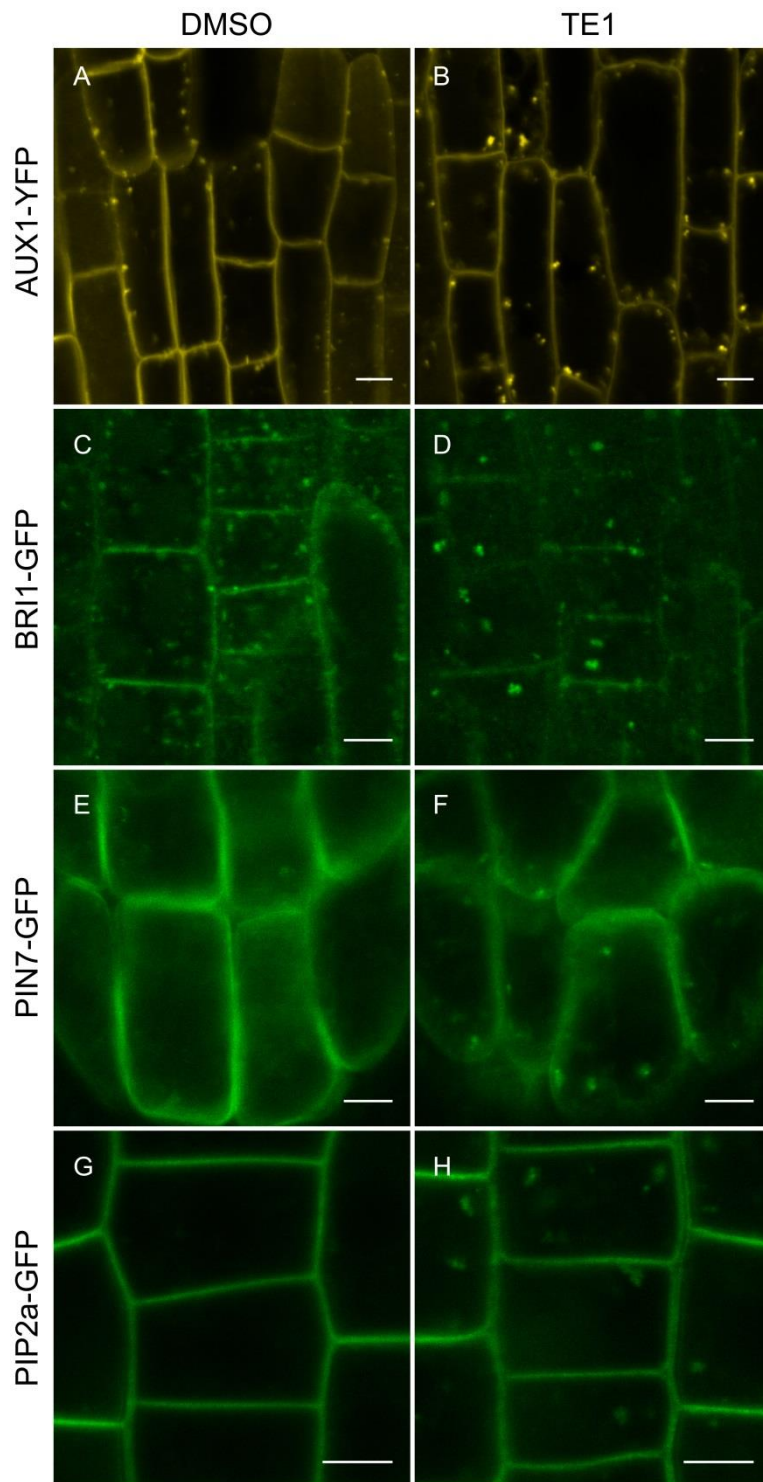
Figure 4.4. TE1 also interrupts trafficking of other membrane proteins.

Roots epidermis of *Arabidopsis thaliana* seedlings expressing AUX1-YFP incubated for 180 min in DMSO (A) and 35 µM TE1 (B), BRI1-GFP 180 min in DMSO (C) and 35 µM TE1 (D), PIN7-GFP for 120 min in DMSO (E) and 25 µM TE1 (F), and PIP2a-GFP 120 min in DMSO (G) and 25 µM TE1 (H), respectively. Scale bars, 5 µm.

4.2.3 Determining the effect of TE1 on endocytosis from the plasma membrane

4.2.3.1 Protein accumulating in TE1 induced compartments does not originate from the plasma membrane

TE1 induces intracellular accumulation of several membrane proteins. This led to a hypothesis that increased endocytosis in the presence of TE1 may shift the balance of endocytic recycling components causing intracellular accumulation. Therefore, it is important to determine the origin of the proteins in the TE1 induced compartments to elucidate the mechanism of TE1 action. To independently assess the role of TE1 in membrane recycling, BFA and auxin were used as pharmacological tools to modulate specific stages of endocytic protein recycling in plants expressing PIN2-GFP. Auxin has been shown to inhibit clathrin-mediated endocytosis of PIN proteins (Paciorek et al., 2005; Robert et al., 2010).

In 0.2% DMSO, PIN2 accumulation is not visible in the intracellular compartments (Figure 4.5A). However, intracellular PIN2 accumulation was visualised after 120 min incubation at 25 µM TE1 (Figure 4.5C). Similarly, 50 µM BFA caused accumulation of PIN2 in BFA bodies after 60 min treatment (Figure 4.5B). Accumulation of PIN2 in BFA bodies was prevented in seedlings pre-treated with 5 µM 1-Naphthaleneacetic acid (NAA) for 30 min (Figure 4.5E) (Paciorek et al., 2005). In contrast, inhibition of PIN2 internalisation with NAA did not prevent the accumulation of PIN2 in the TE1 bodies (Figure 4.5F), suggesting that PIN2 proteins agglomerating in TE1 bodies did not originate from the PM. This result contradicts the hypothesis that in the presence of TE1, increased endocytosis of PIN2 protein leads to protein accumulation at the TE1 compartment. The result suggests that the proteins contained within the TE1 bodies are not likely to be originating from the PM. This data also shows that TE1 has a distinct mode of action in comparison to BFA, which is known to affect protein recycling to the PM (Steinmann et al., 1999; Geldner et al., 2001). This is further backed up by the fact that NAA inhibits accumulation of PIN2 in BFA bodies however protein accumulation in the TE1 bodies is clearly visible.

Contribution of the newly synthesised proteins to the proteins accumulated in the TE1 compartments was also investigated by using cycloheximide (CHX) that is a

known inhibitor of protein biosynthesis (Geldner et al., 2001). PIN2-GFP seedlings incubated in 50 μM CHX for 150 min were comparable to DMSO control (Figure 4.5G) and as expected the BFA compartments in the presence of CHX were also visible as normal (Figure 4.5H). Surprisingly, TE1 bodies were also observed in the presence of CHX (Figure 4.5I). Taken together, these data suggest that TE1 bodies still form even if endocytosis or biosynthesis is inhibited. However, a positive control for CHX treatment was not performed together with these experiments therefore the possibility of newly synthesised proteins contributing to the protein accumulation in the TE1 bodies can not be completely ruled out.
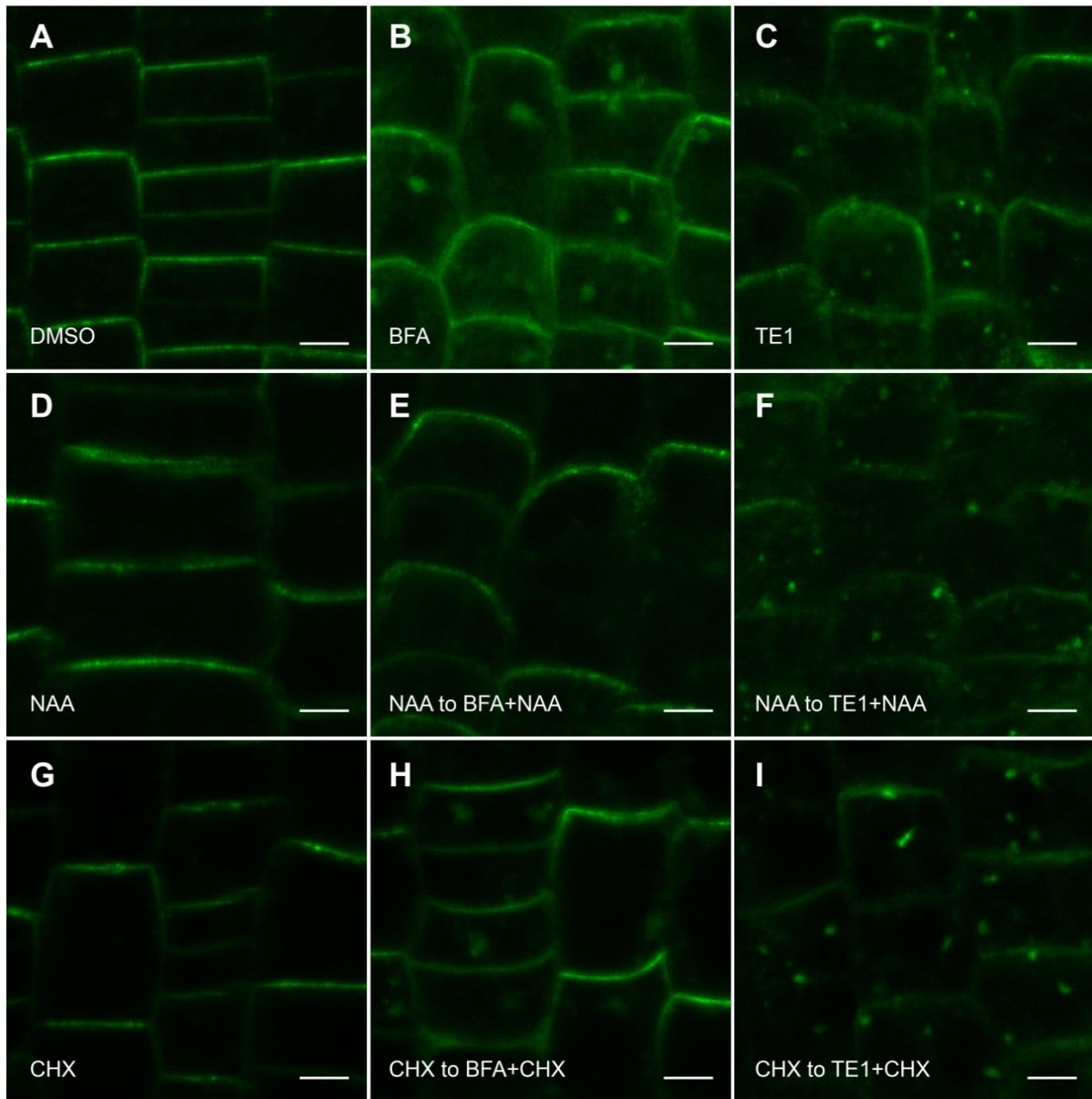
Figure 4.5. Effects of TE1 on PIN2 trafficking.

Roots of *Arabidopsis thaliana* seedlings expressing PIN2-GFP (A-I) were transplanted to DMSO control (A), 50 µM BFA for 60 min (B), 25 µM TE1 for 120 min (C), 5 µM NAA for 150 min (D), 50 µM BFA and 5 µM NAA for 60 min following pre-treatment for 30 min with 5 µM NAA (E), 25 µM TE1 and 5 µM NAA for 120 min following a pre-treatment with 5 µM NAA for 30 min (F), 50 µM CHX for 150 min (G), 50 µM CHX and 50 µM BFA for 60 min following pre-treatment for 30 min with 5 µM CHX (H), and 50 µM CHX and TE1 for 120 min following pre-treatment for 30 min with 50 µM CHX (I). Scale bars, 5 µm.

4.2.3.2 TE1 is an inhibitor of endocytosis

Examining the source of PIN2 proteins in TE1 bodies indicated that they do not originate from the PM. However, TE1 also induces intracellular accumulation of other membrane proteins such as BRI1, AUX1 and PIP2a (Figure 4.4). Therefore, the overall effect of TE1 on endocytosis was examined to determine if any of these proteins in TE1 bodies may source from the PM. A fluorescent probe, FM4-64, that binds to the lipids in the PM through its lipophilic tail was used to monitor endocytic events from the PM. FM4-64 has been widely used in plants to trace endocytosis in plants (Jelinkova et al., 2010). Furthermore, inhibition of clathrin dependent PIN2 internalisation in the presence of tyrphostin A23 (A23), an inhibitor of clathrin mediated endocytosis, did not cause complete inhibition of the FM4-64 uptake (Dhonukshe et al., 2007). Uptake of FM4-64 into the TGN compartments has been reported to take place after just 5 min (Dettmer et al., 2006). Therefore, an image was generated every minute in different seedlings from 4 min to 15 min after FM4-64 staining of seedlings that had been treated with 0.1 % DMSO or 25 µM TE1 for 120 min (Figure 4.6). In control seedlings, FM4-64 uptake was observed 5 min after staining and FM4-64 uptake was generally higher after every minute after staining (Figure 4.6 top rows). In contrast, seedlings treated with TE1 showed no FM4-64 uptake even 15 min after staining (Figure 4.6) suggesting that TE1 is an inhibitor of endocytosis. It can be concluded that endomembrane proteins contained within the TE1 bodies are not being recruited from the PM whether the protein is PIN2, AUX1, BRI1 or PIP2a. This result suggests that TE1 affects early steps of the endocytosis pathway from the PM.
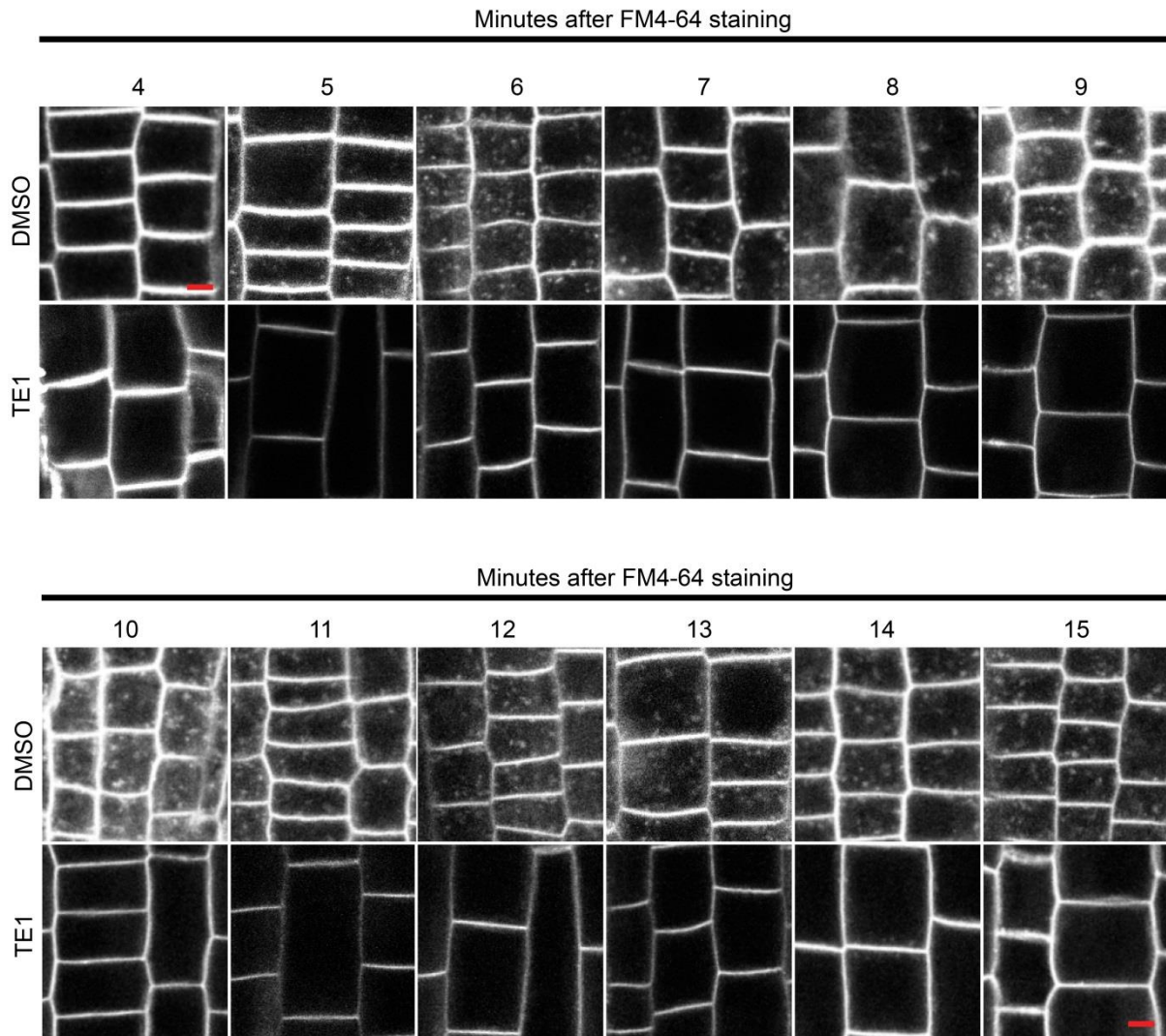
Figure 4.6. TE1 inhibits endocytosis from the plasma membrane.

7 day old wild-type (Col-0) *Arabidopsis thaliana* seedlings were incubated in DMSO (top rows) and 25 µM TE1 (bottom rows) for 120 min. Seedlings were then incubated for 5 min in medium containing 5 µM FM4-64, followed by washes in ½ MS medium ×2 at 4°C. The timer started after taking the seedlings off 4°C, and FM4-64 uptake in root epidermis was monitored from 4-15 min after FM4-64 staining. Scale bars, 5 µm.

4.2.4 Dissection of other trafficking components

4.2.4.1 TE1 does not affect the secretion of newly synthesised proteins

Trafficking of membrane proteins is inhibited by TE1 (Figure 4.2 and Figure 4.4). To investigate if trafficking to the PM and exocytosis is affected by TE1, *Arabidopsis thaliana* lines expressing secreted green fluorescent protein (secGFP) were monitored. In the control condition, secGFP is synthesised in the endoplasmic reticulum (ER) and secreted to the apoplast displaying a weak GFP signal (Figure 4.7A) (Zheng et al., 2004). Similar to the DMSO control, seedlings treated with 25 µM TE1 for 120 min showed faint accumulation of GFP in the apoplast (Figure 4.7C). However, when the trafficking to the membrane is interfered with by BFA treatment, a bright GFP signal is observed in endomembrane compartments and the ER (Figure 4.7B). This result indicates that trafficking to the PM and exocytosis is unaffected in the presence of TE1. Moreover, as the GFP signal was comparable in the presence of TE1 and DMSO, the apoplastic pH is also likely to be unaffected by TE1 as higher apoplastic pH increases GFP signal at the apoplast (Zheng et al., 2004). Increased intracellular accumulation of secGFP in the presence of BFA also indicates that newly synthesised proteins require a BFA sensitive ARF-GEF for membrane trafficking and they are likely to undergo trafficking through post-Golgi intermediate compartment that is likely to be the TGN.
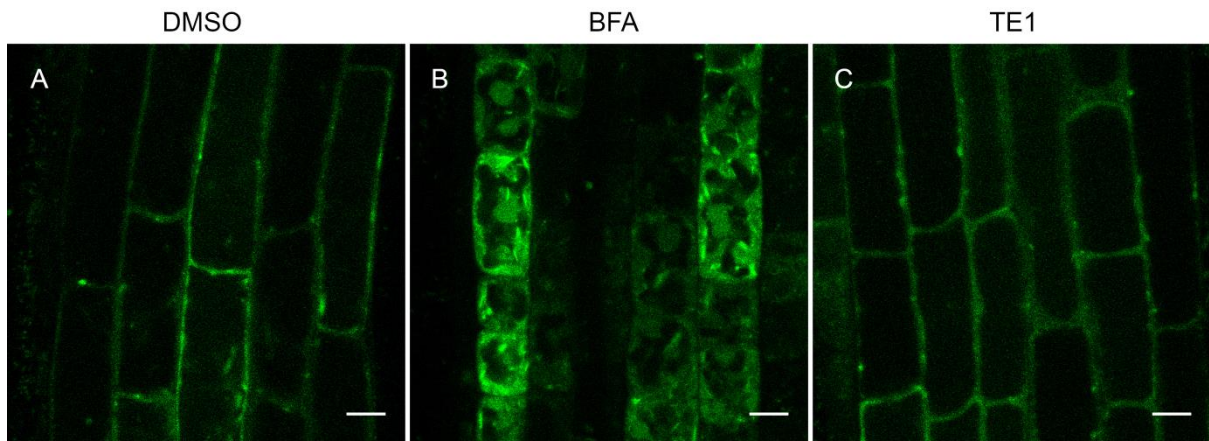
Figure 4.7. Trafficking to the membrane and exocytosis is functional in the presence of TE1.

7 day old *Arabidopsis thaliana* seedlings expressing secreted green fluorescent protein incubated in DMSO (A), 50 µM BFA (B), and 25 µM TE1 (C) for 120 min. Scale bars, 5 µm.

4.2.4.2 TE1 is unlikely to inhibit the exocytosis of membrane proteins

TE1 does not affect the secretion of secGFP (Figure 4.7) however, this does not reflect the secretion of membrane proteins that are undergoing constitutive recycling. Therefore, PIN2-GFP seedlings were used to investigate the effect of TE1 on exocytosis. Seedlings expressing PIN2-GFP incubated in 50 µM BFA for 60 min (Figure 4.8B) showed accumulation of PIN2 in BFA compartments and as expected 120 min incubation in 25 µM TE1 caused the formation of TE1 bodies (Figure 4.8C). The BFA phenotype could be recovered upon transplantation to DMSO media for 120 min (Figure 4.8D). However, when seedlings pre-treated with 50 µM BFA for 60 min were transplanted to media containing 25 µM TE1 for 120 min, the BFA compartments were recovered (not visualised) but TE1 compartments were visualised (Figure 4.8E). And finally, intracellular PIN2 accumulation could be recovered in seedlings pre-treated with 50 µM BFA for 60 min followed by 25 µM TE1 for 120 min and washed out to compound free media for 180 min (Figure 4.8F). These show that BFA bodies can be recovered in the presence of TE1, which suggest that TE1 does not inhibit the secretion of membrane proteins, unless they are directly diverted to TE1 compartments after BFA transplantation to the TE1.
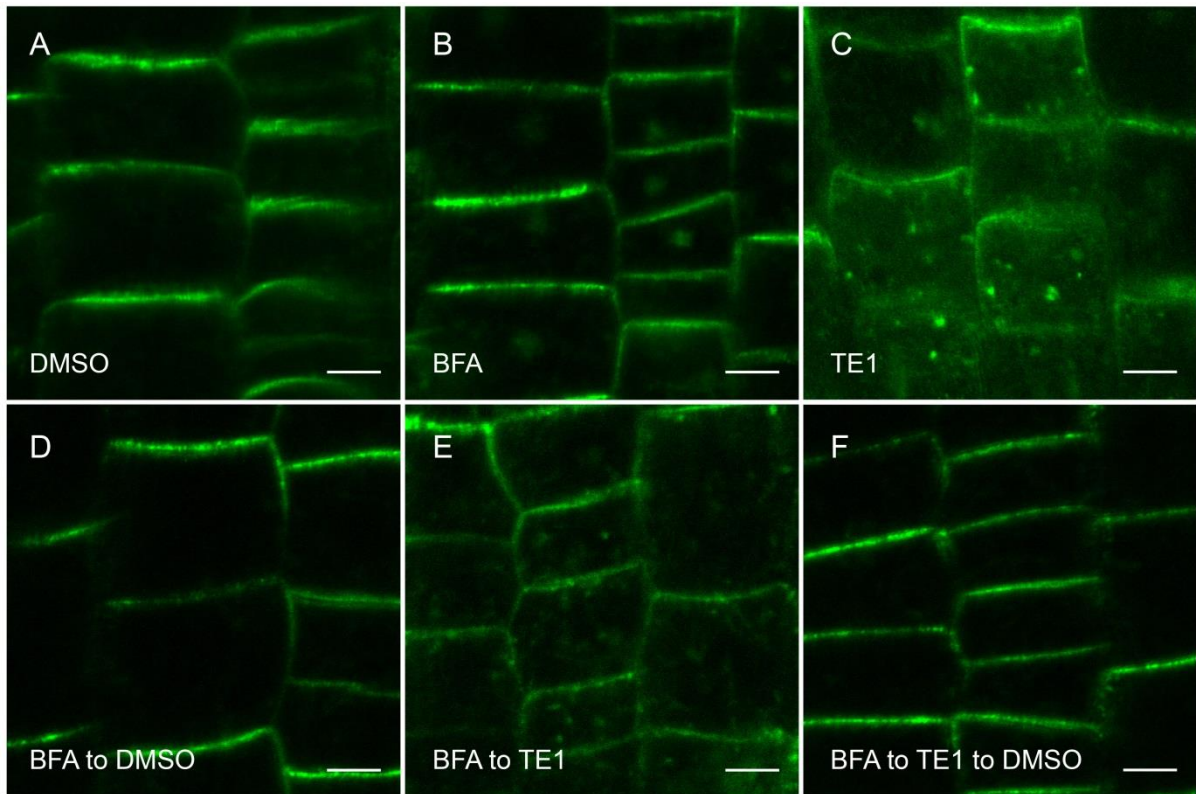
Figure 4.8. BFA bodies maybe recovered in the presence of TE1.

PIN2-GFP seedlings were incubated in DMSO for 6 h (A), 50 µM BFA for 60 min (B) and 25 µM TE1 for 120 min (C). Following 60 min incubation in 50 µM BFA, PIN2-GFP seedlings were also transplanted to DMSO for 120 min (D), 25 µM TE1 for 120 min (E) and finally to TE1 for 120 min followed by washout in DMSO for 180 min (F). Scale bars, 5 µm.

4.2.4.3 Trafficking to the vacuole is functional in the presence of TE1

So far, it is now established that TE1 does not affect the trafficking to the membrane (Figure 4.7) and it seems to inhibit endocytosis (Figure 4.6). Therefore the excess membrane in the TE1 compartments is unlikely to source from the PM (Figure 4.5 and Figure 4.6). Therefore it was hypothesised that the late vacuolar trafficking events to the vacuole may be affected by the action of TE1 causing the intracellular accumulation observed after short-term treatment. The effect of TE1 on vacuolar trafficking was tested by investigating PIN2-GFP trafficking to the lytic vacuole by taking advantage of GFP stability in the lytic vacuole in the dark (Tamura et al., 2003).

Some lytic vacuole labelling with PIN2-GFP was observed in the DMSO control at 6 h in the dark (Figure 4.9A). However, in seedlings treated with 25 µM TE1 for 6 h in the dark, the intensity of GFP in the lytic vacuole was higher compared to DMSO control (Figure 4.9B). However, the intracellular TE1 bodies observed after 120 min in PIN2-GFP lines (Figure 4.2) were not seen after 6 h TE1 treatment (Figure 4.9B). Therefore, the increased vacuolar accumulation and disappearance of TE1 induced compartments after 6 h TE1 treatment suggests that protein retrieval from the late vacuolar trafficking step is also affected by TE1.
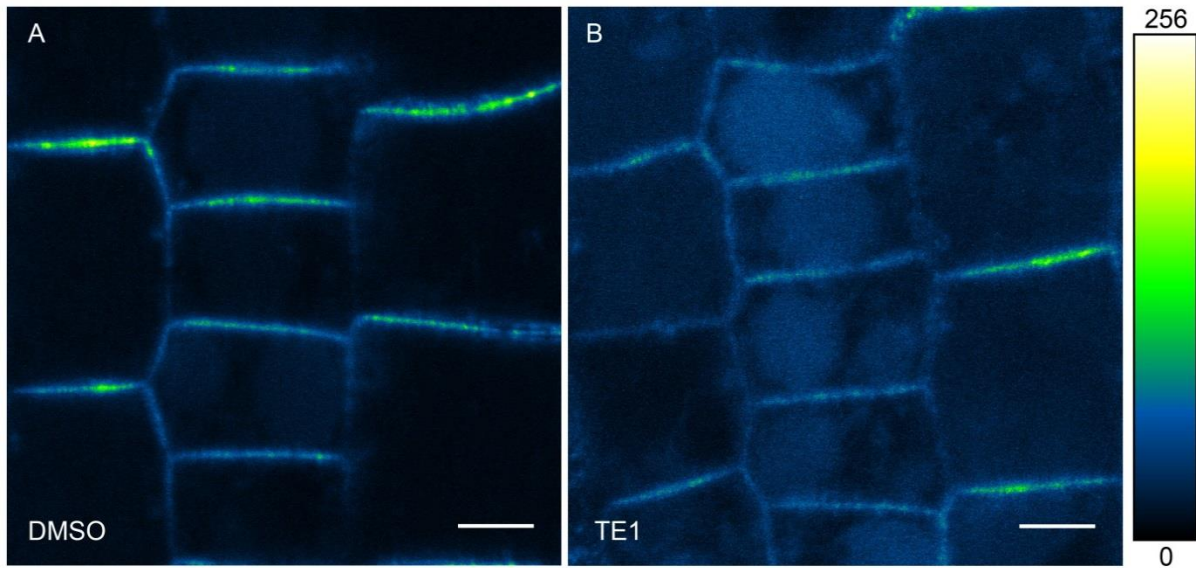
Figure 4.9. Increased vacuolar labelling is observed in the presence of TE1.

Heat map of fluorescence in seedlings expressing PIN2-GFP incubated in DMSO (A) and 25 M TE1 (B) for 6 h in the dark. Colour panel on the right displays relative intensity of PIN2-GFP from 0-256. Scale bars, 5 μm.

4.2.5 Characterising the identity of TE1 induced compartments

Using TE1 and other chemicals as dissection tools to unpick the endomembrane trafficking components has narrowed down the mode of action of TE1 towards the late vacuolar trafficking pathway. However, this conclusion would be incomplete without identification of TE1 bodies. Therefore, to identify the endomembrane compartment in which PIN2 accumulates in the presence of TE1, immuno-localisation using anti-PIN2 antibody was performed in marker lines for different endomembrane compartments (Figure 4.10 and Figure 4.11).

4.2.5.1 TE1 bodies do not co-localise with Golgi or trans-Golgi network compartments

Arabidopsis thaliana seedlings expressing N-acetylglucosaminyl transferase I (NAG)-GFP labelling Golgi (Figure 4.10A), syntaxin of plants 61 (SYP61)-CFP (Figure 4.10B), and vacuolar H^+-ATPase (VHAa1)-GFP (Figure 4.10C) labelling TGN sub-populations, were incubated in 0.1% DMSO or 25 µM TE1, then subjected to immuno detection of PIN2 proteins using anti-PIN2 antibodies. Immuno-labelling revealed that in control seedlings, native PIN2 protein behaves in the same way as the PIN2-GFP in stably transformed *Arabidopsis thaliana* lines (Figure 4.10 and Figure 4.11). As predicted, TE1 bodies identified by anti-PIN2 did not co-localise with Golgi (NAG-GFP; Figure 4.10A), or the TGN (SYP61-CFP and VHAa1-GFP; Figure 4.10B and C).
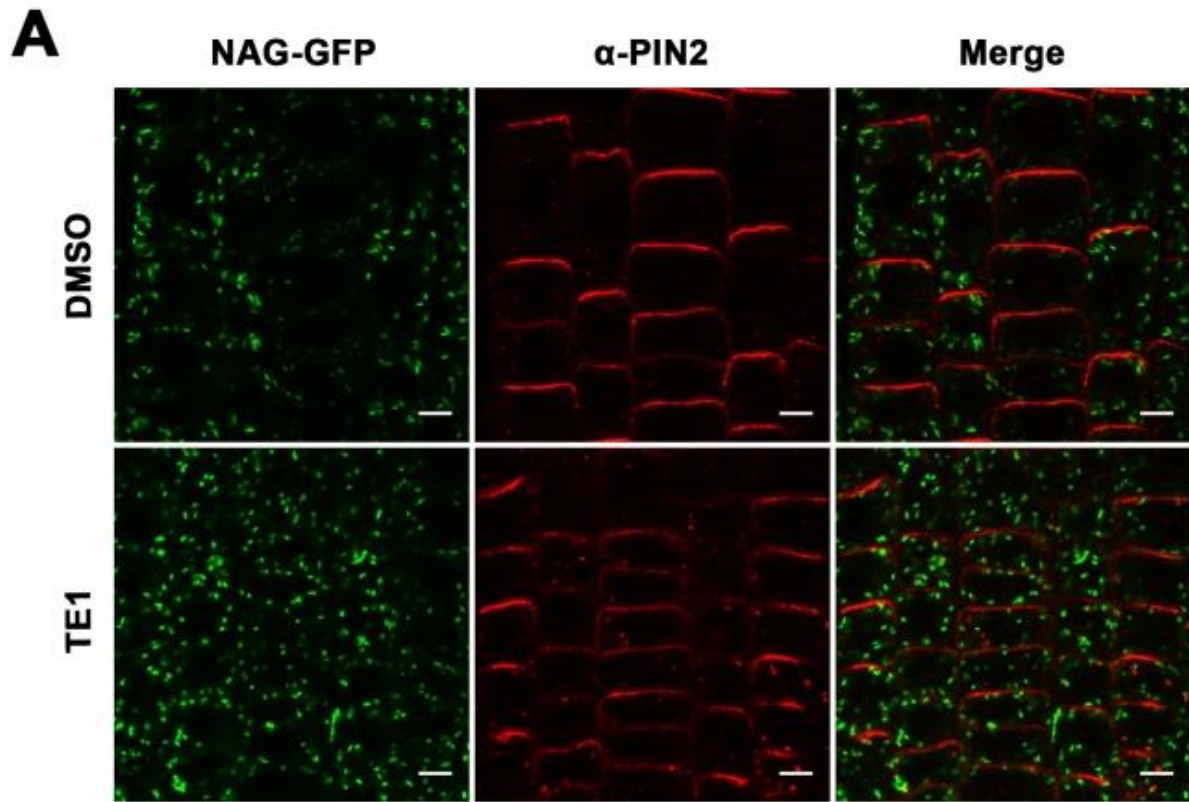
Figure 4.10A
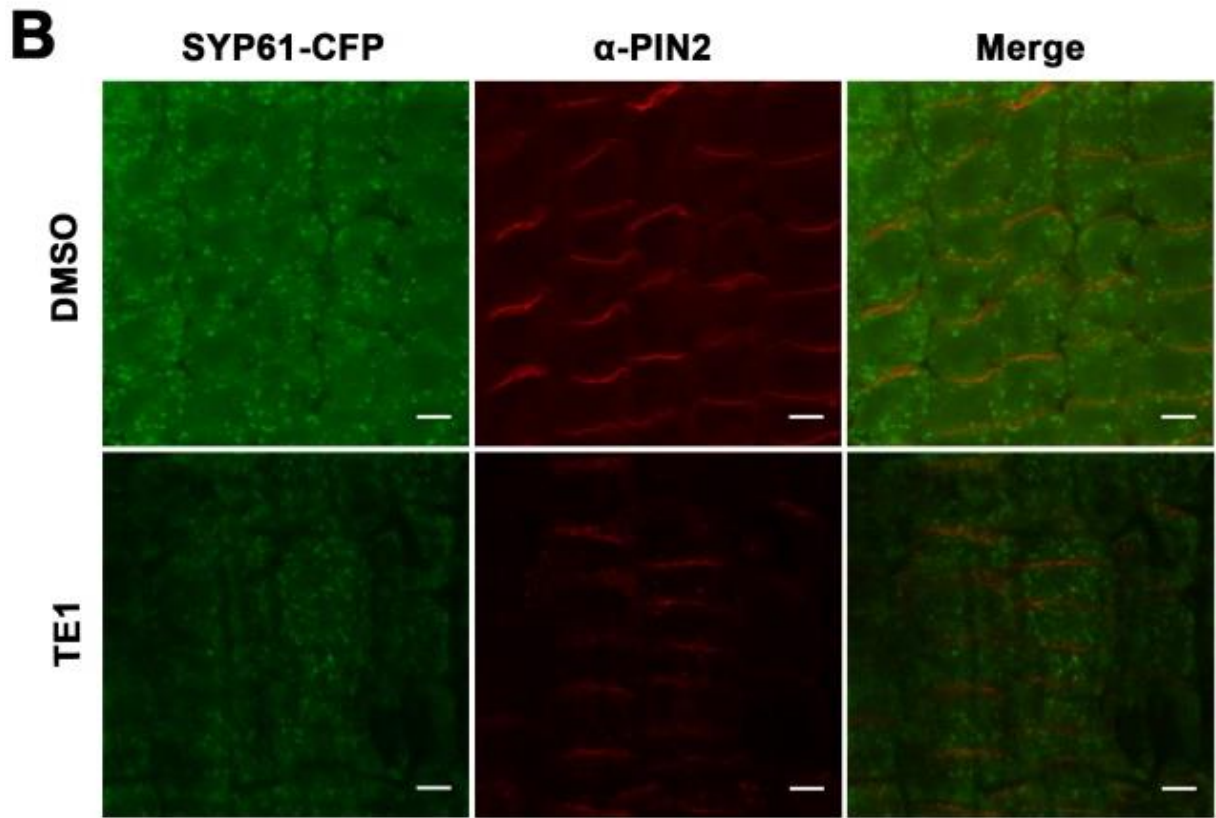
Figure 4.10B
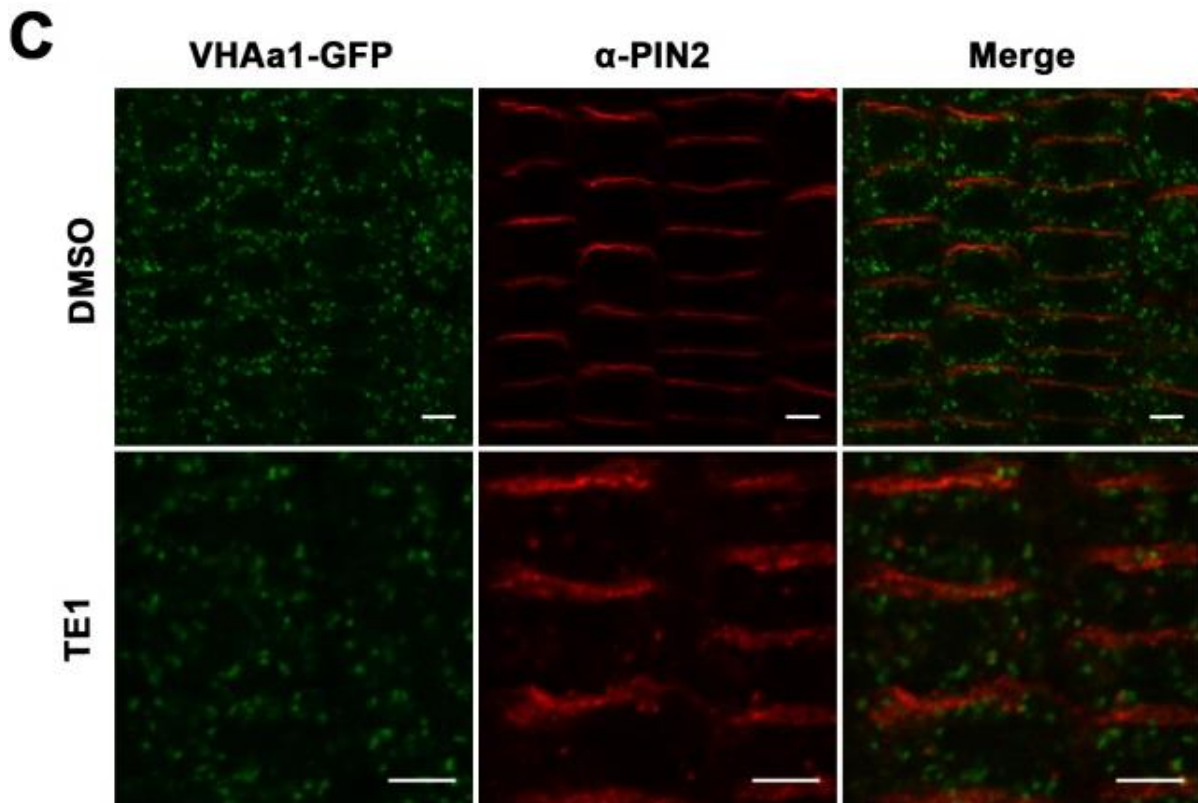
Figure 4.10. Immuno-localisation studies using anti-PIN2.

7 day old seedlings expressing NAG-GFP (A), SYP61-CFP (B) and VHAa1-GFP (C) were incubated in DMSO (top row) and 25 µM TE1 (bottom row) for 120 min and promptly fixed in 4% formaldehyde. Anti-PIN2 was used for immuno-detection of PIN2 proteins (second column). Merged images of anti-PIN2 labelling and respective endomembrane markers can be seen in the third column of each picture group. Scale bars, 5 µm.

4.2.5.2 Immuno-localisation identified TE1 bodies as the pre-vacuolar compartments

Immuno-localisation using anti-PIN2 in seedlings expressing GFP-*Arabidopsis thaliana* Rab GTPase homolog F2B (ARA7) labelling the PVC were performed as described in section 4.2.5.1. TE1 induced intracellular bodies detected with anti-PIN2 co-localised with GFP-ARA7 compartments (Figure 4.11) indicating the TE1 bodies represent the PVC. This result justifies the hypothesis that the retrieval of protein from the PVC to the TGN is inhibited by the action of TE1. Overall the results suggest that TE1 interferes with trafficking to the TGN, either from the PM or the PVC (Figure 4.12), therefore protein accumulation is visible in the PVC after short term TE1 treatment. However a prolonged exposure to TE1 leads protein accumulation to the vacuole.
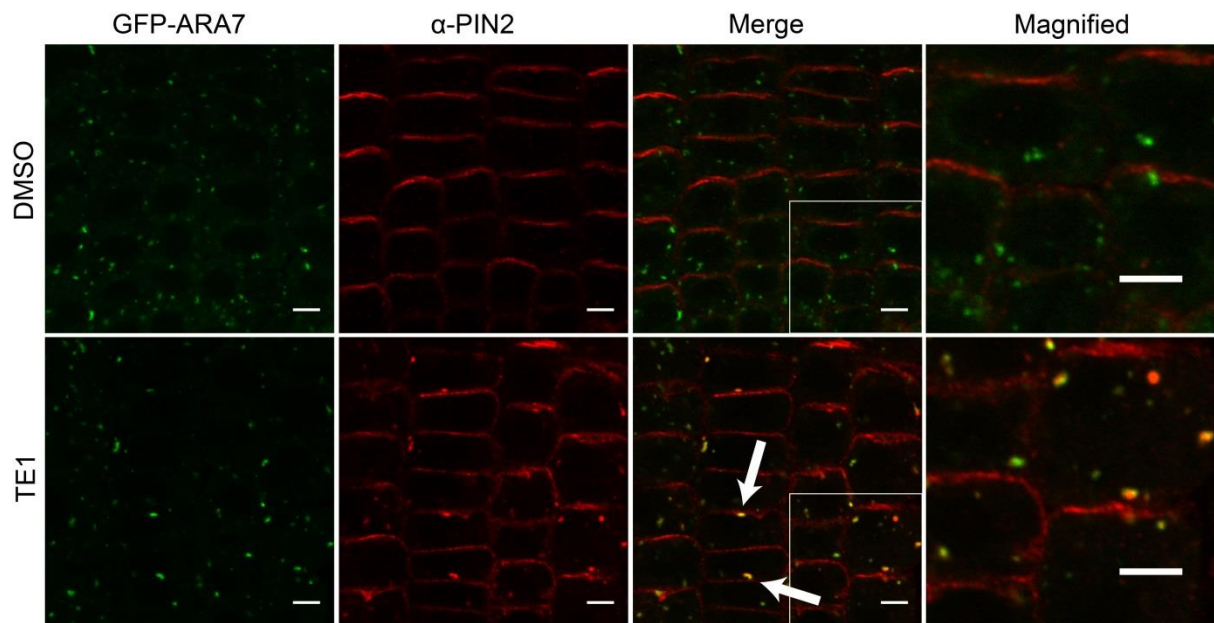
Figure 4.11. TE1 causes protein accumulation at the ARA7 compartment.

Seedlings expressing GFP-ARA7 were incubated in DMSO (top row) and 25 μM TE1 (bottom row) for 120 min. Seedlings were fixed in 4% formaldehyde and anti-PIN2 antibodies (middle column) were used for immuno-localisation of PIN2 proteins. First column shows GFP-ARA7 and last two columns is an overlap (see arrows) of GFP-ARA7 and labelling from anti-PIN2 antibodies that is shown in the second column. Scale bars, 5 μm.
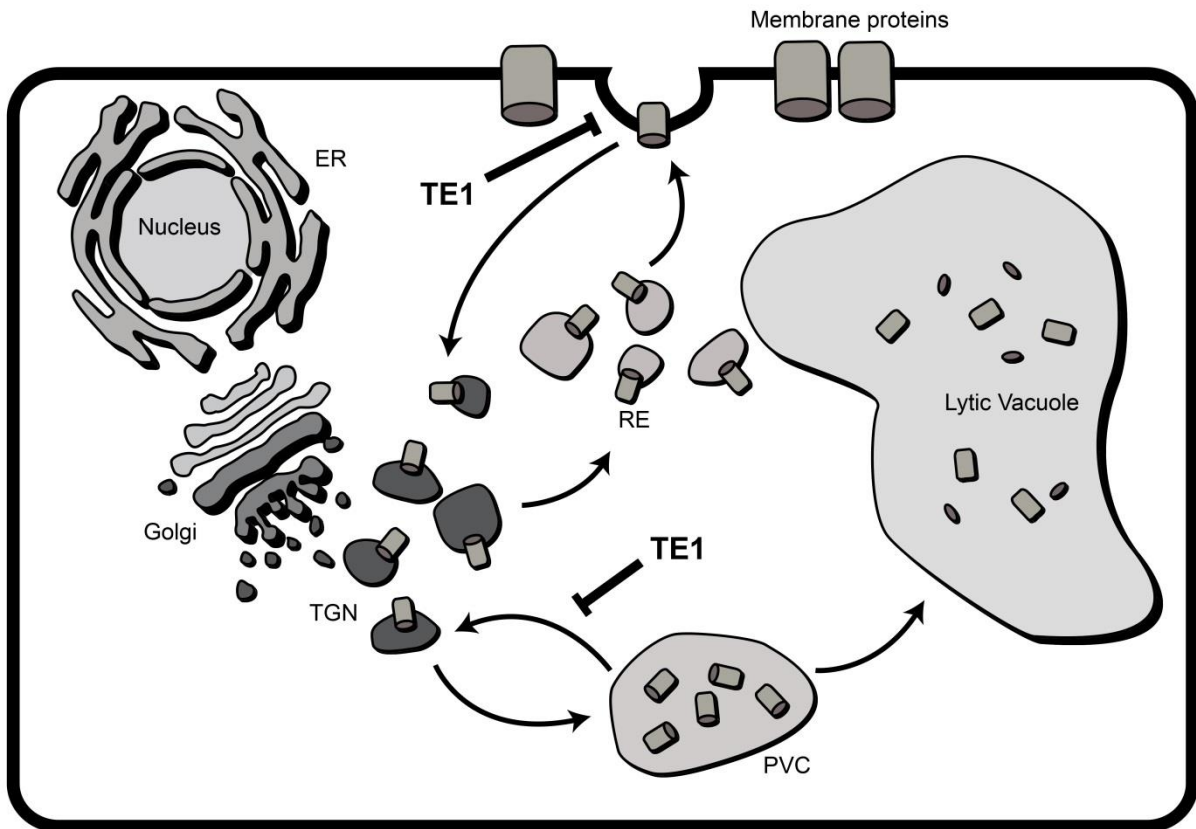
Figure 4.12. Endomembrane protein trafficking and possible mode of action of TE1.

Model shows endosomal trafficking to the plasma membrane and to the lytic vacuole via different endosome compartments and predicted mode of action of TE1.

4.2.6 Characterising the effects of TE1 on the actin cytoskeleton

4.2.6.1 TE1 does not depolymerise actin cytoskeleton at low concentrations

Intracellular agglomeration of membrane proteins has been widely reported upon depolymerisation of the actin cytoskeleton. Furthermore, actin is required for organelle movements in plants (Hawes and Satiat-Jeunemaitre, 2001) and endomembrane based trafficking also requires actin (Geldner et al., 2001; Grebe et al., 2003). Therefore, the effects of TE1 on the actin cytoskeleton and its role in the plant and cellular phenotypes observed were thoroughly investigated.

Arabidopsis thaliana roots expressing GFP fused to actin binding domain 2 (ABD2) from *Arabidopsis thaliana* fimbrin 1, which labels actin filaments, were incubated in 0.1% DMSO for 120 min. These plants showed fine filaments of the actin network throughout the cell (Figure 4.13A). Seedlings incubated in 25 µM TE1 for 120 min still displayed an actin network and filaments, and at a resolution generated by confocal microscopy they were comparable to control seedlings (Figure 4.13B). However, this is very different to the depolymerisation of actin filaments with 100 nM LatB (Figure 4.13C). In fact, even after 48 h incubation at 10 µM TE1 no visible changes in the actin network was observed (Figure 4.14, top row).

As previously demonstrated in Chapter 3, 48 h incubation in TE1 causes loss of gravitropic response in *Arabidopsis thaliana* roots at a concentration as low as 1 µM, Chapter 3 (Figure 3.20). Depolymerisation of the actin filaments by incubating the seedlings in 100 nM LatB for 120 min caused similar intracellular accumulation of PIN2-GFP (Figure 4.14, bottom row) as seen in the presence of TE1. However, this data suggests that the agravitropic growth and the inhibition of membrane trafficking caused by TE1 is not due to depolymerisation of actin filaments (Chapter 5, Figure 5.4A).
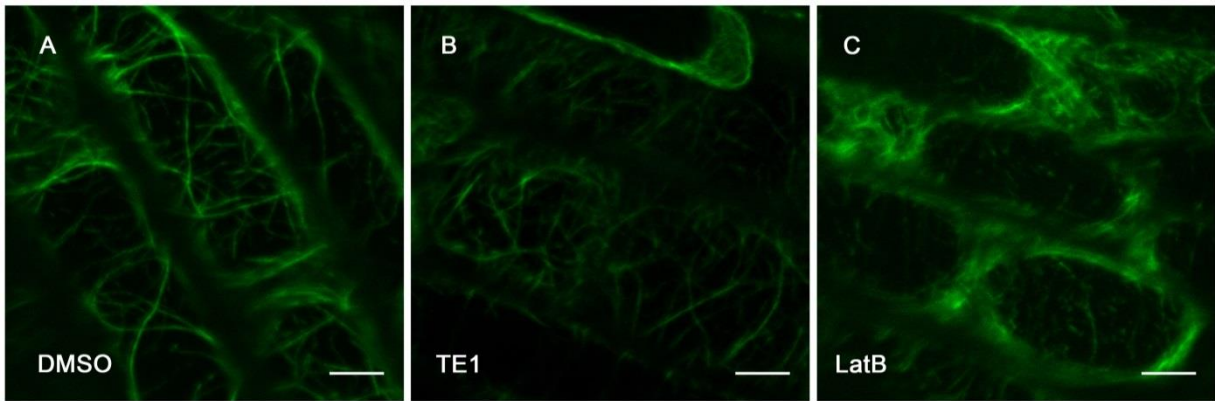
Figure 4.13. No visible effect on the actin cytoskeleton is observed in the presence of TE1.

Actin flaments visualised with GFP-ABD2 in *Arabidopsis thaliana* root incubated for 120 min in the presence of DMSO (A), 25 µM TE1 (B) and 100 nM latrunculin B (C). Scale bars, 5 µm.
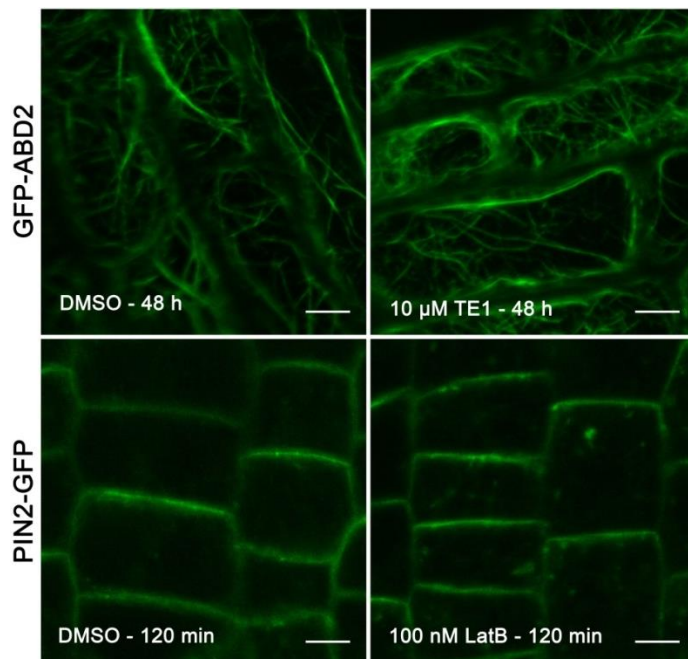
Figure 4.14. Prolonged exposure to low concentration of TE1 does not visibly affect the actin cytoskeleton.

Arabidopsis thaliana seedlings expressing GFP-ABD2 (top row) were incubated in DMSO medium (left column) and in 10 µM TE1 (right column) for 48 h. Seedlings expressing PIN2-GFP incubated (bottom row) in DMSO (left column) and in 100 nM latrunculin B (right column, bottom row) for 120 min are shown. Scale bars, 5 µm.

4.2.7 Structure activity relationship determines side-groups required for biological activity of TE1

Structure activity relationship (SAR) studies were performed to determine side groups required for biological activity of TE1. In a small scale screen, analogues of TE1 were synthesised in the laboratory by James Warren (MChem student, University of Leeds). PIN2-GFP and PIN7-GFP seedlings were incubated in medium containing 25 µM chemicals for 120 min to monitor change in PIN2/PIN7 localisation and distribution with confocal microscopy. Summarised activity of TE1 variants is shown in Figure 4.15. As shown in Table 4-1, SAR studies show that JW4, JW42, JW45, JW47 and JW48 do not show any bioactivity towards PIN2 distribution. However, JW30, JW32 and JW35 caused intracellular accumulation of PIN2-GFP after 120 min incubation as seen in the presence of TE1, although some of the activity was lost in JW35 (Figure 4.15A and Table 4-1). SAR studies performed on PIN7-GFP seedlings can also be seen in Table 4-1. JW30, JW32, JW35, JW42 and JW48 all caused increased intracellular accumulation of PIN7 in the root columella. However, JW4, JW45 and JW47 did not affect PIN7 distribution (Figure 4.15B and Table 4-1). Although intracellular accumulation of PIN7-GFP, unlike PIN2-GFP, was observed in the presence of JW42 and JW48, the biological activity was very weak (Table 4-1).
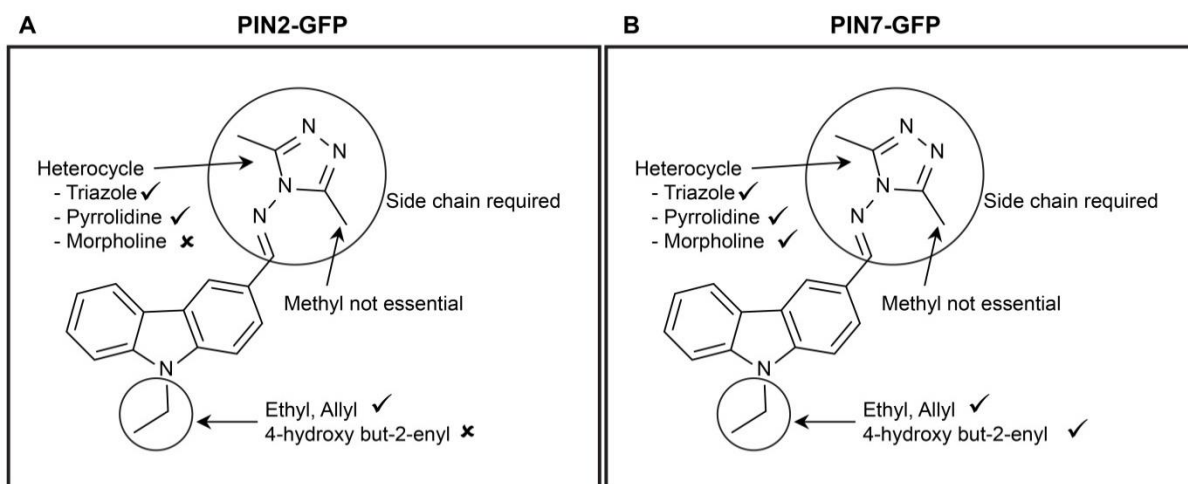
Figure 4.15. Summary of structure activity relationship (SAR) displayed by TE1 analogues on PIN2-GFP and PIN2-GFP.

SAR study performed by incubating seedlings expressing PIN2-GFP (A) and PIN7-GFP (B) in 25 µM compound for 120 min. TE1 variants were considered to be active (✓) if intracellular bodies containing PIN2-GFP/PIN7-GFP were observed in the presence of compound, and inactive (✗) if intracellular bodies were not observed after the incubation for 120 min.

Table 4-1. Biological activity of TE1 analogues in PIN2-GFP and PIN7-GFP

Chemical	Structure	PIN2-GFP after 120 min at 25 µM chemical	Active on PIN2	PIN7-GFP after 120 min at 25 µM chemical	Active on PIN7
DMSO			✗		✗
TE1 $C_{19}H_{19}N_5$ (317.4)			✓		✓
JW4 $C_{14}H_{13}N$ (195.26)			✗		✗
JW30 $C_{20}H_{19}N_5$ (329.4)			✓		✓
JW32 $C_{17}H_{15}N_5$ (289.3)			✓		✓
JW35 $C_{19}H_{21}N_3$ (291.39)			✓ weak		✓ weak
JW42 $C_{19}H_{21}N_3O$ (307.39)			✗		✓ weak
JW45 $C_{10}H_9NO$ (159.18)			✗		✗
JW47 $C_{15}H_{17}N_5$ (267.33)			✗		✗
JW48 $C_{21}H_{21}N_5O$ (359.42)			✗		✓ weak

Table 4-1. **Structure activity relationship study (SAR) of TE1 analogues.**

SAR study to identify functional group required biological activity of TE1, in different cell types, using PIN2-GFP and PIN7-GFP. Seedlings were incubated in 25 µM chemical for 120 min and intracellular accumulation of PIN2-GFP or PIN7-GFP was monitored to determine the biological activity of the compound. Scale bars, 5 µm.

4.3 Discussion

This chapter presents experiments to characterise the short-term cellular effects of the small molecule TE1. It is demonstrated that the short-term exposure to TE1 results in inhibition of endocytosis (Figure 4.6) and the accumulation of PIN2-GFP in the pre-vacuolar compartments (Figure 4.11). Overall results lead to the model as shown in Figure 4.12 and discussed in detail below. Inhibition of endomembrane protein trafficking (Figure 4.2 and Figure 4.4) and impairment of auxin redistribution (Figure 4.1) would explain the decreased gravitropism displayed upon 48 h exposure to the compound, Chapter 3 (Figure 3.20).

TE1 caused intracellular accumulation of PIN2-GFP after 120 min treatment. These intracellular bodies were not visualised upon transplanting the seedlings to DMSO medium for further 180 min (Figure 4.2). This indicates that the target binding of TE1 is not permanent and intracellular processes such as metabolism or excretion is taking place fast to alleviate the cellular phenotype caused by short term exposure to TE1. As seen in Chapter 3, growth inhibition caused by long term TE1 exposure may also be recovered (Figure 3.9). The average fluorescence intensity of GFP after 120 min in 25 μM TE1 was comparable to control, in lines expressing PIN2-GFP (Figure 4.3). This indicates that after 120 min TE1 treatment the PIN2 expression or degradation was unaffected, suggesting that proteins accumulating at the TE1 bodies arise from the steady-state. It has been shown that the synthesis and turnover of PINs is a slow process (Geldner et al., 2001). This indicates that PIN proteins present in the steady-state endomembrane compartments are enough to account for these intracellular accumulations.

TE1 is not a specific inhibitor of PIN2 trafficking since other membrane proteins such as AUX1, BRI1, PIP2a and PIN7 were also affected (Figure 4.4) although some differences in sensitivity were noted. Differential sensitivity shown to TE1 by different membrane proteins could depend on the partially overlapping mechanisms targeted by the compound, differential uptake of the compound by different cell type, rate of trafficking and endocytic recycling may vary in different membrane proteins, or the compound might display stronger binding affinity to a specific target protein compared to others. However even though the markers tested are different the target of TE1 is likely to be the same. This general effect on membrane protein trafficking

could explain the severe growth inhibition and eventual lethal effects of chronic long term TE1 exposure, Chapter 3 (Figure 3.3 – Figure 3.6).

Small molecule inhibitors of endomembrane trafficking are widely reported to affect gravitropism and plant growth, however the cellular effects of TE1 are distinct from the other compounds such as BFA (Geldner et al., 2001), ES1 (Robert et al., 2008) and wortmannin (daSilva et al., 2005). BFA treatment resulted in intracellular accumulation of PIN2-GFP in structures that were distinct in appearance from those formed upon treatment with TE1 (Figure 4.5B and C). The accumulation of PIN2-GFP in the BFA compartments could be prevented by pre-treatment with auxin as previously reported (Figure 4.5E) (Paciorek et al., 2005). However, in TE1 treated cells intracellular accumulation of PIN2-GFP were still visible in the presence of auxin (Figure 4.5F).

Addition of exogenous auxin has been proposed to bind and interfere with the function of auxin-binding protein 1 (ABP1), which contributes to the recruitment of clathrin to the PM for endocytosis (Robert et al., 2010). The contrasting observation that the intracellular accumulation caused by TE1 in the presence of auxin (Figure 4.5) and inhibition of endocytic tracer FM4-64 (Figure 4.6) indicates that TE1 causes total inhibition of endocytosis from the PM. PIN2 proteins were also observed in the TE1 bodies in the presence of protein biosynthesis inhibitor CHX (Figure 4.5G-I), suggesting that no significant contribution from newly synthesised proteins is required for protein accumulation in the TE1 bodies. Overall, the results suggest that protein in the intracellular compartments in the presence of TE1 is likely to be accumulated from proteins already within organelles of the endomembrane system prior to the addition of TE1 although newly synthesised proteins may also make a minor contribution.

The effects of TE1 on the trafficking to the membrane and exocytosis were also investigated. In the presence of TE1, *Arabidopsis thaliana* lines expressing secGFP showed GFP signal at the apoplast that was similar to the DMSO control. In the presence of TE1 all the components required for PM secretory trafficking seem to be functional and no inhibition in biosynthesis is also visible. This is consistent with TE1 inhibiting two distinct steps of membrane trafficking and retrieval of PIN2 from the PVC to the TGN (Figure 4.12) resulting in the increased directional transport of

PIN2-GFP to the vacuole over a period of several hours (Figure 4.9). However, the trafficking of secGFP to the PM/apoplast was blocked by the action BFA as indicated by the GFP accumulation in the intracellular compartments (Figure 4.7).

There has been a lot of controversies and open questions in plant membrane trafficking. One of the questions is whether BFA only specifically inhibits trafficking of proteins that are recycling back to the PM (Geldner et al., 2003) or whether proteins that are newly synthesised share a common trafficking pathway when trafficking to the membrane. There is not concrete evidence so far that suggest that an intermediate compartment is required for protein trafficking between the Golgi and the PM. Inhibition of secGFP secretion in the presence of BFA (Figure 4.7) show that there is a BFA sensitive ARF-GEF pathway required for trafficking of newly synthesised proteins to the PM. BFA does not affect the morphology of Golgi stacks in *Arabidopsis thaliana* roots (Teh and Moore, 2007), suggesting this effect is likely to take place at post-Golgi trafficking pathway. Therefore, newly synthesised proteins are likely to converge with the TGN that require ARF-GEF(s) for PM trafficking. This could also explain the existence of the sub-population of TGNs. This result however does not exclude the possibility of direct trafficking from the Golgi to the PM. To challenge this detailed understanding of trafficking from the Golgi to the TGN is necessary.

BFA bodies were also recovered to TE1 bodies when PIN2-GFP seedlings were transplanted to TE1 (Figure 4.8). This data further reiterates TE1 does not affect the secretion of proteins at the membrane. PIN proteins in the BFA compartments represent the proteins that are internalised from the membrane and being recycled back (Figure 4.5) (Paciorek et al., 2005). Therefore the recovery of the PIN2 accumulated in the BFA compartments eventually starts trafficking towards the PM. Another possibility is that proteins already in the BFA compartments may re-direct towards the TE1 bodies without being transported to the membrane. Therefore, exocytosis is unlikely to be affected by TE1, whether it is for newly synthesised proteins like secGFP or if the proteins are being recycled to the membrane like PIN2 in the BFA compartments.

PIN2 trafficking to the vacuole is inhibited with wortmannin treatment (Kleine-Vehn et al., 2008). However, higher GFP content in the lytic vacuole is observed in PIN2-

GFP seedlings treated with TE1 in the dark compared to non-treated seedlings (Figure 4.9). This result suggests that the function of PI3K, required for vacuolar trafficking, is unaffected in the presence of TE1 and that this compound has a different mode of action to wortmannin. Trafficking to the vacuole maybe up-regulated after prolonged exposure to TE1, which could disrupt the differential degradation of PIN2 protein that is required for gravitropic response (Abas et al., 2006; Kleine-Vehn et al., 2008). However, it is most likely that if the retrieval of proteins to the TGN compartments from the PVC is inhibited then both newly synthesised proteins and those cycling between intracellular endomembrane compartments may be redirected towards the vacuole (Figure 4.9 and Figure 4.12). This is supported by the finding that TE1 induced intracellular PIN2 accumulation co-localises with ARA7-GFP that is a known PVC marker (Figure 4.11).

ARA7 belongs to Rab5 family of Rab GTPases and all the Rab5 members in *Arabidopsis thaliana* can be activated by GEF VPS9a (Goh et al., 2007). A GDP-locked version of ARA7 also had an inhibitory effect on the endocytic uptake of FM4-64 (Dhonukshe et al., 2006). Recent identification of the matured form of PVC, late prevacuolar compartment (LPVC), was shown to act as an intermediate compartment between the PVC and the vacuole in tobacco leaf epidermis (Foresti et al., 2010). However, characterisation of the LPVC has not been reported in *Arabidopsis thaliana* to date. Co-localisation of Rab5 homologs, Rha1 and ARA7, revealed they both localise to the PVC (Lee et al., 2004), and recently Rha1 was shown to be localised to the LPVC in tobacco (Bottanelli et al., 2012). Overexpression of Rab5 GTPases was also reported to cause fusion of TGN with the PVC (Bottanelli et al., 2012), similarly wortmannin treatment also caused fusion of PVCs (Wang et al., 2009). However, in the presence of TE1, no homotypic fusion of Golgi or TGN with the PVC subpopulation was observed, as TE1 induced compartments did not co-localise with NAG-GFP, CYP61-CFP or VHAa1-GFP (Figure 4.10 and Figure 4.11).

Compound ES1 selectively inhibited the trafficking of membrane proteins, where it changed the distribution of BRI1 and apically localised AUX1 and PIN2, whereas basally localised PIN1 and non-polar PIN7 and PIP2a were unaffected (Robert et al., 2008). Interference of ES1 with endomembrane trafficking has recently been linked to the stabilisation of actin filaments caused by the compound (Toth et al., 2012). It is

however interesting that actin stabilisation leading to the depolymerisation by ES1 only selectively disrupted endomembrane trafficking and did not alter plants gravitropic response (Robert et al., 2008). TE1 however, affects trafficking of PIN2, AUX1, BRI1, PIP2a and PIN7.

TE1 does not have a striking effect on the organisation of the actin cytoskeleton either on short term exposure to 25 µM TE1 (Figure 4.13) or 48 h exposure to 10 µM TE1 (Figure 4.14), at least as reported by the appearance of GFP-ABD2, yet the former results in accumulation of PIN2-GFP in the PVC and the latter is an order of magnitude higher than the concentration required to affect the gravitropic response, Chapter 3 (Figure 3.20). Depolymerisation of the actin cytoskeleton is observed in the presence of 100 nM LatB (Figure 4.13). Intracellular PIN2-GFP bodies similar to TE1 bodies are also observed in seedlings treated with 100 nM LatB (Figure 4.14). However, it can be seen that even slight depolymerisation of actin filaments increases root bending in response to gravistimulation, Chapter 5 (Figure 5.4A). Similarly, enhanced gravitropism has been observed up on LatB treatment in maize (Hou et al., 2003) and *Arabidopsis thaliana* (Hou et al., 2004) roots. Depolymerisation of actin cytoskeleton inhibits PIN2 trafficking to the vacuole (Kleine-Vehn et al., 2008), however trafficking to the vacuole remains functional in the presence of TE1 (Figure 4.9). Thus it is unlikely that the cellular effects caused by TE1 are due to a direct effect on the actin cytoskeleton.

The SAR of TE1 was examined by testing the effects of a focussed library of TE1 derivatives on the trafficking of PIN2-GFP and PIN7-GFP (Figure 4.15 and Table 4-1). Taken together, SAR studies show that the carbazole core structure is crucial for the biological activity of TE1, and both the triazole head group and the alkyl chain make contributions although the latter two regions can accommodate minor modifications. Some difference in the bioactivity of the compounds were noted in PIN2 and PIN7 trafficking (Figure 4.15 and Table 4-1). Compound JW42 and JW48 did not change the localisation of PIN2, however JW42 and JW48 induced intracellular accumulation of PIN7-GFP but the biological activity was significantly reduced in these compounds in comparison to TE1.

5 Chapter Five – Identification of *Arabidopsis thaliana* natural accessions that display resistance to TENin1 and genetic mapping of the resistant loci

5.1 Introduction

Chapter 3 and Chapter 4 described long term and short term phenotypes caused by compound TE1. These include reduced gravitropic response and inhibition of root and hypocotyl growth in *Arabidopsis thaliana* seedlings ecotype Columbia (Col-0). These visual phenotypes, caused by the presence of TE1 at micromolar concentrations, make it possible to identify potential resistant mutants in a sensitive background in a forward genetic screen. Loss of function mutant populations can be generated in a number of ways and many mutant populations are available from stock centres world-wide. The initial mutant population may be generated by using a commonly used mutagen such as ethyl methanesulphonate (EMS), which alkylates G bases by adding a methyl group, causing mispairing of the bases. Therefore, instead of pairing with C, an alkylated G pairs with T, resulting in C/G to T/A substitutions (Maple and Moller, 2007).

Mutagenesis by EMS permits the generation of a high level of non-biased point mutations therefore relatively few seeds are required to perform the forward genetic screen. However, only a small number of these point mutations actually cause loss of function of the gene. These may be achieved when a base pair change leads to change in critical amino acid required for protein function or if a premature stop codon is introduced. Another problem with this approach is that individual plants carry multiple mutations, requiring extensive back crossing to isolate the mutation that gives rise to the phenotype of interest and the position of the point mutation is unknown which makes the cloning of the EMS induced mutagenised gene technically demanding and time consuming. This generally requires the identification of tightly linked molecular markers that co-segregate with the phenotype of interest in a mapping population generated by crossing two different accessions that have sufficient genetic variation to allow unique molecular markers to be designed. Although now as the cost of sequencing has fallen rapidly complete genome re-sequencing is a viable alternative to identify causal mutations (Jander et al., 2002).

Another way to generate mutant populations is by insertional mutagenesis, where foreign DNA is inserted into random genomic sites, that can be generated by Agrobacterium mediated transferred DNA (T-DNA) transformation (Alonso et al., 2003), or from maize transposable elements (Parinov et al., 1999). These biological insertions occur at low frequencies and therefore a large number of mutants need to be screened in order to identify candidate genes in a forward genetics screen. However, these insertions act as a molecular marker therefore providing a strong starting point for map based cloning (Liu et al., 1995) or direct isolation of the tagged gene via plasmid rescue or PCR (Sessions et al., 2002). By placing a strong promoter/enhancer adjacent to the border of the T-DNA insertion lines with constitutive over expression of downstream genes can be produced (Weigel et al., 2000).

A third potential way of identifying target genes in *Arabidopsis thaliana* is by exploiting large genotypic and phenotypic variation in wild-type lines. These lines are collected from different geographic locations and therefore are referred as ecotypes or accessions (a more neutral term that does not exclude the fact that the local adaptation may not occur within the ecotype). Over 6,000 *Arabidopsis thaliana* accessions have been collected throughout the world (Weigel and Mott, 2009) and there are now several hundreds of *Arabidopsis thaliana* ecotypes that may be purchased from the Arabidopsis stock centre (http://*Arabidopsis*.info/ or https://abrc.osu.edu/). Therefore, *Arabidopsis thaliana* is an excellent model to study natural variation because of the extensive resources (Koornneef et al., 2004). This approach was successfully used to isolate the target gene for the small molecule hypostatin (Zhao et al., 2007).

First an accession or accessions that differ from the reference accession with respect to the phenotype are identified and the inheritance determined by carrying out appropriate crosses. This determines whether the phenotype corresponds to the inheritance of a single gene or multiple genes, whether the phenotype is dominant or recessive and whether it shows discrete or quantitative variation. If the latter, it is determined a quantitative trait and the loci that determine that trait are termed Quantative Trait Locus (QTL). Therefore, a QTL may be defined as a region of the genome that is associated with an effect on a quantitative trait, which may contain anything between a single gene to thousands of genes. These resources may be

used to map the locus leading to the identification of the genetic source of the phenotype of interest at a high resolution up to single nucleotide polymorphism (Lukowitz et al., 2000; Peters et al., 2003). The *Arabidopsis thaliana* resources that allow the mapping of genes of interest include recombinant inbred lines (RILs) that are usually generated by crossing two different accessions (Figure 5.1), that display difference in the trait of interest, and a genetic map may be created using several molecular markers (Lister and Dean, 1993). A RIL population is essentially a permanent mapping population that can be rescreened many times. Screening a population of RILs allows the identification of the region that contains the mutated gene or QTL(s) responsible for the trait in question. In principle, fully sequenced genomes and high level of nucleotide polymorphisms allow a fast identification. The main disadvantage of using this approach is the resolution of the mapping population. Although mapping resolution is defined by the size of the mapping population, the size of the QTL region may vary from 5 to 20 cM (Wilson et al., 2001; Loudet et al., 2002). This region usually contains hundreds of candidate genes with the coverage up to 5 Mb in the chromosome region. Therefore, once the region that the QTL responsible for the phenotype is identified then there are several fine mapping strategies that may be employed to identify the candidate gene (Lukowitz et al., 2000; Peters et al., 2003). There are several factors that may affect QTL detection that need to be taken into consideration. Some examples include the number of segregating genes in a mapping population, coverage and density of markers, size of the mapping population, variability of the trait screened, and the number of genes controlling the variation in traits.
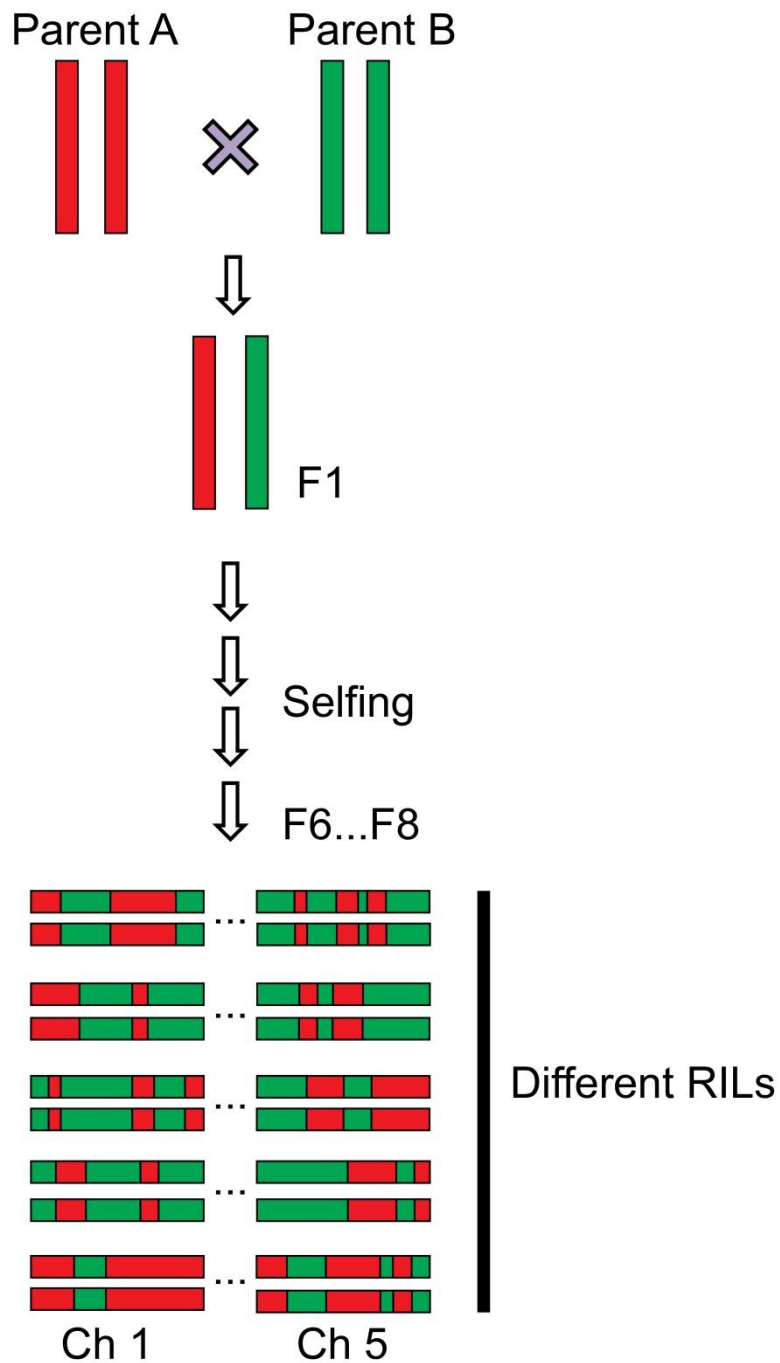
Figure 5.1. Generating recombinant inbred lines (RILs).

Parent A and Parent B that are genetically distant are crossed to generate F1 population. From the F1, RILs are generated by allowing selfing until the F6 to F8 generations, therefore the lines generated are close to homozygosity saturation. Several different RILs can be generated using this way each line containing different genetic regions, generated by recombination events passed on through the generations, from parent A or B within their chromosomes (Ch1 to Ch5).

Arabidopsis thaliana accessions can be highly divergent therefore molecular markers required for fine mapping may be generated. Some of the commonly used PCR based fine mapping techniques use molecular markers such as cleaved amplified polymorphic sequences (CAPS) and simple sequence length polymorphisms (SSLPs). CAPS shows differences in restriction fragment length polymorphism (RFLP) when amplified DNA fragments, generated by PCR using locus-specific primers, are digested with restriction enzymes (Konieczny and Ausubel, 1993). The number of fragments or length generated after restriction endonuclease digestion may be different depending on the single nucleotide polymorphisms (SNPs) between the two accessions that alter restriction enzymes recognition sites (Figure 5.2). SSLPs also use PCR amplified gene fragments of interest that display variability in short repeated sequences therefore allowing identification of different fragment size polymorphisms (Bell and Ecker, 1994).

The aim of this chapter was to use *Arabidopsis thaliana* natural accessions that display altered sensitivity to the effects of TE1 to gain information about the possible molecular target(s) of TE1. The initial screen of 80 different accessions, was performed by Adam Jamaluddin (MSc student, University of Leeds) which revealed two *Arabidopsis thaliana* accessions that display decreased sensitivity to the effects of TE1, including resistance to the agravitropic growth, increased primary root length and higher seedling survival percentage in the presence of TE1. I independently confirmed these results, investigated the inheritance of the resistant phenotype and using a RILs population derived from a cross between one of the resistant accessions, Shahdara, and sensitive accession, Col-0, to identify a locus on chromosome 5 that contains a QTL for increased resistance to TE1.
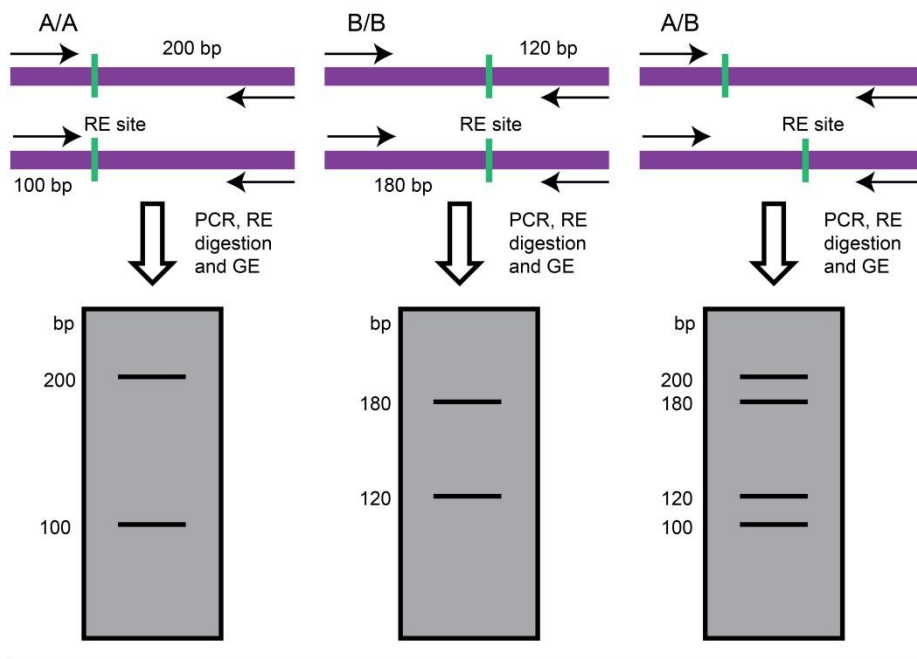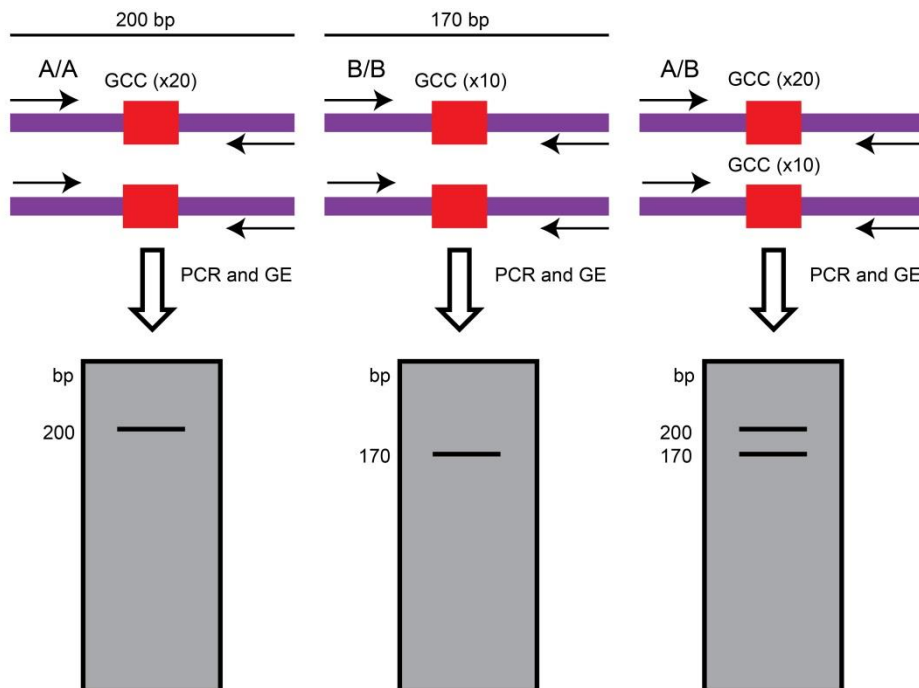
Figure 5.2. Cleaved amplified polymorphic sequence (CAPS) and simple sequence length polymorphism (SSLP) markers for gene mapping.

RE; restriction endonuclease, PCR; polymerase chain reaction, GE; gel electrophoresis. Green lines represent RE digestion site, and red box represent repeated sequences.

5.2 Identification of two *Arabidopsis thaliana* accessions that display reduced sensitivity to the effects of TE1

As discussed above, *Arabidopsis thaliana* is an excellent model to study natural variation (Koornneef et al., 2004). The 1001 Genomes Project aimed to sequence the genome of 1001 *Arabidopsis thaliana* accessions to discover the whole-genome sequence variation. From the selected 1001 accessions, genome information is now available for 80 (Cao et al., 2011). To take advantage of *Arabidopsis thaliana* genetic variation in response to compound TE1, the 80 *Arabidopsis thaliana* accessions from 1001 Genomes Project, along with Columbia (Col-0), Landsberg erecta (Ler) and Wassilewskija (Ws2), were screened (by Adam Jamaluddin, MSc student, University of Leeds) to identify ecotypes that display altered sensitivity to the effects of 1 μM or 2 μM TE1 (Figure 5.3 and Table 5-1).

Primary screening selected for accessions that displayed germination rates higher than 50%, with an average root length of 20 ± 5 mm in 7 day old seedlings, and these were taken forward to the secondary screen that tested gravitropic response in the presence of 2 μM TE1. The gravitropic response assay was performed as described in Chapter 3. Seedlings were grown on ½ MS media for 6 days followed by transplantation for 48 h to fresh ½ MS media containing 0.1% DMSO or 2 μM TE1. The transplanted seedlings were also gravistimulated at 90° for the duration of 48 h. Root growth was also monitored during this 48 h transplant period to see if root growth was comparable for DMSO control and at 2 μM TE1. At 2 μM TE1 root growth of all 39 ecotypes after 48 h transplant were comparable to the DMSO control. The secondary screen yielded twenty ecotypes that displayed some resistance to reduced gravitropic response caused by TE1 (Figure 5.3 and Table 5-1). These twenty ecotypes were re-tested in a tertiary screen that confirmed Shahdara (Sha) and Heiligkreuztal 2 (HKT2-4) to display reduced sensitivity to the effects of TE1 (Figure 5.3 and Table 5-1).
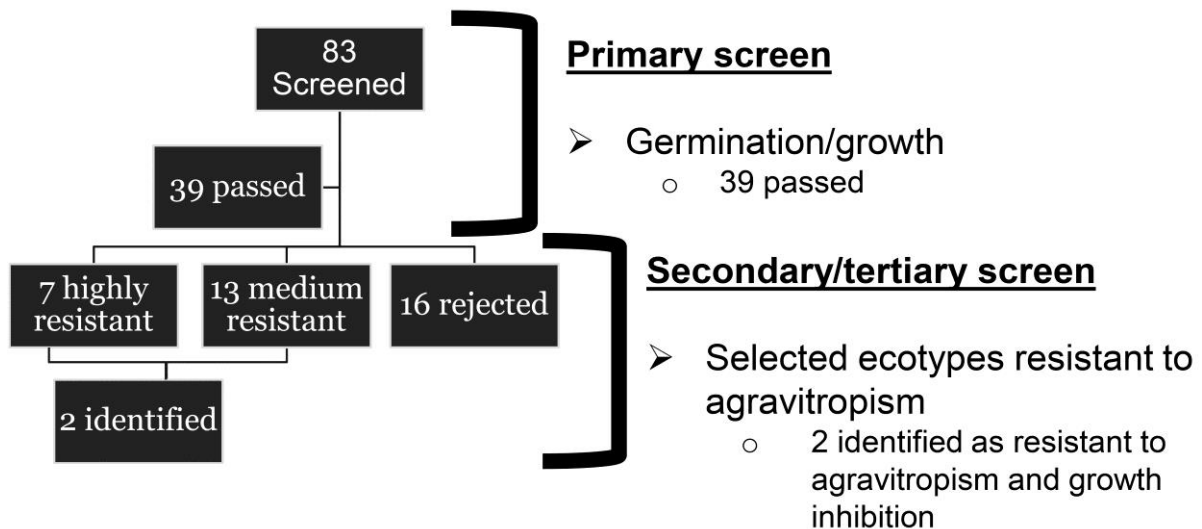
Figure 5.3. Screen to identify *Arabidopsis thaliana* accession(s) that display altered sensitivity to TE1.

83 *Arabidopsis thaliana* accessions were screened in the primary screen of which 39 accessions were taken forward to secondary screen. 47 *Arabidopsis thaliana* accessions that displayed poor germination percentage and growth were excluded at this point. The secondary screen to identify accessions that display resistance to agravitropic growth caused by TE1 resulted in 7 highly resistant and 13 medium resistant ecotypes. These were re-screened for agravitropism in a tertiary screen and two *Arabidopsis thaliana* accessions were identified to display altered resistant to TE1. This screen was performed by Adam Jamaluddin (MSc student, University of Leeds).

NASC Code	Name	Primary	Secondary	Tertiary
N1092	Col-0	✓*	✗*	✗*
N1642	Ler	✓*	✗*	✗*
N1601	Ws2	✓	✗	
N76347	Aitba-2	✗		
N76348	Toufl-1	✗		
N76349	Vezzano-2	✗		
N76350	Vezzano-2	✗		
N76351	Rovero-1	✗		
N76352	Voeran-1	✗		
N76353	Altenb-2	✓	✓	✗
N76354	Mitterberg-1	✓	✓	✗
N76355	Castelfed-4	✓	✓	✗
N76356	Castelfed-4	✓	✓	✗
N76357	Bozen-1	✓	✓	✗
N76358	Bozen-1	✓	✓	✗
N76359	Ciste-1	✗		
N76360	Ciste-2	✗		
N76361	Monte-1	✗		
N76362	Angel-1	✗		
N76363	Moran-1	✓	✗	
N76364	Mammo-2	✓	✗	
N76365	Mammo-1	✗		
N76366	Angit-1	✗		
N76367	Lago-1	✗		
N76368	Apost-1	✗		
N76369	Dobra-1	✗		
N76370	Petro-1	✓	✓	✗
N76371	Lecho-1	✓	✓	✗
N76372	Jablo-1	✗		
N76373	Bolin-1	✓	✓	✗
N76374	Shigu-2	✓	✓	✗
N76375	Shigu-1	✗		
N76376	Kidr-1	✓	✗	
N76377	Stepn-2	✗		
N76378	Stepn-1	✓	✗	
N76379	Sij1	✓	✗	
N76380	Sij2	✓	✗	
N76381	Sij4	✗		
N76382	Sha	✓	✓	✓
N76383	Koz2	✓	✗	
N76384	Kly4	✗		
N76385	Kly1	✓	✗	
N76386	Dog-4	✓	✗	
N76387	Xan-1	✗		
N76388	Lerik1-3	✗		
N76389	Istisu-1	✓	✗	
N76390	Lag2-2	✓	✗	
N76391	Vash-1	✗		

N76392	Bak-2	✓	✓	✗
N76393	Bak-7	✗		
N76394	Yeg-1	✓	✗	
N76395	Kastel-1	✗		
N76396	Koch-1	✓	✗	
N76397	Del-10	✗		
N76398	Nemrut-1	✗		
N76399	Ey1.5-2	✓	✓	✗
N76400	Star-8	✗		
N76401	Tu-Scha-9	✗		
N76402	Nie1-2	✓	✓	✗
N76403	Tu-SB30-3	✓	✗	
N76404	HKT2-4	✓	✓	✓
N76405	Tu-Wa1-2	✗		
N76406	Ru3.1-31	✓	✓	✗
N76407	Tu-V-13	✗		
N76408	Wal-HasB-4	✗		
N76409	Agu-1	✗		
N76410	Cdm-0	✗		
N76411	Don-0	✗		
N76412	Fei-0	✓	✗	
N76413	Leo-1	✗		
N76414	Mer-6	✗		
N76415	Ped-0	✗		
N76416	Pra-6	✗		
N76417	Qui-0	✗		
N76418	Vie-0	✗		
N76419	Slavi-1	✓	✓	✗
N76420	Copac-1	✗		
N76421	Borsk-2	✓	✓	✗
N76422	Krazo-2	✓	✓	✗
N76423	Galdo-1	✗		
N76424	Timpo-1	✗		
N76425	Valsi-1	✓	✓	✗
N76426	Leb-3	✓	✗	

Table 5-1. The list of *Arabidopsis thaliana* ecotypes screened against TE1.

Nottingham Arabidopsis Stock Centre (NASC) code and the accession name are shown in the first column and the second column respectively. Third, fourth and fifth column show primary screen for growth/germination, gravitropism and re-screening to confirm gravitropism, respectively. ✓; passed therefore taken forward to next screen, ✗; failed therefore dropped from the screen, and *; used as control even if it did not pass through the screen. This screen was performed by Adam Jamaluddin (MSc student, University of Leeds).

5.2.1 *Arabidopsis thaliana* accessions Sha and HKT2-4 display resistance to the reduced gravitropic bending observed in reference accessions Col-0 and Ler

The two *Arabidopsis thaliana* natural accessions, Sha and HKT2-4, which displayed resistance to reduced gravitropic response caused by TE1, identified by Adam Jamaluddin were re-tested. 6 day old seedlings grown on ½ MS media containing 0.1% DMSO were transplanted to ½ MS media containing 0.1% DMSO, 1 µM TE1 and 2 µM TE1, respectively, and gravistimulated at 90°. After 48 h transplantation and gravistimulation at 90°, sensitive *Arabidopsis thaliana* accessions, Col-0 and Ler, displayed 70% (60°/85°) and 78% (51°/65°) root bending in 1 µM TE1 compared to their controls. However, resistant ecotypes, Sha and HKT2-4 showed 96% (81°/84°) and 87% (68°/78°), gravity response, respectively relative to control (Figure 5.4 and Figure 5.5). At 2 µM, Sha and HKT2-4 showed 86% and 85% of control response but Col-0 and Ler showed 45% and 61% (Figure 5.4).

To exclude the possibility of differences in the actin cytoskeleton, in Sha and HKT2-4 with respect to Col-0, which could possibly underlie the resistant phenotype, a gravitropic response assay was performed in the presence of the actin depolymerising drug LatB. In the presence of LatB, no inhibition of gravitropism was seen in any line at either 10 or 50 nM although LatB inhibited root growth in all accessions at 50 nM (Figure 5.4A and B). Collectively, these results show that TE1 does not have obvious effects on the actin cytoskeleton at concentrations used and actin depolymerisation does not inhibit gravitropism. Sha and HKT2-4 show reduced effects to the phenotypes caused by TE1 but gravitropic response do not differ in their response to LatB. Therefore, TE1 has a distinct mode of action to LatB and these accessions are useful tools to investigate the effects of this chemical in the future.
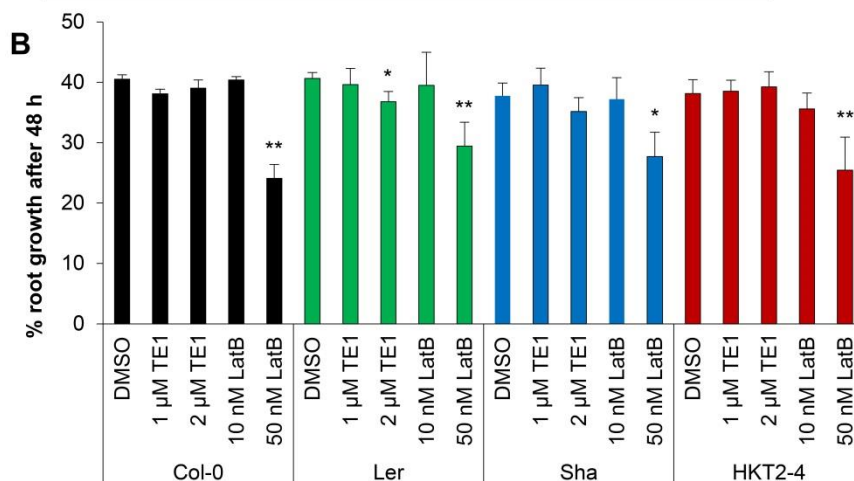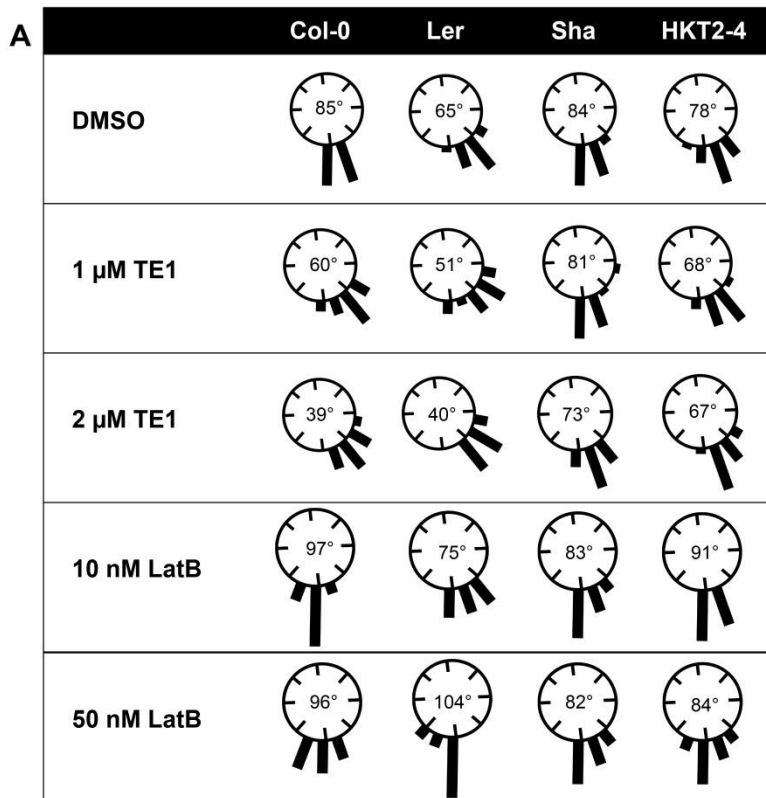
Figure 5.4. *Arabidopsis thaliana* **natural accession screen reveals two ecotypes that display difference in sensitivity to TE1.**

6 day old Col-0, Ler, Sha and HKT2-4 seedlings grown on DMSO control were transplanted and gravistimulated at 90° for 48 h in the presence of DMSO, 1 µM TE1, 2 µM TE1, 10 nM LatB or 50 nM LatB. Histograms of root bending (A), number in the middle of histograms reveal average root bending after 48 h of gravistimulation. Percentage root growth after 48 h of transplant (B). * p ≤ 0.05, ** p ≤ 0.01. The resistant accessions were identified by Adam Jamaluddin (MSc student, University of Leeds) and I independently produced the results displayed above.
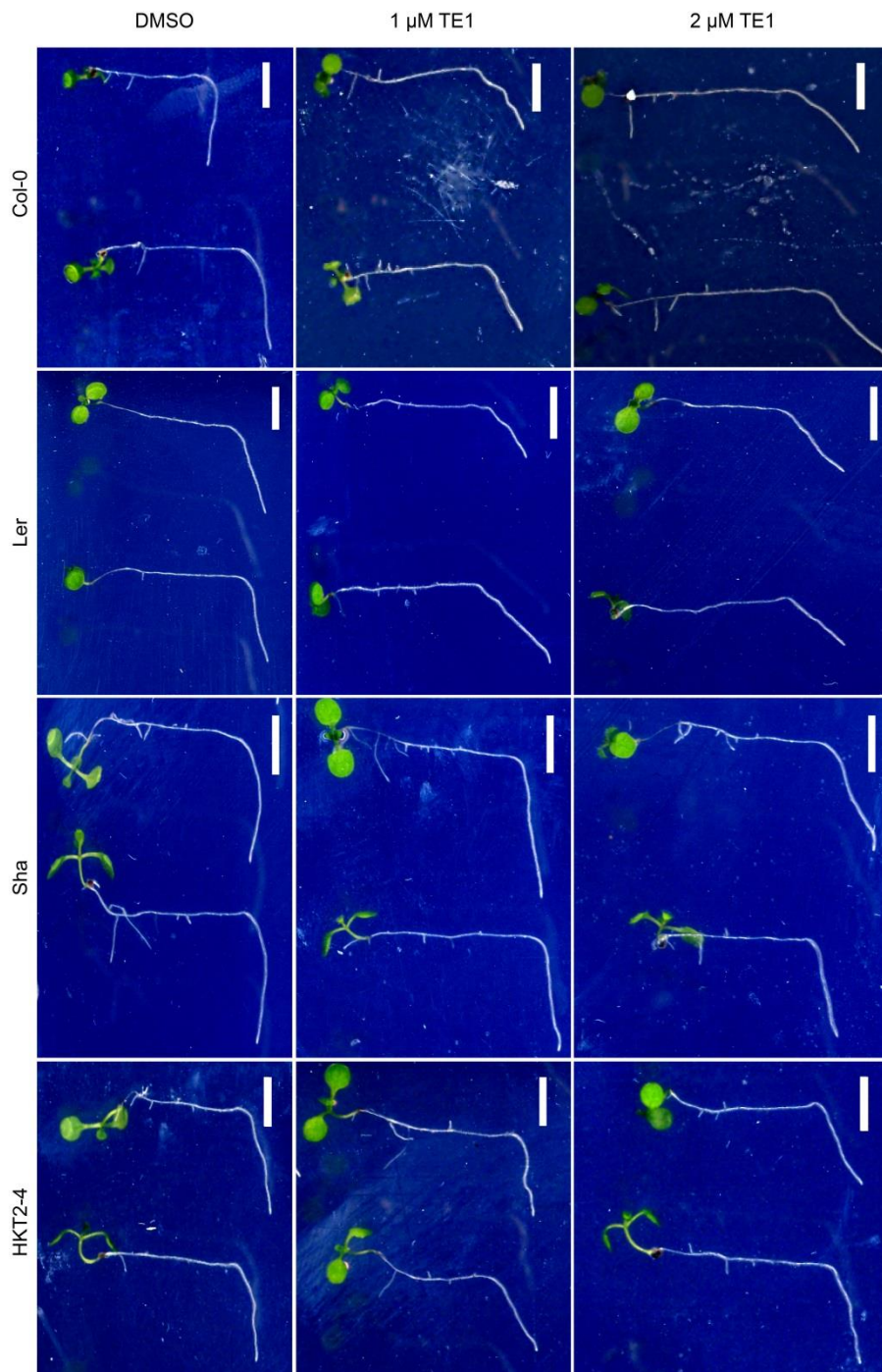
Figure 5.5. *Arabidopsis thaliana* accessions Sha and HKT2-4 display increased gravitropic bending in the presence of TE1.

6 day old Col-0 (first row), Ler (second row), Sha (third row) and HKT2-4 (last row) seedlings grown on DMSO medium were transplanted to medium containing DMSO (first column), 1 µM (middle column) or 2 µM TE1 (third column) and gravistimulated for 48 h. Scale bars, 5 mm.

5.2.2 *Arabidopsis thaliana* accessions Sha and HKT2-4 display increased resistance to the root growth inhibition and survival rates observed in the presence of TE1

To confirm that Sha and HKT2-4 displayed resistance to the effects of TE1, several other phenotypes were also scored. In the reference accession Col-0, compound TE1 inhibited root growth at concentrations above 5 µM (Chapter 3, Figure 3.3). Therefore, the effect of TE1 on root length was measured in resistant accessions Sha and HKT2-4, and sensitive accessions Col-0 and Ler.

7 day old Col-0, Ler, Sha and HKT2-4 seedlings were grown on ½ MS media containing 0.1% DMSO, 10 µM TE1 or 25 µM TE1. The primary root length of the seedlings were measured and displayed as % relative to respective DMSO controls. As observed before, the average length of the primary root at 10 µM and 25 µM TE1 in Col-0 seedlings, relative to DMSO control, were recorded at 54 ± 11% and 27 ± 5%, respectively (Figure 5.6, black bars). The average primary root length of another sensitive accession, Ler, at 10 µM and 25 µM TE1 relative to DMSO control, was recorded at 39 ± 11% and 20 ± 8%, respectively (Figure 5.6, green bars). T-test revealed p values ≤ 0.01, for both 10 µM and 25 µM TE1 in Col-0 and Ler seedlings suggesting the decrease in root length is statistically significant at these concentrations. In comparison the average primary root length of Sha at 10 µM and 25 µM TE1 relative to DMSO control, was recorded at 86 ± 12% and 41 ± 6%, respectively (Figure 5.6, blue bars). According to statistical T-test, the slight decrease in Sha root length observed at 10 µM TE1 was not statistically significant. However, the p value was ≤ 0.01 for 25 µM TE1 revealing that the decrease in Sha root lengths at this concentration is statistically significant. The average primary root length of HKT2-4 at 10 µM and 25 µM TE1 relative to DMSO control was recorded at 90 ± 5% and 51 ± 6%, respectively (Figure 5.6, red bars). Statistical T-test revealed p value ≤ 0.05 for 10 µM TE1 and ≤ 0.01 for 25 µM TE1, suggesting the decrease in root length is statistically significant. However, taken together these data show that both Sha and HKT2-4 show increased resistance to the root growth inhibition caused by TE1.
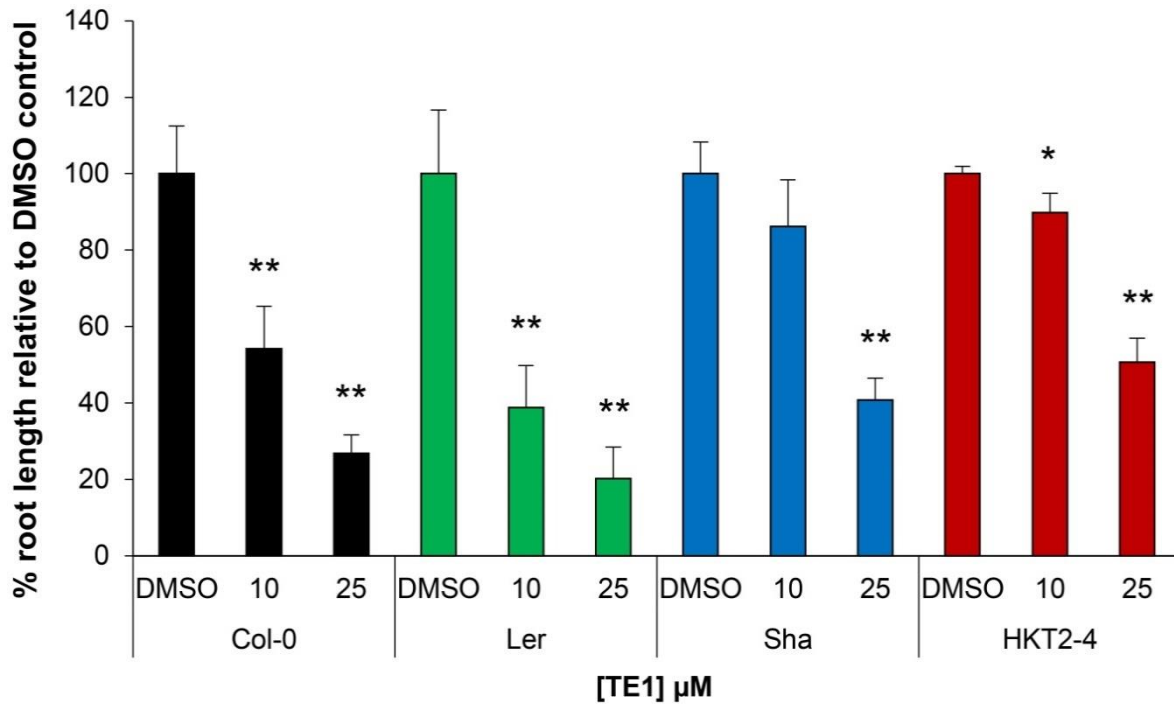
Figure 5.6. *Arabidopsis thaliana* **accessions Sha and HKT2-4 display increased resistance to root growth inhibition caused by TE1.**

Root length of 7 day old Col-0 (black bars), Ler (green bars), Sha (blue bars) and HKT2-4 (red bars) seedlings grown in 16 h light on media containing 0.1% DMSO, 10 μM TE1 or 25 μM TE1 are shown. Root growth of plants grown on TE1 were standardised against DMSO control. A typical data set from three repetitions is shown, total of 20-30 seedlings were scored per condition. Error bars represent SE, * p ≤ 0.05, ** p ≤ 0.01.

5.2.3 *Arabidopsis thaliana* accessions Sha and HKT2-4 show increased survival percentages in the presence of TE1

The survival percentage of reference accession Col-0 also decreased at concentrations above 10 µM TE1 (Chapter 3, Figure 3.6). Therefore a survival assay was carried out to characterise the effects of TE1 on the survival rates of resistant accessions Sha and HKT. Col-0, Ler, Sha and HKT2-4 seedlings were grown in ½ MS media containing 0.1% DMSO, 10 µM TE1 or 25 µM TE1. After 7 days of growth the survival was monitored (Figure 5.7 and Figure 5.8). In the presence of DMSO, survival rates for Col-0, Ler, Sha and HKT2-4 seedlings were scored at 89 ± 4%, 83 ± 3%, 97 ± 3% and 100%, respectively. In the presence of 10 µM TE1, survival rates for Col-0, Ler, Sha and HKT2-4 seedlings were scored at 86 ± 5%, 86 ± 1%, 89 ± 5% and 97 ± 3%, respectively. Finally, in the presence of 25 µM TE1, survival rates for Col-0, Ler, Sha and HKT2-4 seedlings were scored at 40 ± 1%, 54 ± 1%, 79 ± 0.1% and 97 ± 4%, respectively. Statistical T-test gave a p value ≤ 0.01 for both Col-0 and Ler in the presence of 25 µM TE1 suggesting that decrease in survival percentage is highly significant. T-test for Sha at 25 µM TE1 gave a p value of ≤ 0.05 also suggesting decreased survival is significant but no statistical significance was observed in the survival percentage of HKT2-4 in the presence of 10 µM or 25 µM TE1 (Figure 5.7 and Figure 5.8). Overall, the results show that *Arabidopsis thaliana* accessions, Sha and HKT2-4, display resistance to the several phenotypic effects caused by TE1.
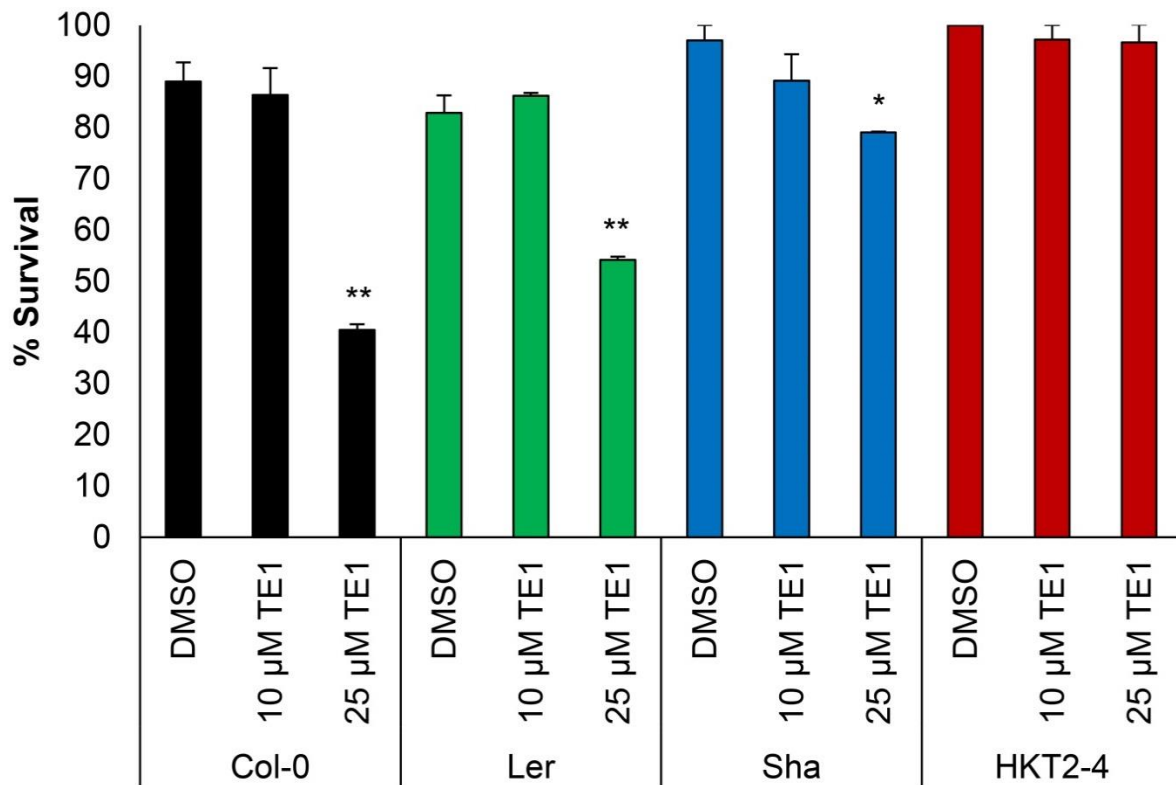
Figure 5.7. *Arabidopsis thaliana* **accessions Sha and HKT2-4 display increased survival percentage in the presence of TE1.**

Percentage survival of 7 day old Col-0 (black bars), Ler (green bars), Sha (blue bars) and HKT2-4 (red bars) seedlings grown on medium containing DMSO, 10 µM TE1 and 25 µM TE1. A typical data set from three repetitions is shown, total of 25-30 seedlings were scored per condition. Error bars represent SE, * $p \leq 0.05$, ** $p \leq 0.01$.
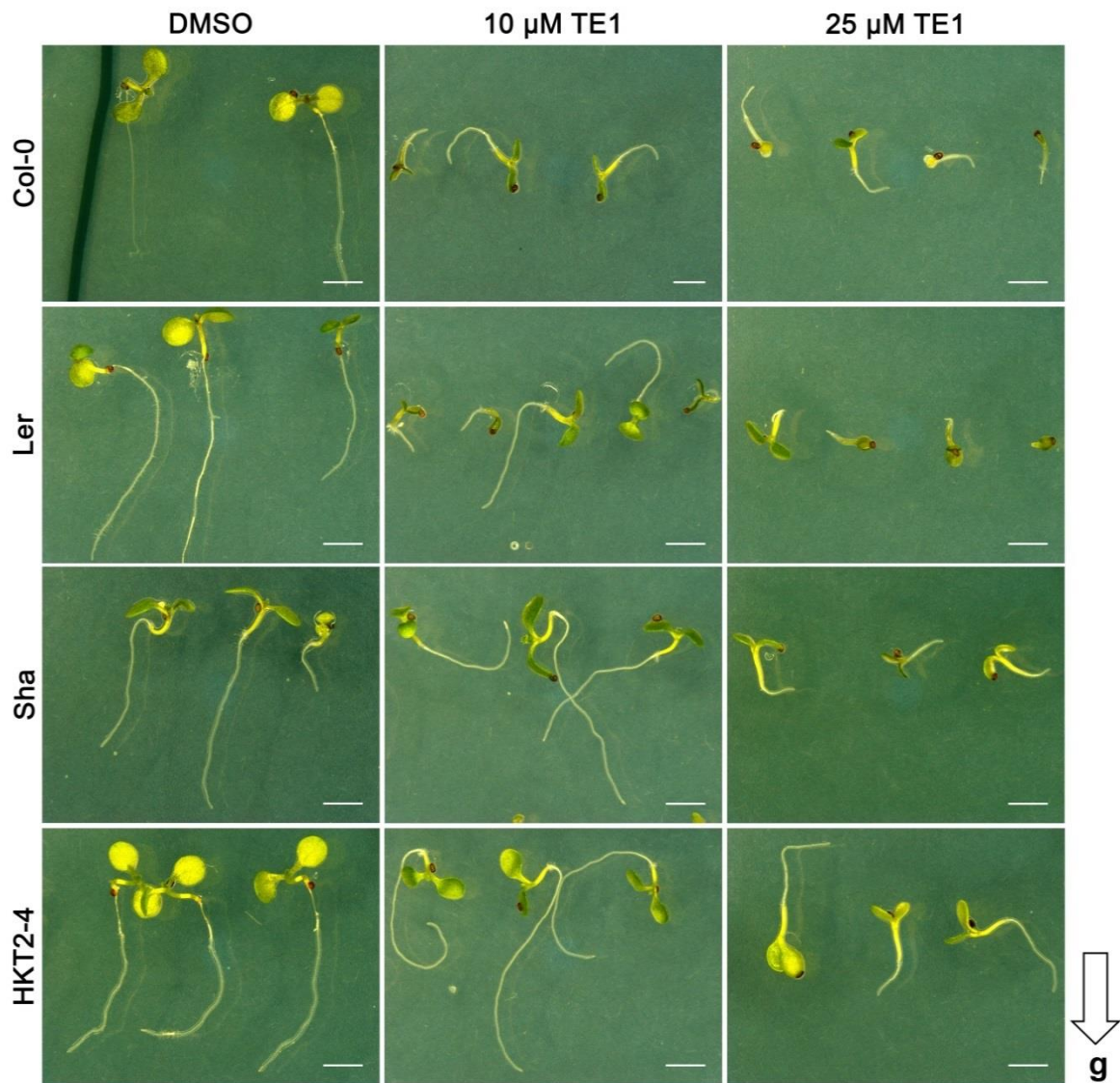
Figure 5.8. Effect of TE1 on whole plant.

7 day old Col-0 (first row), Ler (second row), Sha (third row) and HKT2-4 (last row) seedlings grown on 0.1% DMSO (first column), 10 µM TE1 (middle column) and 25 µM TE1 (third column) are shown. Arrow represents gravitry (g) vector. Scale bars, 2 mm.

5.2.4 *Arabidopsis thaliana* accessions Sha and HKT2-4 show partial resistance to the inhibition of endocytosis caused by TE1

As shown in Chapter 4, TE1 inhibited internalisation of endocytic tracer FM4-64 indicating that TE1 is an inhibitor of endocytosis (Chapter 4, Figure 4.6). Therefore, to complement the investigation of TE1 mediated whole plant phenotypes, FM4-64 uptake was monitored in these accessions to investigate cellular level phenotypes (Figure 5.9 and Figure 5.10). As expected, in DMSO FM4-64 internalisation was visualised after 7 min in Col-0, Sha and HKT2-4 root epidermal cells. However, in the presence of 25 µM TE1, Col-0 root epidermal cells showed no uptake of FM4-64, even after 15 min. Similarly, in the Sha and HKT2-4 roots no uptake of FM4-64 was observed after 7 min staining in seedlings treated with TE1. Sha and HKT2-4 displayed slight internalisation of FM4-64, 11 min after staining. However, the total endocytic uptake in the respective TE1 resistant accessions was still significantly lower in the presence of TE1 (Figure 5.9 and Figure 5.10). This result suggest that although the endocytic uptake is slowed by 25 µM TE1 in Sha and HKT2-4, it is not totally inhibited like it is in Col-0 root epidermis cells. This shows that Sha and HKT2-4 display increased resistance to both whole plant and cellular phenotypes caused by TE1.
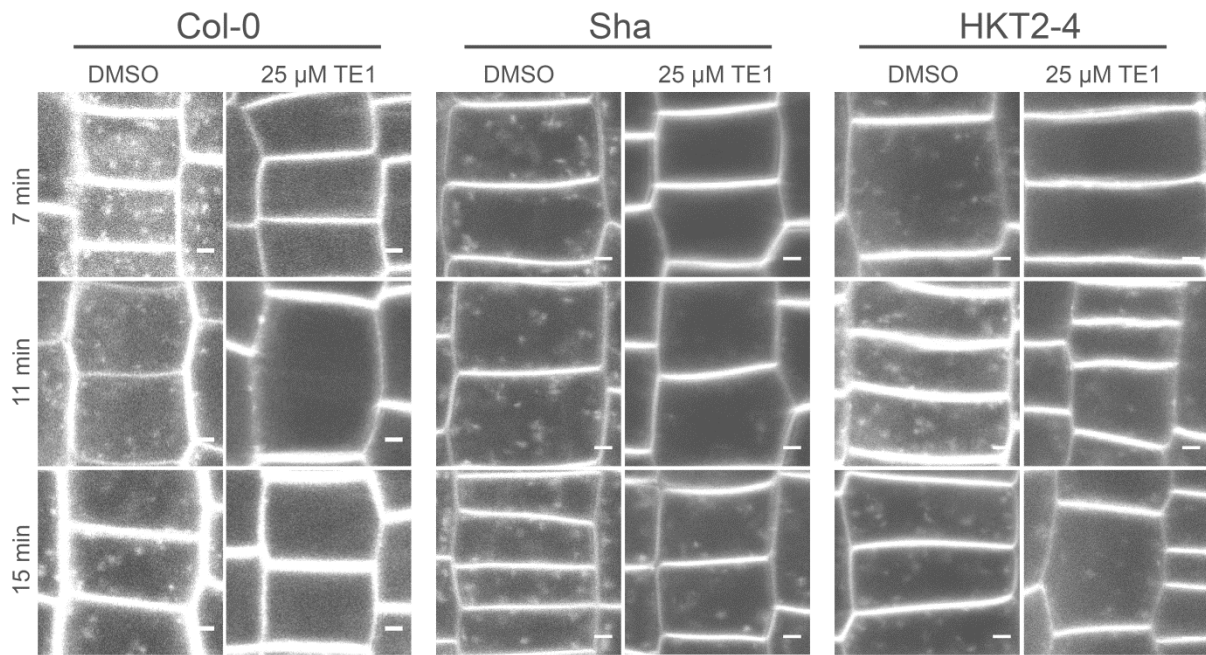
Figure 5.9. Sha and HKT2-4 are only partially sensitive to the TE1 dependent inhibition of endocytosis.

7 day old *Arabidopsis thaliana* ecotypes Col-0, Sha and HKT2-4 were incubated in DMSO or 25 µM TE1 for 120 min. Seedlings were then incubated for 5 min in ½ MS medium containing 5 µM FM4-64, followed by washes in ½ MS medium ×2 at 4°C. The timer started after taking the seedlings off 4°C, and images generated by confocal microscope, 7, 11 and 15 min after FM4-64 staining are shown. Scale bars, 2 µm.
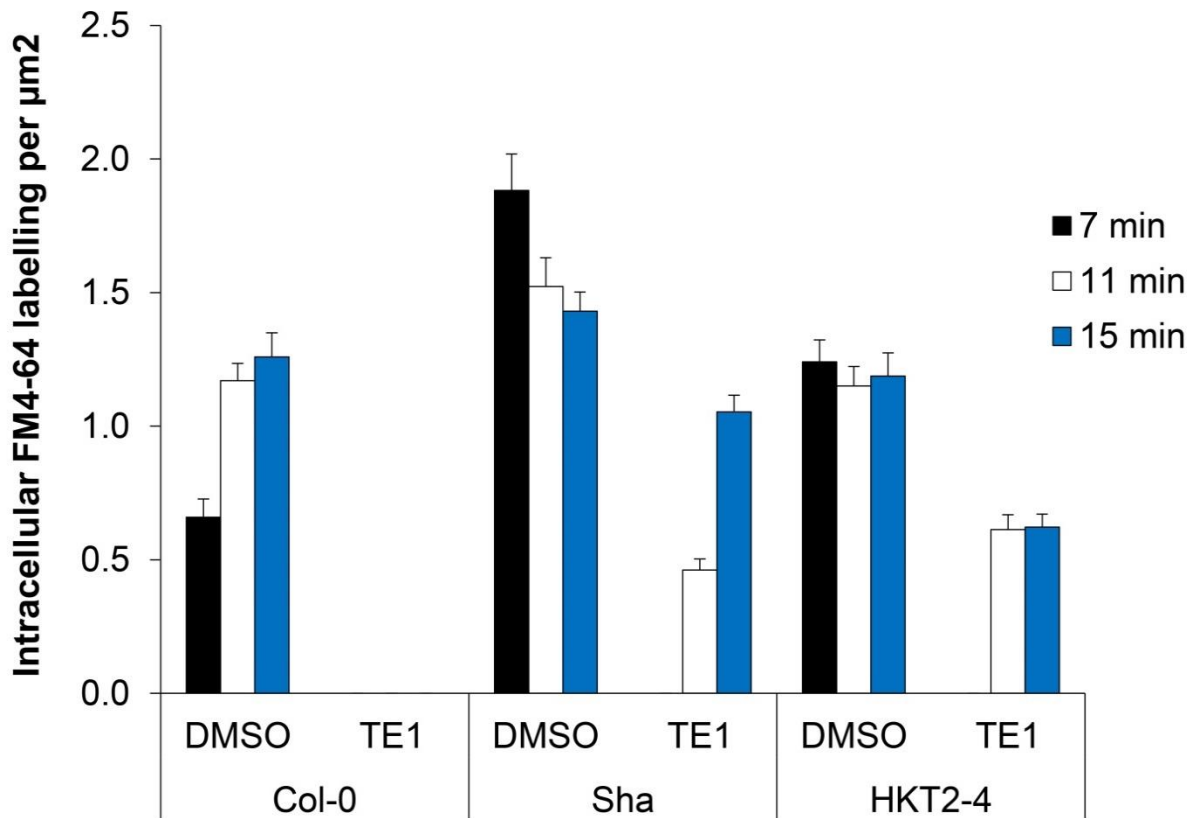
Figure 5.10. Resistant accessions show endocytic uptake in the presence of TE1.

7 day old *Arabidopsis thaliana* ecotypes Col-0, Sha and HKT2-4 were incubated in DMSO or 25 µM TE1 for 120 min. Seedlings were then incubated for 5 min in ½ MS medium containing 5 µM FM4-64, followed by washes in ½ MS medium ×2 at 4°C. The graph displays uptake of FM4-64 observed in intracellular endosomal compartments per μm^2, 7, 11 and 15 min after FM4-64 staining, in TE1 treated and untreated seedlings. Error bars represent SE.

5.3 Genetic basis of the TE1 resistant accessions Sha and HKT2-4

To understand the nature of TE1 resistance displayed by Sha and HKT2-4, several crosses were generated for Sha x Col-0 and HKT2-4 x Col-0 (using Col-0 as both male (♂) and female (♀) parents). Crosses were also generated for Sha x HKT2-4 using both ecotypes and male and female parent. In the F1 population, each homologous chromosome is obtained from a different parent. This allows determination of the nature of the resistant trait displayed by Sha and HKT2-4. Therefore, F1 seeds were screened for two distinct traits, survival rates and root length, in the presence of 25 µM and 10 µM TE1, respectively. F1 crosses were also tested for germination rates.

F2 populations were also generated by allowing selfing of the F1 plants. The F2 seedlings were also screened for root length phenotype in the presence of 10 µM TE1. The segregation of the of the root length in F2 seedlings the presence of 10 µM TE1 should theoretically allow the determination of the nature of the trait (dominant or recessive) but this is also dependent on the number of loci that are responsible for the TE1 resistant trait and whether the two accessions have genetically determined naturally different root lengths.

5.3.1 Genetic interrogation of the F1 crosses

Genetic investigation of the F1 crosses was carried out by using Col-0 and Sha/HKT2-4 as parental P1 population to generate the F1 cross. Since all F1 lines are heterozygous, when survival or root length is investigated in the presence of TE1 the same trait is expected in all the seedlings. This should give an indication of the nature of the trait, either dominant or recessive.

5.3.1.1 Germination of F1 is unaffected by TE1

Before screening the F1 lines for root length and survival rates, germination rates were measured for each cross that was generated. Germination of F1 seeds and parental ecotypes was monitored after 7 days growth in ½ MS media containing 0.1% DMSO or 10 µM TE1 (Figure 5.11). The seeds tested in DMSO control included, Col-0, Sha, HKT2-4, Col-0 (♂) x Sha (♀), Sha (♂) x Col-0 (♀), Col-0 (♂) x HKT2-4 (♀), HKT2-4 (♂) x Col-0 (♀), Sha (♂) x HKT2-4 (♀) and HKT2-4 (♂) x Sha (♀).

As seen previously for Col-0, Germination percentage was unaffected by the presence of TE1 in all the lines that were tested (Figure 5.11). In Col-0, 92% and 100% germination was observed in the presence of DMSO and 10 µM TE1, respectively. In Sha and HKT2-4, 100% germination was recorded in the presence of DMSO and 10 µM TE1. In Col-0 (♂) x Sha (♀), 93% and 100% germination was recorded in DMSO and 10 µM TE1, respectively. In Sha (♂) x Col-0 (♀), 0% and 11% germination was observed in DMSO and 10 µM TE1, respectively. In Col-0 (♂) x HKT2-4 (♀), 100% germination was recorded for both DMSO and 10 µM TE1. In HKT2-4 (♂) x Col-0 (♀), no germination was observed in the presence and absence of TE1. In Sha (♂) x HKT2-4 (♀), 100% and 96% germination was observed in DMSO and 10 µM TE1, respectively. And finally in HKT2-4 (♂) x Sha (♀), 75% and 73% germination was observed in DMSO and 10 µM TE1, respectively (Figure 5.11).

These results indicate that the germination percentage in the presence of TE1 is unaffected in the F1 crosses. However, it is also clear that when Col-0 is the female parent in crosses with either Sha or HKT2-4, the germination percentage is very low in the F1 crosses. This indicates that there is a strong maternal effect; Col-0 as a female parent is unfavourable for germination in a cross with Sha or HKT2-4 but this effect is independent of any effect of TE1.
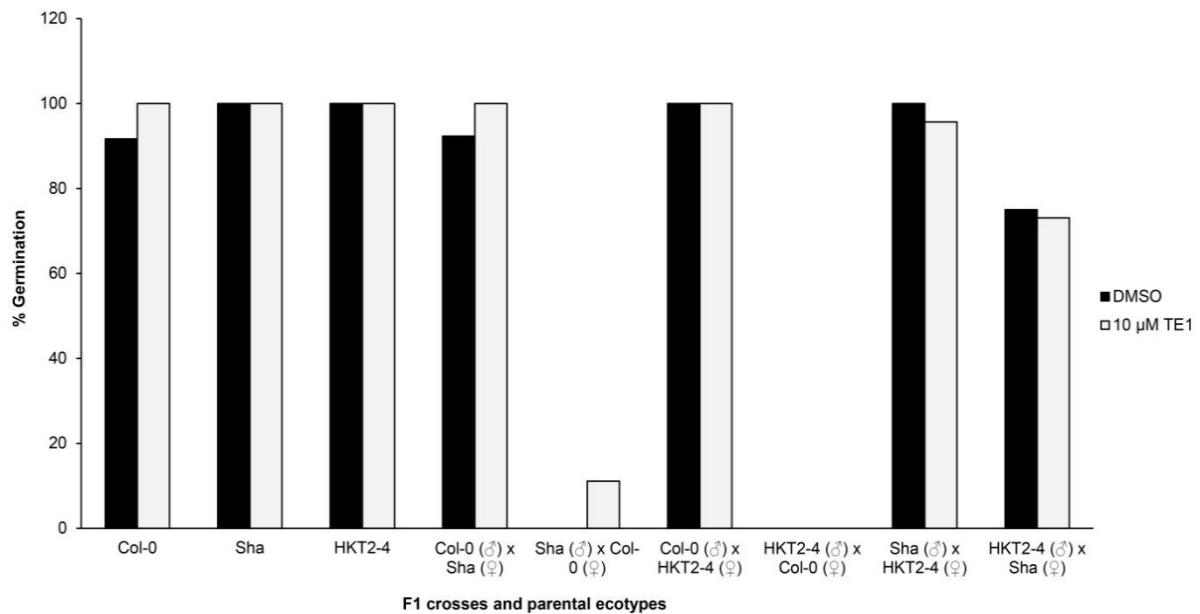
Figure 5.11. Germination rates of F1 crosses.

Germination percentage is shown for F1 crosses in the presence of 0.1% DMSO (black bars) and 10 µM TE1 (grey bars). Germination was monitored after 7 days growth. In DMSO control, Col-0 (n=24), Sha (n=15), HKT2-4 (n=17), Col-0 (♂) x Sha (♀) (n=13), Sha (♂) x Col-0 (♀) (n=10), Col-0 (♂) x HKT2-4 (♀) (n=16), HKT2-4 (♂) x Col-0 (♀) (n=13), Sha (♂) x HKT2-4 (♀) (n=9) and HKT2-4 (♂) x Sha (♀) (n=8), F1 seeds were tested for germination. In the presence of 10 µM TE1, Col-0 (n=21), Sha (n=15), HKT2-4 (n=24), Col-0 (♂) x Sha (♀) (n=23), Sha (♂) x Col-0 (♀) (n=18), Col-0 (♂) x HKT2-4 (♀) (n=25), HKT2-4 (♂) x Col-0 (♀) (n=22), Sha (♂) x HKT2-4 (♀) (n=23) and HKT2-4 (♂) x Sha (♀) (n=26), F1 seeds were tested for germination.

5.3.1.2 Survival rates of F1 crosses are decreased by TE1

F1 crosses along with the parental ecotypes, Col-0, Sha and HKT2-4, were plated in ½ MS media containing 0.1% DMSO or 25 µM TE1. After 7 days growth the seedlings were scored for survival percentages. Survival percentage was monitored in F1 lines, Col-0 (♂) x Sha (♀) and Col-0 (♂) x HKT2-4 (♀) (Figure 5.12). As shown above the F1 crosses using Col-0 as a female parent resulted in a poor germination therefore survival rates were not screened for Sha (♂) x Col-0 (♀) or HKT2-4 (♂) x Col-0 (♀) F1 lines.

Percentage survival for Col-0 seedlings was 96% in DMSO and 19% in 25 µM TE1. In Sha and HKT2-4 seedlings, 100% survival was observed in DMSO for both accessions, and 60% and 88% respective survival rates was observed in 25 µM TE1. In Col-0 (♂) x Sha (♀) F1 seedlings, 100% survival was seen in DMSO control and 17% survival was observed in 25 µM TE1. Finally in Col-0 (♂) x HKT2-4 (♀) F1 seedlings, 100% survival was seen in DMSO control and 40% survival was observed in the presence of 25 µM TE1. Therefore, the survival rates decrease in the F1 crosses when compared to respective parents Sha and HKT2-4 (Figure 5.12). These results indicate that the nature of TE1 resistance displayed by the accessions is not dominant, as the heterozygous diploid chromosome consists of a chromosome from Col-0 and Sha or HKT2-4. In the presence of 25 µM TE1 in Col-0 (♂) x Sha (♀), the percentage survival is similar to the Col-0 indicating that TE1 sensitivity trait displayed by Col-0 is genetically dominant over the more resistant Sha phenotype. In the presence of 25 µM TE1 in Col-0 (♂) x HKT2-4 (♀), the percentage survival is approximately intermediate between the survival percentage between Col-0 and HKT2-4 indicating that the TE1 resistance maybe a semi-dominant. It is also important to consider the possibility of multiple genes that could be contributing to the resistant phenotype displayed by HKT2-4. However the percentage survival assay is somewhat subjective and a more quantitative measure is preferable.
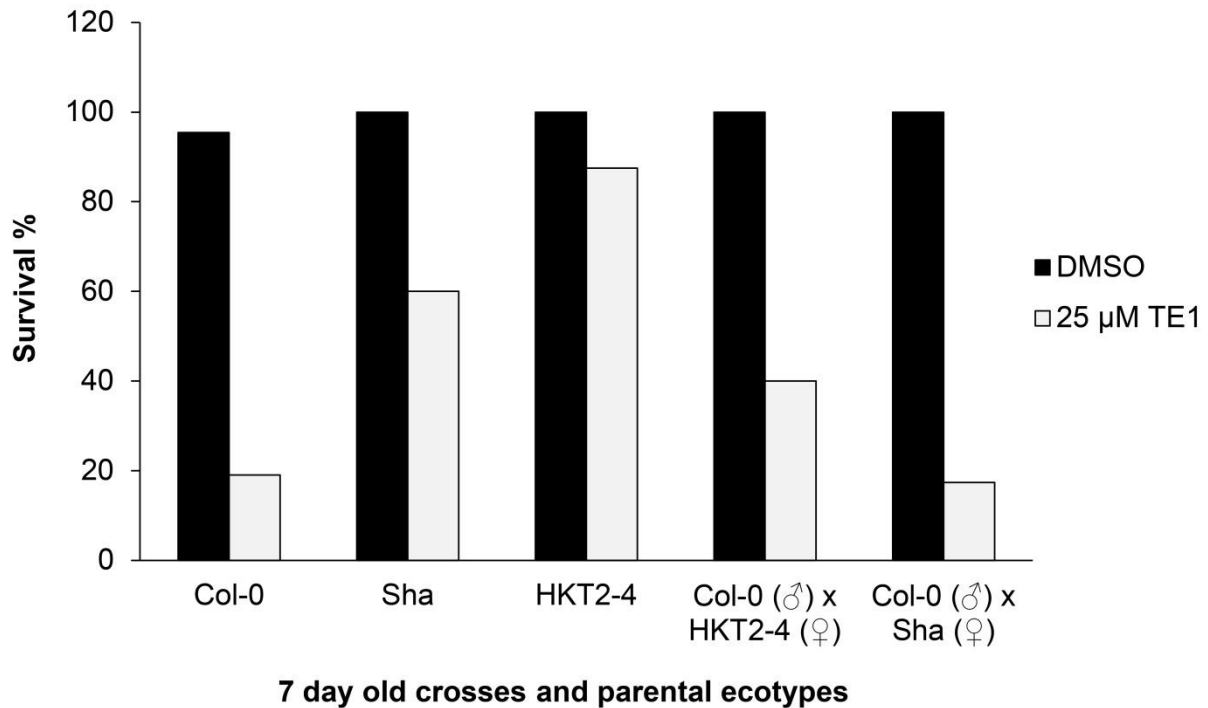
Figure 5.12. Survival rates of F1 crosses.

7 day old seedlings grown on ½ MS media containing 0.1% DMSO (black bars) or 25 μM TE1 (grey bars). In DMSO control, Col-0 (n=24), Sha (n=15), HKT2-4 (n=17), Col-0 (♂) x Sha (♀) (n=13) and Col-0 (♂) x HKT2-4 (♀) (n=16), F1 seedlings were tested. In 25 μM TE1, Col-0 (n=21), Sha (n=15), HKT2-4 (n=24), Col-0 (♂) x Sha (♀) (n=23) and Col-0 (♂) x HKT2-4 (♀) (n=25), F1 seedlings were tested for percentage survival.

5.3.1.3 Difference in average root length is observed in F1 crosses

F1 crosses together with parental ecotypes, Col-0, Sha and HKT2-4 were also plated in ½ MS media containing 0.1% DMSO or 10 µM TE1. After 7 days growth the primary root length of the seedlings were measured. Average root length was measured for F1 lines, Col-0 (♂) x Sha (♀), Col-0 (♂) x HKT2-4 (♀), Sha (♂) x HKT2-4 (♀) and HKT2-4 (♂) x Sha (♀) (Figure 5.13).

In DMSO, average root length for Col-0, Sha and HKT2-4 was 8.6 ± 1 mm, 8.8 ± 0.7 mm and 13.7 ± 0.3 mm, respectively. In the presence of 10 µM TE1, average root length for Col-0, Sha and HKT2-4 was 4.6 ± 0.5 mm, 7.5 ± 0.9 mm and 12.3 ± 0.6 mm, respectively. F1 lines in DMSO, Col-0 (♂) x Sha (♀), Col-0 (♂) x HKT2-4 (♀), Sha (♂) x HKT2-4 (♀) and HKT2-4 (♂) x Sha (♀), displayed average root length of 5.8 ± 0.7 mm, 4.8 ± 0.4 mm, 11.7 ± 1.3 mm and 1.9 ± 0.1 mm, respectively. In comparison, the F1 lines Col-0 (♂) x Sha (♀), Col-0 (♂) x HKT2-4 (♀), Sha (♂) x HKT2-4 (♀) and HKT2-4 (♂) x Sha (♀), in 10 µM TE1 showed average root length of 4.6 ± 0.8 mm, 3.8 ± 0.2 mm, 7.6 ± 0.4 mm and 1.5 ± 0.1 mm, respectively (Figure 5.13).

The crosses display a high level of resistance to root growth inhibition if only DMSO and 10 µM TE1 is being compared within each ecotype. The Col-0 x (♂) x Sha (♀) F1 crosses showed no significant reduction in root length in comparison to DMSO control. In comparison, other crosses showed slight reduction in root length, but these were still significantly more resistant than Col-0. However, the average root length of the crosses is generally smaller in comparison to the average root length of the respective parents, even in the presence of DMSO. In the Sha x HKT2-4 F1 crosses using Sha as maternal parent, average root length was short. However, root length was much longer in the F1 cross that used HKT2-4 as the paternal parent (Figure 5.13). This also indicates that HKT2-4 as a female parent displays longer root growth when crossed with Sha. Therefore, it is difficult to make any definitive conclusions based on these results.
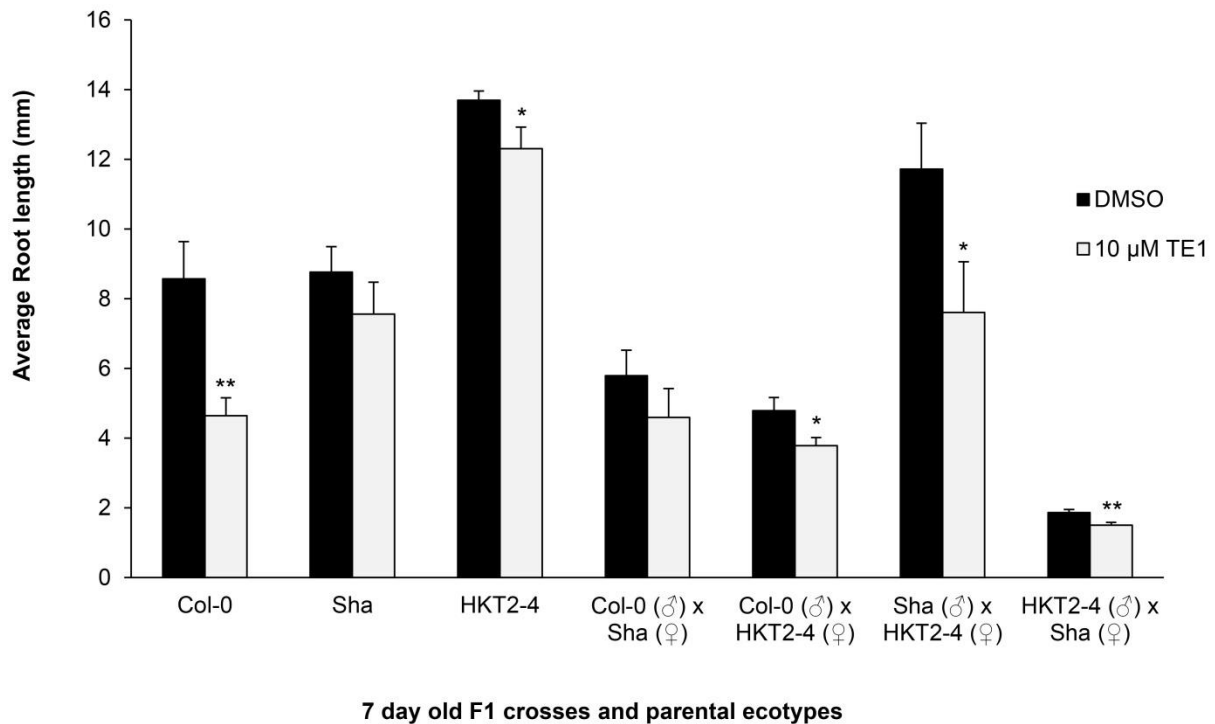
Figure 5.13. Average root length of F1 crosses.

7 day old seedlings grown on ½ MS seedlings containing 0.1% DMSO (black bars) or 10 µM TE1 (grey bars). In DMSO control, Col-0 (n=30), Sha (n=63), HKT2-4 (n=45), Col-0 (♂) x Sha (♀) (n=30) and Col-0 (♂) x HKT2-4 (♀) (n=55), Sha (♂) x HKT2-4 (♀) (n=31) and HKT2-4 (♂) x Sha (♀) (n=31), seedlings were tested for root length. In 10 µM TE1, Col-0 (n=20), Sha (n=20), HKT2-4 (n=33), Col-0 (♂) x Sha (♀) (n=22) and Col-0 (♂) x HKT2-4 (♀) (n=33), Sha (♂) x HKT2-4 (♀) (n=16) and HKT2-4 (♂) x Sha (♀) (n=21), seedlings were tested for root length. Error bars represent SE, * $p \leq 0.05$, ** $p \leq 0.01$. T-TEST was performed between DMSO and 10 µM TE1 treatment on each line.

5.3.2 Genetic investigation of the F2 seedlings

Genetic tests on the F2 lines generated were also performed. In the F2, the paired alleles, gained in the F1 from parents P1, segregate randomly following the recombination events that take place during meiosis. Therefore, as the F2 gametes are formed the TE1 resistant allele(s) are segregated randomly. Therefore, if root length at 10 μM TE1 is used as a phenotype to screen the F2 seedlings, theoretically, this will result in four different phenotypic outcomes. (1) Long root/long root, (2) long root/short root, (3) short root/long root and (4) short root/short root phenotypes will be observed. Combination (1) and (4) are homozygous and (2) and (3) are heterozygous. Therefore, this can be used to further confirm the nature of TE1 resistance (dominant/recessive). It would be easier to predict this, if there is a single gene responsible for resistance which would result in a 3:1 ratio depending on whether the allele is dominant of recessive.

5.3.2.1 Investigation of the F2 crosses Sha x Col-0 and HKT2-4 x Col-0

F2 crosses along with parental ecotypes, Col-0, Sha and HKT2-4 were plated in ½ MS media containing 0.1% DMSO or 10 μM TE1. After 7 days growth, root lengths of seedlings were measured and the distribution of root length was plotted as histograms or cumulative distribution frequency (CDF) graphs (Figure 5.14 – Figure 5.16). Root length of 7 day old Col-0 (Figure 5.14), Sha (Figure 5.15) and HKT2-4 (Figure 5.16) seedlings were measured in the presence of DMSO (black lines) and 10 μM TE1 (red lines). Root length of 7 day old F2 seedlings, Sha (♂) x Col-0 (♀) and Col-0 (♂) x Sha (♀) (Figure 5.15), and HKT2-4 (♂) x Col-0 (♀) and Col-0 (♂) x HKT2-4 (♀) (Figure 5.16), grown in the presence of 10 μM TE1 were also measured.

As it can be seen that the distribution of root length in the presence and in the absence of TE1 may be effectively shown as a histogram (Figure 5.14A) or as a CDF (Figure 5.14B). Therefore, both histograms and CDFs are shown for the crosses and the parental ecotypes. As expected in Col-0 seedlings, there is a clear inhibition in the root length in the presence of 10 μM TE1 (Figure 5.14).

However, the Sha seedlings did not display similar root growth to what was previously observed as Sha root lengths in previous experiments were significantly higher in the presence of DMSO (see Figure 5.13). In this experiment the root growth in the presence of 10 μM TE1 in Sha seedlings is similar to DMSO and the F2

crosses Sha (♂) x Col-0 (♀) and Col-0 (♂) x Sha (♀) (Figure 5.15). The result suggests that Sha displays a dominant trait over Col-0. This contradicts the observation that was previously made that the Col-0 trait displays dominance over Sha (Figure 5.12). However, during the experiment the root growth of wild-type Sha seedlings were shorter than observed previously even on DMSO although the crosses and Col-0 parent grew normally. Therefore, it is difficult to make this conclusion without a proper control. The dotted lines in the figure show data for Sha root lengths from another independent experiment where more normal root growth was observed. Although it is not ideal to compare data from different experiments this suggests that the F2 crosses that were generated may be more sensitive than the Sha parent (Figure 5.15). Clearly this experiment needs repeating to make a robust conclusion but this batch of Sha seed now consistently shows poor root growth and there was insufficient time to generate a new batch.

In the HKT2-4 seedlings, the root length was much more uniform in the presence of DMSO (similar to what was observed previously in Figure 5.13) and high level of resistance to root growth inhibition is observed in the presence of 10 µM TE1. The distribution of root growth of HKT2-4 is shown as a histogram (Figure 5.16A and C) and as CDF (Figure 5.16B and D). Root length of the F2 crosses HKT2-4 (♂) x Col-0 (♀) and Col-0 (♂) x HKT2-4 (♀) were also measured in the presence of 10 µM TE1. HKT2-4 x Col-0 crosses (using Col-0 as male or female parent) showed similar root growth pattern (Figure 5.16A and B). Therefore the root length for reciprocal crosses were merged and displayed F2 HKT2-4 x Col-0 (Figure 5.16C and D). As expected, segregation of the root lengths in the presence of 10 µM TE1 was observed in the F2 HKT2-4 x Col-0 seedlings. However, a large percentage of inhibition of root growth in the presence of 10 µM TE1 in the F2 seedlings were observed, and this trait seems to be intermediate between Col-0 and HKT2-4. This result is consistent with previous observation that suggested that TE1 resistant trait displayed by HKT2-4 may be of semi-dominant nature.
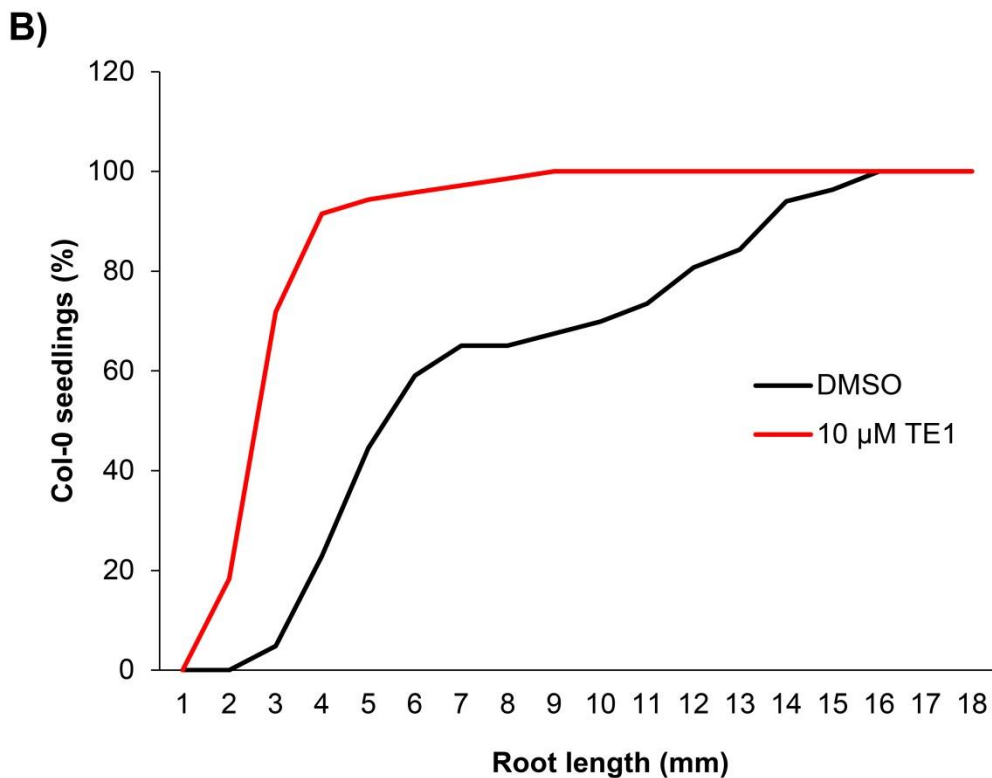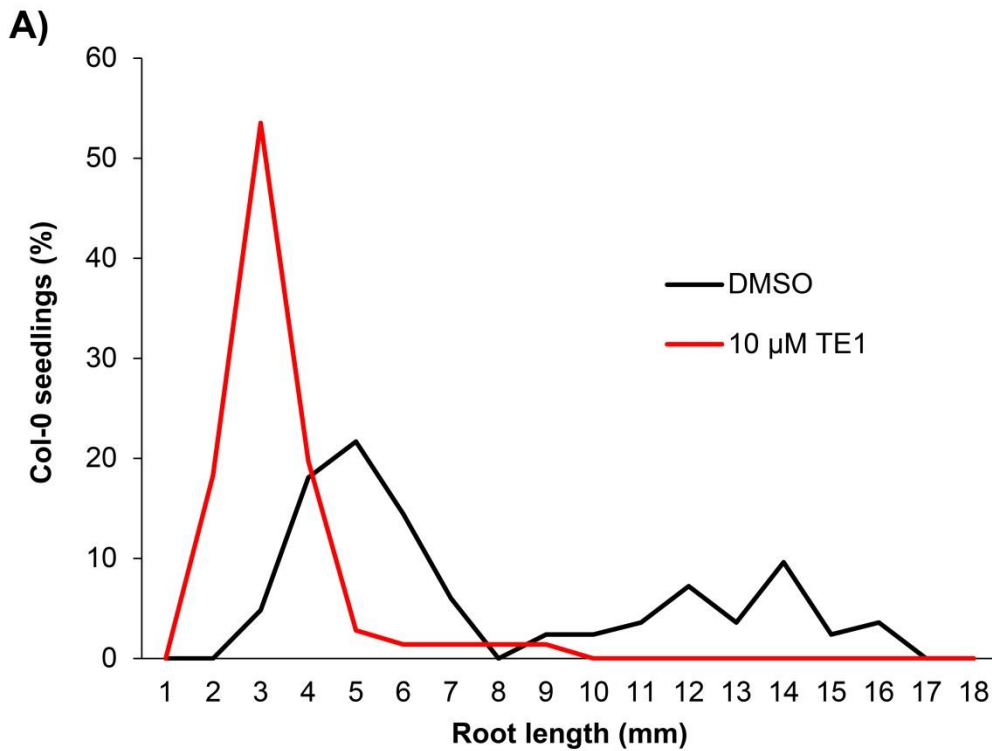
Figure 5.14. Distributions of Col-0 seedlings root length.

Histogram (A) and cumulative distribution frequency (CDF) graphs of Col-0 seedlings grown on ½ MS media containing 0.1% DMSO (black line; n=83) or 10 µM TE1 (red line; n=71). The graph represents a dataset from an experiment repeated two times.
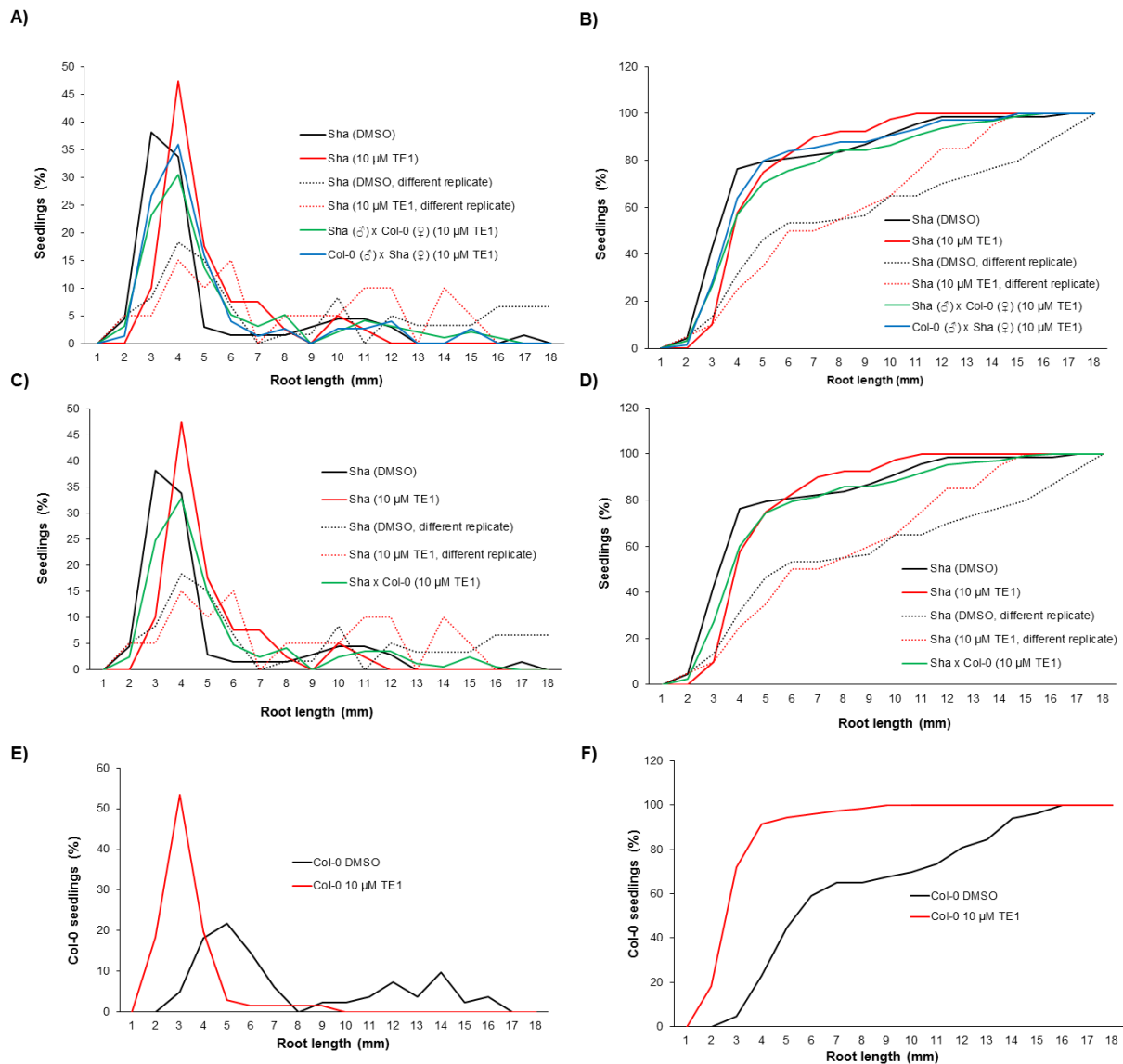
Figure 5.15. Distributions of Sha and Sha x Col-0 F2 seedlings root length in the presence of 10 µM TE1.

Histogram (A, C and E) and CDF (B, D and F) graphs of root length of 7 day old seedlings. Sha seedlings were grown on ½ MS media containing 0.1% DMSO (A-D) (black line; n=68) or 10 µM TE1 (A-D) (red line; n=40). F2 crosses, Sha (♂) x Col-0 (♀) (A and C) (green; n=75), and Col-0 (♂) x Sha (♀) (A and C) (blue line; n=95), were grown on media containing 10 µM TE1. Sha x Col-0 reciprocal crosses (using Col-0 as both male and female P1) showed similar pattern therefore they were merged (n=170) and shown as histogram (C; green line) and CDF (D; green line). Dotted lines represent Sha root growth data from a previous experiment is labelled different replicate. Distributions of root length in 7 day old Col-0 seedlings are also

shown as histogram (E) and as CDF (F). Col-0 seedlings were grown in ½ MS media containing 0.1% DMSO (black line; n=83) and 10 µM TE1 (red line; n=71). The graphs represent a dataset from experiment repeated two times.
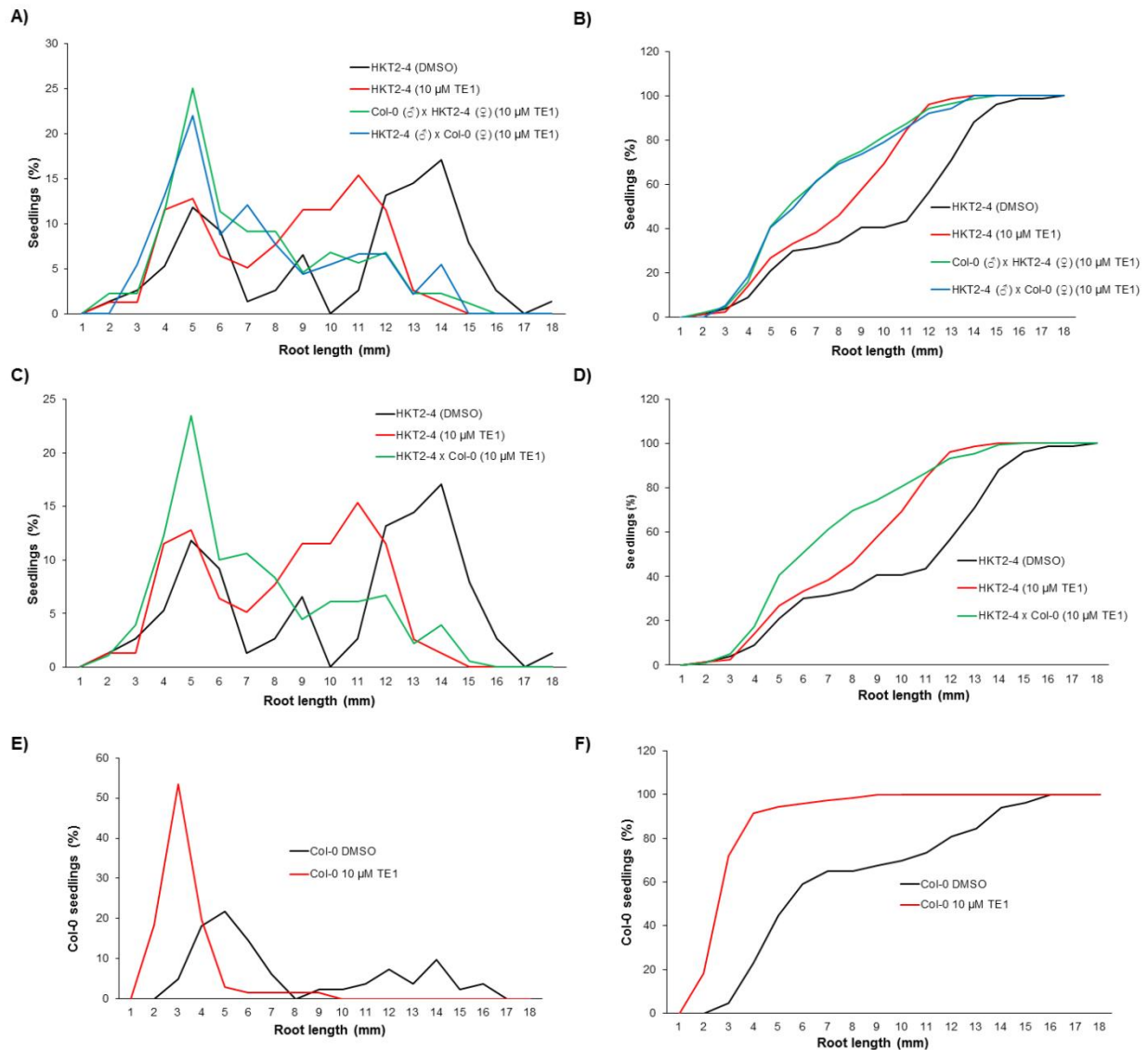
Figure 5.16. Distribution of HKT2-4 and HKT2-4 x Col-0 F2 seedlings root growth in the presence of 10 µM TE1.

Histogram (A and C) and CDF (B and D) graphs of root length of 7 day old seedlings. HKT2-4 seedlings were grown on ½ MS media containing 0.1% DMSO (A-D) (black line; n=76) or 10 µM TE1 (A-D) (red line; n=78). F2 crosses, Col-0 (♂) x HKT2-4 (♀) (A and C) (green; n=88), and HKT2-4 (♂) x Col-0 (♀) (A and C) (blue line; n=91), were grown on media containing 10 µM TE1. HKT2-4 x Col-0 reciprocal (using Col-0 as both male and female P1) crosses showed similar pattern therefore they were merged (n=179) and shown as histogram (C; green line) and CDF (D; green line). Distributions of root length in 7 day old Col-0 seedlings are also shown as histogram (E) and as CDF (F). Col-0 seedlings were grown in ½ MS media

containing 0.1% DMSO (black line; n=83) and 10 μM TE1 (red line; n=71). The graphs represent a dataset from experiment repeated two times.

5.4 Mapping QTL responsible for the resistance to TE1

As highlighted in the introduction the use of RILs to map QTL provides a powerful tool as lines are almost homozygous and allows phenotypic and genotypic analysis of different traits under various conditions on the same material. The two *Arabidopsis thaliana* accessions, Sha and HKT2-4, that display decreased sensitivity to the effects of TE1, provide ideal tool to screen the RILs generated by crossing with Col-0 using survival percentage phenotype at 25 µM TE1 (Figure 5.7) or to quantify average root length at 10 µM TE1 (Figure 5.6). RILs are not available for HKT2-4 as yet. However, RILs have been generated for Bay-0 x Sha (Loudet et al., 2002) and Ler x Sha (Clerkx et al., 2004). However, all of the experiments were performed in Col-0 background therefore Sha x Col-0 RILs (Simon et al., 2008) was chosen to screen against TE1.

5.4.1 Screening RILs using survival rates traits

An easy to observe phenotype(s) needs to be chosen to screen the RILs. Therefore, survival percentage after 7 days at 25 µM TE1 (Figure 5.7) was chosen as one of the phenotypes that was screened. The authors that generated the Sha x Col-0 RILs have picked out a set of RILs they describe as 'core population', that is an optimal subset to screen for a phenotype without losing much QTL identification power (Simon et al., 2008). The criteria used by the authors to select this subset of RILs were: selecting lines that were mostly homozygous that display higher recombination events and contain extensive data (Simon et al., 2008). Therefore, 174 Sha x Col-0 RILs were plated in ½ MS medium containing 25 µM TE1. Approximately 1,700 seedlings were studied, therefore on average 10 seedlings per RIL were represented in the screen. The seedlings were allowed growth for 7 days and scored for survival rates (Figure 5.17).

The distribution of the phenotypic values representing survival percentages in the presence of 25 µM TE1 for all 174 RILs is shown in Figure 5.18. Some RILs display trait values that are more extreme that displayed by the parent accessions. Overall, significant amount of variation was observed between RILs as indicated by the traits observed (Figure 5.17 and Figure 5.18).

The raw data of the percentage survival for each RIL was inputted into the QTL cartographer software (http://statgen.ncsu.edu/qtlcart/). QTL analysis was performed in QTL cartographer using composite interval mapping (CIM) feature, see materials and methods (Chapter 2) for details. CIM generated an output of the graph that predicts the logarithm of odds (LOD) scores of the predicted region where QTL is likely to reside. Based on the survival rates of the RILs screened, three QTLs were identified (Figure 5.19 and Table 5-2). QTL PSR1 (percentage survival 1) was mapped to chromosome 1 between marker 2 and 3. This is predicted to lie in between 5-7 cM, approximately from 2.2-3 Mb at the chromosome 1. Two QTLs, PSR5a and PSR5b, residing very close to each other were identified in chromosome 5. PSR5a is predicted to be within marker 8 around 39-42 cM, approximately 9 Mb in chromosome 5. Meanwhile, PSR5b is predicted to be within marker 10 and 11, between 47-58 cM, approximately 2.47-2.79 Mb in chromosome 5 (Figure 5.19 and Table 5-2). There are roughly 350 genes in PSR1, 300 genes in PSR5a and 800 genes in PSR5b.
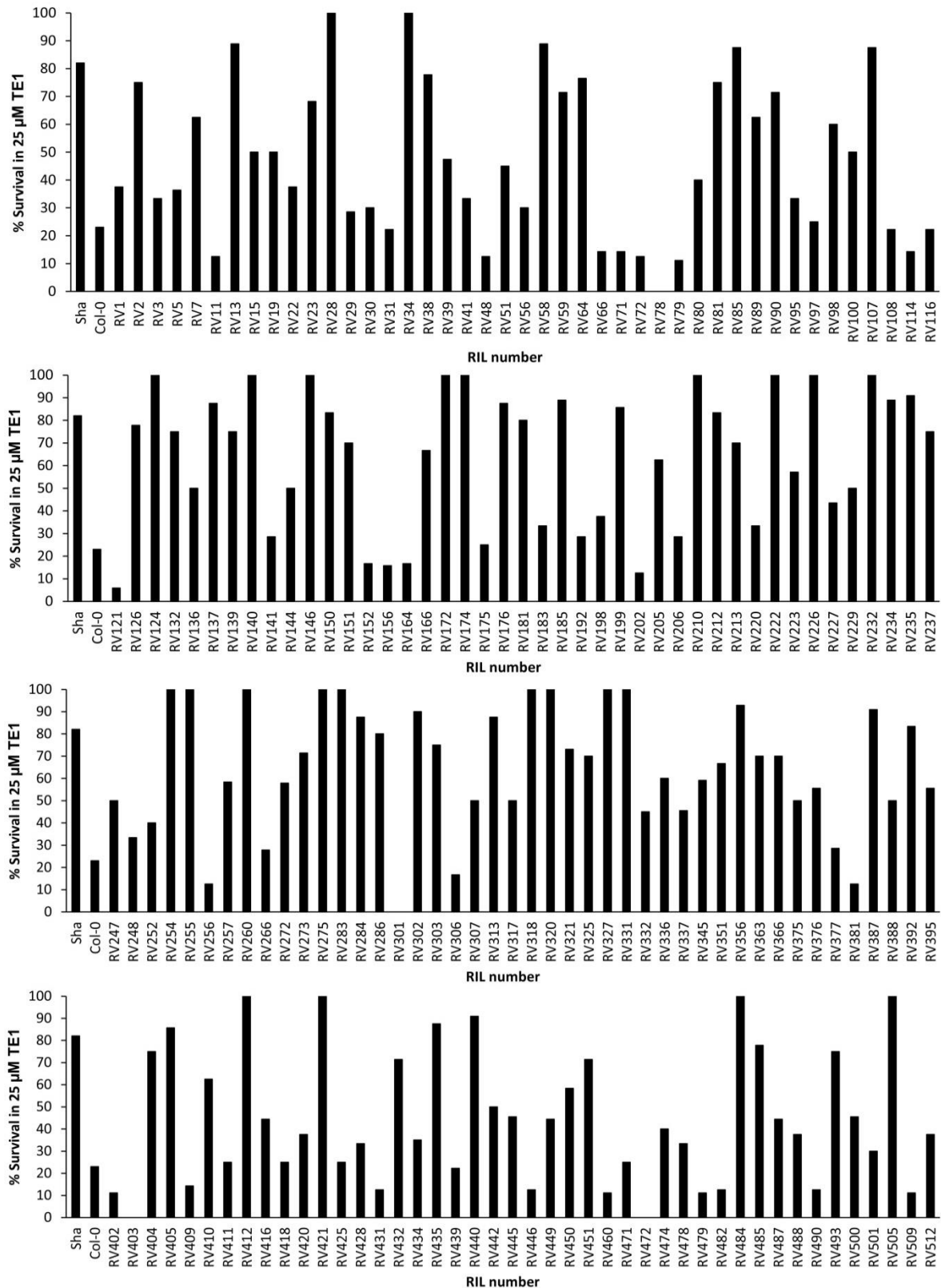
Figure 5.17. Survival percentage of 7 day old Sha x Col-0 RIL seedlings.

174 RILs (Simon et al., 2008) along with parent Sha and Col-0 seedlings were grown in media containing 25 µM TE1 and scored for survival rates.
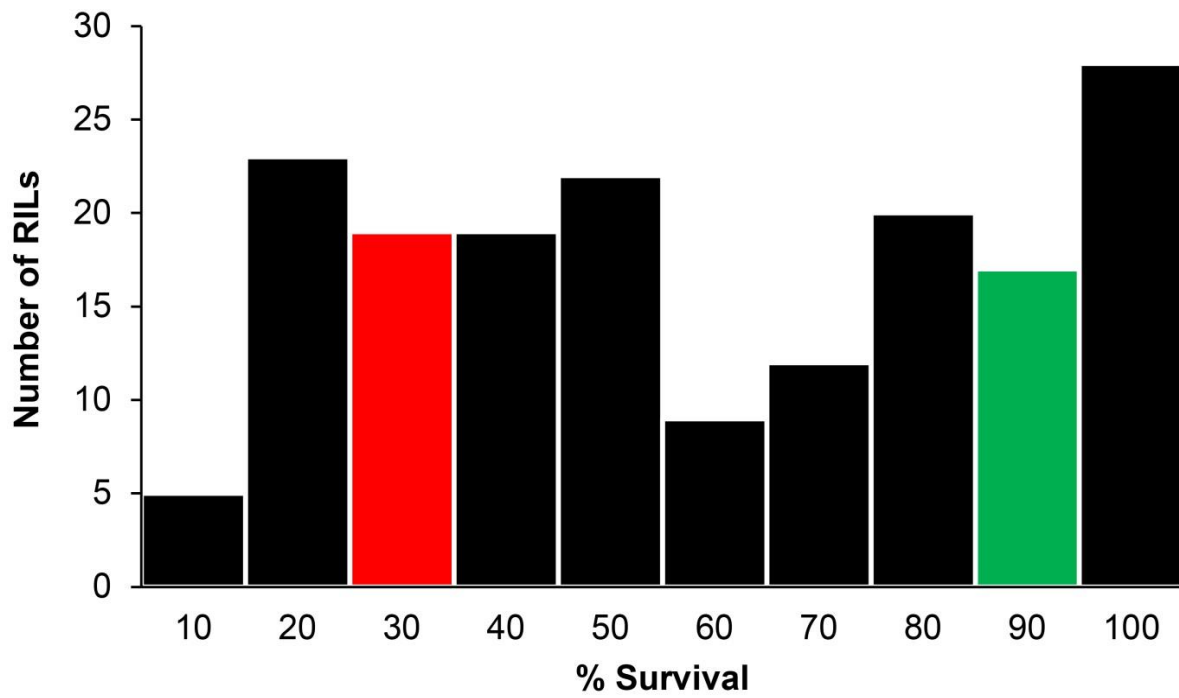
Figure 5.18. Distribution of non-normalised data for the survival trait displayed by Sha x Col-0 RIL populations.

Total 174 RIL lines were screened for survival rates after 7 days growth in medium containing 25 µM TE1. Red and green bars represent survival percentage value obtained for parental accession Col-0 and Sha, respectively.
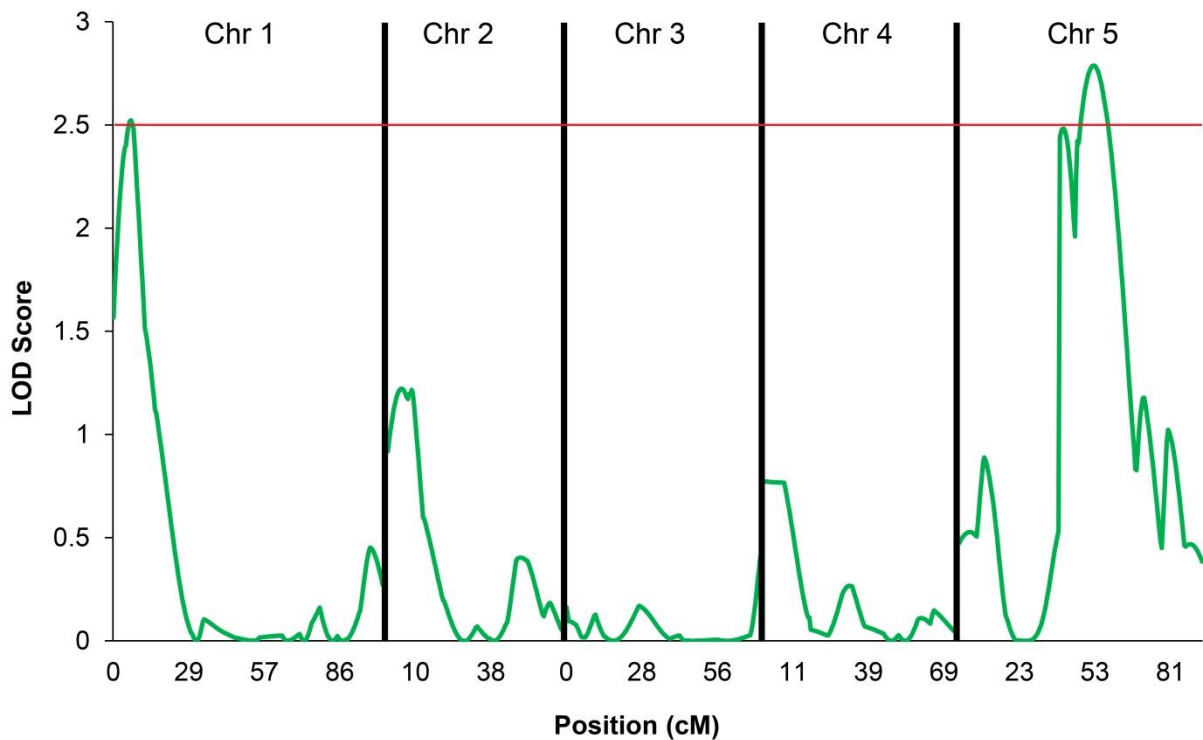
Figure 5.19. LOD score graphs predicting QTL responsible for resistance to TE1.

LOD scores are shown for Chromosome 1-5. 174 RILs (F8) generated by crossing Sha x Col-0 (Simon et al., 2008) grown on 25 μM TE1 were scored for survival percentage (see Figure 5.17). The data generated from survival rates of the 174 RILs were inputted into QTL cartographer software (**http://statgen.ncsu.edu/qtlcart/**) that predicts QTL responsible for resistance (Silva Lda et al., 2012).

5.4.2 Screening RILs using root length trait

Screening the RILs with survival percentage phenotype identified regions in chromosome 1 and chromosome 5 to contain the QTLs responsible for resistance trait in Sha (Figure 5.19). However, accuracy of the QTL positioning, detected by LOD peak, especially by screening the RILs may shift a few cM to the left or to the right. This factor can be controlled by reducing environmental variation, by screening more RILs or by screening for several phenotypes affected by the gene in a pleiotropic manner (Korol et al., 2001; Price, 2006). If the size of the QTL is small then this shift of the LOD peak could be misleading and may lead to fine mapping in the wrong region. Re-screening the RILs with a different phenotype also allows the association of the QTL region to a trait of interest. Therefore, if a gene controls several traits and QTL curves show relative similar QTL pattern, then confidence on the QTL is significantly higher and multiple trait mapping strategy may be employed to generate LOD scores for identified QTL from both traits.

The frequency distribution of RIL population screened for survival rates in the presence of 25 µM TE1 did not show a normal distribution, therefore this needs to be backed up by additional tests (Figure 5.18). To screen the RILs with a second phenotype, root growth was monitored in 7 day old RILs grown on ½ MS media containing 10 µM TE1. In total 174 Sha x Col-0 RILs were screened. Primary root lengths of approximately 2,000 seedlings were measured, which averages about 12 seedlings per RIL. However, the 57 RILs from RV1 to RV152 that were screened grew poorly due to being placed on a different shelf, which may have been colder, in the growth room to the other lines. Therefore, these 57 RILs were excluded from the analysis and this left a total of 117 RILs there were used for QTL analysis. Figure 5.20 shows the average primary root length of the RIL populations grown in the presence of 10 µM TE1. The distribution of the root growth trait in the presence of 10 µM TE1 for the 117 RILs used for QTL analysis is also shown in Figure 5.21. Overall, the RILs display significant variation in the root growth in the presence of 10 µM TE1 (Figure 5.20 and Figure 5.21).

The average root length growth for each RIL was inputted into the QTL cartographer software, and CIM procedure was used as explained before (see Chapter 2). The output graph predicting LOD scored for predicted QTL region was then generated (Figure 5.22). From this one major QTL, ARL5 (average root length 5), was identified

approximately in the same region as PSR5a and PSR5b. ARL5 is predicted lie between markers 8, 9 and 10 in chromosome 5 (Figure 5.24). This is approximately 40-50 cM or 9-13.6 Mbp in chromosome 5 (Figure 5.22 and Table 5-2). Identification of ARL5 overlapping with PSR5a and PSR5b suggest that both traits screened against TE1 are controlled by this major QTL. There are approximately 1150 predicted genes in the region covered by ARL5.
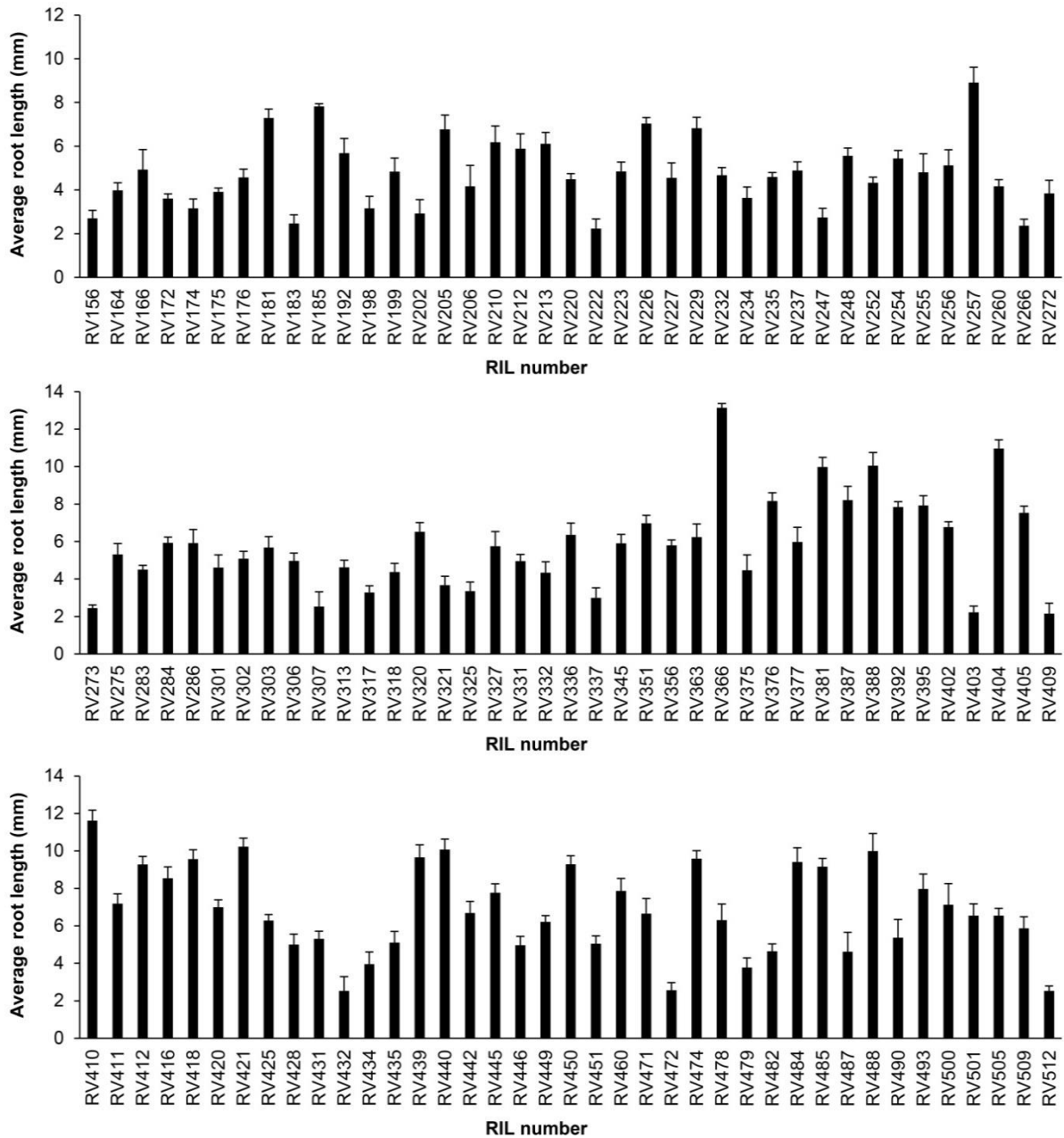
Figure 5.20. Average root length of 7 day old Sha x Col-0 RIL seedlings.

Average primary root length is shown of 117 RIL (Simon et al., 2008) seedlings were grown in media containing 10 µM TE1. Error bars represent SE.
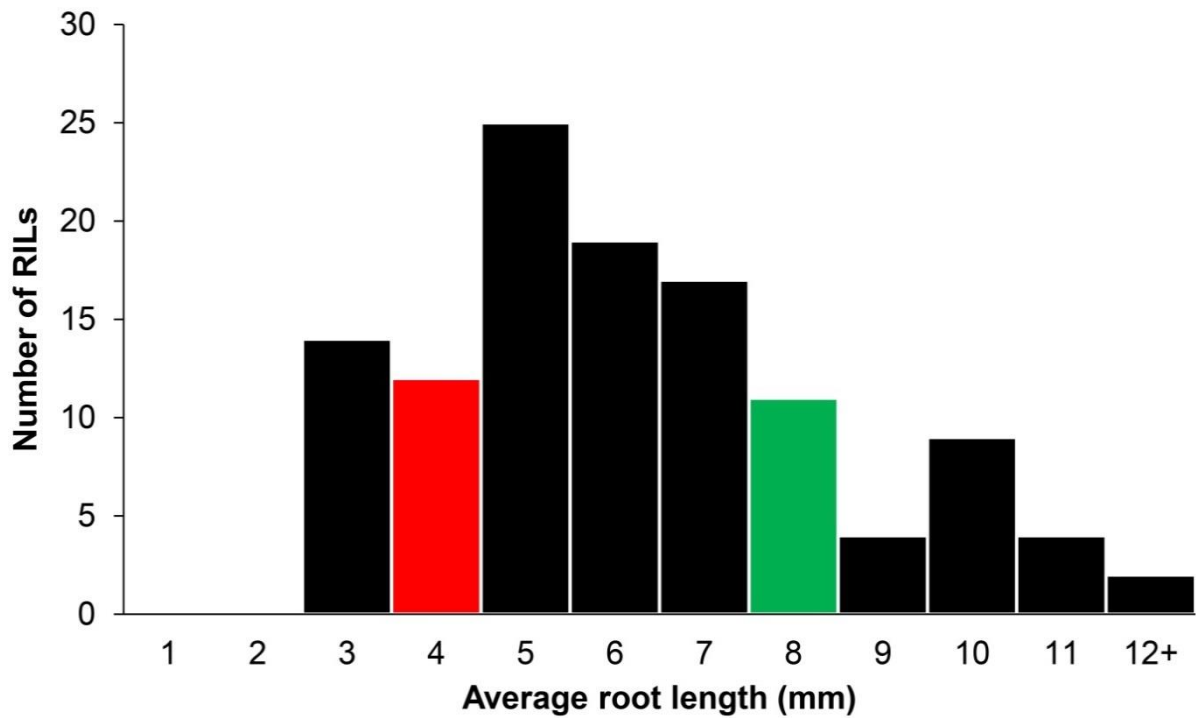
Figure 5.21. Distribution of non-normalised data for the average root length trait measured in Sha x Col-0 RIL populations.

Total 117 RIL lines were screened for average primary root length after 7 days growth in medium containing 10 µM TE1. Red and green bars represent average root length measured for parental accession Col-0 and Sha, respectively.
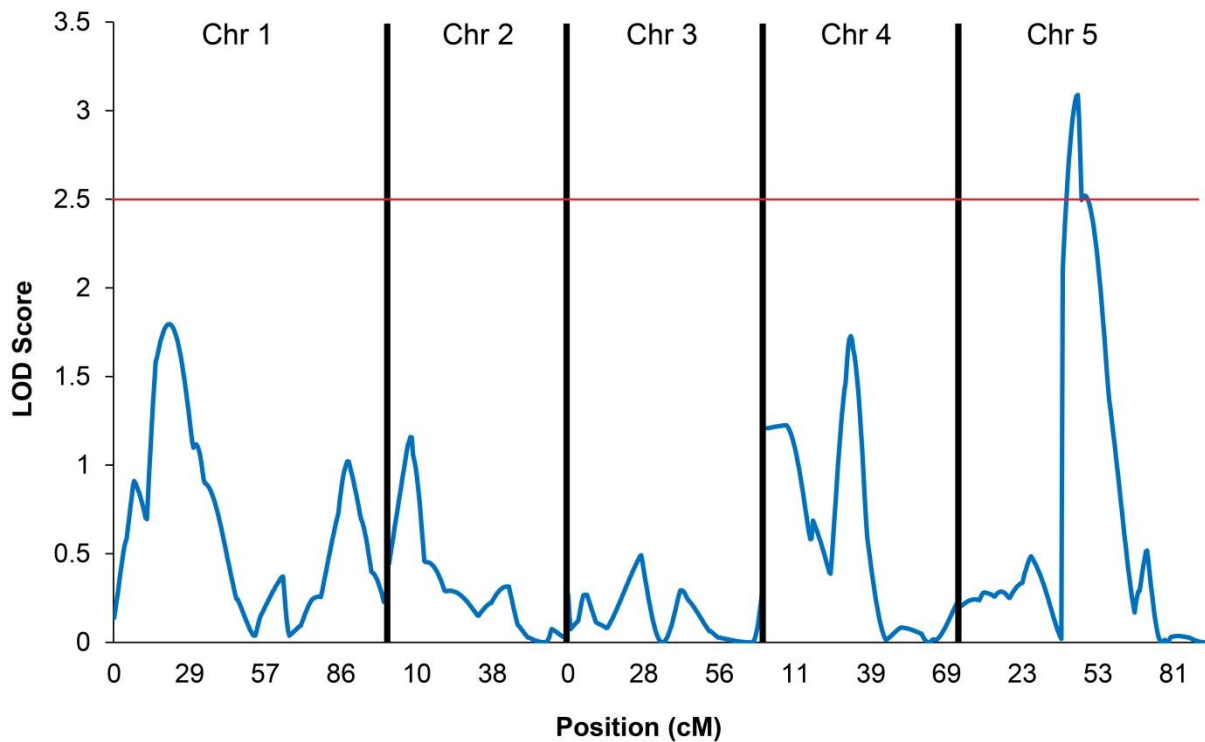
Figure 5.22. LOD score graphs predicting QTL responsible for resistance to TE1.

LOD scores are shown for Chromosome 1-5. 117 RILs (F8) generated by crossing Sha x Col-0 (Simon et al., 2008) grown on 10 µM TE1 and quantified average root length (see Figure 5.20). The data generated from average root lengths of the 174 RILs were inputted into QTL cartographer (**http://statgen.ncsu.edu/qtlcart/**) that predicts QTL responsible for resistance (Silva Lda et al., 2012).

5.4.3 Multiple trait analysis to predict TE1 resistant QTL

The data generated by screening RILs for survival rates in the presence of 25 µM TE1 and average root length in the presence of 10 µM TE1 could be used to analyse QTL by considering multiple traits. Therefore, multiple-trait analysis feature in QTL cartographer was used for CIM by inputting the data generated for both traits (see details in Chapter 2). CIM using multiple-trait analysis detected three significant QTLs, multi-trait 1a (MTR1a), MTR1b and MTR5 (Figure 5.23 and Table 5-2). MTR1a was mapped to chromosome 1 between marker 1 and 3. That is approximately 2-11 cM, which is 0.6-3 Mb in chromosome 1. MTR1b is close to MTR1a, it resides between marker 4 and 5, roughly 13-22 cM or 4.1-5.6 Mb in chromosome 1. Finally, a major QTL MTR5 was mapped to chromosome 5, between marker 8 and 11, approximately 39-61 cM or 9-16.3 Mb (Table 5-2 and Figure 5.24). All together these data suggests that the QTL detected in chromosome 5 is responsible for TE1 resistance for both traits, root length and survival rates. However, the QTL in chromosome 1 is required for survival rate, when plants are exposed to higher concentration of TE1. Therefore, the effects of the QTLs can be elucidated at different concentrations as the QTL is does not peak over LOD 2.5 in chromosome 1 when plants are only exposed to 10 µM TE1 (Figure 5.23 and Table 5-2). MTR1a covers approximately 1000 genes, MTR1b has 640 genes, and MTR5 has 1900 genes. Therefore, due to the large number of genes present in the QTLs detected it is difficult to carry out further investigation using a candidate based approach.
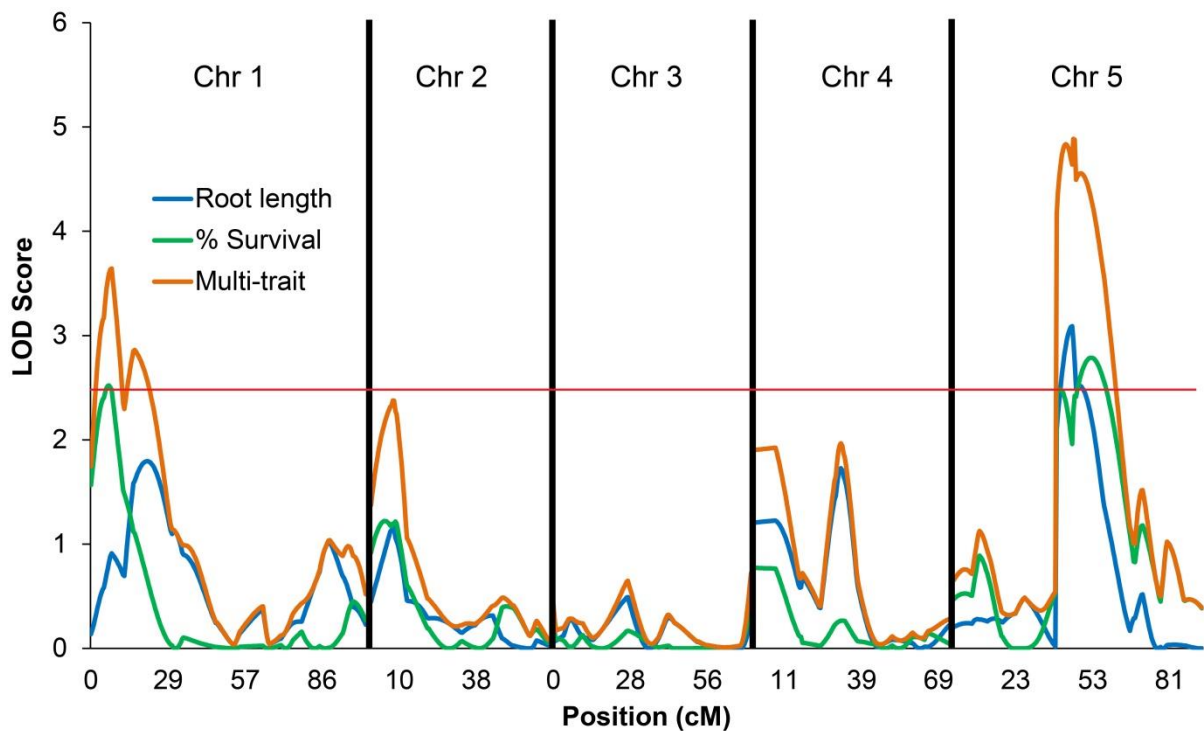
Figure 5.23. Multiple-trait mapping of predicted QTL responsible for resistance to the effects TE1.

Overlapping LOD scores for traits screened for % survival in the presence of 25 µM TE1 (green line; Figure 5.19) and average root length (blue line; Figure 5.22) are shown. The orange line shows QTL prediction by taking LOD scores for both traits in consideration. The data generated by multiple trait analysis using QTL cartographer (**http://statgen.ncsu.edu/qtlcart/**) that predicts QTLs responsible for resistance (Silva Lda et al., 2012).

Table 5-2. QTL analysis of two traits, % survival and average root length in Sha x Col-0 RIL populations

Trait	QTL	Chr – Marker	cM (Mbp)	LOD score
Survival rate	PSR1	Chr1 – 2 and 3	5-7 (2.2-3.0)	2.52
	PSR5a	Chr5 – 8	39-42 (9.0)	2.48
	PSR5b	Chr5 – 10 and 11	47-58 (13.6-16.3)	2.47-2.79
Root length	ARL5	Chr5 – 8, 9 and 10	40-50 (9.0-13.6)	2.44-3.09
Multi-trait	MTR1a	Chr1 – 1, 2 and 3	2-11 (0.6-3.0)	2.38-3.64
	MTR1b	Chr1 – 4 and 5	13-22 (4.1-5.6)	2.45-2.85
	MTR5	Chr5 – 8 to 11	39-61 (9.0-16.3)	2.51-4.89

Table 5-2. Major QTLs detected by screening Sha x Col-0 RILs for different traits.

QTLs detected for percentage survival (PSR) in the presence of 25 µM TE1 and average root length (ARL) in the presence of 10 µM TE1 are shown. QTLs detected by multiple-trait analysis (MTR) are also displayed. Chromosomes (Chr) and marker numbers and LOD scores for the detected QTLs are also shown. cM (Mbp) represents position of the QTL.
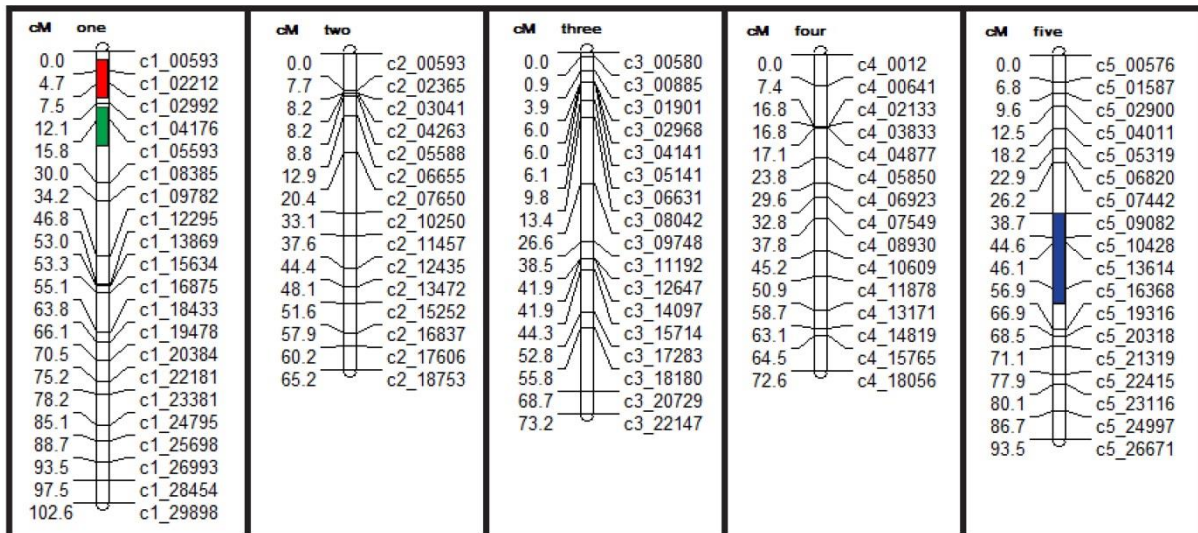
Figure 5.24. Position of the markers and QTLs mapped by screening Sha x Col-0 RILs.

The chromosomal map shows markers (the code on the right side of each chromosome map) used by Simon et al., (2008), to map the recombination in Sha x Col-0 RILs. The QTLs in chromosomes identified by multi-trait mapping is shown as red for MTR1a and green for MTR1b. MTR5 is also shown in chromosome 5 indicated in a blue region. The numbers on the left side of the chromosome maps indicate the position in cM, and chromosome numbers are indicated by the numbered letters on the top.

5.5 Identifying SNPs within the putative QTLs

One way of identifying candidate genes responsible for the TE1 resistance trait displayed by Sha and HKT2-4 is to identify SNPs in these accessions with reference to Col-0. An ideal place for SNPs identification is within the region covered by the TE1 resistance loci in the chromosome 1 (MTR1a and MTR1b) and chromosome 5 (MTR5). However, the total number of Sha and HKT2-4 SNPs on this region would still be too large for robust conclusions. This could be further narrowed by identifying the SNPs that are present in Sha or HKT2-4 but not present in other TE1 sensitive ecotypes that were screened against gravitropic response from the secondary screen onwards (see Table 5-1). Therefore, SNP identifications in the 39 *Arabidopsis thaliana* accessions, out of which only Sha and HKT2-4 were TE1 resistant, screened in the secondary screen was carried out and SNPs were identified for each accession with reference to Col-0. This was performed using POLYMORPH software, and the polymorphism tool 'SNPs by Region' was used (http://polymorph.weigelworld.org/cgi-bin/webapp.cgi). After the SNPs with reference to Col-0 were identified for each of the 39 accessions, SNPs that are unique to Sha, HKT2-4 (SNPs not present in the other 37 sensitive accessions) or SNPs common to Sha and HKT2-4 but not found in other TE1 sensitive accessions, were also identified (Figure 5.25 and Figure 5.26) (the script to identify unique SNPs was written in python software by Sean Stevenson, University of Leeds).

5.5.1 No correlation in SNP distribution is observed between Sha and HKT2-4 in QTLs in Chromosome 1

Identification of unique SNPs within MTR1a in Sha showed that there are 16 SNPs from 2.8-3.0 Mb which is at least two times the number of SNPs observed in the other regions of MTR1a (Figure 5.25A). However, the number of SNPs in MTR1a is relatively low in comparison with other QTLs. In MTR1b, 24 SNPs unique to Sha were identified from 2.4-2.6 Mb, which is higher than SNPs in other regions (Figure 5.25B). In comparison to Sha, significantly higher numbers of SNPs, unique to HKT2-4, were identified in MTR1a and MTR1b (Figure 5.25B). However, there was no correlation between the distribution of SNPs and the region in both MTR1a and MTR1b. Although the highest number of unique HKT2-4 SNPs in MTR1a was also observed between 2.4-2.6 Mb (Figure 5.25B). There were no unique SNPs shared by both Sha and HKT2-4 in MTR1a and MTR1b.
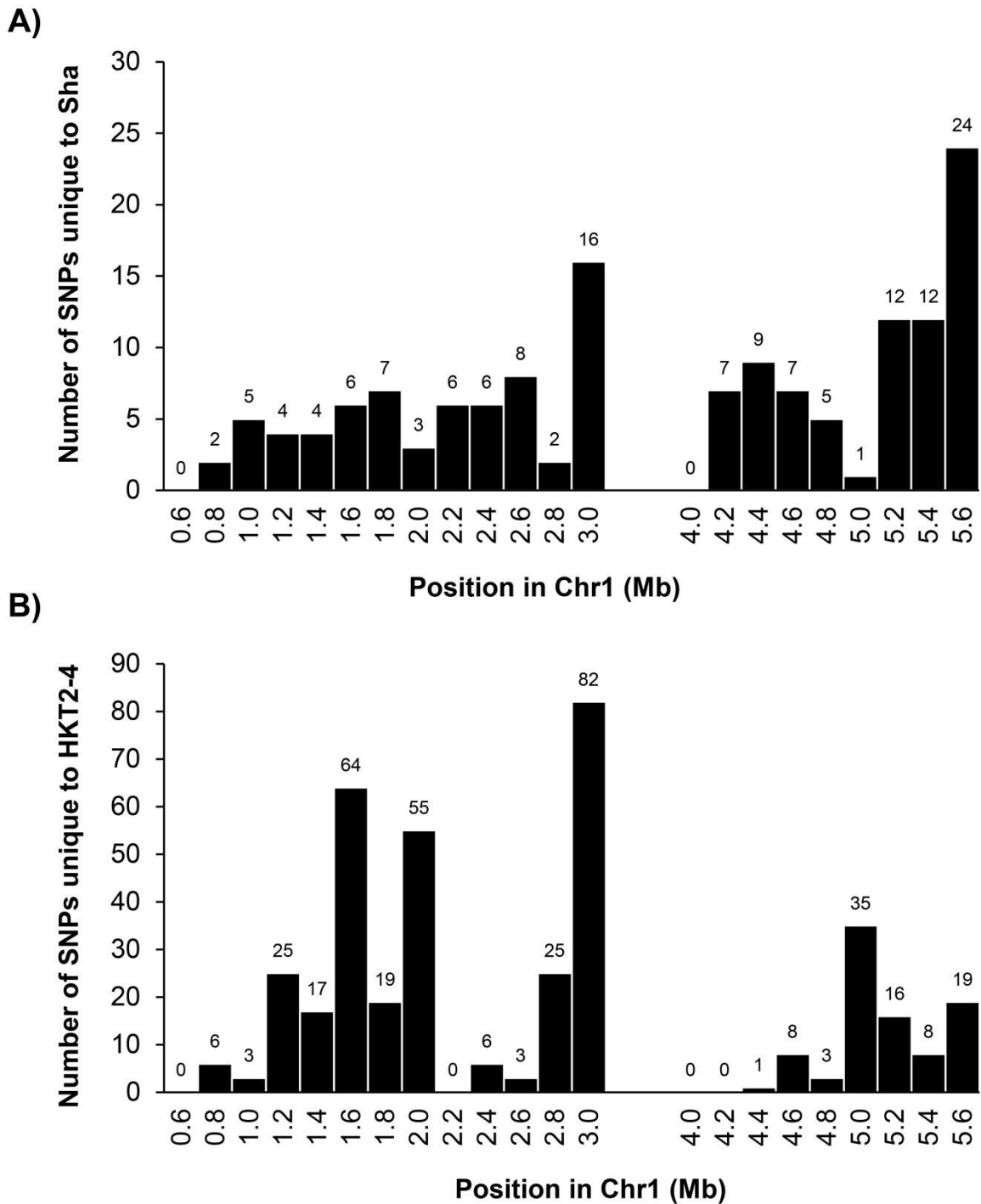
Figure 5.25. Frequency distribution of SNPs that are exclusive to TE1 resistant accessions within QTLs mapped in the chromosome 1.

SNPs were identified with reference to Col-0 for 39 accessions from the secondary screen (Table 5-1). From this, SNPs that are unique to Sha (A) and HKT2-4 (B) in the region covered by MTR1a and MTR1b were further distinguished. Number of SNPs within a region is indicated on top of the bars.

5.5.2 High number of SNPs are observed within MTR5 in chromosome 5

SNPs exclusive to Sha, HKT2-4, and SNPs that are shared by both Sha and HKT2-4 within the MTR5 region was also identified (Figure 5.26). In general a high number of unique SNPs were identified in MTR5 region for both Sha and HKT2-4 (Figure 5.26). In Sha, the number of unique SNPs between 9-13.8 Mb was relatively low in comparison to the number of SNPs identified in region between 14-16.6 Mb in chromosome 5 (Figure 5.26A). However in HKT2-4, high number of unique SNPs was identified in between 10.6-11 Mb and between 13.6-14 Mb (Figure 5.26B). The number of unique SNPs between 11.2-13.4 Mb is relatively low for both Sha and HKT2-4. Unlike in MTR1a and MTR1b, unique SNPs that are common to both Sha and HKT2-4 were identified in MTR5 (Figure 5.26C). Manual analysis of the unique SNPs common to Sha and HKT2-4 was also identified using the GBrowse software (http://gbrowse.tacc.utexas.edu/cgi-bin/gb2/gbrowse/arabidopsis/) that is available from The Arabidopsis information resource (http://www.arabidopsis.org/). This showed that total eight SNPs out of 28 were in the gene coding region. Transposable element gene (AT5G27902.1) contained SNP at 9922653 bp that caused G to A base pair change, with reference to Col-0, in both Sha and HKT2-4. The second gene was Ulp1 cysteine-type peptidase (AT5G28235.1), which is predicted to be located at the plasma membrane. This gene had two unique SNPs at 10202115 bp (A → G) and 10202258 bp (C → T), in the coding region that was common to Sha and HKT2-4. Finally, the third gene encodes 20S proteasome alpha subunit A1 (AT5G35590.1), which is predicted to be localised to the cytoplasm and the vacuolar membrane. This protein contained five unique SNPs present in both Sha and HKT2-4 at 13766369 bp (T → C), 13766371 bp (T → C), 13766372 (G → A), 13766375 (A → G), and 13766487 (T → C). The base pair change indicated is the same for both Sha and HKT2-4, and it is with reference to Col-0.
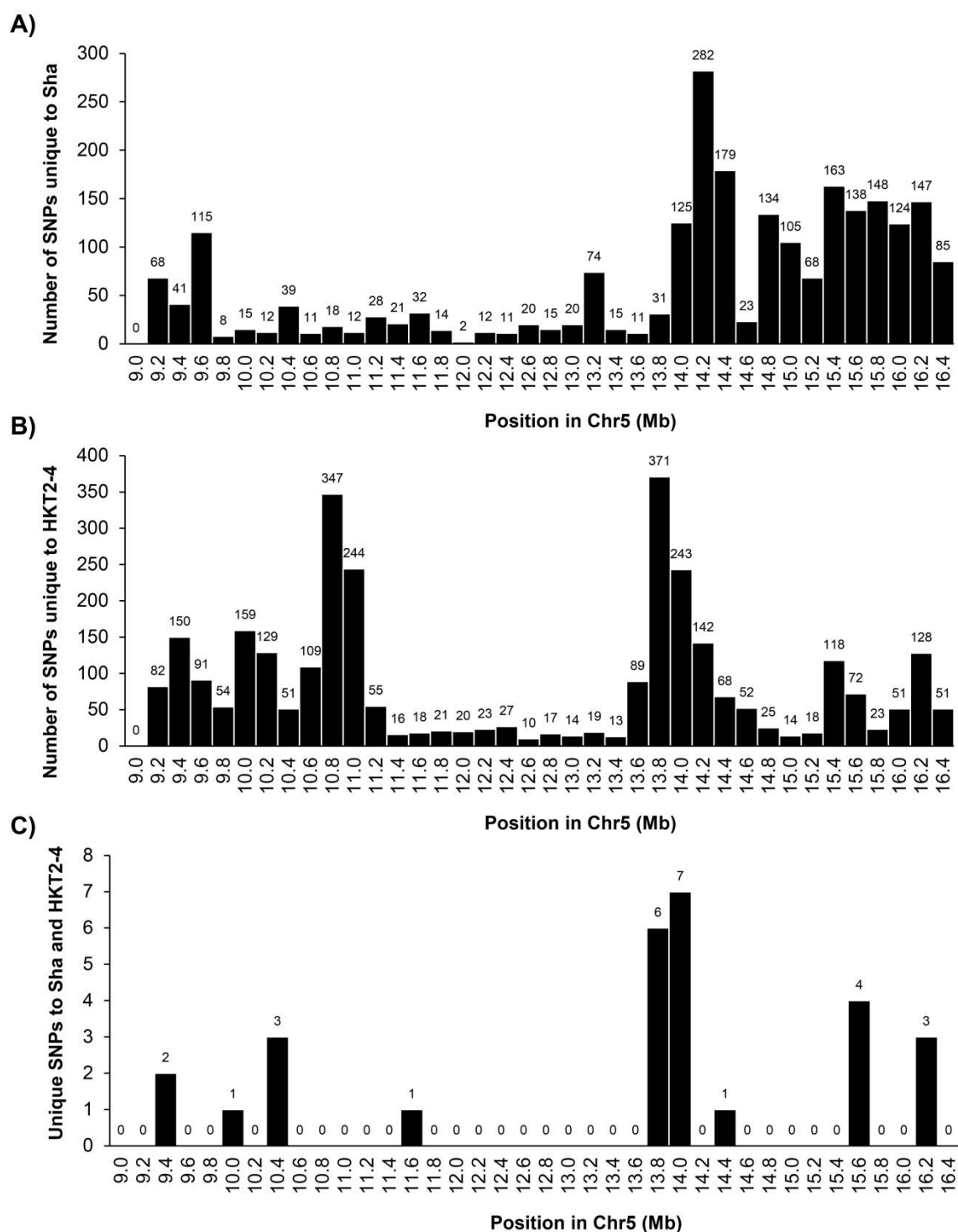
Figure 5.26. Frequency distribution of SNPs that are exclusive to TE1 resistant accessions within QTL mapped in the chromosome 5.

SNPs were identified with reference to Col-0 for 39 accessions from the secondary screen (Table 5-1). From this, SNPs that are unique to Sha (A), HKT2-4 (B), and unique SNPs shared by Sha and HKT2-4 (C) in the region covered by MTR5 were further distinguished. Number of SNPs within a region is indicated on top of the bars.

5.6 Discussion

As previously shown in this thesis, compound TE1 reduces root gravitropic response (Chapter 3, Figure 3.20). Therefore, reduced gravitropic response was used as a phenotype in a genetic screen to identify *Arabidopsis thaliana* natural accessions that display resistance to the effects of TE1. The 83 *Arabidopsis thaliana* accessions were screened by Adam Jamaluddin (MSc student 2012, University of Leeds), and he identified two ecotypes, Sha and HKT2-4 that display reduced sensitivity to the agravitropic growth caused by TE1 (Figure 5.3 and Table 5-1). These *Arabidopsis thaliana* accessions were independently confirmed to display reduced sensitivity to the agravitropic growth caused by 1 µM or 2 µM TE1 (Figure 5.4A and Figure 5.5).

As shown in Chapter 4, depolymerisation of the actin cytoskeleton was not observed, under the confocal microscope, either on short term exposure to 25 µM TE1 or 48 h exposure to 10 µM TE1 (Figure 4.13 and Figure 4.14). Depolymerisation of the actin cytoskeleton is observed in the presence of 10 nM LatB (Figure 4.13). However, it can also be seen that even slight depolymerisation of the actin filaments increases root bending in response to gravistimulation (Figure 5.4A). Similarly, enhanced root bending has been shown upon LatB treatment in maize (Hou et al., 2003) and *Arabidopsis thaliana* (Hou et al., 2004) roots. Sha and HKT2-4, were selected as being resistant to multiple effects of TE1. This included resistance to agravitropic growth, root growth inhibition and increased survival percentages (Figure 5.4 – Figure 5.8). Furthermore, these findings were complemented by the resistance to the TE1 inhibition of endocytosis displayed by Sha and HKT2-4 (Figure 5.9). This suggests there is a common mechanism underlying these effects. Therefore, these accessions were tested for gravitropic response in the presence of TE1 and LatB, which allowed the effects of TE1 and LatB to be further distinguished. As expected, increased gravitropic bending was observed in the presence of LatB in the TE1 sensitive ecotypes Col-0 and Ler. Similarly, in the presence of LatB, the TE1 resistant ecotype HKT2-4 also displayed increased root bending and Sha showed no change in root bending upon gravistimulation (Figure 5.4A). These results indicate that reduced sensitivity to TE1 displayed by Sha and HKT2-4 does not directly involve changes in actin polymerisation. In addition, 50 nM LatB decreased the root growth in both TE1 sensitive and resistant ecotypes (Figure 5.4B), which suggests

that LatB has similar effects on all these ecotypes therefore actin cytoskeleton and its interactions are similar in Sha and HKT2-4 in comparison to Col-0 accession.

The root growth analysis and survival percentage assay reveal that the TE1 resistant accessions, Sha and HKT2-4, are not completely resistant to the effects of TE1. In Sha and HKT2-4 roots, significant reduction in average root bending, upon gravistimulation, was still observed in the presence of 2 µM TE1. However, this effect was much lower in comparison to Col-0 or Ler (Figure 5.4A). Similarly, delayed and reduced uptake of FM4-64 in Sha and HKT2-4 was observed in the presence of 25 µM TE1, whereas in Col-0, TE1 caused total inhibition of endocytic FM4-64 uptake (Figure 5.9 and Figure 5.10). Therefore, it is sensible to acknowledge Sha and HKT2-4 as displaying reduced sensitivity to the effects of TE1, not complete resistance. This observation is further confirmed, as increasing concentration of TE1 causes increased inhibition of root growth in Sha and HKT2-4 seedlings, although this effect is less compared to Col-0 and Ler seedlings (Figure 5.6 and Figure 5.8). With all the results suggesting that Sha and HKT2-4 are still sensitive to the effects of TE1 but that they are more resistant than Col-0 or Ler, it is possible that difference in gene expression may well be the underlying factor for this effect. For example, the gene responsible for resistance against TE1 may be highly expressed in Sha or HKT2-4. The possibility of more than one gene or protein may also contribute to the effect on Sha/HKT2-4 cannot be ruled out. Reduced uptake and high rate of compound metabolism may also be an underlying factor for reduced TE1 sensitivity observed in Sha and HKT2-4.

The accession HKT2-4 was collected from Heiligkreuztal in Germany. However, beside the genome sequence (Cao et al., 2011) not much is known about this accession. Meanwhile, Sha was harvested from the mountainous region of Pamiro-Alay in Tajikistan. This could why Sha is considered to be one of the more resistant accessions to drought (Bouchabke et al., 2008) and salt stress (Ren et al., 2010). It is unlikely that drought resistance feature of Sha is responsible for TE1 resistance. Although, long term chronic exposure of high concentration of TE1 leads to severe growth inhibition of Col-0 seedlings (Figure 5.8), resembling a stress phenotype, no root growth inhibition is observed at 1 µM TE1 (Chapter 3, Figure 3.20). And at 1 µM TE1, inhibition of root gravitropic response is observed without any effect to the root growth (Figure 5.4 and Figure 5.5).

It has also been demonstrated that Sha does not release mucilage (pectinaceous polysaccharides) on seed imbibition (Macquet et al., 2007). This could mean that there is less uptake of the TE1 from the media when the seed is about to germinate, therefore TE1 is less effective on Sha root growth inhibition. But this is unlikely to happen as suggested by few points. (1) As germination rates of TE1 sensitive Col-0 seeds were not affected in the presence of TE1 (Chapter 3, Figure 3.7), it is unlikely that possible decreased uptake of TE1 before germination is likely to affect root growth. (2) The effects of TE1 takes place within 120 min (Chapter 4, Figure 4.2 and Figure 4.4) and growth in sensitive ecotypes, Col-0 and Ler, is seen to be arrested after a certain stage (Figure 5.8) therefore, exposure to the TE1 after germination would arrest the growth after that certain stage if the ecotype was increasingly sensitive. And (3), the gravitropic assay shows that lack of mucilage release in Sha has nothing to do with TE1 activity as the seedlings were already germinated and root was fully exposed to the TE1 in the media by the time seedlings were transplanted to media containing TE1 (Figure 5.4). Therefore, the nature of TE1 resistance displayed by the ecotypes, HKT2-4 and Sha, has not been described before.

Genetic investigation of the F1 and F2 crosses revealed that the TE1 resistance trait displayed by HKT2-4 is not dominant. As suggested by the data, the TE1 resistant trait is semi-dominant (Figure 5.12 – Figure 5.14, and Figure 5.16). Similarly, F1 data suggested that the TE1 resistant trait displayed by Sha is most likely a recessive trait. However, this could not be confirmed by the F2 crosses due to the lack of reliable control seedling growth. However, when this was fitted into expected root growth of Sha seedlings in the presence of TE1, the trait seemed to be recessive, which is in agreement with the F1 data (Figure 5.12 – Figure 5.15). One interesting observation was that the percentage of germination was substantially decreased in F1 crosses with Sha and HKT2-4 that used Col-0 as a female parent. This was consistent in the presence and in absence of TE1, suggesting this was not due to the effects of TE1 (Figure 5.11). One of the reasons for this effect could be that cytoplasmic inheritance from Col-0 may not be compatible with Sha or with HKT2-4.

Sha has been reported to be display differential response to auxin signalling with reference to Col-0 (Delker et al., 2010). The results displayed in this study shows that Sha is slightly more sensitive to auxin mediated root inhibition and increased

hypocotyl elongation at elevated auxin levels grown in higher temperatures but the general pattern was similar, and the magnitude of difference is not very large too. However, auxin-induced gene expression in Sha roots is significantly lower than Col-0, but the endogenous auxin level were similar between Sha and Col-0. Moreover, there was only 34% overlap between the auxin induced genes in Sha and Col-0 (Delker et al., 2010), therefore two third of genes induced by auxin are unique to Sha. However, the genes that display difference in auxin induced expression pattern in Sha and Col-0 (Delker et al., 2010), were not found to be in the major QTL MTR5. So, if Sha is less sensitive to the effects of auxin and if the auxin responsive genes are unique in Sha then this could explain why Sha displays partial resistance to the effects of TE1, which essentially changes the distribution of auxin by interfering with protein recycling required for proper positioning of auxin efflux carriers. Similarly, natural variation in plant hormone induced gene expression, using salicylic acid, revealed wide variation in transcript levels between the *Arabidopsis thaliana* accessions tested (van Leeuwen et al., 2007).

Studies on natural variation of root architecture and growth also revealed wide variation in different accessions (Loudet et al., 2005; Kellermeier et al., 2013). However, the data generated throughout this thesis suggest that the average root growth of Sha is similar to Col-0, although the seedlings did display wide variation in growth even though they were descended from a single seed, obtained from the Nottingham Arabidopsis Stock Centre. However, HKT2-4 displayed much more uniform growth and the average root length was generally longer than Sha and Col-0. Wide variation in root architecture is also observed in Sha accession as determined by lateral root length and density (Loudet et al., 2005). Recently, auxin was reported generate 'anti-gravitropic offset', a force acting against gravity, that determines the non-vertical growth of lateral organs in *Arabidopsis thaliana* (Roychoudhry et al., 2013). Therefore, this variation in root architecture, in comparison to Col-0, may be explained by the differential response to auxin displayed by Sha (Delker et al., 2010).

RILs that display a wide range of traits were seen in Sha x Col-0 lines (Simon et al., 2008) that are readily available. RIL populations also exist between Sha and Bay-0 (Loudet et al., 2002), and Sha and Ler (Clerkx et al., 2004). Sha and Col-0 were chosen for quantitative genetics approach to map the TE1 resistance loci. This is

because all the cell biology investigations took place in Col-0 background. The similarity in root growth between Col-0 and Sha and drastic difference seen in the presence of TE1 also limits environmental variation that may change the outcome of the QTL mapping. The RILs were screened for average root length trait at 10 μM TE1 and survival rates at 25 μM TE1. The QTL output identified a single major QTL ARL5 at chromosome 5 underlying the resistance to root growth inhibition at 10 μM TE1 (Figure 5.22). Similarly, two QTLs PSR5a and PSR5b were also observed at the same region when RILs were screened at 25 μM TE1 against survival rates (Figure 5.19). At 25 μM TE1, a QTL from chromosome 1, PSR1, also contributed to the resistance phenotype, which was not required for 10 μM TE1 (Figure 5.19, Figure 5.22 and Table 5-2). The possibility that independent but linked genes, within the different identified resistant loci, governing both traits cannot be ruled out. Taken together, multiple trait mapping has identified three putative QTLs that are involved in TE1 insensitivity displayed by Sha (Figure 5.23 and Table 5-2). These QTLs provide an excellent platform to identify molecular targets of the compound TE1. Further analysis of the QTL regions in resistant vs sensitive ecotypes revealed identification of SNPs that are exclusive to Sha or HKT2-4. However, due to the large number of SNPs identified it is also not possible to analyse all of them. If the QTL region is still narrowed down then this approach may prove to be useful way of identifying the genes contributing to the resistance. For example, right now the QTL region is too large to work on candidate based approach. But in a narrower region, unique SNP(s) may be detected and this could correlate with SNP(s) in a candidate gene, which may provide additional confidence required to carry out genetic analysis using either knockout or overexpression lines. Narrowing down the QTL region may be carried out by using the RILs that are highly resistance to TE1, which could be used for fine mapping purposes, a process that is already underway in the laboratory using CAPS and derived CAPS markers (by Dr. Heba Ebeed, University of Leeds). These can then be used to narrow down the QTL region and candidate genes may be identified which can be used for complementation in Col-0 and introducing the sensitive version of the gene from Col-0 to Sha to identify molecular target of the compound TE1.

6 Chapter Six – Conclusions, general discussion and future perspectives

6.1 Conclusions and summary

This study characterised the physiological and cellular effects of the small molecule, Trafficking and ENdocytosis inhibitor 1 (TENin1; TE1). TE1 was shown to cause dose-dependent inhibition of root and hypocotyl growth. Upon long term exposure it also changed the morphology of the ER and reduced organelle movements. It was shown to be an inhibitor of root and hypocotyl gravitropism. Molecular dissection of the endomembrane protein trafficking pathway in *Arabidopsis thaliana* roots revealed the mode of action of TE1, demonstrating that it interfered with protein recycling from the PM and the PVC, including that of the auxin efflux carrier PIN2. This leads to protein accumulation at the PVC, and after longer periods, increased protein level is observed in the vacuole. TE1 is ultimately lethal to plants if they are exposed for long periods at high concentrations, but the effects may be reversed if the plants are transferred to compound free media after 5 days. A screen using 83 *Arabidopsis thaliana* natural variants revealed that Sha and HKT2-4 display reduced sensitivity to the effects of TE1. This work was initiated by Adam Jamaluddin (MSc student, University of Leeds) who carried out the screen. This work was continued in this study, characterising the phenotypic and cellular effects on Sha and HKT2-4 and screening a population of Sha x Col-0 recombinant inbred lines for both survival and root growth phenotypes. Three putative QTLs were mapped that may contribute to the TE1 resistance in *Arabidopsis thaliana* accession Sha.

6.2 TE1 mediated inhibition of *Arabidopsis thaliana* seedling growth is likely to be due to the inhibition endocytic recycling

TE1 shows dose dependent inhibition root length and hypocotyl elongation in dark grown seedlings. This is likely to be due to the primary effects of TE1 on endomembrane trafficking, which eventually changes the distribution of hormones required for cell expansion and plant growth. TE1 inhibited the re-distribution of auxin in *Arabidopsis thaliana* roots, which could be a consequence of the inhibition in endocytic recycling of auxin efflux carriers. It is well known that plant hormones such as auxin, gibberellin, brassinosteroid and cytokinin, all influence cell elongation and growth (Hobbie, 1998; Moller and Chua, 1999; Kepinski and Leyser, 2005b).

It is also known that cell elongation requires delivery of cell wall components and enzymes, that are trafficked through endomembrane compartments, coordinated with the dynamic actin cytoskeleton (Hepler et al., 2001). ECHIDNA protein required for secretory trafficking of the cell wall polysaccharides (Gendre et al., 2013) from the TGN was shown to be required for root growth in light and hypocotyl elongation in dark (Gendre et al., 2011). The delivery of these components required for cell expansion is unlikely to be affected by TE1 as secretory trafficking of newly synthesised secGFP was functional in the presence of TE1. However, polarised growth may need polarised endocytic recycling of membrane proteins required for cell wall synthesis. And, there is evidence that already suggest that polarisation of membrane proteins, at least of PIN proteins, is achieved by endocytic recycling (Dhonukshe et al., 2008a; Kleine-Vehn et al., 2009; Dhonukshe et al., 2010). Therefore, the growth effect inhibition by TE1 may be linked to inhibition of endocytic recycling.

6.3 TE1 induced protein accumulation in the ARA7 positive compartment provides a platform to the identification of mechanism of action of TE1

Identification of the molecular target presents a major challenge in chemical biology (Cong et al., 2012). However, this study has identified a mode of action of the chemical TE1. This may be used as a lead to study and characterise the mechanism of action that is interfered by the compound. Small GTP binding, such as the family of Rab and ARF GTPases required for vasicular trafficking (Nielsen et al., 2008), present a potential target of TE1. ARA7 (RabF2b), is localised to a sub-population of the prevacuolar compartment (Kotzer et al., 2004), where TE1 induced protein accumulation is observed, and a dominant negative version of ARA7 also inhibited endocytosis (Dhonukshe et al., 2008a), similar to the effects of TE1. Even though ARA7 is reported to be required for vacuolar trafficking (Kotzer et al., 2004), some interference with components in the ARA7 positive compartment could explain why TE1 is inhibiting endocytosis and recycling from the PVC. In this context it is interesting that a similar compound Rhodblock 4 acts as an inhibitor of rho GTPases mediated pathway during cytokinesis in Drosophila cells (Castoreno et al., 2010). I tested Rhodblock 4, to determine if it alters PIN2 localisation in *Arabidopsis thaliana* roots. However, Rhodblock 4 had no effect on PIN2 localisation, but it remains

possible that differences between the plant and animal small GTPases could account for the lack of activity.

Another possibility is that TE1 affects the components of cytoskeleton and its dynamics. Even though no depolymerisation or bundling of the actin filaments were visualised under the confocal microscope after 120 min at 25 µM TE1 or after 48 h treatment at 10 µM TE1, the possibility of subtle changes in actin dynamics cannot be ruled out. Short term treatment with microtubule depolymerising drug oryzalin did not cause any changes to PIN1 positioning (Geldner et al., 2001). However, recently a report demonstrated that the microtubule binding protein, Cytoplasmic Linker Associated Protein (CLASP), interacts with Sorting Nexin 1 (SNX1) (Ambrose et al., 2013). CLASP has been shown to be required for microtubule polymerisation (Ambrose and Wasteneys, 2008). Similar to the effects of TE1, microtubule depolymerisation caused increased accumulation of PIN2 to the vacuole (Ambrose et al., 2013). This fits in with the model that CLASP interacts with SNX1, which has been shown to be required for PIN2 recycling in a wortmannin sensitive compartment (Jaillais et al., 2006). It is known that the SNX1 protein is a subunit of the retromer complex which is thought to be required for protein recycling from the PVC to the TGN (Oliviusson et al., 2006; Zouhar et al., 2009; Kang et al., 2012; Nodzynski et al., 2013).

6.4 Future prospective

6.4.1 Biochemical approach and the major QTL at chromosome 5 may be used for molecular target identification

Compound TE1 may be used as a tool to dissect trafficking pathways, and identification of the molecular target may provide a significant link between endocytosis and protein recycling from the PVC, a process that is not very well characterised. Identification of the QTLs provides a good platform for the target identification and fine-mapping procedures are already taking place in the laboratory to narrow down the QTL regions and subsequently identify the genetic regions responsible for TE1 resistance. The QTLs were identified by screening for long term effects of TE1 on root growth inhibition and survival rates therefore the inhibition of trafficking events suggest these effects are pleiotropic consequences of membrane trafficking defects, since the partially resistant accessions Sha and HKT2-4 also

showed reduced inhibition of endocytosis by TE1. Given the substantial time and resources, it might be worthwhile to screen the RILs for FM4-64 uptake after 120 min treatment on TE1 and setup a confocal based screen to identify resistant RILs that show FM4-64 internalisation. This could be a more accurate screen because short term inhibition of endocytosis is likely to be closer to a primary inhibition caused by TE1 rather than root growth inhibition and survival rates assay, which is likely to represent a pleiotropic effect after long term chronic treatment in the compound.

An alternative route to the target identification is via a biochemical approach, using derivatives of the compound to label or purify the molecular target (Kumari and van der Hoorn, 2011; Lenger et al., 2012). The SAR study performed on TE1 structural analogues showed that only very limited modification of the molecule could be tolerated and still retain biological activity. This means that the ability to incorporate a reactive group to allow covalent modification of the target or a tag such as biotin into TE1 that might enable an affinity purification based approach could not be followed.

6.4.2 TE1 and other small molecules may be used as a tool to dissect endomembrane trafficking components

Likewise lot of questions are left unanswered in endomembrane biology itself. For example, the theory that BFA specifically affects proteins recycling to the PM is questionable, as shown by the inhibition of secGFP trafficking in the presence of BFA. To further address this question a co-localisation experiment with FM4-64 needs to be performed to ask whether the secGFP is accumulating in the ER surrounding the nucleus or if they are getting stuck in the BFA compartment. If the BFA compartment marked by FM4-64 co-localises with secGFP then it will be appropriate to conclude that newly synthesised proteins undergo trafficking to the PM through the TGN and this requires the action of a BFA sensitive ARF-GEF. Consequently, does BFA affect the morphology of PVC? This is a relatively simple question to answer and needs screening the PVC markers in the presence of BFA. But this could provide us with invaluable insights into the vacuolar trafficking. If the TGN is collapsed in the presence of BFA and trafficking to the vacuole is functional then we can further elucidate the trafficking pathways by looking at endocytic trafficking of FM4-64 and if that reaches the vacuole then perhaps there is evidence that TGN is not required for trafficking of endocytic trafficking to the vacuole. This can also be used on trafficking of newly synthesised proteins.

Trafficking of secGFP was not seen to be affected by TE1. Therefore, it is likely that the soluble proteins trafficking towards the PM do not require additional receptors recycling from the PM, as TE1 inhibits recycling from the PM just after 120 min treatment. Further investigation would be necessary to determine whether this hypothesis is viable or not. This can be performed in a protoplast system by investigating soluble and membrane spanning proteins cargo delivery to the PM. If TE1 does not affect delivery of soluble proteins as seen with secGFP and inhibits delivery of membrane spanning proteins to the PM, then it suggest that additional components recycling from the PM is required the secretory trafficking of membrane proteins. Additionally, the trafficking pathways may be further dissected by using tyrphostin A23, which is reported to specifically inhibit the action of AP-2 (Banbury et al., 2003), therefore inhibiting clathrin mediated endocytosis from the PM (Dhonukshe et al., 2007). This can further determine if clathrin independent endocytosis is able to rescue the trafficking inhibition of membrane protein, given that TE1 inhibits trafficking of newly synthesised membrane proteins.

Is TGN the first endomembrane compartment which the endocytic trafficking merges with? This is a difficult question to answer as constitutive endocytic trafficking takes place at a high rate and overlaps with the secretory trafficking pathway. FM4-64 co-localises with the TGN after 6 min (Dettmer et al., 2006), and due to the limitations of experimental setup it is not feasible to image the marker lines before that time. However, if endocytosis is inhibited by TE1 and washout is performed in the presence of FM4-64 then the endocytosis may be monitored in marker lines i.e. VHAa1-GFP, SYP61-CFP, GNOM-GFP, GFP-ARA7 or other defined endomembrane markers, and observe the co-localisation to see if there is a possibility that endocytic trafficking may quickly pass through a compartment before reaching the TGN after 6 min under normal condition. This is made possible due to the easily reversible effects of TE1, which makes it a more attractive tool for investigation of protein trafficking in different organisms. For example, the proteins accumulated in the PVC may be tested for reversibility and see if they are recycled back to the PM or diverted to the vacuole. This may provide a first direct evidence of protein recycling from the PVC. Compound TE1 should also be useful in the future to dissect the complex endomembrane protein trafficking pathways. Especially, as it

only interferes with endomembrane protein recycling therefore, role of newly synthesised membrane, vacuolar or soluble proteins may be interrogated.

Why does TE1 not affect the trafficking to the vacuole, as seen with wortmannin, if it is inhibiting the recycling of proteins from the PVC? Does this mean there is a vacuolar trafficking pathway that does not require PVC? Does secretory proteins and endocytic protein trafficking require the TGN en route to the vacuole? Does TE1 affect trafficking machinery of other eukaryotic endomembrane system? TE1 and other small molecule inhibitors of endomembrane trafficking systems may be used to address these questions in the future.

7 References

Abas, L., Benjamins, R., Malenica, N., Paciorek, T., Wisniewska, J., Moulinier-Anzola, J.C., Sieberer, T., Friml, J., and Luschnig, C. (2006). Intracellular trafficking and proteolysis of the Arabidopsis auxin-efflux facilitator PIN2 are involved in root gravitropism. Nat Cell Biol **8,** 249-256.

Aikawa, Y., and Martin, T.F. (2005). ADP-ribosylation factor 6 regulation of phosphatidylinositol-4,5-bisphosphate synthesis, endocytosis, and exocytosis. Methods in enzymology **404,** 422-431.

Alonso, J.M., Stepanova, A.N., Leisse, T.J., Kim, C.J., Chen, H., Shinn, P., Stevenson, D.K., Zimmerman, J., Barajas, P., Cheuk, R., Gadrinab, C., Heller, C., Jeske, A., Koesema, E., Meyers, C.C., Parker, H., Prednis, L., Ansari, Y., Choy, N., Deen, H., Geralt, M., Hazari, N., Hom, E., Karnes, M., Mulholland, C., Ndubaku, R., Schmidt, I., Guzman, P., Aguilar-Henonin, L., Schmid, M., Weigel, D., Carter, D.E., Marchand, T., Risseeuw, E., Brogden, D., Zeko, A., Crosby, W.L., Berry, C.C., and Ecker, J.R. (2003). Genome-wide insertional mutagenesis of Arabidopsis thaliana. Science **301,** 653-657.

Ambrose, C., Ruan, Y., Gardiner, J., Tamblyn, L.M., Catching, A., Kirik, V., Marc, J., Overall, R., and Wasteneys, G.O. (2013). CLASP interacts with sorting nexin 1 to link microtubules and auxin transport via PIN2 recycling in Arabidopsis thaliana. Developmental cell **24,** 649-659.

Ambrose, J.C., and Wasteneys, G.O. (2008). CLASP modulates microtubule-cortex interaction during self-organization of acentrosomal microtubules. Molecular biology of the cell **19,** 4730-4737.

Babst, M. (2011). MVB vesicle formation: ESCRT-dependent, ESCRT-independent and everything in between. Current Opinion in Cell Biology **23,** 452-457.

Banbury, D.N., Oakley, J.D., Sessions, R.B., and Banting, G. (2003). Tyrphostin A23 inhibits internalization of the transferrin receptor by perturbing the interaction between tyrosine motifs and the medium chain subunit of the AP-2 adaptor complex. J Biol Chem **278,** 12022-12028.

Band, L.R., Wells, D.M., Larrieu, A., Sun, J.Y., Middleton, A.M., French, A.P., Brunoud, G., Sato, E.M., Wilson, M.H., Peret, B., Oliva, M., Swarup, R., Sairanen, I., Parry, G., Ljung, K., Beeckman, T., Garibaldi, J.M., Estelle, M., Owen, M.R., Vissenberg, K., Hodgman, T.C., Pridmore, T.P., King, J.R., Vernoux, T., and Bennett, M.J. (2012). Root gravitropism is regulated by a transient lateral auxin gradient controlled by a tipping-point mechanism. P Natl Acad Sci USA **109,** 4668-4673.

Bandmann, V., and Homann, U. (2012). Clathrin-independent endocytosis contributes to uptake of glucose into BY-2 protoplasts. Plant J **70,** 578-584.

Bandyopadhyay, A., Blakeslee, J.J., Lee, O.R., Mravec, J., Sauer, M., Titapiwatanakun, B., Makam, S.N., Bouchard, R., Geisler, M., Martinoia, E., Friml, J., Peer, W.A., and Murphy, A.S. (2007). Interactions of PIN and PGP auxin transport mechanisms. Biochem Soc Trans **35,** 137-141.

Bar, M., Sharfman, M., Schuster, S., and Avni, A. (2009). The coiled-coil domain of EHD2 mediates inhibition of LeEix2 endocytosis and signaling. PloS one **4,** e7973.

Barbez, E., Kubes, M., Rolcik, J., Beziat, C., Pencik, A., Wang, B., Rosquete, M.R., Zhu, J., Dobrev, P.I., Lee, Y., Zazimalova, E., Petrasek, J., Geisler, M., Friml, J., and Kleine-Vehn, J. (2012). A novel putative auxin carrier

family regulates intracellular auxin homeostasis in plants. Nature **485,** 119-122.

Barlowe, C., Orci, L., Yeung, T., Hosobuchi, M., Hamamoto, S., Salama, N., Rexach, M.F., Ravazzola, M., Amherdt, M., and Schekman, R. (1994). COPII: a membrane coat formed by Sec proteins that drive vesicle budding from the endoplasmic reticulum. Cell **77,** 895-907.

Barth, M., and Holstein, S.E.H. (2004). Identification and functional characterization of Arabidopsis AP180, a binding partner of plant alpha C-adaptin. Journal of Cell Science **117,** 2051-2062.

Bassil, E., Ohto, M.A., Esumi, T., Tajima, H., Zhu, Z., Cagnac, O., Belmonte, M., Peleg, Z., Yamaguchi, T., and Blumwald, E. (2011). The Arabidopsis intracellular Na+/H+ antiporters NHX5 and NHX6 are endosome associated and necessary for plant growth and development. Plant Cell **23,** 224-239.

Batoko, H., Zheng, H.Q., Hawes, C., and Moore, I. (2000). A rab1 GTPase is required for transport between the endoplasmic reticulum and golgi apparatus and for normal golgi movement in plants. Plant Cell **12,** 2201-2218.

Bell, C.J., and Ecker, J.R. (1994). Assignment of 30 microsatellite loci to the linkage map of Arabidopsis. Genomics **19,** 137-144.

Bender, R.L., Fekete, M.L., Klinkenberg, P.M., Hampton, M., Bauer, B., Malecha, M., Lindgren, K., J, A.M., Perera, M.A., Nikolau, B.J., and Carter, C.J. (2013). PIN6 is required for nectary auxin response and short stamen development. Plant J.

Bethune, J., Wieland, F., and Moelleken, J. (2006). COPI-mediated transport. The Journal of membrane biology **211,** 65-79.

Blakeslee, J.J., Bandyopadhyay, A., Lee, O.R., Mravec, J., Titapiwatanakun, B., Sauer, M., Makam, S.N., Cheng, Y., Bouchard, R., Adamec, J., Geisler, M., Nagashima, A., Sakai, T., Martinoia, E., Friml, J., Peer, W.A., and Murphy, A.S. (2007). Interactions among PIN-FORMED and P-glycoprotein auxin transporters in Arabidopsis. Plant Cell **19,** 131-147.

Boevink, P., Martin, B., Oparka, K., Cruz, S.S., and Hawes, C. (1999). Transport of virally expressed green fluorescent protein through the secretory pathway in tobacco leaves is inhibited by cold shock and brefeldin A. Planta **208,** 392-400.

Bottanelli, F., Gershlick, D.C., and Denecke, J. (2012). Evidence for sequential action of Rab5 and Rab7 GTPases in prevacuolar organelle partitioning. Traffic **13,** 338-354.

Bouchabke, O., Chang, F., Simon, M., Voisin, R., Pelletier, G., and Durand-Tardif, M. (2008). Natural variation in Arabidopsis thaliana as a tool for highlighting differential drought responses. PloS one **3,** e1705.

Brown, L.A., O'Leary-Steele, C., Brookes, P., Armitage, L., Kepinski, S., Warriner, S.L., and Baker, A. (2011). A small molecule with differential effects on the PTS1 and PTS2 peroxisome matrix import pathways. Plant J **65,** 980-990.

Brunoud, G., Wells, D.M., Oliva, M., Larrieu, A., Mirabet, V., Burrow, A.H., Beeckman, T., Kepinski, S., Traas, J., Bennett, M.J., and Vernoux, T. (2012). A novel sensor to map auxin response and distribution at high spatio-temporal resolution. Nature **482,** 103-106.

Calderon Villalobos, L.I., Lee, S., De Oliveira, C., Ivetac, A., Brandt, W., Armitage, L., Sheard, L.B., Tan, X., Parry, G., Mao, H., Zheng, N., Napier, R., Kepinski, S., and Estelle, M. (2012). A combinatorial TIR1/AFB-Aux/IAA

co-receptor system for differential sensing of auxin. Nat Chem Biol **8,** 477-485.

Cao, J., Schneeberger, K., Ossowski, S., Gunther, T., Bender, S., Fitz, J., Koenig, D., Lanz, C., Stegle, O., Lippert, C., Wang, X., Ott, F., Muller, J., Alonso-Blanco, C., Borgwardt, K., Schmid, K.J., and Weigel, D. (2011). Whole-genome sequencing of multiple Arabidopsis thaliana populations. Nature genetics **43,** 956-963.

Carol, R.J., and Dolan, L. (2002). Building a hair: tip growth in Arabidopsis thaliana root hairs. Philosophical transactions of the Royal Society of London. Series B, Biological sciences **357,** 815-821.

Castoreno, A.B., Smurnyy, Y., Torres, A.D., Vokes, M.S., Jones, T.R., Carpenter, A.E., and Eggert, U.S. (2010). Small molecules discovered in a pathway screen target the Rho pathway in cytokinesis. Nat Chem Biol **6,** 457-463.

Chapman, E.J., and Estelle, M. (2009). Mechanism of auxin-regulated gene expression in plants. Annual review of genetics **43,** 265-285.

Chen, R., Hilson, P., Sedbrook, J., Rosen, E., Caspar, T., and Masson, P.H. (1998). The arabidopsis thaliana AGRAVITROPIC 1 gene encodes a component of the polar-auxin-transport efflux carrier. Proc Natl Acad Sci U S A **95,** 15112-15117.

Chen, X., Irani, N.G., and Friml, J. (2011). Clathrin-mediated endocytosis: the gateway into plant cells. Curr Opin Plant Biol **14,** 674-682.

Chen, X., Naramoto, S., Robert, S., Tejos, R., Lofke, C., Lin, D., Yang, Z., and Friml, J. (2012). ABP1 and ROP6 GTPase signaling regulate clathrin-mediated endocytosis in Arabidopsis roots. Curr Biol **22,** 1326-1332.

Chinchilla, D., Zipfel, C., Robatzek, S., Kemmerling, B., Nurnberger, T., Jones, J.D., Felix, G., and Boller, T. (2007). A flagellin-induced complex of the receptor FLS2 and BAK1 initiates plant defence. Nature **448,** 497-500.

Clerkx, E.J.M., El-Lithy, M.E., Vierling, E., Ruys, G.J., Blankestijin-De Vries, H., Groot, S.P.C., Vreugdenhil, D., and Koornneef, M. (2004). Analysis of natural allelic variation of Arabidopsis seed germination and seed longevity traits between the accessions Landsberg erecta and Shakdara, using a new recombinant inbred line population. Plant Physiology **135,** 432-443.

Cong, F., Cheung, A.K., and Huang, S.M. (2012). Chemical genetics-based target identification in drug discovery. Annual review of pharmacology and toxicology **52,** 57-78.

Cutler, S.R., Ehrhardt, D.W., Griffitts, J.S., and Somerville, C.R. (2000). Random GFP::cDNA fusions enable visualization of subcellular structures in cells of Arabidopsis at a high frequency. Proc Natl Acad Sci U S A **97,** 3718-3723.

d'Enfert, C., Wuestehube, L.J., Lila, T., and Schekman, R. (1991). Sec12p-dependent membrane binding of the small GTP-binding protein Sar1p promotes formation of transport vesicles from the ER. J Cell Biol **114,** 663-670.

Dal Bosco, C., Dovzhenko, A., Liu, X., Woerner, N., Rensch, T., Eismann, M., Eimer, S., Hegermann, J., Paponov, I.A., Ruperti, B., Heberle-Bors, E., Touraev, A., Cohen, J.D., and Palme, K. (2012). The endoplasmic reticulum localized PIN8 is a pollen-specific auxin carrier involved in intracellular auxin homeostasis. Plant J **71,** 860-870.

daSilva, L.L., Snapp, E.L., Denecke, J., Lippincott-Schwartz, J., Hawes, C., and Brandizzi, F. (2004). Endoplasmic reticulum export sites and Golgi bodies

behave as single mobile secretory units in plant cells. Plant Cell **16,** 1753-1771.

daSilva, L.L., Taylor, J.P., Hadlington, J.L., Hanton, S.L., Snowden, C.J., Fox, S.J., Foresti, O., Brandizzi, F., and Denecke, J. (2005). Receptor salvage from the prevacuolar compartment is essential for efficient vacuolar protein targeting. Plant Cell **17,** 132-148.

De Marcos Lousa, C., Gershlick, D.C., and Denecke, J. (2012). Mechanisms and concepts paving the way towards a complete transport cycle of plant vacuolar sorting receptors. Plant Cell **24,** 1714-1732.

Delbarre, A., Muller, P., Imhoff, V., and Guern, J. (1996). Comparison of mechanisms controlling uptake and accumulation of 2,4-dichlorophenoxy acetic acid, naphthalene-1-acetic acid, and indole-3-acetic acid in suspension-cultured tobacco cells. Planta **198,** 532-541.

Delker, C., Poschl, Y., Raschke, A., Ullrich, K., Ettingshausen, S., Hauptmann, V., Grosse, I., and Quint, M. (2010). Natural variation of transcriptional auxin response networks in Arabidopsis thaliana. Plant Cell **22,** 2184-2200.

Denecke, J., Botterman, J., and Deblaere, R. (1990). Protein Secretion in Plant-Cells Can Occur Via a Default Pathway. Plant Cell **2,** 51-59.

Dettmer, J., and Friml, J. (2011). Cell polarity in plants: when two do the same, it is not the same. Curr Opin Cell Biol **23,** 686-696.

Dettmer, J., Hong-Hermesdorf, A., Stierhof, Y.D., and Schumacher, K. (2006). Vacuolar H+-ATPase activity is required for endocytic and secretory trafficking in Arabidopsis. Plant Cell **18,** 715-730.

Dharmasiri, N., Dharmasiri, S., and Estelle, M. (2005). The F-box protein TIR1 is an auxin receptor. Nature **435,** 441-445.

Dhonukshe, P., Baluska, F., Schlicht, M., Hlavacka, A., Samaj, J., Friml, J., and Gadella, T.W., Jr. (2006). Endocytosis of cell surface material mediates cell plate formation during plant cytokinesis. Developmental cell **10,** 137-150.

Dhonukshe, P., Aniento, F., Hwang, I., Robinson, D.G., Mravec, J., Stierhof, Y.D., and Friml, J. (2007). Clathrin-mediated constitutive endocytosis of PIN auxin efflux carriers in Arabidopsis. Curr Biol **17,** 520-527.

Dhonukshe, P., Huang, F., Galvan-Ampudia, C.S., Mahonen, A.P., Kleine-Vehn, J., Xu, J., Quint, A., Prasad, K., Friml, J., Scheres, B., and Offringa, R. (2010). Plasma membrane-bound AGC3 kinases phosphorylate PIN auxin carriers at TPRXS(N/S) motifs to direct apical PIN recycling. Development **137,** 3245-3255.

Dhonukshe, P., Tanaka, H., Goh, T., Ebine, K., Mahonen, A.P., Prasad, K., Blilou, I., Geldner, N., Xu, J., Uemura, T., Chory, J., Ueda, T., Nakano, A., Scheres, B., and Friml, J. (2008a). Generation of cell polarity in plants links endocytosis, auxin distribution and cell fate decisions. Nature **456,** 962-966.

Dhonukshe, P., Grigoriev, I., Fischer, R., Tominaga, M., Robinson, D.G., Hasek, J., Paciorek, T., Petrasek, J., Seifertova, D., Tejos, R., Meisel, L.A., Zazimalova, E., Gadella, T.W., Jr., Stierhof, Y.D., Ueda, T., Oiwa, K., Akhmanova, A., Brock, R., Spang, A., and Friml, J. (2008b). Auxin transport inhibitors impair vesicle motility and actin cytoskeleton dynamics in diverse eukaryotes. Proc Natl Acad Sci U S A **105,** 4489-4494.

Ding, Z., Wang, B., Moreno, I., Duplakova, N., Simon, S., Carraro, N., Reemmer, J., Pencik, A., Chen, X., Tejos, R., Skupa, P., Pollmann, S., Mravec, J., Petrasek, J., Zazimalova, E., Honys, D., Rolcik, J., Murphy, A., Orellana, A., Geisler, M., and Friml, J. (2012). ER-localized auxin transporter PIN8

regulates auxin homeostasis and male gametophyte development in Arabidopsis. Nature communications **3,** 941.

Eastmond, P.J., Quettier, A.L., Kroon, J.T., Craddock, C., Adams, N., and Slabas, A.R. (2010). Phosphatidic acid phosphohydrolase 1 and 2 regulate phospholipid synthesis at the endoplasmic reticulum in Arabidopsis. Plant Cell **22,** 2796-2811.

El-Lithy, M.E., Clerkx, E.J.M., Ruys, G.J., Koornneef, M., and Vreugdenhil, D. (2004). Quantitative trait locus analysis of growth-related traits in a new Arabidopsis recombinant. Plant Physiology **135,** 444-458.

Feraru, E., and Friml, J. (2008). PIN polar targeting. Plant Physiology **147,** 1553-1559.

Feraru, E., Paciorek, T., Feraru, M.I., Zwiewka, M., De Groodt, R., De Rycke, R., Kleine-Vehn, J., and Friml, J. (2010). The AP-3 beta adaptin mediates the biogenesis and function of lytic vacuoles in Arabidopsis. Plant Cell **22,** 2812-2824.

Finet, C., and Jaillais, Y. (2012). Auxology: when auxin meets plant evo-devo. Developmental biology **369,** 19-31.

Foresti, O., and Denecke, J. (2008). Intermediate organelles of the plant secretory pathway: identity and function. Traffic **9,** 1599-1612.

Foresti, O., Gershlick, D.C., Bottanelli, F., Hummel, E., Hawes, C., and Denecke, J. (2010). A recycling-defective vacuolar sorting receptor reveals an intermediate compartment situated between prevacuoles and vacuoles in tobacco. Plant Cell **22,** 3992-4008.

Friml, J., Wisniewska, J., Benkova, E., Mendgen, K., and Palme, K. (2002). Lateral relocation of auxin efflux regulator PIN3 mediates tropism in Arabidopsis. Nature **415,** 806-809.

Friml, J., Vieten, A., Sauer, M., Weijers, D., Schwarz, H., Hamann, T., Offringa, R., and Jurgens, G. (2003). Efflux-dependent auxin gradients establish the apical-basal axis of Arabidopsis. Nature **426,** 147-153.

Friml, J., Yang, X., Michniewicz, M., Weijers, D., Quint, A., Tietz, O., Benjamins, R., Ouwerkerk, P.B., Ljung, K., Sandberg, G., Hooykaas, P.J., Palme, K., and Offringa, R. (2004). A PINOID-dependent binary switch in apical-basal PIN polar targeting directs auxin efflux. Science **306,** 862-865.

Fukaki, H., Fujisawa, H., and Tasaka, M. (1996). SGR1, SGR2, SGR3: novel genetic loci involved in shoot gravitropism in Arabidopsis thaliana. Plant Physiol **110,** 945-955.

Fukaki, H., Wysocka-Diller, J., Kato, T., Fujisawa, H., Benfey, P.N., and Tasaka, M. (1998). Genetic evidence that the endodermis is essential for shoot gravitropism in Arabidopsis thaliana. Plant J **14,** 425-430.

Ganguly, A., Lee, S.H., Cho, M., Lee, O.R., Yoo, H., and Cho, H.T. (2010). Differential auxin-transporting activities of PIN-FORMED proteins in Arabidopsis root hair cells. Plant Physiol **153,** 1046-1061.

Ge, M., Cohen, J.S., Brown, H.A., and Freed, J.H. (2001). ADP ribosylation factor 6 binding to phosphatidylinositol 4,5-bisphosphate-containing vesicles creates defects in the bilayer structure: an electron spin resonance study. Biophysical journal **81,** 994-1005.

Geldner, N., Friml, J., Stierhof, Y.D., Jurgens, G., and Palme, K. (2001). Auxin transport inhibitors block PIN1 cycling and vesicle trafficking. Nature **413,** 425-428.

Geldner, N., Hyman, D.L., Wang, X., Schumacher, K., and Chory, J. (2007). Endosomal signaling of plant steroid receptor kinase BRI1. Genes & development **21,** 1598-1602.

Geldner, N., Anders, N., Wolters, H., Keicher, J., Kornberger, W., Muller, P., Delbarre, A., Ueda, T., Nakano, A., and Jurgens, G. (2003). The Arabidopsis GNOM ARF-GEF mediates endosomal recycling, auxin transport, and auxin-dependent plant growth. Cell **112,** 219-230.

Gendre, D., McFarlane, H.E., Johnson, E., Mouille, G., Sjodin, A., Oh, J., Levesque-Tremblay, G., Watanabe, Y., Samuels, L., and Bhalerao, R.P. (2013). Trans-Golgi Network Localized ECHIDNA/Ypt Interacting Protein Complex Is Required for the Secretion of Cell Wall Polysaccharides in Arabidopsis. Plant Cell.

Gendre, D., Oh, J., Boutte, Y., Best, J.G., Samuels, L., Nilsson, R., Uemura, T., Marchant, A., Bennett, M.J., Grebe, M., and Bhalerao, R.P. (2011). Conserved Arabidopsis ECHIDNA protein mediates trans-Golgi-network trafficking and cell elongation. Proc Natl Acad Sci U S A **108,** 8048-8053.

Gendreau, E., Traas, J., Desnos, T., Grandjean, O., Caboche, M., and Hofte, H. (1997). Cellular basis of hypocotyl growth in Arabidopsis thaliana. Plant Physiol **114,** 295-305.

Goh, T., Uchida, W., Arakawa, S., Ito, E., Dainobu, T., Ebine, K., Takeuchi, M., Sato, K., Ueda, T., and Nakano, A. (2007). VPS9a, the common activator for two distinct types of Rab5 GTPases, is essential for the development of Arabidopsis thaliana. Plant Cell **19,** 3504-3515.

Grebe, M., Xu, J., Mobius, W., Ueda, T., Nakano, A., Geuze, H.J., Rook, M.B., and Scheres, B. (2003). Arabidopsis sterol endocytosis involves actin-mediated trafficking via ARA6-positive early endosomes. Curr Biol **13,** 1378-1387.

Grunewald, W., and Friml, J. (2010). The march of the PINs: developmental plasticity by dynamic polar targeting in plant cells. EMBO J **29,** 2700-2714.

Happel, N., Honing, S., Neuhaus, J.M., Paris, N., Robinson, D.G., and Holstein, S.E.H. (2004). Arabidopsis mu A-adaptin interacts with the tyrosine motif of the vacuolar sorting receptor VSR-PS1. Plant Journal **37,** 678-693.

Hawes, C.R., and Satiat-Jeunemaitre, B. (2001). Trekking along the cytoskeleton. Plant Physiol **125,** 119-122.

Hepler, P.K., Vidali, L., and Cheung, A.Y. (2001). Polarized cell growth in higher plants. Annu Rev Cell Dev Bi **17,** 159-187.

Hicks, G.R., and Raikhel, N.V. (2009). Opportunities and challenges in plant chemical biology. Nat Chem Biol **5,** 268-272.

Hicks, G.R., and Raikhel, N.V. (2010). Advances in dissecting endomembrane trafficking with small molecules. Curr Opin Plant Biol **13,** 706-713.

Hicks, G.R., and Raikhel, N.V. (2012). Small molecules present large opportunities in plant biology. Annual review of plant biology **63,** 261-282.

Hobbie, L.J. (1998). Auxin: Molecular genetic approaches in Arabidopsis. Plant Physiol Bioch **36,** 91-102.

Hou, G., Mohamalawari, D.R., and Blancaflor, E.B. (2003). Enhanced gravitropism of roots with a disrupted cap actin cytoskeleton. Plant Physiol **131,** 1360-1373.

Hou, G., Kramer, V.L., Wang, Y.S., Chen, R., Perbal, G., Gilroy, S., and Blancaflor, E.B. (2004). The promotion of gravitropism in Arabidopsis roots upon actin disruption is coupled with the extended alkalinization of the

columella cytoplasm and a persistent lateral auxin gradient. Plant J **39,** 113-125.

Hu, J., Baker, A., Bartel, B., Linka, N., Mullen, R.T., Reumann, S., and Zolman, B.K. (2012). Plant peroxisomes: biogenesis and function. Plant Cell **24,** 2279-2303.

Hu, J., Shibata, Y., Voss, C., Shemesh, T., Li, Z., Coughlin, M., Kozlov, M.M., Rapoport, T.A., and Prinz, W.A. (2008). Membrane proteins of the endoplasmic reticulum induce high-curvature tubules. Science **319,** 1247-1250.

Huss, M., Ingenhorst, G., Konig, S., Gassel, M., Drose, S., Zeeck, A., Altendorf, K., and Wieczorek, H. (2002). Concanamycin A, the specific inhibitor of V-ATPases, binds to the V(o) subunit c. J Biol Chem **277,** 40544-40548.

Jaillais, Y., Fobis-Loisy, I., Miege, C., Rollin, C., and Gaude, T. (2006). AtSNX1 defines an endosome for auxin-carrier trafficking in Arabidopsis. Nature **443,** 106-109.

Jander, G., Norris, S.R., Rounsley, S.D., Bush, D.F., Levin, I.M., and Last, R.L. (2002). Arabidopsis map-based cloning in the post-genome era. Plant Physiol **129,** 440-450.

Jelinkova, A., Malinska, K., Simon, S., Kleine-Vehn, J., Parezova, M., Pejchar, P., Kubes, M., Martinec, J., Friml, J., Zazimalova, E., and Petrasek, J. (2010). Probing plant membranes with FM dyes: tracking, dragging or blocking? Plant J **61,** 883-892.

Jensen, P.J., Hangarter, R.P., and Estelle, M. (1998). Auxin transport is required for hypocotyl elongation in light-grown but not dark-grown Arabidopsis. Plant Physiol **116,** 455-462.

Jiang, L., and Rogers, J.C. (1998). Integral membrane protein sorting to vacuoles in plant cells: evidence for two pathways. J Cell Biol **143,** 1183-1199.

Jung, J.Y., Kim, Y.W., Kwak, J.M., Hwang, J.U., Young, J., Schroeder, J.I., Hwang, I., and Lee, Y. (2002). Phosphatidylinositol 3- and 4-phosphate are required for normal stomatal movements. Plant Cell **14,** 2399-2412.

Kandasamy, M.K., McKinney, E.C., and Meagher, R.B. (2009). A single vegetative actin isovariant overexpressed under the control of multiple regulatory sequences is sufficient for normal Arabidopsis development. Plant Cell **21,** 701-718.

Kandasamy, M.K., Gilliland, L.U., McKinney, E.C., and Meagher, R.B. (2001). One plant actin isovariant, ACT7, is induced by auxin and required for normal callus formation. Plant Cell **13,** 1541-1554.

Kang, H., Kim, S.Y., Song, K., Sohn, E.J., Lee, Y., Lee, D.W., Hara-Nishimura, I., and Hwang, I. (2012). Trafficking of vacuolar proteins: the crucial role of Arabidopsis vacuolar protein sorting 29 in recycling vacuolar sorting receptor. Plant Cell **24,** 5058-5073.

Kato, T., Morita, M.T., Fukaki, H., Yamauchi, Y., Uehara, M., Niihama, M., and Tasaka, M. (2002). SGR2, a phospholipase-like protein, and ZIG/SGR4, a SNARE, are involved in the shoot gravitropism of Arabidopsis. Plant Cell **14,** 33-46.

Kellermeier, F., Chardon, F., and Amtmann, A. (2013). Natural variation of Arabidopsis root architecture reveals complementing adaptive strategies to potassium starvation. Plant Physiol **161,** 1421-1432.

Kepinski, S., and Leyser, O. (2005a). The Arabidopsis F-box protein TIR1 is an auxin receptor. Nature **435,** 446-451.

Kepinski, S., and Leyser, O. (2005b). Plant development: Auxin in loops. Current Biology **15,** R208-R210.

Kiss, J.Z., Hertel, R., and Sack, F.D. (1989). Amyloplasts are necessary for full gravitropic sensitivity in roots of Arabidopsis thaliana. Planta **177,** 198-206.

Kiss, J.Z., Guisinger, M.M., Miller, A.J., and Stackhouse, K.S. (1997). Reduced gravitropism in hypocotyls of starch-deficient mutants of Arabidopsis. Plant & cell physiology **38,** 518-525.

Kleine-Vehn, J., Leitner, J., Zwiewka, M., Sauer, M., Abas, L., Luschnig, C., and Friml, J. (2008). Differential degradation of PIN2 auxin efflux carrier by retromer-dependent vacuolar targeting. Proc Natl Acad Sci U S A **105,** 17812-17817.

Kleine-Vehn, J., Huang, F., Naramoto, S., Zhang, J., Michniewicz, M., Offringa, R., and Friml, J. (2009). PIN Auxin Efflux Carrier Polarity Is Regulated by PINOID Kinase-Mediated Recruitment into GNOM-Independent Trafficking in Arabidopsis. Plant Cell **21,** 3839-3849.

Konieczny, A., and Ausubel, F.M. (1993). A procedure for mapping Arabidopsis mutations using co-dominant ecotype-specific PCR-based markers. Plant J **4,** 403-410.

Koornneef, M., Alonso-Blanco, C., and Vreugdenhil, D. (2004). Naturally occurring genetic variation in Arabidopsis thaliana. Annual review of plant biology **55,** 141-172.

Korol, A.B., Ronin, Y.I., Itskovich, A.M., Peng, J., and Nevo, E. (2001). Enhanced efficiency of quantitative trait loci mapping analysis based on multivariate complexes of quantitative traits. Genetics **157,** 1789-1803.

Kotzer, A.M., Brandizzi, F., Neumann, U., Paris, N., Moore, I., and Hawes, C. (2004). AtRabF2b (Ara7) acts on the vacuolar trafficking pathway in tobacco leaf epidermal cells. J Cell Sci **117,** 6377-6389.

Krecek, P., Skupa, P., Libus, J., Naramoto, S., Tejos, R., Friml, J., and Zazimalova, E. (2009). The PIN-FORMED (PIN) protein family of auxin transporters. Genome biology **10,** 249.

Kumari, S., and van der Hoorn, R.A. (2011). A structural biology perspective on bioactive small molecules and their plant targets. Curr Opin Plant Biol **14,** 480-488.

Lau, S., Slane, D., Herud, O., Kong, J., and Jurgens, G. (2012). Early embryogenesis in flowering plants: setting up the basic body pattern. Annual review of plant biology **63,** 483-506.

Lauber, M.H., Waizenegger, I., Steinmann, T., Schwarz, H., Mayer, U., Hwang, I., Lukowitz, W., and Jurgens, G. (1997). The Arabidopsis KNOLLE protein is a cytokinesis-specific syntaxin. J Cell Biol **139,** 1485-1493.

Lavieu, G., Zheng, H., and Rothman, J.E. (2013). Stapled Golgi cisternae remain in place as cargo passes through the stack. eLife **2,** e00558.

Lee, G.J., Sohn, E.J., Lee, M.H., and Hwang, I. (2004). The Arabidopsis rab5 homologs rha1 and ara7 localize to the prevacuolar compartment. Plant & cell physiology **45,** 1211-1220.

Lee, M.H., Min, M.K., Lee, Y.J., Jin, J.B., Shin, D.H., Kim, D.H., Lee, K.H., and Hwang, I. (2002). ADP-ribosylation factor 1 of Arabidopsis plays a critical role in intracellular trafficking and maintenance of endoplasmic reticulum morphology in Arabidopsis. Plant Physiol **129,** 1507-1520.

Lenger, J., Kaschani, F., Lenz, T., Dalhoff, C., Villamor, J.G., Koster, H., Sewald, N., and van der Hoorn, R.A.L. (2012). Labeling and enrichment of

Arabidopsis thaliana matrix metalloproteases using an active-site directed, marimastat-based photoreactive probe. Bioorgan Med Chem **20,** 592-596.

Li, R., Liu, P., Wan, Y., Chen, T., Wang, Q., Mettbach, U., Baluska, F., Samaj, J., Fang, X., Lucas, W.J., and Lin, J. (2012). A membrane microdomain-associated protein, Arabidopsis Flot1, is involved in a clathrin-independent endocytic pathway and is required for seedling development. Plant Cell **24,** 2105-2122.

Lin, D., Nagawa, S., Chen, J., Cao, L., Chen, X., Xu, T., Li, H., Dhonukshe, P., Yamamuro, C., Friml, J., Scheres, B., Fu, Y., and Yang, Z. (2012). A ROP GTPase-dependent auxin signaling pathway regulates the subcellular distribution of PIN2 in Arabidopsis roots. Curr Biol **22,** 1319-1325.

Lister, C., and Dean, C. (1993). Recombinant Inbred Lines for Mapping Rflp and Phenotypic Markers in Arabidopsis-Thaliana. Plant Journal **4,** 745-750.

Liu, Y.G., Mitsukawa, N., Oosumi, T., and Whittier, R.F. (1995). Efficient isolation and mapping of Arabidopsis thaliana T-DNA insert junctions by thermal asymmetric interlaced PCR. Plant J **8,** 457-463.

Ljung, K., Bhalerao, R.P., and Sandberg, G. (2001). Sites and homeostatic control of auxin biosynthesis in Arabidopsis during vegetative growth. Plant J **28,** 465-474.

Ljung, K., Hull, A.K., Celenza, J., Yamada, M., Estelle, M., Normanly, J., and Sandberg, G. (2005). Sites and regulation of auxin biosynthesis in Arabidopsis roots. Plant Cell **17,** 1090-1104.

Loudet, O., Gaudon, V., Trubuil, A., and Daniel-Vedele, F. (2005). Quantitative trait loci controlling root growth and architecture in Arabidopsis thaliana confirmed by heterogeneous inbred family. Theoretical and Applied Genetics **110,** 742-753.

Loudet, O., Chaillou, S., Camilleri, C., Bouchez, D., and Daniel-Vedele, F. (2002). Bay-0 x Shahdara recombinant inbred line population: a powerful tool for the genetic dissection of complex traits in Arabidopsis. TAG. Theoretical and applied genetics. Theoretische und angewandte Genetik **104,** 1173-1184.

Lukowitz, W., Gillmor, C.S., and Scheible, W.R. (2000). Positional cloning in Arabidopsis. Why it feels good to have a genome initiative working for you. Plant Physiol **123,** 795-805.

Luschnig, C., Gaxiola, R.A., Grisafi, P., and Fink, G.R. (1998). EIR1, a root-specific protein involved in auxin transport, is required for gravitropism in Arabidopsis thaliana. Genes & development **12,** 2175-2187.

Macquet, A., Ralet, M.C., Loudet, O., Kronenberger, J., Mouille, G., Marion-Poll, A., and North, H.M. (2007). A naturally occurring mutation in an Arabidopsis accession affects a beta-D-galactosidase that increases the hydrophilic potential of rhamnogalacturonan I in seed mucilage. Plant Cell **19,** 3990-4006.

Mancuso, S., Barlow, P.W., Volkmann, D., and Baluska, F. (2006). Actin turnover-mediated gravity response in maize root apices: gravitropism of decapped roots implicates gravisensing outside of the root cap. Plant signaling & behavior **1,** 52-58.

Maple, J., and Moller, S.G. (2007). Mutagenesis in Arabidopsis. Methods in molecular biology **362,** 197-206.

Marti, L., Fornaciari, S., Renna, L., Stefano, G., and Brandizzi, F. (2010). COPII-mediated traffic in plants. Trends in plant science **15,** 522-528.

Matsuoka, K., Watanabe, N., and Nakamura, K. (1995). O-glycosylation of a precursor to a sweet potato vacuolar protein, sporamin, expressed in tobacco cells. Plant Journal **8,** 877-889.

McMahon, H.T., and Boucrot, E. (2011). Molecular mechanism and physiological functions of clathrin-mediated endocytosis. Nature reviews. Molecular cell biology **12,** 517-533.

Michniewicz, M., Zago, M.K., Abas, L., Weijers, D., Schweighofer, A., Meskiene, I., Heisler, M.G., Ohno, C., Zhang, J., Huang, F., Schwab, R., Weigel, D., Meyerowitz, E.M., Luschnig, C., Offringa, R., and Friml, J. (2007). Antagonistic regulation of PIN phosphorylation by PP2A and PINOID directs auxin flux. Cell **130,** 1044-1056.

Moller, S.G., and Chua, N.H. (1999). Interactions and intersections of plant signaling pathways. J Mol Biol **293,** 219-234.

Morita, M.T. (2010). Directional gravity sensing in gravitropism. Annual review of plant biology **61,** 705-720.

Morita, M.T., Kato, T., Nagafusa, K., Saito, C., Ueda, T., Nakano, A., and Tasaka, M. (2002). Involvement of the vacuoles of the endodermis in the early process of shoot gravitropism in Arabidopsis. Plant Cell **14,** 47-56.

Mravec, J., Skupa, P., Bailly, A., Hoyerova, K., Krecek, P., Bielach, A., Petrasek, J., Zhang, J., Gaykova, V., Stierhof, Y.D., Dobrev, P.I., Schwarzerova, K., Rolcik, J., Seifertova, D., Luschnig, C., Benkova, E., Zazimalova, E., Geisler, M., and Friml, J. (2009). Subcellular homeostasis of phytohormone auxin is mediated by the ER-localized PIN5 transporter. Nature **459,** 1136-1140.

Muller, A., Guan, C., Galweiler, L., Tanzler, P., Huijser, P., Marchant, A., Parry, G., Bennett, M., Wisman, E., and Palme, K. (1998). AtPIN2 defines a locus of Arabidopsis for root gravitropism control. EMBO J **17,** 6903-6911.

Murphy, A.S., and Peer, W.A. (2012). Vesicle trafficking: ROP-RIC roundabout. Curr Biol **22,** R576-578.

Nagawa, S., Xu, T., Lin, D., Dhonukshe, P., Zhang, X., Friml, J., Scheres, B., Fu, Y., and Yang, Z. (2012). ROP GTPase-dependent actin microfilaments promote PIN1 polarization by localized inhibition of clathrin-dependent endocytosis. PLoS biology **10,** e1001299.

Naramoto, S., Kleine-Vehn, J., Robert, S., Fujimoto, M., Dainobu, T., Paciorek, T., Ueda, T., Nakano, A., Van Montagu, M.C., Fukuda, H., and Friml, J. (2010). ADP-ribosylation factor machinery mediates endocytosis in plant cells. Proc Natl Acad Sci U S A **107,** 21890-21895.

Nebenfuhr, A., Ritzenthaler, C., and Robinson, D.G. (2002). Brefeldin A: deciphering an enigmatic inhibitor of secretion. Plant Physiol **130,** 1102-1108.

Nielsen, E., Cheung, A.Y., and Ueda, T. (2008). The regulatory RAB and ARF GTPases for vesicular trafficking. Plant Physiol **147,** 1516-1526.

Nodzynski, T., Feraru, M.I., Hirsch, S., De Rycke, R., Niculaes, C., Boerjan, W., Van Leene, J., De Jaeger, G., Vanneste, S., and Friml, J. (2013). Retromer Subunits VPS35A and VPS29 Mediate Prevacuolar Compartment (PVC) Function in Arabidopsis. Mol Plant.

Ojangu, E.L., Jarve, K., Paves, H., and Truve, E. (2007). Arabidopsis thaliana myosin XIK is involved in root hair as well as trichome morphogenesis on stems and leaves. Protoplasma **230,** 193-202.

Oliviusson, P., Heinzerling, O., Hillmer, S., Hinz, G., Tse, Y.C., Jiang, L., and Robinson, D.G. (2006). Plant retromer, localized to the prevacuolar

compartment and microvesicles in Arabidopsis, may interact with vacuolar sorting receptors. Plant Cell **18,** 1239-1252.

Ortiz-Zapater, E., Soriano-Ortega, E., Marcote, M.J., Ortiz-Masia, D., and Aniento, F. (2006). Trafficking of the human transferrin receptor in plant cells: effects of tyrphostin A23 and brefeldin A. Plant J **48,** 757-770.

Ovecka, M., Lang, I., Baluska, F., Ismail, A., Illes, P., and Lichtscheidl, I.K. (2005). Endocytosis and vesicle trafficking during tip growth of root hairs. Protoplasma **226,** 39-54.

Paciorek, T., Zazimalova, E., Ruthardt, N., Petrasek, J., Stierhof, Y.D., Kleine-Vehn, J., Morris, D.A., Emans, N., Jurgens, G., Geldner, N., and Friml, J. (2005). Auxin inhibits endocytosis and promotes its own efflux from cells. Nature **435,** 1251-1256.

Parinov, S., Sevugan, M., Ye, D., Yang, W.C., Kumaran, M., and Sundaresan, V. (1999). Analysis of flanking sequences from dissociation insertion lines: a database for reverse genetics in Arabidopsis. Plant Cell **11,** 2263-2270.

Park, M., Song, K., Reichardt, I., Kim, H., Mayer, U., Stierhof, Y.D., Hwang, I., and Jurgens, G. (2013). Arabidopsis mu-adaptin subunit AP1M of adaptor protein complex 1 mediates late secretory and vacuolar traffic and is required for growth. Proc Natl Acad Sci U S A **110,** 10318-10323.

Parry, G., Calderon-Villalobos, L.I., Prigge, M., Peret, B., Dharmasiri, S., Itoh, H., Lechner, E., Gray, W.M., Bennett, M., and Estelle, M. (2009). Complex regulation of the TIR1/AFB family of auxin receptors. Proc Natl Acad Sci U S A **106,** 22540-22545.

Peer, W.A., Blakeslee, J.J., Yang, H.B., and Murphy, A.S. (2011). Seven Things We Think We Know about Auxin Transport. Molecular Plant **4,** 487-504.

Peremyslov, V.V., Prokhnevsky, A.I., and Dolja, V.V. (2010). Class XI myosins are required for development, cell expansion, and F-Actin organization in Arabidopsis. Plant Cell **22,** 1883-1897.

Peremyslov, V.V., Prokhnevsky, A.I., Avisar, D., and Dolja, V.V. (2008). Two class XI myosins function in organelle trafficking and root hair development in Arabidopsis. Plant Physiol **146,** 1109-1116.

Peters, J.L., Cnudde, F., and Gerats, T. (2003). Forward genetics and map-based cloning approaches. Trends in plant science **8,** 484-491.

Petrasek, J., Mravec, J., Bouchard, R., Blakeslee, J.J., Abas, M., Seifertova, D., Wisniewska, J., Tadele, Z., Kubes, M., Covanova, M., Dhonukshe, P., Skupa, P., Benkova, E., Perry, L., Krecek, P., Lee, O.R., Fink, G.R., Geisler, M., Murphy, A.S., Luschnig, C., Zazimalova, E., and Friml, J. (2006). PIN proteins perform a rate-limiting function in cellular auxin efflux. Science **312,** 914-918.

Pracharoenwattana, I., Cornah, J.E., and Smith, S.M. (2005). Arabidopsis peroxisomal citrate synthase is required for fatty acid respiration and seed germination. Plant Cell **17,** 2037-2048.

Price, A.H. (2006). Believe it or not, QTLs are accurate! Trends in plant science **11,** 213-216.

Prokhnevsky, A.I., Peremyslov, V.V., and Dolja, V.V. (2008). Overlapping functions of the four class XI myosins in Arabidopsis growth, root hair elongation, and organelle motility. Proc Natl Acad Sci U S A **105,** 19744-19749.

Rapoport, T.A. (2007). Protein translocation across the eukaryotic endoplasmic reticulum and bacterial plasma membranes. Nature **450,** 663-669.

Reichardt, I., Stierhof, Y.D., Mayer, U., Richter, S., Schwarz, H., Schumacher, K., and Jurgens, G. (2007). Plant cytokinesis requires de novo secretory trafficking but not endocytosis. Curr Biol **17,** 2047-2053.

Ren, Z., Zheng, Z., Chinnusamy, V., Zhu, J., Cui, X., Iida, K., and Zhu, J.K. (2010). RAS1, a quantitative trait locus for salt tolerance and ABA sensitivity in Arabidopsis. Proc Natl Acad Sci U S A **107,** 5669-5674.

Richter, S., Voss, U., and Jurgens, G. (2009). Post-Golgi traffic in plants. Traffic **10,** 819-828.

Richter, S., Geldner, N., Schrader, J., Wolters, H., Stierhof, Y.D., Rios, G., Koncz, C., Robinson, D.G., and Jurgens, G. (2007). Functional diversification of closely related ARF-GEFs in protein secretion and recycling. Nature **448,** 488-492.

Ritzenthaler, C., Nebenfuhr, A., Movafeghi, A., Stussi-Garaud, C., Behnia, L., Pimpl, P., Staehelin, L.A., and Robinson, D.G. (2002). Reevaluation of the effects of brefeldin A on plant cells using tobacco Bright Yellow 2 cells expressing Golgi-targeted green fluorescent protein and COPI antisera. Plant Cell **14,** 237-261.

Robert, S., Chary, S.N., Drakakaki, G., Li, S., Yang, Z., Raikhel, N.V., and Hicks, G.R. (2008). Endosidin1 defines a compartment involved in endocytosis of the brassinosteroid receptor BRI1 and the auxin transporters PIN2 and AUX1. Proc Natl Acad Sci U S A **105,** 8464-8469.

Robert, S., Kleine-Vehn, J., Barbez, E., Sauer, M., Paciorek, T., Baster, P., Vanneste, S., Zhang, J., Simon, S., Covanova, M., Hayashi, K., Dhonukshe, P., Yang, Z., Bednarek, S.Y., Jones, A.M., Luschnig, C., Aniento, F., Zazimalova, E., and Friml, J. (2010). ABP1 mediates auxin inhibition of clathrin-dependent endocytosis in Arabidopsis. Cell **143,** 111-121.

Rojas-Pierce, M., Titapiwatanakun, B., Sohn, E.J., Fang, F., Larive, C.K., Blakeslee, J., Cheng, Y., Cutler, S.R., Peer, W.A., Murphy, A.S., and Raikhel, N.V. (2007). Arabidopsis P-glycoprotein19 participates in the inhibition of gravitropism by gravacin. Chem Biol **14,** 1366-1376.

Roychoudhry, S., Del Bianco, M., Kieffer, M., and Kepinski, S. (2013). Auxin Controls Gravitropic Setpoint Angle in Higher Plant Lateral Branches. Curr Biol.

Sabater, M., and Rubery, P.H. (1987). Auxin Carriers in Cucurbita Vesicles .2. Evidence That Carrier-Mediated Routes of Both Indole-3-Acetic-Acid Influx and Efflux Are Electroimpelled. Planta **171,** 507-513.

Saint-Jore, C.M., Evins, J., Batoko, H., Brandizzi, F., Moore, I., and Hawes, C. (2002). Redistribution of membrane proteins between the Golgi apparatus and endoplasmic reticulum in plants is reversible and not dependent on cytoskeletal networks. Plant J **29,** 661-678.

Sauer, M., Paciorek, T., Benkova, E., and Friml, J. (2006). Immunocytochemical techniques for whole-mount in situ protein localization in plants. Nature protocols **1,** 98-103.

Savaldi-Goldstein, S., Baiga, T.J., Pojer, F., Dabi, T., Butterfield, C., Parry, G., Santner, A., Dharmasiri, N., Tao, Y., Estelle, M., Noel, J.P., and Chory, J. (2008). New auxin analogs with growth-promoting effects in intact plants reveal a chemical strategy to improve hormone delivery. Proc Natl Acad Sci U S A **105,** 15190-15195.

Scheuring, D., Viotti, C., Kruger, F., Kunzl, F., Sturm, S., Bubeck, J., Hillmer, S., Frigerio, L., Robinson, D.G., Pimpl, P., and Schumacher, K. (2011).

Multivesicular bodies mature from the trans-Golgi network/early endosome in Arabidopsis. Plant Cell **23,** 3463-3481.

Sessions, A., Burke, E., Presting, G., Aux, G., McElver, J., Patton, D., Dietrich, B., Ho, P., Bacwaden, J., Ko, C., Clarke, J.D., Cotton, D., Bullis, D., Snell, J., Miguel, T., Hutchison, D., Kimmerly, B., Mitzel, T., Katagiri, F., Glazebrook, J., Law, M., and Goff, S.A. (2002). A high-throughput Arabidopsis reverse genetics system. Plant Cell **14,** 2985-2994.

Sheahan, M.B., Staiger, C.J., Rose, R.J., and McCurdy, D.W. (2004). A green fluorescent protein fusion to actin-binding domain 2 of Arabidopsis fimbrin highlights new features of a dynamic actin cytoskeleton in live plant cells. Plant Physiol **136,** 3968-3978.

Shimmen, T., and Yokota, E. (2004). Cytoplasmic streaming in plants. Curr Opin Cell Biol **16,** 68-72.

Shimomura, S. (2006). Identification of a glycosylphosphatidylinositol-anchored plasma membrane protein interacting with the C-terminus of auxin-binding protein 1: a photoaffinity crosslinking study. Plant molecular biology **60,** 663-677.

Silva Lda, C., Wang, S., and Zeng, Z.B. (2012). Composite interval mapping and multiple interval mapping: procedures and guidelines for using Windows QTL Cartographer. Methods in molecular biology **871,** 75-119.

Simon, M., Loudet, O., Durand, S., Berard, A., Brunel, D., Sennesal, F.X., Durand-Tardif, M., Pelletier, G., and Camilleri, C. (2008). Quantitative trait loci mapping in five new large recombinant inbred line populations of Arabidopsis thaliana genotyped with consensus single-nucleotide polymorphism markers. Genetics **178,** 2253-2264.

Sorieul, M., Langhans, M., Guetzoyan, L., Hillmer, S., Clarkson, G., Lord, J.M., Roberts, L.M., Robinson, D.G., Spooner, R.A., and Frigerio, L. (2011). An Exo2 derivative affects ER and Golgi morphology and vacuolar sorting in a tissue-specific manner in arabidopsis. Traffic **12,** 1552-1562.

Sparkes, I., Runions, J., Hawes, C., and Griffing, L. (2009a). Movement and remodeling of the endoplasmic reticulum in nondividing cells of tobacco leaves. Plant Cell **21,** 3937-3949.

Sparkes, I., Tolley, N., Aller, I., Svozil, J., Osterrieder, A., Botchway, S., Mueller, C., Frigerio, L., and Hawes, C. (2010). Five Arabidopsis reticulon isoforms share endoplasmic reticulum location, topology, and membrane-shaping properties. Plant Cell **22,** 1333-1343.

Sparkes, I.A. (2010). Motoring around the plant cell: insights from plant myosins. Biochem Soc Trans **38,** 833-838.

Sparkes, I.A., Teanby, N.A., and Hawes, C. (2008). Truncated myosin XI tail fusions inhibit peroxisome, Golgi, and mitochondrial movement in tobacco leaf epidermal cells: a genetic tool for the next generation. J Exp Bot **59,** 2499-2512.

Sparkes, I.A., Ketelaar, T., de Ruijter, N.C., and Hawes, C. (2009b). Grab a Golgi: laser trapping of Golgi bodies reveals in vivo interactions with the endoplasmic reticulum. Traffic **10,** 567-571.

Sparkes, I.A., Frigerio, L., Tolley, N., and Hawes, C. (2009c). The plant endoplasmic reticulum: a cell-wide web. Biochem J **423,** 145-155.

Stefano, G., Renna, L., Chatre, L., Hanton, S.L., Moreau, P., Hawes, C., and Brandizzi, F. (2006). In tobacco leaf epidermal cells, the integrity of protein

export from the endoplasmic reticulum and of ER export sites depends on active COPI machinery. Plant J **46,** 95-110.

Steinmann, T., Geldner, N., Grebe, M., Mangold, S., Jackson, C.L., Paris, S., Galweiler, L., Palme, K., and Jurgens, G. (1999). Coordinated polar localization of auxin efflux carrier PIN1 by GNOM ARF GEF. Science **286,** 316-318.

Stolz, A., and Wolf, D.H. (2010). Endoplasmic reticulum associated protein degradation: a chaperone assisted journey to hell. Biochimica et biophysica acta **1803,** 694-705.

Surpin, M., Rojas-Pierce, M., Carter, C., Hicks, G.R., Vasquez, J., and Raikhel, N.V. (2005). The power of chemical genomics to study the link between endomembrane system components and the gravitropic response. Proc Natl Acad Sci U S A **102,** 4902-4907.

Swarup, R., Kargul, J., Marchant, A., Zadik, D., Rahman, A., Mills, R., Yemm, A., May, S., Williams, L., Millner, P., Tsurumi, S., Moore, I., Napier, R., Kerr, I.D., and Bennett, M.J. (2004). Structure-function analysis of the presumptive Arabidopsis auxin permease AUX1. Plant Cell **16,** 3069-3083.

Tamura, K., Shimada, T., Ono, E., Tanaka, Y., Nagatani, A., Higashi, S.I., Watanabe, M., Nishimura, M., and Hara-Nishimura, I. (2003). Why green fluorescent fusion proteins have not been observed in the vacuoles of higher plants. Plant J **35,** 545-555.

Tasaka, M., Kato, T., and Fukaki, H. (1999). The endodermis and shoot gravitropism. Trends in plant science **4,** 103-107.

Teh, O.K., and Moore, I. (2007). An ARF-GEF acting at the Golgi and in selective endocytosis in polarized plant cells. Nature **448,** 493-496.

Teh, O.K., Shimono, Y., Shirakawa, M., Fukao, Y., Tamura, K., Shimada, T., and Hara-Nishimura, I. (2013). The AP-1 mu Adaptin is Required for KNOLLE Localization at the Cell Plate to Mediate Cytokinesis in Arabidopsis. Plant and Cell Physiology **54,** 838-847.

Tolley, N., Sparkes, I., Craddock, C.P., Eastmond, P.J., Runions, J., Hawes, C., and Frigerio, L. (2010). Transmembrane domain length is responsible for the ability of a plant reticulon to shape endoplasmic reticulum tubules in vivo. Plant J **64,** 411-418.

Tolley, N., Sparkes, I.A., Hunter, P.R., Craddock, C.P., Nuttall, J., Roberts, L.M., Hawes, C., Pedrazzini, E., and Frigerio, L. (2008). Overexpression of a plant reticulon remodels the lumen of the cortical endoplasmic reticulum but does not perturb protein transport. Traffic **9,** 94-102.

Tominaga-Wada, R., Ishida, T., and Wada, T. (2011). New Insights into the Mechanism of Development of Arabidopsis Root Hairs and Trichomes. Int Rev Cel Mol Bio **286,** 67-106.

Toth, R., Gerding-Reimers, C., Deeks, M.J., Menninger, S., Gallegos, R.M., Tonaco, I.A., Hubel, K., Hussey, P.J., Waldmann, H., and Coupland, G. (2012). Prieurianin/ endosidin1 is an actin stabilizing small molecule identified from a chemical genetic screen for circadian clock effectors in Arabidopsis thaliana. Plant J.

Tse, Y.C., Lo, S.W., Hillmer, S., Dupree, P., and Jiang, L. (2006). Dynamic response of prevacuolar compartments to brefeldin a in plant cells. Plant Physiol **142,** 1442-1459.

Tse, Y.C., Mo, B., Hillmer, S., Zhao, M., Lo, S.W., Robinson, D.G., and Jiang, L. (2004). Identification of multivesicular bodies as prevacuolar compartments in Nicotiana tabacum BY-2 cells. Plant Cell **16,** 672-693.

Tsien, R.Y. (1998). The green fluorescent protein. Annual review of biochemistry **67,** 509-544.

Ueda, H., Yokota, E., Kutsuna, N., Shimada, T., Tamura, K., Shimmen, T., Hasezawa, S., Dolja, V.V., and Hara-Nishimura, I. (2010). Myosin-dependent endoplasmic reticulum motility and F-actin organization in plant cells. Proc Natl Acad Sci U S A **107,** 6894-6899.

Utsuno, K., Shikanai, T., Yamada, Y., and Hashimoto, T. (1998). Agr, an Agravitropic locus of Arabidopsis thaliana, encodes a novel membrane-protein family member. Plant & cell physiology **39,** 1111-1118.

van Leeuwen, H., Kliebenstein, D.J., West, M.A.L., Kim, K., van Poecke, R., Katagiri, F., Michelmore, R.W., Doerge, R.W., and Clair, D.A. (2007). Natural variation among Arabidopsis thaliana accessions for transcriptome response to exogenous salicylic acid. Plant Cell **19,** 2099-2110.

Vert, G. (2008). Plant signaling: brassinosteroids, immunity and effectors are BAK ! Curr Biol **18,** R963-965.

Vitale, A., Ceriotti, A., and Denecke, J. (1993). The Role of the Endoplasmic-Reticulum in Protein-Synthesis, Modification and Intracellular-Transport. Journal of Experimental Botany **44,** 1417-1444.

Volker, A., Stierhof, Y.D., and Jurgens, G. (2001). Cell cycle-independent expression of the Arabidopsis cytokinesis-specific syntaxin KNOLLE results in mistargeting to the plasma membrane and is not sufficient for cytokinesis. J Cell Sci **114,** 3001-3012.

Wang, J., Cai, Y., Miao, Y., Lam, S.K., and Jiang, L. (2009). Wortmannin induces homotypic fusion of plant prevacuolar compartments. J Exp Bot **60,** 3075-3083.

Wang, J.G., Li, S., Zhao, X.Y., Zhou, L.Z., Huang, G.Q., Feng, C., and Zhang, Y. (2013). HAPLESS13, the Arabidopsis mu1 Adaptin, Is Essential for Protein Sorting at the trans-Golgi Network/Early Endosome. Plant Physiol **162,** 1897-1910.

Wee, E.G., Sherrier, D.J., Prime, T.A., and Dupree, P. (1998). Targeting of active sialyltransferase to the plant Golgi apparatus. Plant Cell **10,** 1759-1768.

Weigel, D., and Mott, R. (2009). The 1001 genomes project for Arabidopsis thaliana. Genome biology **10,** 107.

Weigel, D., Ahn, J.H., Blazquez, M.A., Borevitz, J.O., Christensen, S.K., Fankhauser, C., Ferrandiz, C., Kardailsky, I., Malancharuvil, E.J., Neff, M.M., Nguyen, J.T., Sato, S., Wang, Z.Y., Xia, Y., Dixon, R.A., Harrison, M.J., Lamb, C.J., Yanofsky, M.F., and Chory, J. (2000). Activation tagging in Arabidopsis. Plant Physiol **122,** 1003-1013.

Wilson, I.W., Schiff, C.L., Hughes, D.E., and Somerville, S.C. (2001). Quantitative trait loci analysis of powdery mildew disease resistance in the Arabidopsis thaliana accession kashmir-1. Genetics **158,** 1301-1309.

Yamauchi, Y., Fukaki, H., Fujisawa, H., and Tasaka, M. (1997). Mutations in the SGR4, SGR5 and SGR6 loci of Arabidopsis thaliana alter the shoot gravitropism. Plant & cell physiology **38,** 530-535.

Yano, D., Sato, M., Saito, C., Sato, M.H., Morita, M.T., and Tasaka, M. (2003). A SNARE complex containing SGR3/AtVAM3 and ZIG/VTI11 in gravity-sensing

cells is important for Arabidopsis shoot gravitropism. Proc Natl Acad Sci U S A **100,** 8589-8594.

Yokoyama, R., and Nishitani, K. (2001). Endoxyloglucan transferase is localized both in the cell plate and in the secretory pathway destined for the apoplast in tobacco cells. Plant & cell physiology **42,** 292-300.

Zhao, Y., Chow, T.F., Puckrin, R.S., Alfred, S.E., Korir, A.K., Larive, C.K., and Cutler, S.R. (2007). Chemical genetic interrogation of natural variation uncovers a molecule that is glycoactivated. Nature Chemical Biology **3,** 716-721.

Zheng, H., Kunst, L., Hawes, C., and Moore, I. (2004). A GFP-based assay reveals a role for RHD3 in transport between the endoplasmic reticulum and Golgi apparatus. Plant J **37,** 398-414.

Zouhar, J., Hicks, G.R., and Raikhel, N.V. (2004). Sorting inhibitors (Sortins): Chemical compounds to study vacuolar sorting in Arabidopsis. Proc Natl Acad Sci U S A **101,** 9497-9501.

Zouhar, J., Rojo, E., and Bassham, D.C. (2009). AtVPS45 Is a Positive Regulator of the SYP41/SYP61/VTI12 SNARE Complex Involved in Trafficking of Vacuolar Cargo. Plant Physiology **149,** 1668-1678.

Zwiewka, M., Feraru, E., Moller, B., Hwang, I., Feraru, M.I., Kleine-Vehn, J., Weijers, D., and Friml, J. (2011). The AP-3 adaptor complex is required for vacuolar function in Arabidopsis. Cell research **21,** 1711-1722.